ENVIRONMENTAL EFFECTS ON FATIGUE DAMAGE IN NOTCHED CARBON FIBRE COMPOSITES

by

Sotiris Kellas, MSc (Eng), DIC

A thesis submitted for the degree of

PhD

in the Faculty of Engineering

Department of Aeronautics

Imperial College of Science and Technology

University of London

London, SW7 2BY

May 1988

ABSTRACT

Notched coupons, fabricated from a standard carbon epoxy system (XAS/914), were fatigue tested under reversed axial loading. Two notch types were investigated, 5mm circular hole and 10mm sharp slit, located centrally in the 50mm wide coupon specimens. Several destructive and non-destructive methods were used to study the effect of absorbed moisture and/or heat on the fatigue properties of symmetric (0°/±45°) CFRP laminates.

The main objective was the understanding of the mechanisms of fatigue damage propagation around the notches under hot and/or wet environments. The fatigue performance was assessed mainly by means of residual strength measurements. It was found that the shape and extent of fatigue damage around the notches is highly dependent upon the environments considered. Furthermore, it was shown that the residual strength or fatigue life depends upon the stacking sequence for a given environment.

Major emphasis was placed on a thorough study of the standard system but the results obtained were used to describe and predict the fatigue behaviour in more advanced carbon fibre reinforced composite systems (aromatic thermoplastic polymer, toughened epoxy, and bismaleimide).

Damage development around the notches was compared for each material system. The effects of moisture exposure and temperature are included in the comparison, residual tensile and compressive strength measurements were also made. It was found that the toughened system gave better fatigue damage tolerance than the standard epoxy system. The epoxy as well as the bismaleimide systems were more sensitive to wet environments and underwent a change in the fatigue damage mode as a result of moisture pick-up. The thermoplastic-based system was more stable and relatively insensitive to wet environments. However, when tested at high temperature (130°C) a significant reduction in the static properties was observed.

Critical changes in damage mechanisms have been isolated, related to residual strengths (tensile and compressive) and correlated with fatigue life (S-N curves). The most important of which is the transition from width-wise damage growth to length-wise. The fatigue amplitude at which this occurs is denoted by S_t, the transition stress. A simple screening method for fatigue damage tolerant composite structures is proposed. Experimentally determined parameters such as S_t are used in the approach.

ACKNOWLEDGEMENTS

The author wishes to thank his supervisor, Dr John Morton, sincerely for his valuable help and encouragement: even though, in January 1987 he became a professor at VPI in the United States he continued his supervision throughout the course of the research work. The author also wishes to thank all the members of the composite centre, and in particular Bill Godwin, for their advice and guidance. Thanks are also due to the Department's technical staff, and in particular Ray Wilkins. The help of Mr Ken Stevens, on financial matters as well as on editing the thesis is also acknowledged. Moreover, Mr Dennis Hitchings is acknowledged for his advise on the computational study.

The financial support provided by the Procurement Executive Ministry of Defence is gratefully acknowledged. The author would also like to acknowledge ICI and BP for the free-of-charge supply of the materials.

Finally the author wishes to thank the contract monitors, Dr Sarah Bishop and Dr Paul Curtis, for their support and fruitful discussions.

LIST OF SYMBOLS

S -Fatigue amplitude (stress).
S_{st} -Static strength (stress).
S_{HW} -Hot/wet (130°C/1.4%) static strength (stress).
S_t -Transition stress: amplitude at which the fatigue damage undergoes a transition in the direction of propagation.
N -Fatigue life.
R -Ratio of minimum to maximum cyclic load amplitude.
R_{ms} -Ratio of maximum stress in the 0° plies divided by the corresponding maxinum stress in the ±45° plies.
L -Cyclic load amplitude.
Lh -Standard cyclic load amplitude for 5mm circular holes.
Ln -Standard cyclic load amplitude for 10mm sharp notches.
A -Primary stacking sequence: (±45°/03°/±45°/0°)s.
B -Secondary stacking sequence: (0°/±45°/02°/±45°/0°)s.
D -Moisture diffusion coefficient.
M -Moisture equilibrium level.
α -Constant, being expressed as a percentage.
β -Constant.
Tg -Glass transition temperature.
$2a$ -Sharp notch length.
$2a_n$ -Nominal sharp notch length.
E_{ii} -Linear elastic stiffness in the direction i, where i=1,2,3; the ply local axes or i=x,y,z; the laminate axes.

G_{ij} -Shear stiffness in the plane ij, where i,j=1,2,3; the ply local axes or i,j=x,y,z; the laminate axes.

ν_{ij} -Poisson's ratio in the plane ij, where i,j=1,2,3; the ply local axes or i,j=x,y,z; the laminate axes.

σ_x -Component of the direct stress in the direction x, the loading direction.

σ_y -Component of the direct stress in the direction y, transverse to the loading direction.

σ_z -Component of the direct stress in the direction z, at right angles to the plane of the specimen.

σ_{ij} -Component of the shear stress in the plain ij, where i,j=x,y,z.

t -time.

I -Second moment of area.

$E_{ij}I$ -Bending stiffness in the direction ij where i,j=1,2,3; the ply local axes or i,j=x,y,z; the laminate axes.

LIST OF ABBREVIATIONS

BP -British Petroleum
BSI -British Standards Institute
CFRP -Carbon Fibre Reinforced Plastic
C-C -Compression-Compression fatigue loading
CTE -Coefficient of Thermal Expansion
ESM -Electron Scanning Microscope
FEA -Finite Element Analysis
FRP -Fibre Reinforced Plastics
ICI -Imperial Chemical Industries
ILSS -Interlaminar Shear Strength
NDE -Non-Destructive Examination
PEEK -Poly-Ether Ether-Ketone
PLS -Primary Longitudinal Splits
POS -Primary Off-axis Splits
PTFE -Poly-Tetra-Fluoro-Ethylene
RAE -Royal Aircraft Establishment
RH -Relative Humidity
RT -Room Temperature
SCF -Stress Concentration Factor
SLS -Secondary Longitudinal Splits
SOS -Secondary Off-axis Splits
T-C -Tension-Compression fatigue loading (R=-1)
T-T -Tension-Tension fatigue loading
UV -Ultra-Violet
VTOL -Vertical Take-Off and Landing
0-C -"Zero-Compression" fatigue loading ($R=\infty$)
0-T -"Zero-Tension" fatigue loading (R=0)

LIST OF CONTENTS

		Page
1.	**INTRODUCTION**	11
2.	**LITERATURE SURVEY**	14
2.1	INTRODUCTION	14
2.2	MOISTURE ABSORPION IN FIBRE REINFORCED COMPOSITES	14
2.2.1	Effect of Moisture on Epoxy Matrices	15
2.2.2	Effect of Temperature on Moisture Pick-up Rate	20
2.2.3	Effect of Relative Humidity on Equilibrium Level	21
2.2.4	Effect of Moisture Pick-up Upon the Mechanical Properties	22
(a)	Shear Strength	23
(b)	Compressive Strength	24
(c)	Tensile Strength	26
2.2.5	Effect of Moisture on Other Matrices	27
(a)	Bismaleimide	27
(b)	*Polyether Etherketone*	28
2.3	FATIGUE OF COMPOSITE MATERIALS	28
2.3.1	Unnotched Behaviour	29
(a)	Unidirectional	29
(b)	Multidirectional	30
2.3.2	Notched Behaviour	32
(a)	Unidirectional	32
(b)	Multidirectional	32
2.3.3	The Effect of Hygrothermal Environment	33
3.	**EXPERIMENTAL PROGRAMME**	36
3.1	INTRODUCTION	36
3.2	APPARATUS	37

3.2.1	Anti-buckling Guides	37
3.2.2	Test Chamber	38
3.2.3	Test Machines	39
3.2.4	Environmental Cabinets	40
3.2.5	Non-destructive Examination Equipment	40
3.2.6	Destructive Examination Equipment	41
3.3	SPECIMEN PREPARATION	41
3.3.1	Plain Specimens	42
3.3.2	Notched Specimens	43
(a)	Sharp Notches	43
(b)	Circular Holes	43
3.3.3	Environmental Conditioning	44
(a)	60°C/84% RH	44
(b)	RT/100% RH	44
(c)	Weather Conditioning	44
3.4	STATIC TESTS	45
3.4.1	Plain Specimens	45
(a)	Static Strength Tests	45
(b)	Interlaminar Shear Strength Tests	46
(c)	Mechanical Property Determination	46
3.4.2	Notched Specimens	47
(a)	Notched Strengths	47
(b)	Proof Loading	47
(c)	Residual Strengths	48
3.5	FATIGUE TESTS	48
3.5.1	Sharp Notches	49
3.5.2	Circular Holes	50
3.6	DAMAGE DETECTION	51
3.6.1	Non-Destructive Examination	51

(a)	Ultrasonic C-scan	51
(b)	X-ray Radiography	52
3.6.2	Destructive Examination	52
(a)	Optical Microscopy	52
(b)	Scaning Electron Microscopy	53
(c)	Deply	53
(d)	Slicing	54
4.	**EXPERIMENTAL RESULTS AND OBSERVATIONS**	**55**
4.1	INTRODUCTION	55
4.2	MOISTURE CONDITIONING	55
(a)	60°C/84% RH	55
(b)	RT/100% RH	56
(c)	Weather Conditioning	56
4.3	STATIC TESTS	57
4.3.1	Plain Specimens	57
(a)	Static Tensile Strengths	57
(b)	Interlaminar Shear Strengths	58
(c)	Mechanical Properties	59
4.3.2	Notched Specimens	59
(a)	Sharp Notches	59
(b)	Circular Holes	61
4.4	FATIGUE TESTS	63
4.4.1	Fatigue and Residual Strength Tests	63
(a)	Sharp Notches	63
(b)	Circular Holes	65
4.4.2	Fatigue Tests to Failure	67
(a)	Sharp Notches	68
(b)	Circular Holes	68
4.5	DAMAGE DETECTION	69
4.5.1	Non-Destructive Examination	69
(a)	Ultrasonic C-scan	69

(b)	X-ray Radiography	71
4.5.2	Destructive Examination	74
(a)	Optical Microscopy	74
(b)	Deply	77
(c)	Scanning Electron Microscopy	78
4.6	FINITE ELEMENT ANALYSIS	79
4.6.1	Sharp 10mm Notch	80
4.6.2	Circular 5mm Hole	82
5.	**NEW MATERIALS**	**84**
5.1	INTRODUCTION	84
5.2	EXPERIMENTAL PROGRAMME	85
5.2.1	Toughened Epoxy Matrix	85
(a)	Static Tests	86
(b)	Fatigue Tests	86
5.2.2	Thermoplastic Matrix	86
(a)	Static Tests	86
(b)	Fatigue Tests	86
5.2.3	Bismaleimide Matrix	87
(a)	Static Tests	87
(b)	Fatigue Tests	87
5.3	EXPERIMENTAL OBSERVATIONS	88
5.3.1	Toughened Epoxy Matrix	88
(a)	Moisture Conditioning	88
(b)	Static Tests	88
(c)	Fatigue and Residual Strength Tests	88
(d)	Damage Evaluation	89
5.3.2	Thermoplastic Matrix	90
(a)	Moisture Conditioning	90
(b)	Static Tests	90
(c)	Fatigue and Residual Strength Tests	91
(d)	Damage Evaluation	92

5.3.3	Bismaleimide Matrix	93
(a)	Moisture Conditioning	93
(b)	Static Tests	93
(c)	Fatigue and Residual Strength Tests	94
(d)	Damage Evaluation	95
6.	**DISCUSSION**	**97**
6.1	INTRODUCTION	97
6.2	DAMAGE STUDIES	98
6.2.1	Sharp Notch	98
6.2.2	Circular Hole	99
6.3	COMPUTATIONAL STUDIES	100
6.3.1	Sharp Notch	101
6.3.2	Circular Hole	102
6.4	STRENGTH STUDIES	103
6.4.1	Static	103
(a)	Tension	103
(b)	Compression	107
6.4.2	Fatigue	109
(a)	Residual Strength Tests	110
(b)	Fatigue Tests to Failure	114
6.5	NEW MATERIALS	120
6.5.1	Toughened Epoxy Matrix	120
6.5.2	Thermoplastic Matrix	123
6.5.3	Bismaleimide Matrix	124
7.	**CONCLUSIONS AND FURTHER WORK**	**127**
7.1	CONCLUSIONS	127

7.1.1	Static Strength Studies	127
(a)	Plain Specimens	127
(b)	Notched Specimens	127
(c)	Computational Studies	128
7.1.2	Fatigue Studies	129
(a)	Damage Evaluation	129
(b)	Residual Strength Tests	130
7.2	FURTHER WORK	131
	REFERENCES	**132**
	APPENDIX I - Moisture Absorption Prediction Models	**140**
	APPENDIX II - Evaluation of the Elastic Constants	**145**
	FIGURES	**148**
	Chapter 3	148
	Chapter 4	158
	Chapter 5	229
	Chapter 6	255
	TABLES	**269**

1. INTRODUCTION

Fibre reinforced materials consist of high strength and stiffness fibres (eg; carbon, boron, glass or aramid) embedded in a matrix of lower strength and stiffness and usually higher ductility (eg; plastic or metal). The continuous fibre reinforced plastic materials are often referred to as advanced composites.

Today one of the most common reinforcing fibres is carbon, having a typical stiffness between 220 and 400 GPa and failure strain of 1 to 1.8%. These fibres are usually used as reinforcement in plastic matrices such as epoxy, bismaleimide, polyimide, or a thermoplastic polymer (eg; Polyether Etherketone, PEEK). An epoxy matrix material has a typical stiffness of about 5 GPa (at 0.2% strain) and a failure strain of about 4%.

The structural advantages (high strength and stiffness to weight ratios) of advanced fibre composites are well known. These materials have therefore found a potential for application in the aerospace industry where their comparatively high raw materials cost is offset by weight savings, more efficient mass component production, and perhaps by service cost reductions. However, the greatest advantage that composite materials possess is the flexibility that they offer in their design to enhance or suppress observed or anticipated structural behaviour. If engineers can eventually develop a deep understanding of the short and long term behaviour of these materials very much improved structural designs will be realised.

Owing to their anisotropy and inhomogeneity composites are very complex materials. Unlike metals, the behaviour of a single composite cannot be translated to the behaviour of another. In other words, there are no available generalised rules applicable to the behaviour of these materials, in different load and/or material configurations. Consequently as a result of conservatism and lack of fundamental understanding (and sufficient databases), engineers and manufacturers are still very cautious about the wider use of such materials. To overcome these barriers, the long term integrity of these materials must be well defined and understood. Furthermore, weaknesses, and advantages must be identified so that they may be avoided or exploited in structural designs.

A well known long term weakness that all materials possess is fatigue. This is defined as the material degradation or failure which occurs after the application of dynamic loads, which are of smaller amplitude than the material's static strength. Engineers have been familiar with such behaviour for over a century, and in homogeneous materials have associated fatigue with self-similar crack growth. Crack growth rates and damage tolerance have, therefore, become the most common design parameters for dealing with fatigue. However, the fatigue behaviour of composite materials cannot be described in an equivalent way since the complexity of the internal microstructure of these materials introduces a wide range of damage modes, which results in the absence of well defined damage states.

It has been pointed out that the long term quality of fibre reinforced plastics may be threatened by environmental exposure. Moisture in particular is thought to have an exceptionally detrimental effect on damaged material where deterioration maybe accelerated by the access to the material's internal microstructure. The damaging effects of moisture on epoxy matrices was recognised over fifteen years ago. Since then, a vast pool of knowledge has been gained through rigorous research on this subject. However, the effect of moisture on the composite's long term behaviour and residual strength are not so well understood. The coupling of environment with additional damaging factors such as fatigue or impact loading presents a further degree of complexity and uncertainty concerning the composite's long term structural integrity.

It is the ultimate objective of the present research work to study and characterise the fatigue damage mechanisms in notched carbon fibre reinforced composite laminates typical of thin aircraft structures such as wing skins. One of the most damaging forms of fatigue: tension-compression, T-C, will be assessed experimentally in its simplest form (ie sinusoidal loading at constant amplitude and frequency) for a range of quasi-uniform hygrothermal conditions.

The research programme is divided into two sections;

(a) the main programme, in which a single standard carbon/epoxy system is thoroughly examined, including a variation in stacking sequence, notch type, and level of moisture conditioning and,

(b) a secondary programme, in which the behaviour of three relatively new fibre/matrix systems is each briefly examined and compared to the standard system in (a).

The fatigue damage initiation and propagation in the various environmental conditions are identified with the aid of destructive and non-destructive techniques such as C-scan, X-ray radiography, optical and scanning electron microscopy, and deply. In addition a finite element analysis is used to obtain an estimate of the pre-damaged state of stress concentration around the notches. The damage state is correlated with the residual strength or fatigue life of the materials. Finally, an attempt is made to define an empirical screening method that would allow an appropriate material system and/or stacking sequence (from a given lay-up) to be selected, to offer the best fatigue resistance under a given environmental condition.

2. LITERATURE SURVEY

2.1 INTRODUCTION

Composite materials have, for many years now, been strong candidates for aerospace applications where weight savings are in constant demand. The uncertainty regarding long term behaviour, which may involve factors such as exposure to hostile environments, fatigue and impact or a combination of these, must be resolved if the full potential of these materials is to be realised by designers and the airworthiness authorities.

There is a wide range of environments that can affect the mechanical behaviour of fibre reinforced plastic materials, eg aviation fuel, degreasing fluids, ultra-violet (UV) and electron radiation, moisture, heat etc. The extent to which the environment affects the composite's behaviour has been the subject of research for some time. A wet and in particular a hot/wet environment has been the main concern for most of these studies, mainly because such environments are likely to be seen in many structural applications. The present review will concentrate upon the effects of hot and/or wet environments upon the mechanical behaviour of fibre reinforced plastics, FRP. Emphasis will be placed on carbon fibre reinforced epoxies.

The fatigue behaviour of composite materials is briefly reviewed under a range of loading conditions and specimen geometries, with the emphasis on carbon fibre reinforced plastics, CFRP. In particular a more detailed investigation is carried out upon the effect of moist environments upon the fatigue behaviour of CFRP.

2.2 MOISTURE ABSORPTION IN FIBRE REINFORCED COMPOSITES

During their service lifetime composite materials usually absorb moisture from their surroundings. An early review study by Wright (1) revealed that all the epoxy systems considered (10 different carbon fibres in 40 different epoxy resins) showed an affinity for water. Following his comprehensive study, in 1979, Wright concluded that, at least for the cases examined, there was no significant effect on mechanical behaviour when the materials were tested at room temperature, RT, but there were adverse effects at elevated temperatures. It is perhaps worth noting that most of the mechanical tests involved shear or flexure tests. Matrix plasticisation and softening were also reported. Other important conclusions were that, the moisture content in a composite depended upon the matrix; the rate of pick-up depended upon the temperature of exposure and not the relative humidity (RH); the maximum equilibrium level depended upon the RH and only very slightly upon the

temperature of exposure, and finally, the reduction in mechanical properties depended upon the amount of water absorbed and not the conditions under which it was absorbed.

In a later, (1983), literature review Komorowski, (2), also stated that all matrix resins used in advanced composite materials absorbed moisture. The work by Komorowski consisted of a series of reviews concerning all aspects relating to moisture absorption in composite materials in general. Only four out of the seven reviews were available to the author, (2-5), and are thus included in the present work. Although these investigations contain a lot of useful information, selected from 328 relevant papers, they do not contain many straight forward conclusions regarding the understanding of the mechanisms that relate to moisture and temperature. Instead they contain a lot of recommendations for further work. Some of Komorowski's worthwhile conclusions concerning the effect of moisture on the mechanical properties were: in general, environment had a greater effect on specimens without defects; moisture and temperature had no significant effect on the notch or defect sensitivity; fibre dominated properties were only slightly affected by moisture and temperature. On accelerating the conditioning, he stated that care should be taken, as a residual stress state may result which would not be found under normal service conditions.

Wright (1) identified some important areas in which work had to be done, some of these areas were: more studies were needed to assess the effect of moisture on properties such as compression, fracture energy and fatigue. Such studies should include elevated temperature tests. The degree of recovery on drying out should also be studied. He also suggested that the effect of moisture be studied for structures under stress. In addition, Komorowski (2-5) recommended work on temperature and humidity gradients, standard methods of testing and preconditioning, adequate material characterization and further work on generalised models for degradation prediction. These are some of the areas that the present review will attempt to identify.

2.2.1 Effect of Moisture on Epoxy Matrices

The basic transport mechanism of moisture into a polymer is provided by the kinetics of the polymer molecules, which carry the water molecules deeper into the polymer network (6). The diffusion process is usually in good agreement with Fick's law of diffusion and many investigators still assume or use this law for moisture concentration predictions, although, modified and more sophisticated models are also available allowing for varying temperature and/or moisture situations. Some

examples of the most widely used moisture prediction models can be found in appendix I.

In a given neat cast resin, water absorption may depend upon the curing process, (7). In a composite this may also depend upon the reinforcing fibre (8). Furthermore, Dews and Favre, (9), have shown that the diffusion process in a composite is more complicated than that in neat resins due to additional variable factors such as fibre/matrix interface, fibre volume fraction, and specimen geometry. These findings appear to contradict the early (1976) assumption suggested by Shen and Springer (10), that moisture absorption in CFRP depends only on the matrix.

Wright (1), reported that, in cast resins, the desorption rate did not differ from the rate of absorption by more than about 20% in either direction. In a composite, however, the rate of desorption was generally higher than that of absorption. In general, reports on the diffusion rates in composites appear to be in conflict. For example, a recent work by Jackson and Weitsman (11), indicated that absorption and desorption rates, in AS4/3502 carbon/epoxy, were approximately equal, whereas, Hertz (12) found that, for a GY-70/X-3 carbon/epoxy, desorption was slower than absorption and highly dependent on the moisture distribution.

In general the diffusion rates in composites appear to be less than those in neat resins (9,13). To the contrary, Piggot (8) reported that in pultruded composites (with a relatively high void content), the main conductivity path for water was provided by the voids in the composite and this was greater than that in neat resin. The conductivity path of the interface appeared to be less effective. Carter and Kibler (14) were the first to appreciate the sensitivity of diffusion upon factors such as resin composition, cure quality, void content, and interfacial bond. They even suggested that moisture diffusion could be used as a screening test for these parameters. Harper and co-workers (15), have studied the effects of voids upon the hygral and mechanical properties of CFRP in some detail. They reported that both the diffusion rate and the moisture equilibrium level depended on void content. Furthermore, they found that low void content composites in general had exhibited a Fickian diffusion, whereas, higher void content material (of the same volume fraction) showed an anomalous behaviour.

The effect of drying out is of particular interest to engineers because it is a process that real structures will undergo in a weather environment during their service lifetime. It is generally agreed that the effect of drying out results, in nearly all cases, in an increase of moisture equilibrium level on reconditioning (1,11), although, there is evidence to suggest (11) that this depends on the degree of drying

out. Jackson and Weitsman (11) have carried out an excellent experimental work in which they studied the effects of cyclic variations in relative humidity. They have shown that more matrix damage was caused by such variations when compared to cases of constant humidity. Moreover, the extent of damage depended upon the past history of exposure to cycling environments, rather than on the current level of moisture content. Apicella and Nicolais (16), reported absorption data for neat epoxy resin which also showed a dependence on past environmental history. Samples absorbed more moisture and displayed lower diffusion coefficients when dried and exposed for a second time. No significant change in either value was observed for additional cycling.

The effect of drying out should be of particular importance to researchers who are interested in the actual value of the equilibrium level. Drying specimens out before conditioning may be bad practice. This may result in higher than usual moisture levels. Curtis and Moore (17), have identified this effect and suggested that traveller specimens (specimens that are used for weight monitoring) should be dried after equilibrium is reached. In this way the effects of thermal cycling are eliminated and a true figure for the moisture level may be obtained.

The bond between fibre and matrix appears to be part chemical and part mechanical. A mechanical bond would be expected to be weakened by moisture and to reform on drying out. However, once chemical bonds are ruptured, such damage may be classified as irreversible, (18). The process whereby water molecules appear to become permanently bound to resin may also be irreversible (19, 20). The recovery of the mechanical properties has been studied by many researchers and this will be discussed below in 2.2.4.

Murayama (21), Studied the effects of moisture and temperature upon the dynamic behaviour of polymers. He concluded that neat resin behaviour could not be translated directly into composite behaviour. Putter et al (22), showed that for a carbon/epoxy composite, frequency effects were quite small in all environmental cases (wet or dry, in a temperature range from RT-93°C). Frequency dependence was greater for matrix dominated lay-ups: furthermore, damping increased with moisture saturation. Museux and co-workers (23), reported that the dynamic response of the ±45° laminates was very sensitive to environmental conditions which is consistent with a softening of the matrix with moisture.

The effect of stress upon moisture absorption has also been the subject for investigation (24-31). Gillat and Broutman (24) found that an applied tensile stress could increase both the rate of diffusion and the maximum equilibrium value. Similar findings have been reported by Neumann and Marom (30), who also found

that the stress effect was related to the matrix loading. In addition they reported that the effect of increasing the fibre volume fraction was to increase the stress effect. Curtis and Moore (17), have determined that combined load cycling and environmental exposure, led to increased rates of moisture absorption and equilibrium levels. Collings and Stone (25), have found that the rate of moisture uptake in all (0°/90°) laminates was greater than that in the unidirectional laminates and this was attributed to the effect of interlaminar residual stresses. Blikstad et al, (31) have also studied the effect of interlaminar residual stresses for several systems and humidity exposures. They found a small but consistent dependence of moisture content on lamination angle. Symmetric ±45° laminates showed the lowest moisture content and the ±5° laminates showed the largest content. This effect was attributed to the residual stress state of each laminate. Although the ±45° laminates exhibit the largest residual stress (in the dry state) they do not end up with the largest moisture content. A stress reversal has been suggested, in which case a compressive interlaminar stress reduced the rate of absorption and the maximum equilibrium level. Furthermore, a higher moisture absorption rate was obtained for the T300/914 system when the material was not post cured: ie, when the dry state interlaminar stresses had not been reduced. It may be concluded that tensile matrix loading results in both moisture level and diffusion rate increases. In contrast, compressive matrix loading has an opposite effect.

Since Wright's early conclusions on the effect of moisture on epoxy matrices, no further important revelations have been reported in the published literature. Matrix plasticisation (and hence Tg reduction) and swelling are the most important effects of moisture upon epoxy matrices.

Komorowski, (3), stated that the glass transition temperature, Tg, is an important parameter, since it constitutes the upper temperature limit for structural application of composite materials. In general, all researchers agree that there is a reduction in Tg with increasing moisture content. In particular, Wright has suggested a rough rule of thumb which proposes that, for each 1% of water pick-up (by the epoxy matrix) there is a drop in Tg of about 20°C. He also reported that experimental results were usually in good agreement with the equation by Kelley and Bueche (32) based on the free volume theory. On the other hand, Komorowski, (3), concluded that the best method available for predicting Tg was the entropy model proposed by Carter and Kibler, (33). Barton and Greenfield (34), have used the dynamic mechanical method to study the effects of moisture on Tg: they reported 57°C reduction in Tg when the moisture content was 4.3%. This value does not seem to follow Wright's rule of thumb. However, they have stated that the definition of Tg is rather arbitrary. They also reported that values of measured Tg depended not only upon the geometry of specimens used but also on the degree of cure. Marchetti and co-

workers (35), also reported Tg reductions with water content, but they stated that this phenomenon could not be correlated only to the percentage of water absorbed. They suggested that the phenomenon could be beyond water absorption alone, but also due to the nature of the reinforcing fibres, which may accelerate hydrolytic processes of the matrix, particularly when the composite is subjected to tensile stresses (36,37). Marchetti et al (35), have also stated that when moisture conditioning occurs at RT, the dry Tg value is completely recoverable on drying, but not so in the case of thermal spiking. A reasonable conclusion, then, is that Tg depends upon the damage state of the matrix as well.

Swelling or moisture expansion of FRP is a problem of dimensional stability very similar to that of thermal expansion. Wright (1) has addressed this problem and found a linear relationship between volume expansion and water up-take, at least up to about 1.5% water content. Furthermore, he stated that for the same equilibrium level the expansion may differ by a factor of two for different systems. Adamson (38) has investigated this problem in detail and concluded that swelling is a three stage process that can be best explained with the free volume concept, which accounts for the fact that the network structure of epoxy resins is not homogeneous. During the first stage water diffuses into a free volume and swelling is caused by those water molecules that become bound to the epoxy network. This stage is identified by the straight line region in a moisture versus square root of time graph. In the second stage the material volume change is equal to the volume of absorbed water. Finally the third stage consists of water occupying the volume contained by the less dense microgel resin particles (micelles). According to Adamson (38), the free volume depends on the temperature, being larger at lower temperatures.

The most widely understood effect of swelling is the reduction of the thermally induced residual stresses. This is usually a beneficial effect, although, in certain cases, fibre/matrix debonding may occur, caused by constrained swelling of the resin as it absorbs and desorbs moisture, (11). Matrix swelling can be particularly important whenever the shape of a non-symmetric laminated composite is a significant design consideration. This problem has been studied by Harper (39), who stated that specific lay-up, average moisture content and distribution, are all very important parameters in determining the shape of anti-symmetric cross-ply laminates.

Matrix expansion by moisture swelling seems to be very similar to thermal expansion. In fact Komorowski (3), concluded that swelling can be predicted in the same way as the thermal expansion. Henriksen et al, (40), have studied the effects of thermal cycling upon the thermal expansion of carbon/epoxy composites. They observed an increase in the coefficient of thermal expansion, CTE, after 10 thermal

cycles. They attributed this effect to fibre/matrix debonding. After 30 cycles, however, a decrease in CTE was observed due to matrix delamination. Therefore, matrix damage may be expected to have similar effects on swelling.

2.2.2 Effect of Temperature on Moisture Pick-up Rate

Temperature increases the molecular mobility of the matrix thus increasing the transport mechanism of water into the matrix. This is the most important, most commonly known, effect of temperature-of-exposure in a wet environment and the result is to increase the diffusion coefficient. Researchers have exploited this phenomenon and used it to accelerate specimen conditioning. Edge (18), has studied the implications of laboratory accelerated conditioning. He concluded that 95°C and 95% RH was the maximum acceptable limit. He dismissed conditioning by water immersion and in particular boiling water, as unrealistic of real service conditions. He concluded that the effects of outdoor weather conditioning were less than those observed in a mild laboratory condition (RT/65% RH).

Wright's work (1), revealed that large moisture diffusion rates may occur above 50-60°C. In fact, Collings and Stone (25), suggested that in many commonly used resins, the diffusion process becomes non-Fickian above about 60°C. Furthermore, Hiel and Adamson (6), reported that the molecular mobility increases significantly above 100°C due to the disruption of intermolecular hydrogen bonds.

It is generally accepted (1,8 and 41), that temperature does not have any significant effect on the moisture equilibrium level. Dewas and Favre (9), however, have found significant increases in the moisture equilibrium level of neat resins, depending upon the material used. For example, Narmco 5208 epoxy resin exhibited an equilibrium level, M=4.98%, by weight, and a diffusion coefficient, $D=1.01 \times 10^5$ cm^2/h at 40°C, compared to M=6.30% and $D=6.29 \times 10^5$ cm^2/h at 90°C, whereas, Ciba 914 epoxy resin, at 40°C, showed an M=5.21% and a $D=1.55 \times 10^5$ cm^2/h, compared to M=9.40% and $D=3.18 \times 10^5$ cm^2/h. Loosely translated, this means that, for the temperature difference of 50°C, both the diffusion coefficient and the equilibrium level, in 914 epoxy, have shown an increase close to 100%, while 5208 showed a marked increase in the diffusion rate alone. Loos and Springer (41), have studied the effect of temperature and found no changes in the equilibrium level. However, when specimens were immersed in water this was no longer true, in fact the moisture level depended on both temperature and time of immersion. Three different systems were considered in this study; T300/1034, AS/3501-5 and T300/5208.

Adamson, (38) has shown experimentally that the equilibrium level in a composite sample, stored at 75°C, had been further increased when the temperature was dropped while the RH was kept at the same level. He called this effect the reversed thermal effect. This increase in water capacity was attributed to an increase in the free volume.

Thermal spiking is another real service life situation that troubles aeronautical engineers. This can arise from several flight situations during an aircraft's service life. Such flight situations are; acceleration through to supersonic flight, and ground-reflection of efflux during low hovering of a VTOL aircraft. A less likely situation can arise from hot gases from missile efflux. Air friction in supersonic flight is the most common spike and temperature in such occasions can reach 135°C (26). The review by Wright (1) has shown that thermal spiking resulted in both a higher equilibrium level and rate of diffusion possibly due to matrix microcracking. Since then, thermal spiking has become a common subject for research in the area of moisture absorption, (25,26,35,42 and 43).

Collings and co-workers (42), have shown that in XAS/914C carbon/epoxy system, moisture equilibrium level was affected only when subjected to thermal spikes of 127°C and over. Furthermore, they showed that the increase in equilibrium level was due to microcracks formed during spiking. This had also been observed previously by Collings and Stone (25), who reported moisture levels doubling as a result. Collings et al, (42), have carried out thermal spiking in wet specimens and observed effects on both diffusion rates and moisture content for moisture equilibrium levels of 1.13% and over. In addition, they found that moisture kinetics in specimens with moisture gradient have been modified: an increase in the diffusion rate was observed. Pritchard and Stansfield (26), suggested that cooling from maximum temperatures may be responsible for damage during spiking. Morgan et al (43), attributed the effect of thermal spiking on free volume increases that involve configurational changes within the epoxy network. These changes are frozen in during the rapid cooling following a thermal spike.

2.2.3 Effect of Relative Humidity on Equilibrium Level

The effect of relative humidity is in general the exact opposite to that of temperature. RH has a marked effect on the equilibrium level and very little effect upon the rate of pick-up. The equilibrium level reaches a maximum, the saturation level, at 100% RH. Loos and Springer (41), have found that materials exposed to humid air in general obeyed Henry's law;

$$M=\alpha(RH)^{\beta}$$

where M is the percentage weight gain and α, β are material constants; α being expressed as a percentage. They stated that the exact values of the constants may vary due to differences in the curing processes. Piggott (8), mentioned values of α for epoxies in the range 5-10% and values for β in the range 1-3. Furthermore, he stated that α depends only very slightly upon temperature. In general the problem of water capacity is more complex than Henry's law would suggest. Void content, curing process, fibre volume fraction, fibre/matrix interface, reinforcing fibre, and past history of exposure are parameters that can contribute to discrepancies, (7,8,9,11 and 15).

2.2.4 Effect of Moisture Pick-up Upon the Mechanical Properties

In his review Wright (1), stated that the bulk of information suggested that there was no significant effect of absorbed water upon RT properties. However, he added that there were many divergences which called for caution in making such an assumption.

In recent years many researchers have concentrated their efforts on examining the effects of environment upon properties such as shear strength, fracture toughness, compression, notch sensitivity, etc. Such effects are usually attributed to the degradation of the matrix and/or fibre/matrix interfacial bond. It is generally accepted that the carbon fibres themselves do not degrade by exposure to moisture, and neither do they absorb any significant amount of water. Piggott (8), has presented data on free fibre moisture exposure at 23°C and 98% RH. Carbon fibres have absorbed 0.02% water by weight, as compared to 0.12% in glass fibres. Results from Dickson et al, (44), show that Kevlar fibres may absorb as much or even more water than the matrix itself (Code 69, epoxy). In general, organic fibres like kevlar, are expected to absorb much more moisture than inorganic fibres, like carbon and glass.

In some cases moisture-induced matrix cracking or void content may expose the fibres to air resulting in either oxidation of the fibres or degradation of the interface (45). Unlike carbon fibre, glass fibre may be attacked by moisture directly. White and Phillips (46), have shown such attacks to occur in a seawater environment, at a temperature of 60°C and a stress equal to 25% UTUL, (a quantity defined in British Standard 4994, 1973).

There is a large amount of published work on the effect of moisture upon the mechanical behaviour of composite materials and it would be an impossible task to consider all of the subjects covered. Therefore, only the very relevant (to the

present research) subjects such as static tension or compression, shear strength, and fatigue will be considered. The subject of fatigue, being the most relevant, will be referred to in a separate section below, 2.3.3.

(a) Shear Strength

Shear strength is a matrix related property and as such it is usually the first to be assessed in most environmental research programmes. In general it is suggested that the shear strength is reduced by moisture and/or temperature. Edge (18), has presented interlaminar shear strength, ILSS, data for CFRP, HTS/914C and AS/3501/5A, at RT and 130°C for a range of moisture contents. It is made clear that the RT ILSS values for both materials depended upon the moisture content but also upon the method of conditioning: (ie, boiling water immersion, 50°C/95% RH, or 21°C 65% RH). Apart from the boiling water conditioned specimens, ILSS at RT in general showed a relatively small decrease with moisture content. The effect of the method of conditioning disappeared when tests were performed at 130°C, in which case a linear decrease in ILSS strength with moisture content was observed. A reasonable conclusion may be drawn from this behaviour, that at RT (or low temperatures), ILSS is fibre/matrix-interface dominated, whereas at 130°C it becomes a matrix dominated parameter. Joshi (47), has also studied the effect of moisture upon the shear properties of CFRP. In a similar data presentation (to that of Edge) she confirmed a decrease in ILSS with moisture content and the difference between methods of conditioning. Furthermore, she studied the effect of fibre treatment and showed an increase in ILSS with fibre treatment, which also depended upon the method of conditioning: boiling water conditioning yielded the lowest ILSS value. Porter (48), presented ILSS results for different CFRP lay-ups and moisture levels. These results indicated a small decrease in ILSS at RT depending upon lay-up. In addition, he reported decreases in ILSS with temperature, and cure pressure. Dickson et al, (44) presented shear strength versus moisture content results, obtained from 4-point bending tests on carbon/epoxy, at RT. These indicate only slight reductions in ILSS strength, with moisture content. ILSS degradation with moisture has also been reported by Collings et al, (42). Such degradation increased with test temperature or thermal spiking. Furthermore, Collings and Stone (25), have stated that when conditioning at 60°C/96% RH, both the equilibrium moisture content itself and the time of exposure at this moisture content had reduced the ILSS. Bishop (49), has studied the effect of moisture upon the notch sensitivity of CFRP. Contrary to most reported results, she found no evidence of shear strength reduction on absorption of moisture.

The disagreement may be attributed to the interpretation of flexure tests in which case the definition of strength may depend upon the failure mode. For example,

a dry specimen of certain size may fail in shear following a 3 or 4-point bend test, however, an identical wet specimen may fail in a mixed mode. The translation of failure load into ILSS in the latter case may not be appropriate: flexure strength in such situation may be a more appropriate parameter (44).

Some data on the recovery of ILSS on drying has been presented by Edge (18). At least for boiling water conditioning, recovery is not complete: moreover, it depends upon the material system. For example 914C showed a steady increase in strength recovery with moisture content, whereas, AS/3501/5A, in general showed a decrease in recovery with moisture content. Ellis and Mason (50), have shown that, following in-service flight conditioning, CFRP test pieces exhibited a negligible degradation in ILSS at RT. A significant decrease in ILSS, however, was observed at 120°C. After about 9,000 flight hours, the material showed a 24.5% reduction in ILSS when tested at 120°C: in this case the moisture content was 1.02%. After 10,500 service hours the moisture content had fallen to 0.44%, despite that, the ILSS showed no signs of recovery. A small but irreversible loss in ILSS was also observed when the material was tested at RT.

A decrease in ±45° tensile strength with moisture level at 130°C was reported by Pritchard and Stansfield (26). A decrease of the shear modulus, at 130°C, with moisture content was also observed. Similar reductions in shear stiffness with moisture were reported by Museux et al (23). A steady reduction of wet ±45° tensile strength with increasing temperature was also observed by Joshi (47). Garg (51), amongst other lay-ups, has also presented tensile strength results for ±45°, wet and dry carbon/epoxy (T300/934), laminates. Results for dry specimens show a decrease in strength with increasing temperature in the range between -48°C to 93°C. An even greater decrease is shown for wet specimens from 25°C to 93°C.

The effect of environment upon the static tensile or compressive strengths has been widely studied (see 18,42,48,50,51,52 and 53). It is particularly difficult to arrive at any solid conclusions since results may be depend upon the material used, lay up, and method of testing (especially in compression). Added stress raisers (eg; cut-outs) usually present an extra degree of complexity.

(b) Compressive Strength

The bulk of information suggests that the worst affected mechanical property is compression. Grimes, (52), presented compression data for AS/3501-6, carbon/epoxy, for a range of lay-ups. Results showed a consistent degradation of plain compressive strength with moisture (1.1% by weight) and/or temperature

(103°C). The worst affected case appeared to be that of a 0° lay-up when tested hot/wet. In this case an 81% reduction (from RT dry condition) in strength was observed, while the modulus and Poisson's ratio remained unaffected. The hot/wet condition was also responsible for a 54% reduction in strength in the 90° lay-up. In this case some degradation in the elastic modulus was also observed. In contrast, the ±45° laminates were affected by temperature rather than moisture. 61% reduction in both hot/wet and hot cases were reported: both modulus and Poisson's ratio were affected by the hot/wet condition. Finally, results on a mixed type lay-up, (0°/90°/45°), showed worse degradation by temperature rather than moisture. A 72% reduction was observed in the hot/wet environment. Furthermore, he reported some differences in results for different test methods. Curtis and Moore (17) have also presented compression data for hot and/or wet environments. Two material systems were considered: XAS/914C and T300/N5208, in a symmetric (0°/90°/45°) type stacking sequence. Both materials showed reductions in strength when tested hot/wet. The reduction in strength appeared to be dependent upon the moisture content (moisture gradient). The 914C system showed a 28% reduction (from RT dry) when tested at 100°C and containing 75% (of the equilibrium level) moisture. Some recovery in strength (8%) was obtained when the moisture content reached the equilibrium level (ie; without a moisture gradient). Similarly, a maximum 22% degradation in strength was observed in 5208 with a moisture content of 50%, while minimum degradation occurred at 75% moisture content. Edge (18) has presented compression results for CFRP following natural weather conditioning for 18 months. It appears that weathering had no significant effect on the strength, even though in such case a moisture gradient is bound to be present.

Notched Compressive strength in a hot/wet condition has currently become one of the key design parameters so far as military aircraft are concerned, (54). Recent studies (42,53 and 54) on the environmental degradation of notched CFRP in compression have been carried out. The first two reports contain work on 914C laminates with centrally located holes. In both cases the lay-ups used consisted of 50% 0° and 50% 45° plies.

Potter and Purslow (53) have studied the effects of preloading upon the compressive strength. They found no significant effect when specimens were preloaded in compression. So far as the notched strengths are concerned, they reported that the effect of laminates with blocked plies was to increase the strength (in RT/dry condition) compared to laminates with well distributed plies. However, when tests were performed in a hot(120°C)/wet(1.0%) condition the effect of lay-up had disappeared. Fractographic analysis revealed that initial failure took the form of protrusion of the discontinuous (due to the hole) 0° fibres, followed by protrusion of the 45° (discontinuous) fibres. Final failure occurred as a result of out-of-plane

buckling of the 0° plies, starting from the outer plies. They suggested that degradation of the fibre/matrix interface is to be blamed for the 0° fibre buckling. In contrast 0° fibre buckling in the dry case was found to be related to 45° ply damage. Furthermore, they suggested that the 0° fibre buckling load may be be considerably reduced by the presence of shear stresses. Associated with the fibre microbuckling situation, Curtis (54) has identified an important consideration, that is the fibre diameter, which is becoming smaller with the arrival of stronger (defect free) fibres. Clearly, even though the tensile strength may be greatly improved, the compressive strength will suffer as a result, especially in the hot/wet condition where matrix support and interface are weakened.

Collings et al (42), have studied the effect of thermal spiking upon the notched compressive strength. They reported that the strength, at RT, remained relatively unaffected by moisture and/or spiking: the maximum decrease in strength appears to be around 11% when the moisture level had been increased to 1.8% due to spiking. A 48% degradation in strength was observed in a similar condition when specimens were tested at 120°C. Similar degradations in strength were also reported by Curtis (54). Furthermore, Collings and co-workers (42) have suggested, on the basis of Potter and Purslow's findings, that when moisture gradients are present it is probable that the notched compressive strength is largely governed by the moisture content at the free edge.

(c) Tensile Strength

So far as the tensile strength is concerned, there is a general agreement of a lesser effect of moisture as compared to the compressive case. In many cases there are reports of increases in RT strength depending upon the material system, lay-up, and the specimen geometry.

Garg (51), has presented plain tensile strength data for CFRP specimens for various environments and lay-ups. He reported a strength increase in dry (0°/90°) laminates with temperature in the range between -50°C to 93°C. In contrast wet specimens (1.82% moisture) showed a steady decrease in tensile strength with increasing temperature. However, at RT the wet laminates appeared to be stronger than the dry ones and a crossover in strengths appeared to have occurred at about 45°C. Similar results were obtained for a (0°/45°/90°) type lay-up, however, in this case the RT wet strength was lower than the dry equivalent. Curtis and Moore (17), have presented data for a (0°/45°/90°) type lay-up for two material systems, 914C and T300/N5208. Although in general the 914C system yielded a greater strength than the 5208, it appeared to have suffered a greater reduction in

tensile strength when tested wet at 100°C: a maximum of 16% reduction in strength was observed as compared to 6% in the 5208 system.

Porter (48), has investigated the effect of moisture and temperature on the damage development and fracture response of CFRP. He considered both notched and unnotched specimens from two lay-ups, (0°/45°/90°) and (0°/90°) symmetric laminates: preloading prior to moisture conditioning was also investigated. He concluded that the effect of preloading, moisture and temperature on the notched tensile behaviour were minimal. In contrast, unnotched specimens suffered greater losses in tensile strength. Bishop (49), has investigated the effect of moisture upon the notch sensitivity of (0°/45°) CFRP laminates. She concluded that the tensile notch sensitivity depends on the ply stacking sequence and shear strength. These relate to the ability of the material to split or delaminate and thus are the most important factors as blunting of the notch may result.

2.2.5 Effect of Moisture on Other Matrices

Epoxy matrices were the first to be used in the production of advanced application composite materials and in general exhibit a relatively low hot/wet operating limit, about 130°C. The need to extend the operating temperature of FRP has led to the commercial development of bismaleimide matrices.

(a) Bismaleimide

A review by Scola (55), shows that, like epoxies, bismaleimide resins also absorb water which results in a reduction of Tg and interlaminar shear strength. Currently the Tg of bismaleimides in the dry state varies between 200°C and 400°C which results in a maximum operating temperature limit in excess of 200°C. A major disadvantage of this type of matrix over the epoxies is their brittle nature and low strain to failure. This has led to the development of toughened systems like Narmco 5245C, which is a blend of epoxy and bismaleimide and is referred to as a bismaleimide-modified-epoxy. Beland et al (56), have shown that 5245C can undergo significant plastisisation under combined temperature and moisture and that the material did not seem to be tougher than a standard epoxy system. Furthermore, the diffusivity of this material appeared to be much higher compared to the standard epoxy. High desorption rates for bismaleimides were reported by McKague et al (57). They found that the RT dry properties of a V378A carbon/polyimide (a special case of bismaleimide with highly cross-linked structure) were similar to that of standard epoxies. However, at higher temperature (177°C) the polyimide system maintained a larger percentage of the matrix-dominated properties. The overall hot/wet behaviour of the polyimide system was also superior. In a recent study of the

M751 bismaleimide Barrie et al (58), showed that, in common with most epoxies, the moisture capacity is independent of the temperature of exposure and that this capacity is increased following a drying out and a further exposure to moisture.

(b) Polyether Etherketone

Other matrices of interest are the thermoplastic resins: in theory at least thermoplastic-based composite systems have potential for more efficient structural component processing, compared to thermoset systems. In contrast to bismaleimides these matrices have a very low Tg; lower than the epoxies, and until very recently these could not be considered for advanced aircraft designs. In 1981 a range of polyether etherketone (PEEK) resins were introduced onto the market by ICI with a Tg in the excess of 140°C (59). PEEK is a crystalline polymer with good environmental resistance as other aromatic thermoplastic polymers. Early work on PEEK composites (APC-1) has shown that the material absorbs very little water, has good resistance to hydraulic fluid and paint strippers (even when under stress), and can retain most of its mechanical properties up to about 100°C when wet (59,60). In a more recent study on a semi-crystalline thermoplastic matrix composite, Curtis (54) found no difference in the tensile strength of wet and dry (±45) laminates when tested at 120°C, although some loss in strength compared to the RT dry case was observed. Furthermore, he concluded that future effort on this thermoplastic based material should concentrate on the fatigue behaviour.

There are many other matrices both plastic and metallic that can be affected by moisture but it would not be possible to even briefly mention such effects in this particular work since more relevant subjects are still to be addressed.

2.3 FATIGUE OF COMPOSITE MATERIALS

The phenomenon of fatigue is associated with the failure of a structural component subjected to fluctuating loads below the ultimate strength. For homogeneous isotropic materials fatigue is correlated to the initiation and self-similar propagation of a single crack, and crack growth rates and damage tolerance have become the most common design approach for dealing with such behaviour.

The fatigue response of composite materials cannot be described in a simple way, since the complexity of their internal microstructure introduces a wide range of fatigue damage modes. Such damage usually consists of various combinations of matrix cracking, fibre/matrix debonding, delamination, void growth, and local fibre fracture. Furthermore, the mechanism, character, and distribution of damage depend upon the material system, stacking sequence of plies, fabrication techniques,

geometry of the component, environmental exposure, stress state, and loading history.

There is a very large amount of published work on the fatigue of composite materials and a state-of-the-art review can be a very difficult task. The present section will therefore be a short synopsis on the fatigue of composite materials in general, but with special emphasis placed on fibre reinforced plastics and in particular CFRP. An attempt will be made to briefly classify the different cases of fatigue and identify the way fatigue damage develops in each case. Most of the information is gathered from published literature surveys from 1973 to 1986, (61-71).

It is apparent from the literature that, since the early years of fatigue research, the areas of interest have been changing according to the needs of the designers, the arrival of new material, the advent of new test methods, and the level of understanding. For example up to 1973 most of the work was concentrated on glass composites and mainly those reinforced with discontinuous fibres. Work on continuous fibre reinforcement was mainly carried out on unidirectionally reinforced laminates. The loading was primarily in tension, (61). In 1977 Harris (62), pointed out the well established, by then, characteristic mode of failure for composites: fibre microbuckling under compressive loading. The weakness of composites in torsion and environmental exposure were also identified. In their 1978 review, Stinchcomb and Reifsnider (63), recognized the need for understanding of the complex fatigue damage mechanisms, rather than the generation of vast amounts of fatigue data. By the early 1980's most of the research work was carried out on carbon/epoxy systems (5), and today a lot of attention is placed on higher performance plastics like toughened epoxies, polyimides, and thermoplastics reinforced with high performance carbon fibres (71).

For convenience in the description and classification of fatigue behaviour, the subject will be divided into two natural categories: the behaviour of unnotched and notched composite materials.

2.3.1 Unnotched Behaviour

(a) Unidirectional Composites

Unidirectional composites represent the simplest form of continuous fibre reinforced materials. Even though the practical application of such composites is limited, because of their poor properties transverse to the fibres, research is still carried out even today. The main objective of such research is the understanding of

the fatigue process in this relatively simple configuration. The hope of translating data from this simple form of a composite to the more complex (multidirectional) must also be a driving force for such research.

In general, the fatigue behaviour of unidirectional composites involves matrix degradation rather than fibre failures except in situations involving very high loads (65). It is agreed that fatigue damage in unidirectional composites occurs in the matrix in the form of fibre/matrix debonding and that the overall behaviour depends upon the relative strain-to-failure of the fibres and the matrix. Other factors such as reinforcement type, fibre/matrix bond, and fibre diameter are also important as they can contribute to fibre/matrix debonding, or fibre failure in the case of fatigue sensitive fibres like aramid (71). The fatigue behaviour of unidirectional composites suffers when the direction of loading is not parallel to the fibre direction. At large deviations from the loading direction, fibres carry less load and, as in torsion, the weakest parts of the composite (matrix and the interface) are loaded directly by shear forces, with the consequence of poor fatigue performance.

Most of the work to-date on the fatigue of unidirectional composites has been carried out in tension, and therefore less is known about the compressive behaviour of these materials. Even so, in general, it is agreed that the additional mode of failure, fibre microbuckling, will result in poorer performance especially when the integrity of the matrix as the supporting element is threatened. Some discrepancies in such case have also been reported due to the test method (64).

(b) Multidirectional Composites

Multidirectional symmetric laminates represent the most practical form of composites and compared with unidirectional composites exhibit a reduced degree of anisotropy. However, there are additional factors that contribute to the complexity of these materials depending upon lamination and material geometry. The most important factors influencing fatigue are free-edge stresses, coupling effects between plies within a laminate and thermal residual stresses (or curing stresses). The latter are a result of the thermal anisotropy of composite materials, and in some cases these stresses may be large enough to initiate matrix cracks in weaker plies which can propagate under cyclic loading. All of these effects are a direct result of lamination (65). Coupling or constraint between layers is responsible for the through-thickness distribution of the in-plane load, and edge stresses are responsible for the generation of out-of-plane stresses and therefore edge delamination. According to Reifsnider (65), the effect of coupling is particularly important in bending, shear, and compressive behaviour. Even so, coupling effects on fatigue response have received very little attention in the literature. The

effectiveness, of the edge stresses has been demonstrated by Lucas and Sainsbury-Carter (72), via the testing of ±45° boron/epoxy tubes and flat specimens. The tube specimens gave a better fatigue performance. Another demonstration has been reported by Schutz (69), in which, compression tests were performed on flat CFRP specimens with the aid of anti-buckling guides. Fully supported specimens showed an improved fatigue performance compared to partly supported ones (with unsupported free edges).

In general, typical laminated composites have a large proportion of the fibres arranged in the principal loading direction (0°), a smaller number at ±45° for torsional rigidity and perhaps a smaller number of fibres at 90° to support any transverse loads. Fatigue damage in these composites usually occurs at the free edges in the form of delamination. In addition, transverse matrix damage appears in the off-axis plies usually very early on (71). On some occasions, transverse cracking induced shear stresses are thought to interact with the edge stresses thus promoting more delamination (73). Extensive delamination may lead to either decoupling (65, 66), or ply buckling in the presence of compressive loading (69), thus, tension-compression fatigue is the most damaging form of uniaxial loading (69, 71). In any case the effect of matrix cracking and/or fibre fracture is to reduce the residual strength and stiffness (69).

The effect of reducing the number of 0° plies in a laminated composite is to increase the rate of fatigue deterioration as compared with the unidirectional (100% 0° plies) case (71). It has been suggested by Harris (62), in 1977, that any matrix and/or fibre/matrix interface toughening should improve fatigue resistance since these are the weakest parts in a composite. Today there are many composites that meet these requirements, however, the recent review by Curtis and Dorey (71) suggests that the fatigue performance of such improved composites, relative to their static strength, has not been as good as one would expect. They have attributed this behaviour to possible new failure processes that trigger excessive fibre/matrix debonding. This can only reinforce one's view on how complex the failure mechanisms in these materials are and why generalised statements about their behaviour are not valid.

Compressive microbuckling is thought to be a characteristic mode of failure in fibre reinforced materials. Harris (66) believes that local matrix shear failures are responsible for initiating such damage, consequently, further fatigue damage may occur as a result. It follows, therefore, that composites are prone to premature failure in the presence of high interlaminar shear stresses. An important point made by Harris (66) is the detrimental effect of fully reversed shear loading (reversed bending) as compared to "half" shear loading.

2.3.2 Notched behaviour

All practical composites are bound to have some defects arising from manufacturing, or other stress concentrators as a result of a structural detail. Impact induced perforation or damage during service is also common. The fatigue response of notched composites should therefore be an area of particular importance. However, the 1978 review by Stinchcomb and Reifsnider (63) revealed that this was an area of special ignorance.

(a) Unidirectional Composites

Like the unnotched case, damage in notched unidirectional composites (under moderate or low fatigue amplitudes) is governed by the direction of the fibres and not the direction of the applied load. In polymeric matrix composites fatigue damage consists primarily of shear failure initiating at the notch tips and running along the fibre direction. Beaumont and Harris (74), have shown that centre notched 0° unidirectional CFRP specimens under tensile fatigue loading developed shear failure initiating at the notch tips at all loads below 80% of the static strength. At higher loads fibre failure resulted in a sudden and rapid propagation of the notch. Moreover, edge-notched specimens developed shear failure at all loads.

(b) Multidirectional Composites

So far as notched composites are concerned, multidirectional material has received more attention as compared to unidirectional due to the wider applicability in structural designs. It is generally agreed that notched composites are less sensitive to fatigue than they are to static loading (64,71). This behaviour is attributed to the neutralisation of the stress raisers, mainly by fibre splitting.* Apparent increases in strength following fatigue have been reported by many researchers (63, 71). The beneficial effect of fatigue damage is usually referred to as "wear in". According to Stinchcomb and Reifsnider (63), metal matrix composites have a lesser tendency for splitting and therefore "wear in" is less common (63, 69). This effect has been demonstrated by Stinchcomb et al (75): in tests on symmetric boron/epoxy and aluminium/epoxy (0°/±45°) type laminates with a central hole they have shown that damage in the polymer matrix composite developed predominantly in the longitudinal direction: in contrast the metal matrix composite developed more transverse damage. This is an important effect showing the role of the matrix and/or the interface in controlling the development of damage. As a direct result of "wear in", fractures away from the holes have been observed (66).

---

* Defined as a shear crack within a ply along the direction of the fibres.

Failure mechanisms in notched composites have been found to vary with fibre diameter as well as matrix materials (69). The direction in which damage will extend from a notch in polymeric matrix composites seems to depend upon laminate structure (76, 77), but especially on layer constraints (63, 69). According to Reifsnider (65), suppression of longitudinal damage is usually ascribed to the superior shear resistance of the ±45° plies. The importance of ply constraint in notched CFRP was very well demonstrated by Stinchcomb and co-workers (76). They concluded that the in-plane constraint is the principal contributor to notched strength and fatigue damage development. More importantly, they have shown that it is the nature, rather than the amount, of damage that controls the residual strength.

The problem of accelerating fatigue testing by load cycle frequency increase appears to have attracted considerable attention particularly in the case of notched FRP. It is argued that in the vicinity of high stress concentrations, high temperature increases (due to the viscoelastic nature of the matrix) may cause additional complications to the stress field and hence damage characteristics. Is thought that this problem is greatest in the case of non-conducting fibres like glass in which case local build-up of heat may result. Many researchers believe that 10 Hz is acceptable for most CFRP laminates, although strictly speaking an absolute value should depend on the type of composite system, lay-up, and loading.

Finally, bearing in mind the importance of the matrix and the fibre/matrix interface in controlling fatigue damage mechanisms and behaviour in general, one cannot disregard the effect of environment.

2.3.3 The Effect of Hygrothermal Environment

It appears from the literature that the fatigue of composites in general, does not present a great problem (5,71). This is thought to be a direct result of the relatively low (0.4%), maximum design strain allowables which are determined by the static hot/wet notched compressive performance of these materials (71). However, future composites with smaller diameter, higher tensile strength and strain to failure fibres may well develop a problem in fatigue, especially in the hot/wet conditions under compressive load regimes (5,71). It follows, therefore, that a thorough understanding of the fatigue processes in such conditions is urgently needed.

Pioneering work on this subject has been carried out by Beaumont and Harris (74) in 1971. Following repeated torsion fatigue tests at a fixed strain limit, on unidirectional CFRP with 40% fibre volume fraction, they concluded that the fatigue behaviour of this material was controlled by the toughness and fatigue properties of

the matrix rather than the interface. The effect of the interface and environment appeared to be important only to the local processes of crack propagation in the matrix. Sumsion and Williams (78), have carried out torsional and flexure fatigue tests on both 0° unidirectional and ±45° crossply CFRP in air and in water at RT and 74°C. Their results show that the major effect of temperature but especially of hot/wet environment in torsion, was to reduce the torsional stiffness. The crossply specimens were more fatigue and environment sensitive than the unidirectional ones. The authors attributed this fact to interface degradation. In flexure, specimens showed significant damage in both air and water when subjected to fully reversed bending and the effect of water appeared to be greater on the unidirectional material. Flexure tests on crossply laminates in various moist environments have been carried out by Dickson et al (44). Three types of fibres; carbon, glass and aramid, were used in epoxy resin code 69. They reported marginal strengthening for CFRP following treatment in boiling water. They related this effect to a beneficial effect of resin plasticisation and reductions in the thermal residual stresses. In contrast, moisture had affected the axial fatigue behaviour of CFRP especially in the matrix dominated ±45° ply sequence. An important point was made as a result of this work, that there appeared to be an optimum state of ductility for the matrix due to moisture conditioning. In this state the matrix appears to be tougher and more fatigue resistant. For the particular matrix used this condition was 65% RH. In the dry condition the matrix appeared to be too brittle and in boiling water the resin was degraded. Similar matrix strengthening effects in epoxy resins following moisture absorption have been reported by Hoa (79), and Hojo et al (80). Grimes (52) has carried out compressive fatigue tests on wet and dry CFRP laminates with four types of lay-up: (0°), (±45°), (90°) and (45°/90°/0°). He concluded that apart from the (90°) laminate the rest were virtually unaffected by moisture.

The mechanisms of fatigue delamination have been studied by Hojo et al (80). They have shown that the ductility of the wet matrix may bring about a decrease in the fatigue crack propagation rate but strictly speaking this depends on the fibre/matrix interface as well. For example a composite with weak interface will show an enhanced crack rate growth no matter what happens to the matrix itself. Since the interface is weakened and the matrix is plasticised with increasing moisture level, there must be an optimum state in a composite, as mentioned by Dickson et al (44), corresponding to the limiting strength of the interface, below which any fatigue crack will propagate in the matrix.

The effect of elevated temperature on the tensile fatigue behaviour of angleply CFRP has been investigated by Rotem and Nelson (81). Their results show a general fatigue strength deterioration with increasing temperature. In a relatively recent survey of the hygrothermal effects on the fatigue behaviour of FRP, Komorowski (5)

concluded that, in general, temperature has a greater effect upon fatigue than moisture does.

A comparison between notched (circular holes) and unnotched CFRP in a combination of hygrothermal and fatigue environments has been conducted by Ryder and Walker (82). They tested two types of lay-ups, a (0°/90°/45°) with 25% 0° plies and a (0°/45°) with 67% 0° plies. Both tension-tension and tension-compression fatigue load regimes were employed. The only observed difference in damage modes (in the different environments) was a faster accumulation of damage in hot/wet specimens compared to the RT/dry case. Consequently the life of the hot/wet specimens was decreased especially in the case of the (notched) matrix dominated lay-up. When they carried out residual strength tests they found a greater reduction in compressive strength, especially in the hot/wet condition.

The problem of realistic load and environmental exposure has been addressed by Gerharz (69). He presented results (taken from the literature) which show that the effect of simultaneous environmental and mechanical loading (representative of that on an upper wing skin) is much more detrimental, to fatigue, than the effect of consecutive environmental exposure and mechanical loading in otherwise identical conditions. These results show that there is an interaction between environment and long-term mechanical loading that influence damage formation and life. This is an important problem that is often ignored in the attempt to cut down costs and accelerate testing.

3. EXPERIMENTAL PROGRAMME

3.1 INTRODUCTION

The usual constraints of time and expense govern all experimental investigations, but this is especially the case when fatigue testing advanced composites. A successful outcome will depend upon a well designed experimental programme which will optimise the information obtained from each long-term test. The programme must take into account that for specimen manufacture, environmental exposure and testing, subsequent examination and damage assessment, a wide range of equipment has to be assembled.

A main programme was designed with the objectives of the work in mind and is summarised in figures 3.1 & 3.2, for stacking sequences A and B respectively. Specimen coupons of type A were notched with centrally located 5mm holes or 10mm sharp slits. Type B specimens were notched with sharp slits only. The notched specimens were tested in reversed axial fatigue (R=-1) in a range of hygrothermal environments (RT/dry, RT/wet, 90°C/dry and 90°C/wet) at a predetermined stress level and number of cycles. The objective of the work was to provide an understanding of the fatigue damage processes and the way these are affected by environment and stress concentrators. The correlation of residual strength or fatigue life with fatigue damage was also an important objective. Fatigue damage in each condition was therefore thoroughly evaluated and both tensile and compressive residual strengths were determined.

Due to possible batch-to-batch property variations in pre-preg material, The whole amount needed for the main programme (plus an extra 25%) was ordered in a single batch. 150 m^2 of unidirectional 914C/XAS-5-34 was ordered from Ciba Geigy Plastics and delivered in May 1985.

Two different stacking sequences rather than lay-ups were chosen so as to highlight any not so obvious effects on damage initiation and/or propagation. For example, it is immediately apparent that a (0°/90°) or a (0°/90°/45°) lay-up will promote more widthwise damage as compared to a (0°/45°) type lay-up, tested under the same conditions. However it is not so obvious, prior to testing, that a slight change in the positioning of one ply within the same lay-up will have any significant effect. The 50% 0° and 50% 45° type lay-up combines very good axial and torsional strengths and is therefore a strong candidate for aircraft wing skins. The chosen stacking sequences were;

(a) $(\pm 45°/0°_3/\pm 45°/0°)_S$, main lay-up, denoted type **A** and,

(b) $(0°/\pm 45°/0°_2/\pm 45°/0°)_S$, denoted type **B**.

Both laminates were (16 ply) symmetric with a nominal thickness of 2mm and fibre volume fraction of about 60%: B type Specimens were to be used in selected tests only.

3.2 APPARATUS

The test machines, loading fixtures and laboratory equipment, some of it purpose built, are described in the following sub-sections.

3.2.1 Anti-buckling Guides

Due to the compressive nature of the loading an anti-buckling support had to be provided. Several anti-buckling devices have been used and reported in the literature by different researchers. Typical examples can be found in references. (17,52,69 and 77). Black and Stinchcomb, (83), have actually developed a method where no anti-buckling support was needed in compressive fatigue testing. However, in practice only thick specimens (greater than 4mm) can be tested in this way (in order to have an acceptable gauge length). All of these devices and methods were considered but it was thought that a better alternative was the jig previously used by the author (84), with minor modifications as shown in figure 3.3. This is a relatively simple device, which was easy to use (requiring no tools) and providing excellent specimen to specimen repeatability. It basically consists of two flat plates, sandwiching the test specimen, with a central window around the notch to ensure unconstrained damage growth. This apparatus was also used for the notched static compressive tests as well as the residual compressive strength measurements. All bolts were tightened by hand so as to ensure an even as well as a repeatable pressure.

The load capacity of these guides is relatively low due to the out of plane weakness at the lower part of the device, see figure 3.3. This was so designed as to prevent (or minimise) longitudinal movement constraints during dynamic loading. However, this part is sensitive to out of plane loading, eg eccentric loading due to jaw misalignment. Loading beyond the so called "capacity load" causes failure. The capacity, for a given specimen, also depends upon the clamping pressure, being increased at higher pressures. It was found that, with a jaw alignment accurate to 0.1mm and a grip pressure reading of 3000 psi, the static test load capacity (for a 2mm thick specimen, type A) was about -65 kN.

Below the capacity load, specimen buckling occurred only in the window area and that depended upon the load and the window size. Two different window sizes were used, 30x23mm and 30x19mm, for specimens with (10mm) sharp notches and (5mm) circular holes respectively. A smaller width size was chosen for the "hole" because higher test loads as well as longitudinal damage growth, rather than widthwise, (compared to the sharp notch) were expected. It has been shown (84), that for a 30x25mm window size and a notched CFRP specimen, the maximum acceptable fatigue load was about 32 kN. Below this value insignificant or no specimen bending at all occurred within the window area.

3.2.2 Test Chamber

For hot testing an appropriate heating chamber had to be designed and tested. This is shown in figure 3.4. The two modified "Black & Decker" paint strippers provided the heating power in the custom built chamber, which fitted directly on to the fatigue machine grip. The temperature was regulated via a temperature controller, first used by Morton and Praulitis (85), suitably modified to drive a second "heating gun". Other features added to the controller were a temperature cut-out thermostat, protecting the hydraulic grips, and a timer cut-out. The chamber was fully tested and calibrated using two sizes of instrumented specimens, 25mm and 50mm wide. The 50mm wide specimens were evaluated both with and without anti-buckling guides. Temperature readings were taken from four different thermocouples, two in either surface of the dummy specimen, one embedded through the thickness of the specimen and one permanently fixed (and well insulated) at a "reference" point inside the chamber. All temperature readings were monitored via a "Comark" electronic thermometer. Optimum procedures (minimum time to desired temperature) were identified for each test condition and were subsequently employed in testing. Such procedures usually involved two different controller settings. A high one A_1 to start with and a lower one A_2, once the maximum desired temperature was reached, see figure 3.5. Optimum procedures and reference (air) temperature values were identified for nine different conditions, these were;

(1) 90°C, 50mm wide specimen with guides

(2) 90°C, 50mm wide specimen without guides and,

(3) 90°C, 25mm wide specimen without guides.

Cases 1,2 and 3 were repeated for 130°C and 200°C test temperatures.

It was assumed that for given external conditions (ie controller setting, cooling airspeed, etc) the relationship between reference and specimen desired temperature remained constant. Therefore, the reference (air) temperature alone could be relied upon during testing.

From the thermocouple readings it was estimated that the temperature fluctuation was about 2% of the desired mean temperature. Furthermore, repeated tests showed that the desired mean temperature could be reached with an accuracy of about 3%. These values were dependent on whether the anti-buckling guides were used or not. In general the temperature fluctuation was increased by about 1% (to 3%) and the desired temperature accuracy decreased by about 0.5% (to 2.5%) when no guides were used.

A major disadvantage of the test chamber was the fact that it could only provide a dry environment. This meant that wet conditioned specimens were partially dried out during testing. The drying out versus time was thoroughly studied using the slicing technique. This technique was carried out at RAE Farnborough. Details of this programme may be found below under the section of destructive examination, 3.6.2.

Due to the fact that the fatigue machine grips were hydraulic it was necessary to thermally isolate the chamber from the grips. The grip temperature was monitored via a thermocouple permanently stuck on to the top jaw, using silver loaded epoxy. Even though the top and bottom inner surfaces of the chamber were well insulated (lined with fire clay) and the top and bottom cut-outs sealed with high temperature silicon rubber, see figure 3.4, some excess heating did occur at the grip surfaces when the chamber was used for long periods of time. The solution to the problem was a, 1hp, centrifugal fan that was used in conjunction with a specially designed (and custom built) flow deflector to blow cooling air on to the grips, figure 3.6.

3.2.3 Test Machines

A 100 kN "Losenhausen", servo-hydraulic, fatigue machine equipped with "Dartec" hydraulic grips, was used for the fatigue and most of the static testing. A small amount of testing (material property measurements and interlaminar shear strength, ILSS, tests) was carried out on a 200 kN "Zwick", screw actuated, test machine equipped with manual wedge-type grips. The advantage of this machine was a computer controlled facility, which also provided the user with data storage and manipulation options, including curve plotting and curve fitting. This facility was developed by Kretsis (86) in the Department of Aeronautics at Imperial College.

Although the clamping force applied by the grips was adjustable by regulating the hydraulic supply pressure (a range of 0 to 3000 psi was available) it was found that, because of the coarse surface of the jaws, tensile testing of plain (unnotched) specimens was extremely difficult. Failure consistently occurred near or within the jaw area, yielding an invalid test. An easy way round this problem is the use of abrasive cloth (84), however, when expensive hydraulic grips are used this is not such a good idea since abrasive particles, which usually litter the grips following such testing, can seriously damage the hydraulic pistons of the grips or indeed any other moving part. An alternative is the use of end tabs as recommended by the various standards institutions. This technique was initially employed, and both fibre glass and aluminium end tabs were used. Fibre glass was found to be the more suitable of the two. However, because of the expense involved as well as the time consumed in the preparation and bonding, another solution to the problem was sought. This led to the design of a set of support plates, which accommodated a set of suitable jaws (from an old grip set) and fitted over the existing jaws figure 3.7. This arrangement provided a fine but rough surface which together with an appropriate clamping pressure (1500 psi) eventually yielded valid failures.

3.2.4 Environmental Cabinets

For the accelerated "wet" conditioning a "Gallenkamp" non-injection humidity oven (OVR-200 series) was used. This was operated at 60°C and, with the use of potassium nitrate (99.5% pure) saturated solution, 84% RH moist environment was obtained. A nitrate salt was chosen instead of a chloride to avoid possible corrosion of the stainless steel liner of the cabinet. The condition was monitored with the aid of a wet and dry hygrometer which was conveniently mounted on one of the cabinet's shelves. Suitable custom built specimen holders also had to be provided to increase the cabinet's capacity and ensure an evenly spaced load. The "dry" specimens were stored in a desiccator, over self-indicating Silica gel, at room temperature, RT.

A further batch of "wet" specimens was stored over distilled water in a sealed cabinet at room temperature so that saturation could be obtained in a non-accelerated state.

3.2.5 Non-destructive Examination Equipment

Two methods were employed for the non-destructive evaluation of fatigue and proof loading induced damage. These were, ultrasonic C-scan and X-ray radiography. C-scans were obtained for every single specimen prior to any further testing or another damage evaluation technique. A "Meccasonics" ultrasonic C-scanning machine was used.

To make damage visible, the X-ray technique requires the introduction of an X-ray opaque fluid (eg zinc iodide, tetrabromoethane, diiodobutane, etc) into the damaged specimen which makes it a rather tedious method. This technique was thus used for selected specimens only, based upon the initial C-scan evaluation. At least one specimen from each condition was examined in this way using a "Hewlett Packard" 43804N Faxitron series X-ray system. The zinc iodide enhancing agent used in this technique was introduced into the damaged area under vacuum, using the apparatus shown schematically in figure 3.8.

3.2.6 Destructive Examination Equipment

Following X-ray examination, all specimens were then destructively examined using techniques such as sectioning and deply.

Microscopic examination of damaged sections was carried out on an "Olympus" BO71 microscope. This was equipped with an "Olympus" PM-10AD photographic system. Both a 35mm camera and a large format adaptor were available. In most cases a "Polaroid" type 55 (large format) positive/negative film was used for instant results.

Specimen deply is achieved by partial pyrolysis of the resin matrix. For this a furnace is required. Ideally pyrolysis should be carried out in an inert gas (eg argon) environment and the furnace vented to the outside. For this particular research work an ordinary "Gallenkamp" FR574 furnace was used. This was placed under an extractor fan so that fumes could be passed outside.

The study of fracture surfaces is usually called fractography. In the present study fractography was performed with the aid of a ("Jeol" JSM-T200) scanning electron microscope, SEM (in the Materials Department at Imperial College).

3.3 SPECIMEN PREPARATION

Laminated panels (measuring 530x300x2mm) were hand layed up in the stacking sequences mentioned above, from unidirectional pre-preg. These were then cured in an autoclave following the manufacturer's cycle for temperature and pressure and then post cured in an air circulating oven at the recommended temperature and time, 190°C for 4 hours. Initially 45 such panels were fabricated, 40 in stacking sequence **A** and 5 in **B**. A series of (0°) and (±45°) panels were also made for strength and stiffness measurements. All panels were fabricated in the Department of Aeronautics at Imperial College.

At a later stage in the programme, three additional panels of 914C material were fabricated, two of type A and one of type B. Furthermore, type A panels of three additional CFRP systems (T400/6376 toughened epoxy, R25 bismaleimide and APC-2 thermoplastic) were either fabricated in house or supplied by the manufacturer for a complementary experimental programme. This programme will be presented independently in chapter 5.

3.3.1 Plain Specimens

Specimens intended for plain (unnotched) static tensile tests were machined from the edge of the panels using a diamond saw. The size of these specimens was about 25x250mm. No attempt was made to follow any standards, since in general there is no agreement to what the best size for a given lay-up is, eg, Sottos (87). The size chosen above was a convenient one (a result of the panel size) and it happened to be closest to the size and configuration of the specimen recommended by the British Standards Institution, BSI (88). Each specimen's average thickness and width were recorded. Specimens intended for "wet" conditioning had their weights recorded too, prior to conditioning and immediately after fabrication. All weight measurements were carried out with the aid of "Stanton" F4 scales, accurate to 0.0001g.

An attempt was made, initially, to test (unnotched) specimens without end tabs. However, valid tensile failures within the test sections were rare, especially in the case of stacking sequence B. Specimens were then provided with end tabs (55x25x2mm): both aluminium and unidirectional glass fibre were used. A quick-set adhesive ("Stabilit express" by "Henkel") was used to avoid (or minimise) drying out of "wet" specimens. Following preliminary tests, fibre glass was chosen as the best material for end tabs. Specimen preparation proved to be time consuming as well as expensive. The process of bonding could be made easier if the end tab laminates were bonded on to the specimen laminate before the actual specimen coupons were machined, as recommended by the BSI (88). Such a method could not be utilized in this programme since plain specimens were off-cuts; ie each 530x300mm panel produced ten 250x50mm, (notched specimens) and two 250x25mm, (plain specimens). In order to avoid end-tabbing, a set of appropriate jaws was used, as explained above in 3.2.3. This method enabled plain specimens to be tested without end tabs and it was therefore used in all subsequent tests, of this nature. All specimens tested in this way had a test section (gauge length) of about 110mm. Any quoted results for plain strength will be referred to this particular test arrangement only, unless otherwise stated.

3.3.2 Notched Specimens

Notched specimens were machined from the laminated panels in the same way as plain ones: these measured 250x50mm. Two types of centrally located cut-outs were introduced into the specimens;

(a) 10mm sharp slit, in the transverse direction and,

(b) 5mm diameter circular hole:

B type specimens were notched with sharp slits only.

The sharp notches were cut in by hand using a jeweller's piercing saw with a very fine blade, 0.2mm thick, which produced a 0.25mm wide cut. A small, 1mm, central hole served as the starting point. Usually several blades were expended per slit making the whole process tedious and time consuming. The length of the cut was roughly monitored using a vernier caliper. An exact and final measurement was obtained with the aid of a "Pye" travelling microscope accurate to 0.01mm. It was found that the length of the notch, on either side of the specimen, was in general different, therefore for each specimen both sizes were measured and the average value was recorded and denoted 2a.

The holes were introduced into the specimens using a "Titex plus" tungsten carbide tip drill bit. It was found that an ordinary drill bit did not produce as clean a cut and moreover, it needed sharpening after a single use.

It was anticipated that the actual positioning of the notch could be an important parameter so far as strength was concerned, therefore, every possible care was taken in centering the notches. This proved particularly difficult in the case of the sharp notches. In many specimens the notch had to be extended beyond 10mm, in order to be near central. It was therefore necessary to use some kind of normalisation factors to allow for these variations in notch lengths. These are discussed in more detail in chapter 4.

Hole size variation was also examined. It was found that this was very small (5.00-5.04mm from a sample of 20 specimens), since the same drill bit was used throughout. Naturally, no account was taken of the hole size variation. A nominal hole diameter of 5mm was assumed for all specimens concerned.

As in the case of plain specimens the cross-sectional details of each specimen were recorded prior to conditioning. Specimens were then conditioned as described below in 3.3.3.

In addition to the stress concentrators two dowel holes were introduced in either end of each specimen. These were needed for locating the anti-buckling plates, figure 3.3, and were introduced prior to testing.

3.3.3 Environmental Conditioning

Three wet conditions were employed;

(a) 60°C/84% RH

Type A and B specimens were stored over a saturated solution of potassium nitrate at 60°C, 84% relative humidity, RH. This was the main wet environmental condition. The expression "wet specimens" refers to this particular environment unless otherwise specified. Both notched and plain specimens were stored under this environment. Weight gains in "traveller specimens" were periodically monitored. Traveller specimens were actual test specimens, 250x50mm and 250x25mm in size. Eleven traveller specimens from different positions inside the chamber were used. The absorbed moisture equilibrium level of about 1.4% by weight was reached after a period of about four months. The exact time to equilibrium could not be estimated because some drying out occurred when the environmental cabinet developed a leak. The exact temperature and moisture level were monitored via wet and/or dry thermocouples. A total of about 220 notched and 40 plain specimens were stored in this environment.

(b) RT/100% RH

A smaller number (20 from each notch type and 5 plain) of type A specimens were stored over distilled water at room temperature. In this 100% RH wet environment saturation could be achieved in a non-accelerated fashion (ie without the use of above ambient temperature). The moisture pick-up was monitored periodically as outlined above. Moisture saturation level, about 2.0%, was reached after a period of about eight months. Only five traveller specimens were used here.

(c) Weather Conditioning

Another small batch of type A Specimens (10 from each notch type and 5 plain) was stored outdoors on the roof of the building for natural weather

conditioning. This conditioning lasted for a period of over two years. Specimen weight was monitored, in the usual way. However, it was noted that matrix material had been eroding away from the surface. Additional, non-moisture related, weight changes meant that moisture content could not be calculated correctly.

All wet specimens were stored dry at RT, prior to any conditioning, that is, they were at no stage stored in an undetermined (laboratory) environment.

Finally, dry conditioned specimens were stored under a single condition, that is, over Silica gel at RT. Both types of specimens, **A** and **B**, were stored in this environment. A total number of about 230 notched and 50 plain specimens were stored in this environment prior to testing.

3.4 STATIC TESTS

Static testing consisted of measurement of plain tensile strengths, notched tensile and compressive strengths and proof loading. Such tests were carried out on the "Losenhausen" machine under displacement control. The output was obtained in the form of load versus cross head displacement and recorded on a "Rikadenki" X-Y plotter. A smaller amount of testing was carried out on the "Zwick" machine using the computer controlled facility. Any self-contained test programmes, ie ILSS and elastic constants measurements, were conducted on the "Zwick" machine.

3.4.1 Plain Specimens

(a) Static Strength Tests

Plain (unnotched) specimens of types A and B were tested in tension in order to determine their plain tensile strength in various environments; eg, wet, dry, hot/wet, etc. The results from these tests were to be compared to the notched static results so that an indication of stress concentration could be obtained (for each test condition). Consequently these tests were conducted on the "Losenhausen" machine under displacement control. A rate of about 3mm per minute, was used.

It was found that valid hot test results could not be obtained, since failures persistently occurred just outside the chamber at the cold portion of the test piece, figure 3.9. A solution to this problem was thought to be long end tabs, long enough to reach inside the chamber. In fact, a test panel (300x300mm) was fabricated with moulded end tabs: a specimen from this end tabbed panel is shown in figure 3.10a. Unfortunately this was not an appropriate solution to this complex problem, since the reinforcing end tabs delaminated prior to failure resulting once more in a

fracture away from the test section. In a further attempt, waisted specimens, figure 3.10b, were also tried without success. The lack of a suitable test machine equipped with a test chamber that would heat the total length of the specimen, rather than the test section alone, meant that this part of the programme had to be abandoned. Consequently, only RT tests were carried out for both wet and dry conditions. All three wet conditions were investigated, ie; 1.4% wet, 2.0% wet and weather conditioning.

(b) Interlaminar Shear Strength Tests

Interlaminar shear strength, ILSS, tests were performed on unidirectional wet and dry specimens (12x10x2mm) to assess the effect of moisture pick-up as well as the effect of ageing during conditioning. It was reported by Collings and Stone (25), that ageing in a hot wet environment (60°C and 96% RH) had caused a reduction in ILSS in carbon/epoxy composites. The large amount of fatigue testing involved in the present programme meant that such ageing was unavoidable, since testing of the wet conditioned specimens lasted for more than a year. It was therefore essential, on the basis of Collings and Stone's observations, to check periodically for possible fluctuations in the ILSS of the wet conditioned specimens (under hot wet conditioning). For these tests the "Zwick" machine was used in conjunction with the test jig shown in figure 3.11. These tests were carried out under displacement control at a rate of 2mm per minute.

(c) Mechanical Property Determination

For the purpose of a 3-D Finite Element Analysis (FEA), an experimental programme was devised to determine the material properties for wet and dry specimens. All six independent properties (E_{11}, E_{22}, G_{12}, G_{23}, ν_{12} and ν_{23}) had to be evaluated to enable the complete set-up of the 6x6 stiffness matrix of the material. The relative, rather than the absolute, values were needed, therefore all the properties had to be evaluated from a single (if possible) laminated panel. A 180 ply unidirectional panel, measuring 200x150x22mm was fabricated. Specimens were then cut from this block with dimensions and fibre orientations as shown in figure 3.12. All specimens were cut slightly oversize using a diamond saw and then precisely ground flat to the desired dimensions. It was originally intended that all properties be measured at elevated temperatures too. Therefore, all specimens were instrumented with high temperature gauges, TML type NFLA-3, capable of withstanding temperatures up to 250°C. Due to time constraints, however, no high temperature tests were carried out. Two specimens for each test condition were available. All properties were evaluated in tension only. These tests were conducted on the "Zwick" machine under displacement control at various rates of displacement.

A minimum rate of displacement was generally used for a particular type of specimen. This was determined by the available computer memory, since all the data (load, grip displacement and strain gauge output) were stored for each test, before being saved on a flexible disc. A typical unidirectional test with two strain gauge readings (averages from the longitudinal and transverse directions) would have produced about 200 sets of data points at a rate of 2mm per minute and a maximum strain of about 0.8%.

In order to check the validity of some of the tests mentioned above, 16 ply $(\pm 45°)_s$, $(0°_{16})$ and $(90°_{16})$ laminated specimens, of similar sizes, were also tested. The $(\pm 45°)_s$ test specimens were used for checks on the in-plane shear stiffness, G_{12}, the (0°) and (90°) specimens to check the direct, E_{11}, and transverse, E_{22}, stiffnesses respectively.

3.4.2 Notched Specimens

These tests were conducted on the "Losenhausen" machine under displacement control at a speed of about 3mm per minute. Both tensile and compressive tests were performed. Compression specimens were supported in the anti-buckling guide.

(a) Notched Strengths

In the case of type A specimens, both sharp notches and circular holes were investigated under six environmental conditions, RT/dry, 90°C/dry, 130°C/dry, RT/wet, 90°C/wet, and 130°C/wet. Three specimens per condition, load case and notch type were tested in this way, resulting in a total number of 72 specimens.

Type B specimens contained sharp notches only and were tested in the same environments as type A specimens. Two specimens per condition and load case were tested, 24 specimens in total.

(b) Proof Loading

A series of proof load tests was also performed on type A specimens only. Fatigue damaged as well as undamaged specimens were tested in various environments in both tension and compression. These tests were carried out once the appropriate average failure load for each condition was known. The proof loading was usually of the order of 90% of the average respective strength. The resulting damage shape from such testing was recorded by means of C-scanning. Some tests had to be repeated, with the load being increased beyond the initial 90% value, by small increments until damage was detectable. Six specimens were lost in this part of the

programme. Following initial C-scan damage evaluation, some specimens were then X-rayed so that better damage definition could be obtained. A total of 20 specimens were tested in this part of the programme.

(c) Residual Strengths

Residual strength tests, both in tension and compression, were carried out on fatigue damaged specimens. Following fatigue, these specimens were statically tested as outlined above. Two specimens were tested in each condition.

A summary of the experimental programme, including the above tests, can be found in figures 3.1 and 3.2.

It should be noted that all wet specimens intended for further residual strength tests were returned to the wet environment so that equilibrium moisture level could be restored. Hot-tested specimens were reconditioned for at least one week before further static (eg; residual strength) testing.

3.5 FATIGUE TESTS

Fatigue tests were performed on the "Losenhausen" machine under constant load control. Even so, the machine was not able to cope with the specimen's stiffness changes with fatigue cycles. A small drop in the maximum fatigue amplitude often occurred, therefore occasional checking and manual adjustment was necessary, especially when fatigue cycling at (reversed) amplitudes greater than 25 kN. Notched specimens were supported in the anti-buckling guide and subjected to a sinusoidal reversed axial fatigue loading, R=-1, at a frequency of 20 Hz. Two temperature levels were investigated; RT and 90°C, for both wet and dry specimens.

The rather high test frequency was used because of the large amount of testing involved. It was assumed that the only high frequency related effect was heat build-up, due to specimen internal friction. For this reason, specimens tested at RT were cooled with the help of the blower, which (as already stated) was otherwise used during hot tests for cooling the grips: the flow deflector was not used in this case. Specimens were sprayed with PTFE dry lubricant so as to minimise surface friction due to the support plates, which were also sprayed. The specimen surface temperature (locally to the notches) was monitored for representative test cases, using attached thermocouples. It was found that the surface temperature depended upon the load amplitude. With the cooling fan on, and a maximum cyclic load of 20 kN the temperature increased from about 22°C to 27°C and at a maximum load of 30 kN it rose from about 22°C to 29°C. This was thought to be acceptable since the high

temperature fatigue tests were carried out at 90°C: there is clearly a significant difference between 90°C and 29°C (nominal RT). For higher than 30 kN load amplitude tests the frequency had to be reduced below 20Hz in order to keep the specimen temperature at about 30°C. Typically the frequency had to be decreased by 1Hz for every kN increase in fatigue amplitude above 30kN.

All fatigue tests are summarised in figures 3.1 and 3.2 for specimen types A and B respectively.

In the case of hot (90°C) fatigue testing, a further (controller) adjustment, to the original procedure, (see section 3.2.2) was needed, due to the extra build up of heat mentioned above. It was found that after a period of 10 minutes of testing the temperature setting on the controller had to be slightly reduced in order to keep the reference reading at the desired position. For example in the case of 90°C tests, the reference (air) temperature should have been 113°C when equilibrium was reached.

3.5.1 Sharp Notches

Preliminary fatigue tests to failure were carried out on type A dry specimens at RT only. An appropriate load level, denoted Ln, was identified that would produce detectable (using the available damage evaluation techniques) amounts of damage after 10^3 cycles and a life in excess of 10^6 cycles. The chosen load, Ln, was 20 kN: for the dry type A specimens this corresponded to an approximate remote strain of 0.3%. Type A specimens were then tested at this load for 10^3 and 10^5 cycles. Thirteen specimens were tested in each condition (dry/RT, dry/90°C, wet/RT and wet/90°C), and cycle case. Tensile and compressive residual strengths were then carried out at, RT, 90°C, and 130°C. Two specimens were tested in each case. A single specimen (per condition) containing an average amount of damage was carefully selected, following C-scan evaluation of all thirteen specimens, and used for further damage examination. A total number of at least 104 specimens were tested in this part of the programme.

Type B specimens were fatigue tested at the same load level Ln, at RT and for 10^5 cycles only. Nine specimens were tested in each condition (wet and dry). Residual strengths at RT were not carried out in this case. At least one specimen was fatigued in the remaining two conditions (dry/90°C and wet/90°C) for damage evaluation purposes. At least 22 specimens were tested in this way.

Saturated wet specimens of type A were also fatigue tested at the same load level (Ln=20 kN) for 10^5 cycles. Both RT and 90°C fatigue tests were performed. Residual strength tests were carried out in both tension and compression under two

conditions; RT and 90°C. Nine specimens were fatigue tested in each condition resulting in a total number of 18 specimens. One specimen from each condition was used for detailed damage evaluation. As above the selection of these specimens was based upon the C-scan evaluation of all fatigue tested specimens, in the same condition.

Weather-conditioned specimens were fatigue tested to failure at various constant load amplitudes. Damage studies were carried out on selected cases only.

3.5.2 Circular Holes

An appropriate load level, Lh, was also determined in this case so as to satisfy the same requirements as in the case of the sharp notches. This was found to be 30 kN corresponding to a remote strain of about 0.4%. Only type A specimens were available in this case. Fatigue and residual strength tests were carried out in exactly the same way as described above for sharp notches.

During initial residual strength tests, large increases in both tensile and compressive strengths were observed. In many cases failure occurred at the pin hole rather than at the original stress concentration. Consequently specimens were tested without pin holes. This had made loading of specimens in the grips slightly more difficult, since prior to clamping the bottom anti-buckling plates were loose.

Damage examination of fatigue tested specimens revealed that, in the hot/wet case, damage around sharp notches was very similar in nature to that in circular holes. In order to investigate further this unexpected effect, a wet specimen with a 10mm circular hole was prepared. This particular specimen was fatigue tested at 90°C at a stress level Ln=20 kN (that same as for the 10mm notches). Damage propagation was monitored periodically using the C-scan. To avoid drying out, this specimen was tested for periods of less than two hours at a time and was re-conditioned before further testing. For comparison, type A and B specimens containing sharp notches were also tested in an identical manner.

Saturated wet specimens were destined for RT and 90°C fatigue tests, as in the equivalent sharp notch case. However, it was found that the first three specimens failed prematurely (short of 10^5 cycles) when tested hot. Therefore fatigue tests were carried out at RT only. The remainder were statically tested in compression at RT and 90°C.

3.6 DAMAGE DETECTION

One of the main objectives of the present work was damage characterization. A lot of time was, therefore, invested in evaluating fatigue induced damage. It was thought vital to the success of this work to identify clearly any individual damage mechanisms responsible for observed strength or life behaviour. At least one specimen per condition, stacking sequence, and notch type, was examined in detail using a range of destructive and non-destructive methods.

3.6.1 Non-Destructive Examination

Two non-destructive examination (NDE) techniques were extensively used in the present work; ultrasonic C-scan, and enhanced X-ray radiography.

(a) Ultrasonic C-scan

C-scan is a relatively simple method for evaluating damage, requiring no special specimen preparation prior to testing. This technique was therefore widely used for evaluating both damaged and undamaged material. Moulded panels were scanned for defects before being cut into specimens. It was found that all panels were acceptable for testing.

Following fatigue or proof load testing, every specimen was examined in this way for an initial damage evaluation. All C-scans were performed at 2 dB steps. It was the original intention that all scans be carried out at the same settings throughout however this was not possible since the attenuation of the signal varied slightly with time, depending upon the condition of the probe. For consistency specimens from the same conditions were usually scanned together.

It was found that the dry lubricant which was used in fatigue to reduce surface friction had to be removed from the specimen's surface prior to C-scanning. Trichloroethylene could be used to remove the lubricant, however Owens (89) has observed some small (of the order of 4%) reduction in flexural strength follows a short exposure of carbon fibre samples to this substance. To avoid cleaning the lubricant from the surface, specimens were not sprayed in the central (50mm long) section where damage was expected. This had little effect on friction since some of this area was taken up by the anti-buckling guide window. Washing-up fluid was used to clean thoroughly the specimen surfaces before scanning. This ensured a grease-free surface. In addition washing-up liquid acts as a wetting agent so minimising the chances of surface bubble formation.

(b) X-ray Radiography

At least one specimen from each test case, load condition, stacking sequence and notch type, was examined using X-ray radiography. Polaroid type 52 (positive only) film was used throughout. Although, in general, X-ray film gives a better definition, the polaroid film was used because it provided an instant photograph and evaluation of the damage state. Furthermore, any mistakes (eg exposure time, X-ray intensity, inadequate enhancer penetration etc) could be identified and corrected on the spot.

Zinc iodide solution was used to highlight the damage region. The enhancer is usually a penetrating fluid capable of absorbing X-ray radiation thus enhancing contrast of the damaged area. Up to six specimens at a time could be treated with penetrant with the aid of the apparatus, shown in figure 3.8. The penetrant consisted of 60g of zinc iodide, 10ml of water, 10ml of alcohol and 10ml of a wetting agent, as described by Jamison and Reifsnider (90). The influence of zinc iodide on the mechanical response of carbon/epoxy has been investigated by Rummel et al (91), who reported no observed effects. Even so, in the present study specimens subjected to zinc iodide were not used in further mechanical tests, eg residual strength tests.

It was found that a very well enhanced damage picture could be obtained if the penetrant was introduced into the damaged area twice; (a) a day before, and (b) a short while before the exposure to X-ray. During the first introduction, the penetrant is given the chance to reach and permeate even the smallest cracks and, therefore, the total damaged area can be identified. The second introduction is needed to replace any penetrant which usually dries out from the very badly damaged surface areas.

Unfortunately, all up-to-date NDE methods alone are inadequate for a complete damage evaluation. When a detailed damage examination is needed other, destructive, methods have to be employed.

3.6.2 Destructive Examination

Several destructive examinations were used in order to achieve a detailed damage characterization. These are; optical microscopy, specimen deply, fractography, and slicing.

(a) Optical Microscopy

For the purpose of microscopic examination two through-thickness sections were carefully removed from each specimen using a diamond saw. Section *A* tangential to the notch tip, along the loading direction, and section *B* perpendicular to *A*. In the case of badly damaged specimens, a larger area was removed and the area of interest was revealed by grinding the, embedded in resin, pieces using a rotary grinder. A polished surface finish was obtained with the aid of a "Metaserv" auto-polisher and ("Brasso") metal polish as the abrasive agent.

Polished specimens were then mounted on holders and examined optically under the microscope. Regions of typical damage were photographed. Usually, two pictures per fatigued specimen were taken, one from each section, (*A* and *B*)

(b) Specimen Deply

Specimen deply was carried out using the technique originally developed by Freeman (92). Specimens were deplied by partial pyrolysis of the matrix in a furnace at a temperature of 418°C for about one hour. Specimens were then separated into individual plies using a trimming knife and mounted on a card using double sided adhesive tape. Initially, gold chloride solution was used to stain the damaged regions prior to deply, however, because of the expense involved due to the large number of specimens, zinc iodide was used instead. Zinc iodide is not as effective but it is much cheaper and more convenient to use: X-rayed specimens could thus be deplied without further preparation.

A major disadvantage of the deply technique is the fact that no photographic recording of the whole damaged area can be made. It is possible to use an electron microscope to identify damage but several pictures are usually needed to be put together in order to make up the total damaged area. If this process is repeated for every ply it can become very expensive and time consuming. An easier method but equally time consuming is the recording (sketching) of damage by hand. This method was adopted in the present work.

(c) Scanning Electron Microscopy

Fractographic analysis was used to characterise the effects of environment upon the fracture behaviour by examining the state of fibre matrix interface. Small pieces of broken plies were removed from statically tested specimens and mounted on cylindrical (9.5mm in diameter) aluminium holders. Silver-loaded epoxy was used to secure the specimen pieces on to the holders which were then gold plated prior to examination in an SEM. Of the two available stages in this microscope, the upper one was used for better definition and a wider choice of angles of view.

(d) Slicing

The slicing technique was employed to enable through thickness moisture distribution to be evaluated. This part of the programme was carried out at RAE Farnborough. Six unidirectional wet specimens (50x40x2mm) were dried in an air circulating oven, operated at 90°C, for different intervals of time. Specimens were exposed to the dry environment for 0, 30, 60, 90, 120 and 150 minutes. Specimens were sliced, using a custom built apparatus, immediately after conditioning (drying).

The apparatus consisted of a height adjustable horizontal specimen holder on which the specimen was attached using double sided adhesive tape. A sharp blade moved back and forth, in the horizontal plane, using a moment arm and series of links. At least 12 in-plane slices were removed from each (2mm thick) specimen with a single clean cut at a time. The weight of each ply was recorded immediately before and after complete drying-out in a vacuum oven which was operated at 60°C. In this way a complete through-thickness moisture content for each test piece was determined.

4. EXPERIMENTAL RESULTS AND OBSERVATIONS

4.1 INTRODUCTION

In the present chapter the way the experimental results were obtained and reduced to a presentable form will be discussed. For well established materials, like most metals, there are standard methods available for reducing and presenting data, however, when it comes to composites, researchers are usually faced with a wide range of non-standard methods and, in many cases, they are forced to provide reasons for their choices. Such choices had to be made in the present research work and these together with the experimental results from the main programme will be discussed below.

The present chapter is divided into five major sections: moisture conditioning; static tests; fatigue tests; damage detection and finite element analysis. The results in these sections will be referred to the main material system, XAS/914C. The results of the secondary programme will be presented independently in the next chapter.

4.2 MOISTURE CONDITIONING

Three wet environmental conditions were employed in the present programme;

(a) 60°C/84% RH,

(b) RT/100% RH and,

(c) natural weathering.

The moisture absorption characteristics of the 914C composite system, under the above conditions, are shown in figures 4.1, 4.2 & 4.3 respectively. In the case of the main environmental condition (a), the drying out time (see section 3.3.3) had to be roughly estimated and accounted for in figure 4.1. It appears that a 1.4% equilibrium level was reached after about three months and remained approximately constant thereafter. In the second environmental case (RT/100% RH), the diffusion appears to be much slower due to the lower temperature of exposure and the equilibrium level higher (at about 2.0%) due to the higher relative humidity of exposure, figure 4.2. In this case equilibrium (saturation) has been reached after about sixteen months of exposure. In both cases the moisture equilibrium level in the 25mm wide specimens appears to be slightly lower compared with the 50mm wide

specimens. This was attributed to a small difference in the thickness of the two specimen geometries. It has been stated in section 3.3.1 that the 25mm wide specimens were off-cuts from the edge of the moulded panels where the thickness tends to be slightly smaller than the nominal thickness (2mm) of the rest of the panel. The fact that the moisture level appears to be sensitive to small thickness (fibre volume fraction) variations indicates that most of the moisture is taken up by the matrix itself rather than the fibre matrix interface.

A marked difference in the moisture absorption characteristics between the two specimen geometries has been observed when the material was weather conditioned, figure 4.3. In this case, the 25mm wide specimens appear to have (at a given time) gained a greater percentage weight than the 50mm wide specimens. This can be attributed to the surface matrix erosion. Such effect must be more pronounced in the 50mm wide specimens which have twice as much free surface area compared to the 25mm wide specimens. The effect of surface matrix loss is also demonstrated by the trend of the weight gain versus real time plot in figure 4.3. The average weight gain during three successive Winters appears to decrease (from 0.8% in January 1986 to about 0.4% in January 1988) while the overall moisture content in the specimens maybe actually increasing. The loss of surface matrix in these specimens resulted in fibre exposure: on cleaning the specimen's surface, the fibres were visible by eye.

The through-thickness moisture distribution during drying out of wet unidirectional 914C, at 90°C, has been investigated by slicing the material. The results from this part of the investigation are shown in figure 4.4. Plot (a) shows the moisture distribution before drying out. Ideally the moisture content versus thickness curve should have been near flat since moisture equilibrium had been reached at the time of test. The resultant trend (shown in plot a) is thought to be a consequence of moisture loss during transportation of the specimens to RAE Farnborough and subsequent moisture conditioning prior to slicing. Another, more likely, explanation for the apparent moisture loss (prior to testing) could be the oven leak, as stated in the section 3.3.3. In any case the equilibrium level at the mid-thickness point should represent the moisture equilibrium level. Furthermore, since each slice from the conditioned specimen was completely dried in vacuum immediately before the dry weight was recorded, this value (short of 1.4%) should represent a true moisture content. A similar value for the moisture content was also obtained from figure 4.1, which implies that the traveller specimens used for weight monitoring may also have been completely dry prior to conditioning. Such a conclusion can be fully justified only if it is assumed that the moisture kinetics in both types of lay-ups (0°/±45°) and unidirectional are identical. The rest of the plots in figure 4.4 indicate the degree of drying out as well as the moisture

distribution after time intervals of thirty minutes, following an exposure to a dry environment at 90°C. A discrepancy has occurred at time t=90 minutes (plot d) in which case the moisture content at the mid-thickness point appears to be lower than that in the plots (e) and (f). In general, all plots show a steady moisture loss from the surface plies with time, while the moisture content in the middle plies remains more or less constant even after two and a half hours of drying (plot f). The fact that some moisture loss did occur prior to drying at 90°C (plot a), suggests that the true moisture content in the surface plies should have been slightly higher than that indicated in plots (b-f).

4.3 STATIC TESTS

Static tests were carried out on both notched and plain specimens.

4.3.1 Plain Specimens

(a) Static Tensile Strengths

Static tests on plain (unnotched) specimens were performed in tension and at RT only. Both types of laminates, A and B, were tested. Table 1 summarises the static tensile test results for wet and dry specimens obtained from valid failures only. A valid failure has been defined as one occurring within the test section. Type B specimens having a 0 deg ply on the surface were more likey to produce a failure in the gripped region as compared to type A specimens, furthermore, the smaller number of available specimens meant that no valid tests were obtained for dry type B specimens.

There are four points worth noting from table 1;

(1) the relatively low moisture level in the wet specimens (1.22% instead of approximately 1.4%),

(2) the variation in strength with moisture level and/or method of conditioning,

(3) the variation in strength with stacking sequence and,

(4) the effect of ageing (in the 60°C/84% RH environment) on the tensile strength: this appears to be negligible.

The first observation is thought to be a direct result of specimen thickness as explained above.

The variation in tensile strength with moisture conditioning may be attributed to a number of possible causes such as; the alteration of the residual stress state, the state of the matrix material, or the ply coupling effects, or a combination of these. It appears that when the specimens were "1.4%" wet an optimum material state was realised, since the strength was at a maximum. In the dry state, however, the residual (curing) stresses are at a maximum and the matrix could be too brittle, thus final fracture may easily initiate from any small fibre or even matrix defect, resulting in a lower strength (4.8%), compared with the 1.4% wet case. Ply coupling is also at a maximum in the dry state, thus making the initiation of final failure from a defect more likely. On the other hand when the material was "2.0%" wet the matrix appeared to be too degraded to offer any crack resistance and hence a lower strength was obtained: a possible cause for the matrix degradation may be the matrix microcracking as a result of excess matrix swelling. A similar tensile strength value to that of "2.0%" wet material has been obtained from the weather conditioned specimens. In this case the relatively low strength may be attributed to a weakening of the exposed fibres following matrix erosion.

Visual examination of the fractured surfaces revealed that specimens that sustained the highest loads appeared to exhibit a larger fracture area compared to the weaker specimens which in general resulted in a rather "clean" fracture. Typical failures, in type A specimens, are shown in figure 4.5.

The large difference (8.2%) in tensile strength between wet type A and B specimens is rather surprising, since the state of the matrix in the two composite specimen types is the same. Such difference in strength could therefore be attributed to other possible causes, for example; the residual stress state or the ply coupling, or a combination of these. The residual stress effect, if any, should be minimal, since the two stacking sequences are very similar. Likewise, it is very difficult to see how the ply coupling effect could have such a large influence on strength. If this is true, then the only possible explanation for the observed behaviour must be the sensitivity of the outer layer to the applied load. For example, during a test the tensile loading is transmitted through shear (applied by the jaws) onto the specimen's surface ply which in turn transmits the load to the rest of the specimen. In the case of sequence A the load transmission may be very smooth due to the flexible nature of the 45° ply. However, in the case of sequence B, most of the load is initially carried by the single outer 0° ply in which case damage may easily initiate from a weak spot, triggering the final failure.

(b) Interlaminar Shear Strengths

Interlaminar shear strength tests were carried out in order to check for any ageing effects in the main environmental condition (60°C/84% RH), see section 3.4.1. These results are summarised in table 2. Looking at the 3, 19 and 29 months of exposure specimens, it appears that ageing effects are minimal. The somewhat higher strength obtained after 13 months of conditioning may be attributed to the different curing batch of specimens. In general, it appears that the effect of moisture content is much more important than any ageing effects, since a near 10% reduction in ILSS, from the dry case, was obtained when the material was "1.4%" wet.

(c) Mechanical Properties

A method has been developed that allows all six independent material properties (E_{11}, E_{22}, G_{12}, G_{23}, ν_{12} and ν_{23}) to be calculated from a single unidirectional thick plate. The average results from this experimental programme are listed in table 3, for both wet and dry 914C material system. Due to time and financial constraints, only two specimens were tested in each case. Ideally, a larger number of specimens should have been tested if a true absolute value was to be obtained. In any case, the present results do show some consistent variation in the elastic constants for wet and dry material, see table 3. A small amount of complementary tests were also performed to check the validity of some of the results (E_{11}, E_{22}, ν_{12} and G_{12}). The method of derivation of all results from the experimental data can be found in appendix II. The greatest deviation in the results has been observed in the trends of the in-plane shear stress versus shear strain plots, figure 4.6, where a somewhat larger value for G_{12} has been obtained from the ±45° tests. The actual variation of G_{12} with shear strain for wet and dry specimens, from the 10° off-axis test is shown in figure 4.7. The largest difference in the G_{12} value (for dry and wet material) appears to occur at about 1.0% shear strain, while, initially (at very low strain) the difference in the "wet" and "dry" value of G_{12} is minimal. The same is also true at very high strain.

4.3.2 Notched Specimens

Static tests on notched specimens were performed on both wet and dry specimens at a range of test temperatures (RT, 90°C, and 130°C) for both types of notch geometries (10mm notch and 5mm hole). The purpose of these tests was to obtain a datum for later comparison with the residual strengths, following tension compression fatigue.

(a) Sharp Notches

Both types of specimens, A and B, were tested in this part of the programme. The results are summarised in tables 4, 5 and 6 for type A, and tables 7 and 8 for type B.

It was stated in section 3.3.2, that the notches were cut by hand and therefore an exact length of 10mm could not be produced. Consequently, a normalisation process has been employed to account for such variations. This is the same as the one previously used by the author (84), whereby the assumption was made that the notched strength is proportional to $1/\sqrt{(a)}$. It has been shown, in (84), that over a small variation of notch length this assumption can be justified. Furthermore, the specimens in this part of the programme were carefully selected (from the total amount of specimens) so that for each specimen as well as test case, the average notch length was as close as possible to 10mm, see tables 4-8.

The test results were obtained as maximum load to fracture which was subsequently divided by the true specimen cross sectional area to give the strength in MPa. Each strength result was then normalised by multiplying by $\sqrt{(2a/10)}$, where 2a is the notch length. A nominal thickness of 2mm rather than the true thickness could have been used in calculating the cross sectional area since the amount of fibres, which control the strength, should be the same in all specimens. However, the true thickness and hence area was used so that a clear indication of the scatter in the material could be obtained. When in sample calculations of strength, the nominal thickness of 2mm was used, instead of the true thickness, the scatter of results (first standard deviation) was reduced by about 10%.

Plots of strength versus test temperature, figures 4.8 and 4.9, show a consistent increase in tensile strength with increasing temperature and a decrease in compressive strength with increasing temperature. These trends appear to be true for both wet and dry specimens and for both stacking sequences A and B. Another point of interest is that the moisture itself appears to have the same effect on notched strength as temperature does. This is true in all cases apart from the tensile tests at RT of dry type A specimens (table 4). In this case the average strength appears to be slightly higher (2.3%) than the equivalent wet value. However, within the experimental scatter this could be disregarded. As a result of moisture/temperature equivalence there exists a point on the strength versus temperature plots (figures 4.8 and 4.9) where the strength in the "dry" and "wet" curves has the same value. These points for all the cases concerned, (sequence A and B, tension and compression) approximately correspond to 130°C for dry and 90°C for wet cases. Moisture/temperature equivalence is also demonstrated by the fracture modes. Some examples of tensile fractures are shown in figures 4.10 and 4.11 for sequence A and B respectively. It appears that a reasonable moisture/temperature equivalence

occurs at 130°C/dry and 90°C/wet cases for both stacking sequences A and B. Furthermore, at these conditions both types of specimens A and B fail in a 45° shearing mode and with a minimum amount of delamination, see figures 4.10 and 4.11.

Comparing the strengths obtained for the two stacking sequences, A appears to be generally superior to B, figures 4.12 and 4.13. An exception is the RT wet case (table 8) where the tensile strength of B appears to be relatively higher. This can be attributed to the surface 0° fibre splitting (figure 4.11) which reduces the stress raising effectiveness of the notch. Splitting, in this case, is possible because the surface ply is relatively unconstrained. The compressive strength of type B specimens appears to be lower in all test conditions. However, in the wet case and especially at 130°C the difference in compressive strength, between the two sequences, becomes minimal, figure 4.13. This indicates that at high temperatures, the ply constraints (or the stacking sequence effects) are also minimum. Other factors like the integrity of the matrix in supporting the fibres become more significant.

The compressive fracture modes for both types of specimens appear to follow a consistent pattern with increasing temperature. At low temperature a rather large fracture path initiates from the notch tips and follows a near 45° direction. Delamination is also evident especially in the dry case. On increasing the test temperature, the fracture path tends to align with the notch direction which at 130°C results in a clean (straight line) failure, figure 4.14.

(b) Circular Holes

This part of the investigation involved specimens with stacking sequence A only. Both wet and dry specimens were tested at RT, 90°C, and 130°C.

A summary of the results can be found in tables 9-12. As in the case of sharp notches the strength was obtained by dividing the fracture load by the true area (specimen width times the thickness). In this case no normalisation was necessary since the variation of the hole size was found to be negligible. In general, a consistent increase in tensile and a decrease in compressive strength has been observed with increasing test temperature, see figure 4.15. The only exception occurred in tension in the 130°C/wet case. It appears that the tensile strength in the hot/wet condition reaches a maximum at 90°C and then drops off at 130°C, figure 4.15. This may be attributed to an interaction between two or more mechanisms that have an opposite effect on tensile strength. Such mechanisms are the blunting of the stress concentration, which has a beneficial effect on strength, and the change in the state of

the matrix material, which appears to reach an optimum state at about 90°C (when the material is wet) and deteriorate at 130°C. The deterioration of the matrix in the hot/wet condition appears to have an adverse effect on tensile strength. The reduction in compressive strength with moisture content is further demonstrated by the 2.0% wet condition in figure 4.15. An almost 12% reduction in compressive strength has occurred compared to the 1.4% condition.

Examples of tensile fracture modes for wet and dry specimens are shown in figure 4.16. Moisture/temperature equivalence appears to occur in two sets of conditions; (a) 90°C/dry and RT/wet, and (b) 130°C/dry and 90°C/wet. Figure 4.15 shows that a good match in tensile strengths also occurs at the conditions (a) and (b). A point of interest in figure 4.16 is the extent of damage in the specimens in (b). It appears that longitudinal 0° splits were responsible for blunting the hole, thus causing a failure equivalent to that usually observed in plain (unnotched) specimens. Figure 4.17, shows that the the average net-section strength at 90°C/wet approaches 1050 MPa, reasonably close to the RT/dry strength of plain specimens. This is an indication of the neutralization of the stress concentration.

Compressive fracture modes are shown in figure 4.18, for 1.4% wet specimens. Unlike the sharp notches all fracture paths appear to follow a straight line perpendicular to the loading direction. The only apparent difference between modes is the reduction of delamination with increasing temperature and/or moisture.

It has been shown above, that in the case of the sharp notch, the compressive strength in the hot/wet conditions appeared to be insensitive to the stacking sequence. Moreover, it appears that the compressive strength (in the hot/wet condition) is also insensitive to stress raisers, see figure 4.17. At 130°C the net-section strength of specimens with 10mm notches is identical to that calculated from specimens with 5mm holes. However this behaviour does not apply to the tensile strength. The tensile results in figure 4.17 suggest that there always exists a subtle difference between the stress raising effects of the sharp notch and the circular hole. It appears that the tensile strength of the sharp notched specimens is largely controlled by ply coupling. When ply coupling is reduced, by some mechanism, the tensile strength increases, but the final fracture is always triggered by the notch. However, the tensile strength of the holed specimens appears to be controlled by a hole blunting effect as a result of the initiation of longitudinal fibre splitting, the larger these splits are, the greater the resulting strength is. This effect usually results in a wider fracture area which in some cases spreads by as much as 60mm above and below the hole, figures 4.16 and 4.19. The subtle difference in the two notch type cases is very well demonstrated by the tensile fracture modes of wet specimens, tested at 130°C, in figure 4.19. Although the two fracture modes look superficially similar, there is a difference in

the way the 0° fibres have failed and this is reflected in the net-section strength values in figure 4.17. In the case of the circular hole the multiple 0° fracture mode resulted in a 28% higher net-section strength, compared to the sharp notch.

Tables 4-12 show that, in general, the scatter (first standard deviation) in the average values of strength is greater for the circular hole. Furthermore, the scatter in the compressive strength of holed specimens appears to be the greatest with values reaching 17% in some cases. A possible reason for such large scatter in the compressive strength may be the actual test method used. The maximum loads endured by the holed specimens were in some cases close to the antibuckling guide load capacity. Possible reduction of the specimen's bending stiffness by a combination of moisture and temperature could result in instability within the window area and hence premature failure.

4.4 FATIGUE TESTS

Two distinctly different types of fatigue test were performed. The first type involved fatigue testing at a predetermined load amplitude and number of fatigue cycles, followed by residual strength measurements. The second type consisted of fatigue tests to failure at different maximum values of stress amplitude. All tests were carried out in tension-compression (R=-1) at constant sinusoidal load amplitude: a frequency of 20 Hz was used in most tests (see section 3.5). In both cases, several environmental conditions were investigated.

4.4.1 Fatigue and Residual Strength Tests

Notched specimens were fatigue tested in tension-compression at a predetermined load amplitude, Ln or Lh for sharp notches and circular holes respectively. A range of environmental conditions was examined: RT/dry; 90°C/dry; RT/wet; and 90°C/wet. Preliminary fatigue tests to failure were also performed for both circular holes and sharp notches.

(a) Sharp Notches

Dry specimens of stacking sequence A were initially fatigue tested, at RT, to failure in order to determine a suitable load amplitude to be used in subsequent tests. The preliminary results are presented in figure 4.20, in the form of stress amplitude (S) versus fatigue life (N). A load amplitude, Ln=20 kN, which in terms of stress is equivalent to approximately 200 MPa, was selected. This stress level corresponds to a fatigue life in excess of 10^6 cycles, see figure 4.20. In terms of remote strain the stress amplitude of 200 MPa (for the dry condition) corresponds

to just below 0.3% strain, see figure 4.21. Subsequent fatigue tests were carried out at a normalised load amplitude Ln $\sqrt{(10/2a)}$, where $\sqrt{(10/2a)}$ is a normalisation factor which accounts for notch deviations, from the nominal 10mm length. Following fatigue testing, specimens were then statically tested in tension or compression in a range of test temperatures (RT, 90°C and 130°C). The results of residual strength (in MPa) were reduced in a similar way to the notched static strength results, see section 4.3.2.

The residual strength results, for the sharp notches, can be found in tables 13-22, for stacking sequence A, and tables 23-24, for sequence B. For the purpose of comparison, the results are also presented in the form of histograms of average strength against test condition, figure 4.22 and 4.23 for sequence A and B respectively. The static test results are also included in these figures. It is apparent (from the two figures), that in general, the tensile strength increases with moisture content and/or elevated temperature. However, the contrary appears to be true in compression. Another point of interest is the exceptionally high tensile strength attained by the 2.0% wet specimens at RT, following fatigue testing at 90°C, figure 4.22. This value, translated to net-section strength, is only 5.8% below the corresponding unnotched strength value, see table 1. This signifies that, under the above test conditions, the stress concentrating effect of the sharp notch has been completely eliminated. Furthermore, figure 4.22 shows a drop-off in tensile strength of the 2.0% wet specimens at 90°C. This implies that the combination of fatigue damage and the 2.0% moisture content results in an optimum state of specimen strength at RT.

The effect of fatigue loading on the residual strength, for type A and B specimens, is demonstrated in figures 4.24 and 4.25 respectively. The percentage variation in residual strengths (with respect to the corresponding static values) are shown for each specimen and fatigue test condition.

Figure 4.24 suggests that fatigue loading had a largely beneficial influence on the residual strength. The occasional relative reductions in strength appear to be small enough to be neglected. Furthermore, the tensile residual strength appears to be more sensitive to the number of fatigue cycles than the compressive strength. After 10^3 cycles the effect of fatigue damage on tensile strength appears to be negligible, compared to the effect on the compressive strength. Near 20% increases in the compressive strength have been obtained after as little as 10^3 cycles. Such large percentage increases in strength were commonly attained in the wet specimens. The most significant increases in strength have been exhibited by the wet specimens following elevated temperature fatigue loading. Strength increases by up to 57% in tension and 45% in compression have been recorded after 10^5 cycles. Figure 4.25

shows that, at least for the conditions examined, the positive effect of fatigue loading on the residual strength is less obvious in the case of B type specimens. This is particularly true when comparing the wet specimens of type B with A.

Examination of the tensile fracture modes revealed that in most cases the fracture modes of pre-fatigued specimens were very similar to those obtained in "sharp notched" static tests; eg figure 4.26. An exception was the hot/wet fatigue tested specimens which exhibited fracture modes similar to those of the holed specimens in static tests. Examples of such modes of failure are presented in figure 4.27. Longitudinal growth of damage appears to blunt the notch thus causing an increase in the tensile strength. The more extensive the damage appears to be, the higher the strength attained, eg figure 4.28.

A similarity in the failure modes has also been observed between residual compressive and static compressive tests. An exception is the dry material in the following fatigue conditions; RT/10^5 and 90°C/10^5. It would appear that the residual compressive strength is controlled by the state of the matrix material as well as the amount of delamination local to the notch tips. This is demonstrated by figure 4.29. The difference in the fracture modes between the first two specimens is some apparent local (to the notch) delamination. It is thought that the 15% difference in strength between the two cases is due to the local delamination in the second specimen. The third specimen in figure 4.29, appears to have developed less notch tip delamination, as compared to the second, however, its residual strength is slightly (3.3%) lower. This may be attributed to the weak state of the matrix and/or interface in the hot wet condition. The fourth (2.0% wet) specimen in figure 4.29, shows a distinctly different mode of failure. It would appear that a combination of matrix toughening and fatigue damage have contributed to an exceptionally high compressive strength, see figure 4.22.

(b) Circular Holes

Preliminary fatigue tests to failure were conducted on dry specimens at RT. The results from this part of the programme are presented in figure 4.30, in the form of an S-N plot. A load amplitude, Lh=30 kN, which in terms of stress is equivalent to approximately 300 MPa, was selected. As in the case of the sharp notch, this stress level corresponds to a fatigue life in excess of 10^6 cycles, see figure 4.30. In terms of remote strain the stress amplitude of 300 MPa (in the dry condition) corresponds to just over 0.4% strain, see figure 4.21. Fatigue tests at load amplitude Lh, were then followed by residual strength determination. Both tensile and compressive strengths were evaluated.

A summary of the residual strength results can be found in tables 25-33. These results can also be found plotted in the form of histograms of average strength versus test condition in figure 4.31. For the purpose of comparison the static test results are also included in this figure. The arrows indicate that the actual strengths are higher than marked. Specimens in such cases failed at locations away from the central 5mm hole. In tension, specimens failed prematurely at the dowel hole: for example see figure 4.32. To avoid such failures, specimens were subsequently provided with aluminium end tabs: an example is shown in figure 4.32. In compression, specimens failed prematurely when the anti-buckling guide capacity (see 3.2.1) of about -65 kN, was exceeded. Such premature failure, is shown in figure 4.33. Figure 4.31 shows that the largest tensile values have been obtained after 10^5 fatigue cycles. It is interesting to note that under the same fatigue condition the 2.0% wet specimens appear to have the same residual strength as the 1.4% wet specimens. It has been stated in section 3.5.2 that, hot/wet (2.0%) fatigue testing was not possible. This was due to the fact that the life of several specimens was much shorter than 10^5 cycles. Figure 4.31 shows that the compressive strength of the 2.0% wet specimens at 90°C is only slightly higher than 300 MPa, the selected fatigue amplitude.

The effect of fatigue loading on the residual strength is presented in figure 4.34. The relative residual strength variation for each test condition is presented in the form of histograms. It is apparent that the fatigue loading has a beneficial effect on the residual tensile strength, especially in the cases of 10^5 fatigue cycles. In general, the effect of fatigue loading on the compressive residual strength appears to be more pronounced than it is on tensile residual strength. Both beneficial and adverse effects on compressive strength have been observed. Up to 72% relative increase in strength has been observed in the hot/wet case after 10^5 cycles. On the other hand a 23% relative reduction in residual strength has been observed in the RT/dry case after as little as 10^3 fatigue cycles, see figure 4.34. It is worth noting that under the same condition (RT/dry), but after 10^5 cycles, the relative strength showed an increase of about 21%. This behaviour implies that there are two or more fatigue damage mechanisms that have a simultaneous but opposite effect on compressive strength. The observed behaviour suggests that such damage mechanisms must be propagating at a different rate. Furthermore, it would appear that elevated temperature and/or moisture content have a beneficial effect on the relative residual compressive strength.

Examples of tensile fractures of fatigue tested specimens are shown in figures 4.32 and 4.35. These fracture modes appear to be very similar in nature to those obtained in the static case (4.3.2). As in the static case, strong specimens exhibited a large amount of damage during failure. A point of particular interest is the failure

mode of the second specimen in figure 4.35. This specimen was slightly damaged during the drilling of the central hole. A small aluminium chip, off the supporting aluminium back plate, had cut slightly into the hole edge. This damage was detected by subsequent C-scan examination. Even though the specimen was rejected it was fatigue tested in order to evaluate the effect of such superficial damage on strength. Surprisingly, this small initial damage had a great influence on the final failure mode (figure 4.35) as well as the strength. A 30% reduction in strength was observed. This sensitive behaviour of holed specimens on the state of the hole may be responsible for some of the observed scatter in the results, see tables 9-12, for static, and 25-33, for residual strengths.

The marked effect of fatigue loading on the residual compressive strength was also evident from the failure modes. Figures 4.36-4.38 demonstrate the effect of fatigue loading and/or elevated temperature on the fracture modes in wet and dry specimens. It appears that as a result of fatigue loading an inconsistency in the residual compressive fracture modes has been observed. Such examples are shown in figure 4.36. The first two specimens have been tested in an identical manner, but they fail in slightly different manner: the same is true for the last two specimens. However, in this case the difference in the failure mode as well as in strength appears to be much greater. The high strength attained by the third specimen in figure 4.36 is accompanied by a large fracture area. An important point is that final failure in this particular specimen has not initiated from the hole. It would appear that fatigue damage must have neutralised the original stress concentration. The largest compressive residual strength has been obtained in the RT/dry condition after 10^5 cycles and RT residual compression. An example of the failure mode in this condition is shown in figure 4.37. Some out of plane damage is evident in the central unsupported region of the specimen (anti-buckling guide window area) but overall it would appear that the specimen failed in an "out-of-width" mode. In general, the strongest specimens appeared to fail in a similar fashion; eg the second and third specimen in figure 4.37. The only difference between the wet and dry specimen failures is the amount of matrix damage. Dry specimens usually exhibited more extensive matrix damage than the equivalent wet specimens, see figure 4.37. Figure 4.38 shows that the matrix splitting (during failure) is further reduced when the specimens are 2.0% wet. The same figure also shows the effect of fatigue loading on final failure.

4.4.2 Fatigue Tests to Failure

Tension-compression fatigue tests to failure were carried out on specimens with stacking sequence A. In this part of the programme failure has been defined as the stage, during the course of a test, at which the specimen's load carrying

cabability is reduced below the maximum value of the applied cycling load. In most cases this corresponded to fracture. On some occasions, however, due to large stiffness reduction, the machine could not apply the required displacement to produce specimen fracture, but it was simply tripped off by the control safety switches. All tests were performed at RT. Both types of notch geometries, sharp notch and circular hole, were evaluated in a range of environmental conditions.

(a) Sharp Notches

In the case of the 10mm notches, three environmental conditions were investigated; dry, 1.4% wet, and weather conditioning. Specimens were fatigue tested at a constant load amplitude until failure. The results from these tests can be found in tables 34 and 35. These results are also presented in the form of S-N curves in figure 4.39; the stress amplitude, S, has been obtained by dividing the load amplitude by the specimen's true area. The static compressive values are also plotted corresponding to 0.25 cycles (on the fatigue life axis). The compressive rather than the tensile values were plotted since these were the lowest in every case. The arrows in this figure indicate longer than shown lives. Excluding the static strength values, all other points (in each environmental condition) appear to lie on a straight line, see also figure 4.20. For clarity, lines through the experimental points have not been drawn. If lines were drawn, then the ones corresponding to dry and 1.4% wet specimens would have been approximately parallel, with the "dry" line drawn below the "wet" one. This may indicate that the RT fatigue behaviour of the wet specimens is superior overall, despite the fact that the dry specimens exhibited a greater static compressive strength than the wet ones. The behaviour of the weather-conditioned specimens appears to be very similar to that of the 1.4% wet specimens, although some points, at short lives, do lie closer to the dry ones. Figure 4.40 shows a plot of normalised stress amplitude, with respect to the corresponding static value, versus fatigue life. From this point of view the difference in the fatigue performance between wet and dry is further increased. At this stage no attempt will be made to correlate the observed fatigue behaviour to the fatigue damage. Such an attempt, however, will be made in chapter 6, where a better way of presenting the fatigue data will be proposed.

(b) Circular Holes

Owing to a shortage in specimens, fewer specimens with circular holes, compared with the number of specimens with sharp notches, were tested in this part of the programme. Furthermore, no 1.4% wet specimens were tested. The results for dry and weather conditioned specimens can be found in tables 36 and 37. A comparison between the two conditions is presented in figures 4.41, in the form of

S-N plots. As with the notches, the stress amplitude was calculated by dividing the load amplitude by the individual specimen true cross-sectional area. It appears that most of the comments made for the sharp notch also apply to the circular hole, so far as the trends of the S-N plots are concerned. Figure 4.42 shows a plot of the normalised stress amplitude, with respect to the corresponding static value, versus fatigue life. Due to the very small difference in the static strength between wet and dry specimens (unlike the sharp notch case), figure 4.42 appears to be very similar to figure 4.41.

4.5 DAMAGE DETECTION

It has been stated in the previous chapters that the correlation of damage with observed fatigue behaviour is the main objective of this research work. Thus damage detection and evaluation form the most important sections of the research programme. Several destructive and non-destructive methods have been employed in a detailed fatigue damage study: the results from these studies are presented below.

4.5.1 Non-Destructive Examination

Two non-destructive examination techniques were used extensively in the present work; ultrasonic C-scan, and X-ray radiography.

(a) Ultrasonic C-scan

Owing to its simplicity the C-scan method was the most extensively used technique. Every single fatigue tested specimen was examined in this way. This technique proved to be ideal for initial fatigue damage evaluation. Some examples of such use are shown in figures 4.43-4.46. It appears that, in each one of these figures, the fatigue damage is reasonably repeated from specimen to specimen. This behaviour is a good indication of the degree of accuracy and repeatability of the experimental tests, as well as the quality of the material used. Based on C-scan damage evaluation, specimens were chosen in pairs (as shown in the figures) for subsequent residual strength tests. A typically damaged specimen (not shown in the figures), per test case, was also selected for subsequent non-destructive and destructive damage examination. A point of interest is the suppression of the widthwise damage propagation in the wet specimens, with circular holes (figure 4.46), which is evident in the dry specimens, figure 4.45.

The C-scan technique was also employed for monitoring the development of fatigue damage during successive fatigue tests. These results are shown in figure 4.47. Surprisingly, the hot/wet fatigue behaviour of the type A specimens appears to

be independent of the notch geometry. Plots of damage area against the number of fatigue cycles suggest that the rate of damage propagation in the hot/wet condition is also independent of the notch geometry, see figure 4.48. Furthermore, figure 4.47 highlights the difference between the stacking sequences A and B. Both the damage development and the fatigue life appear to be different. Bearing in mind the similarity in the two stacking sequences (see section 3.1), the vast apparent difference in their fatigue behaviour is an important finding.

The C-scan technique was also extensively used for the evaluation of proof loading induced damage. On some occasions, tests had to be repeated many times before damage due to proof loading could be detected. Consequently, the C-scan technique proved to be a very convenient method for monitoring the damage development. Examples from these tests are presented in figures 4.49-4.53, for sharp notches and circular holes. In the case of the sharp notches, detectable damage could be obtained following elevated temperature tensile loading, see figure 4.49. Both wet and dry undamaged specimens have developed damage following a tensile loading at 130°C. The main difference between the nature of the damage in dry and wet specimens appears to be the propagation in the widthwise direction. In the dry specimen the damage propagated towards the specimens free edges (away from the notch tips), whereas, in the wet specimen the damage was contained within the notch tips. In the case of the pre-damaged specimen (third in figure 4.49) some small increase in damage area has been observed, following tensile proof loading at 130°C. Compared to the damage development in the other two specimens, in figure 4.49, the damage propagation in the pre-fatigued specimen is negligible, which indicates that fatigue damage suppresses any further damage. In compression, damage could not be detected. It was observed that, under compressive loading, damage development was immediately followed by specimen fracture. Therefore, test interruption was not possible.

Interesting results have also been obtained from the proof loading of specimens with circular holes. As in the case of the sharp notches, damage mainly propagated under elevated temperature tensile loading, for example see figures 4.50. Such damage propagated in the longitudinal direction and appeared to be very similar in nature to that obtained during the fatigue tests of wet specimens, eg the first specimen in figure 4.51. The result of the longitudinal propagation of damage, was to eliminate the stress concentration of the hole, so initiating final failure at a point away from the hole, for example, see figure 4.51 (third specimen).

A moisture effect was also highlighted by the proof loading tests. Comparing the first specimens in figures 4.51 and 4.52, it can be seen that some widthwise damage has propagated in the dry specimen, following tensile proof loading at RT. In

contrast, no widthwise damage development was observed in the wet specimen. As in the case of the sharp notches, the detection of damage under compressive proof loading was extremely difficult, especially at high temperatures (130°C). This phenomenon may be attributed to the different nature of the final failure mode in tension as compared to compression. These differences will be discussed in some detail in chapter 6. In general, C-scan detectable damage development under compressive loading was only possible at relatively low temperatures, see figure 4.53.

(b) X-ray Radiography

In order to correlate accurately the fatigue damage with the residual strength or fatigue life it is essential that the nature of damage initiation and propagation be defined on a macro as well as micro scale. The C-scan technique is ideal in providing an integrated picture of the overall damage shape, without much information on the individual damage modes. When better definition and differentiation of damage modes are needed, the enhanced X-ray radiography technique becomes essential. Examples of X-ray radiographs can be found in figures 4.54 and 4.55 for sharp notches and circular holes respectively. In these figures, individual damage modes such as delamination, fibre splitting and fibre fracture are evident. The radiographs in these figures were carefully selected to highlight the most important effects of environment, stacking sequence, notch geometry, fatigue number of cycles, and fatigue amplitude.

Figure 4.54 demonstrates some of the above effects as applied to the sharp notches. The effect of environment for example is demonstrated by the first two pictures; the effect of stacking sequence by the first and third; the effect of fatigue cycles by the second and fourth; and the effect of cyclic amplitude by the last three pictures. Before going any further into the description of the damage it would seem proper to define the individual damage modes as seen in the radiographs. Any straight line represents a fibre split (0° or 45°); the grey areas represent delamination damage, and the very short and fat dark lines represent fibre fracture. Furthermore, for convenience from now on, any fibre splitting that is tangential to the notch tip will be referred to as primary splitting. Moreover, the 0° splits will be referred to as primary longitudinal splits, PLS, and the 45° splits will be referred to as primary off-axis splits, POS. Any splits other than the primary will be referred to as the secondary splits: SLS and SOS for 0° and 45° respectively.

It appears that in the hot/wet condition, first radiograph in figure 4.54, delamination damage develops within a region defined by two PLS. Some damage in the form of 45° fibre splits is also apparent. However, only a very small amount

appears to extent beyond the boundaries of the PLS, along the widthwise direction. Both longitudinal and off-axis primary splits are also evident in the second radiograph. However, the lack of moisture in this specimen resulted in completely different overall damage development. The delamination damage developed along two perpendicular 45° paths and extended both within and beyond the PLS, mainly aided by the development of some secondary 0 and 45° splitting. The resulting damage shape resembles a butterfly. This was the most commonly observed shape in all fatigue conditions excluding the hot/wet case of stacking sequence A.

The main difference between the stacking sequences A and B is depicted in the third radiograph of figure 4.54. This particular specimen was fatigue tested in the same condition as the specimen of the first radiograph. As in stacking sequence A, most of the fatigue damage appears to be contained within two PLS which appear to be much longer than the POS. However, some, SLS, developed close to the PLS, towards the free edges of the specimen. The combination of 45° splitting and SLS is thought to be responsible for the subsequent widthwise development of delamination damage and final failure, as shown in the C-scans of figure 4.47.

The development of fatigue damage after a large number of fatigue cycles, at the load level Ln, is shown in the fourth radiograph of figure 4.54. This radiograph is representative of the expected form of a "late" damage development in a type A specimen fatigue tested at a load amplitude Ln (20kN) in any one of the three environmental combinations; RT/dry, 90°C/dry, or RT/wet. There are two important points worth noting here; the multiplicity of secondary 0° splitting which appears to be associated with the 45° splits, and the 0° fibre failures, which are associated with the darker delamination area, see the right hand side of the notch (on the radiograph). It is difficult, at this point, to make any firm comments on the nature of the darker area, but it would seem reasonable to assume that such dark areas should either represent a severe delamination (or cavity) between two layers or a milder form of delamination between three or more plies, located vertically above one another, or even a combination of the two.

The effect of load amplitude is illustrated in the last two radiographs of figure 4.54. At high load amplitudes (greater than Ln), the fatigue damage consists mainly of severe, local to the notch tips, delamination which extends towards the specimen's free edges. Associated with this delamination some 0° fibre fractures are also evident. In contrast, at low load levels (lower than Ln), delamination and fibre fractures are not observed. Instead, damage in the form of fibre splitting extends along the longitudinal direction. This is an important observation, and it will be shown in chapter 6, that such behaviour can be very well correlated with the fatigue life.

Representative forms of fatigue damage for the holed specimens are shown in figure 4.55. The first radiograph in this figure represents the damage development after a small number of fatigue cycles at the standard load level Lh. Such damage consists of a pair of PLS and some delamination within the splits. The actual shape of the delamination, shaded region, suggests that a set of four POS are also present. These splits appear to be in the early stage of development and it is not very clear from the radiograph whether they extend beyond the boundaries of the PLS. The effect of higher number of fatigue cycles, is to promote the length of the PLS and the delamination area that is contained within these splits, for example see second, third, and fourth radiographs. However, on closer look, a series of very fine fibre splits are also evident. As demonstrated by these three radiographs the extent of both the primary and secondary splits as well as the associated delamination depends upon the environment and/or the number of fatigue cycles. Moisture appears to suppress both fibre splitting and delamination, as well as the widthwise extent of secondary splitting, compare the second with the third radiograph.

The last two radiographs demonstrate the effect of the cyclic load level upon the development of the fatigue life from a circular hole. The chosen radiographs are from weather conditioned specimens, but they represent typical forms of expected fatigue damage in any one of the environmental conditions used. Unlike the damage development from a sharp notch, the fatigue damage from a circular hole develops mainly along the longitudinal direction. Even at a load level as high as 38 kN, most of the fatigue damage prior to final failure was contained in an oblong shaped region in the centre of the specimen, bound by two longitudinal fibre splits and extending as far as the gripped area. It would appear that final failure, in this particular specimen, was triggered by a relatively sudden growth of transverse delamination local to the hole. In general the damage development from a circular hole depends more upon the number of fatigue cycles than the cyclic stress amplitude. For example the specimen that survived 18 million cycles (fifth radiograph) will eventually undergo a similar damage development and final fracture as the specimen of the sixth radiograph after perhaps 25 or even 30 million cycles. Likewise, the third specimen is expected to undergo the damage states shown in the last three radiographs.

The most interesting observation so far has been the apparent similarity in the nature, rate of growth, and shape of damage in the 10mm notch and hole in the hot/wet environment (figure 4.47). To confirm further the observed behaviour, all specimens in figure 4.47 were subsequently X-rayed so that a clearer view of the damage could be obtained. The radiographs of these specimens are shown in figure 4.56. These do confirm that the fatigue damage from the sharp notch is very similar to that from the 10mm hole. Furthermore the third radiograph of the stacking

sequence B specimen shows a clearer (than C-scan) view of the vast difference in the damage development between the two stacking sequences A and B.

Proof loading induced damage is shown in better definition in the radiographs of figure 4.57, as compared with the C-scans of figure 4.49. The first radiograph shows that the widthwise development of damage, in the dry specimen, consists of a set of well defined primary longitudinal and off-axis splits of about the same length. These are accompanied by delamination damage, triangular in shape, on either side of the notch. In the case of the wet specimen, second radiograph, only two well defined PLS are present along with some delamination which is contained within the notch tips. In this case no off-axis fibre splitting is evident. The proof loading induced damage in both wet and dry specimens appears to be very similar in nature to that obtained during fatigue loading, perhaps at a lesser number of fatigue cycles than 10^5; compare the first and second radiographs in figures 4.54 with the first two radiographs in figure 4.57. The only obvious difference between the fatigue and proof loading induced damage appears to be the lack of secondary fibre splitting and any delamination damage that is associated with it. A reasonable conclusion may be drawn from the above observation: the primary splitting is a result of the stress concentration of the notch and thus can be triggered by any substantial load, cyclic or not, whereas the secondary fibre splitting is a unique characteristic of the cyclic loading alone.

The effect of proof loading on the damage development of a pre-fatigued specimen is shown in the third radiograph of figure 4.57. It is clear that the only mode of further induced damage is delamination, shown by the darker area on the left hand side of the picture. It appears that the pre-existence of fibre splitting was responsible for the development of such delamination, following proof loading. Furthermore, it appears that the effect of pre-existing PLS was to suppress any further development of fibre splitting by neutralising the notch.

4.5.2 Destructive Examination

A preliminary understanding of damage initiation and propagation has been obtained by the use of the non-destructive methods as described above. However, the lack of adequate information on details such as the through-thickness position as well as the extent of the damage, and the state of the fibre/matrix interface, requires destructive examination. Three such techniques were employed; optical microscopy, scanning electron microscopy, and deply. The results from these examinations are presented below.

(a) Optical Microscopy

Relative to the other damage detection techniques, both destructive and non-destructive, this is the most time consuming method, due to to the lengthy specimen preparation procedure involved. However, this technique, when properly used, produces some very valuable information that would otherwise have been overlooked. Such information includes very fine fibre splits or matrix cracks and fibre breakages. This information is particularly important during the early stages of damage development in which case other techniques, X-ray for example, cannot detect the very fine detail. Furthermore, the microscopic technique can give a very clear indication of the through-thickness position of damage such as ply delamination, fibre splitting, and fibre fracture. An indication of the in-plane extent of the damage at a particular cross section can also be obtained.

At least one specimen per fatigue condition and stacking sequence has been examined microscopically. Some of the most important findings can be found in figures 4.58-4.60, for both the sharp notch and the circular hole. As explained in the section 3.6.2, two through-thickness sections were usually examined per specimen. For convenience, the section along the longitudinal direction will be referred to as section'A', and the one along the transverse direction will be referred to as 'B'. Both sections contain the notch tip line which on the actual micrographs of figures 4.58-4.60 is indicated by the two arrows.

Figure 4.58 consists of three micrographs from wet and dry stacking sequence A specimens. These micrographs represent typical through-thickness damage development from a sharp notch, after a small number (10^3) of fatigue cycles, at a load amplitude Ln. The first one is a micrograph of a dry specimen fatigue tested at RT. The picture belongs to a section 'A' which is approximately two ply thicknesses away from the notch tip, and located between the notch tip and the specimen's free edge. Four important points are depicted in this micrograph; the initiation of the POS; the delamination between the surface 45° and the 0° plies; the delamination between the 45° plies themselves which is contained within the POS; and the preferred accumulation of damage in the surface plies. The last two micrographs are from a wet specimen fatigue tested at 90°C. The first of the two pictures belongs to a section 'B', and shows the PLS in all three stacks of 0° plies. Some delamination between the 0° and the 45° plies is also evident, however, no SLS can be seen. The third picture belongs to a section 'A' that is located in an identical position to the section of the first micrograph (figure 4.58). It appears that some POS do develop in this (hot/wet) case, however, no delamination between the 0° and 45° plies is evident, at this particular section. Both the first and the third micrographs show the development of some very fine SOS.

A further development of fatigue damage in sharp notched specimens is depicted in figure 4.59 for stacking sequences A and B, tested at a load amplitude Ln. The first micrograph represents the fatigue damage development after 10^5 cycles in a dry specimen of type A, which was fatigue tested hot. The picture belongs to a section 'A' which is located about one ply thickness away from the notch tip line. The interesting features here are; the large delamination between the outer 0° and 45° plies, and the development of a rather large number of SOS. The second micrograph represents the damage development in a B type specimen tested in an identical fashion to that of the specimen in the first micrograph. The most important difference between the two micrographs is the 0° fibre fracture in the second one. This fibre damage appears to be a result of ply separation that initiated in the surface plies. The third micrograph allows a comparison to be made between the hot/dry and the hot/wet cases of type B specimens. It is clear that under the hot/wet condition the damage is less severe compared with the hot/dry case. However, some 0° fibre fracture in the outer ply did occur. In the case of type A specimens no fibre fractures were observed, at least up to 10^5 cycles.

An inside view into the fatigue damage development from a 5mm circular hole in different environments, at a load amplitude Lh, is shown in figure 4.60. The first micrograph is taken from a section 'B' and shows the state of damage in a dry specimen which was fatigue tested at RT for 10^3 cycles. There are two important features in this micrograph;

(1) the PLS that led to delamination between the 0° and 45° plies and,

(2) the initiation of 45° splitting, which appears in the micrograph in the form of very fine matrix cracks in the ±45° plies.

The delamination appears to be contained within two imaginary longitudinal lines tangential to the hole, whereas some very fine 45° splits appear to develop both within and outside these imaginary lines. A further stage of fatigue damage development (in the hot/wet condition) is shown in the second micrograph. At this stage a large amount of delamination between the 0° and the 45° plies is evident. Furthermore, a considerable amount of secondary splitting is also evident. In the case of dry specimens, under an identical condition, such splitting was even worse. The third micrograph represents the damage development after 10^6 cycles in a dry specimen. This picture is taken from a longitudinal section, which is located within the shaded region, shown in the fourth X-ray of figure 4.55. It appears that most of the damage is concentrated in the surface plies with a large amount of delamination both between the 45° plies themselves as well as between the 45° and the 0° plies.

(b) Deply

The microscopic examination is usually limited to the plane of the polished sections. Despite the large number of available sections, the microscopic examination, effectively, is a "two-dimensional" technique. In principle this technique can be made quasi "three-dimensional" by the process of consecutive regrinding and repolishing. However, when a large amount of different specimens have to be examined, such process is impractical. On such occasions the deply technique can be very useful indeed.

Deply is a relatively simple technique for determining a three-dimensional picture of the damage state in a laminated composite. A major drawback of this technique is related to the presentation of the results, since no ordinary photographic recording can be obtained. Examples of the uses and results from this method are presented in figures 4.61-4.65. These consist of hand drawn sketches of the observed damage modes in individual ply interfaces. The shaded areas represent delamination; the straight lines along the fibre directions represent fibre splitting; and the lines at angles other than those of the fibre direction represent fibre fractures. The fibre direction is indicated by the arrow on the top left hand corner of each box. Each box represents an individual off-axis ply, or a stack of two or three plies in the case of 0° layers. The numbers in the small boxes indicate the ply interface in each case. It has to be stated that, because the damage was studied mainly by eye, fine details could not be observed. Therefore damage such as secondary fibre splitting, for example, could not be identified.

Figure 4.61 shows the through-thickness distribution of fatigue damage state in a dry specimen tested at RT, at a load amplitude slightly higher than Ln, for 2 million cycles. It is interesting to note that after a large number of fatigue cycles, the through-thickness amount of damage appears to be quite uniform from layer to layer. Another interesting point is the randomness of the fibre fractures which are not associated with the notch tips. It appears that in the absence of delamination, fibre splitting in a 45° ply for example, may initiate fibre fracture in a neighbouring 0° stack of plies and vice versa: see the eighth and ninth boxes, in figure 4.61, and note the 45° fibre fracture in the 0° plies. This is a good example of the influence of ply coupling on damage development.

A comparison of the fatigue damage development between the stacking sequence A and B, in the hot/wet condition, is demonstrated in figures 4.62 and 4.63, respectively. The damage development in these particular specimens has also been investigated by C-scan (figure 4.47) and X-ray (figure 4.56) techniques. It was established by the previous methods that the major difference in the damage

development in the two stacking sequences is the direction in which the fatigue damage propagates. The preferential path of damage propagation for the type A specimen is along the longitudinal direction, whereas for B it is in the transverse direction. Moreover, figures 4.62 and 4.63 suggest that there is an additional difference in the through-thickness development of damage. In the case of stacking sequence B, more damage appears to accumulate in the surface plies compared with the sequence A. A similar effect was also observed in other test conditions, which indicates that there is a difference in the way the applied load is transferred and distributed through the thickness of each stacking sequence.

A typical through-thickness damage distribution in a specimen with circular hole is shown in figure 4.64. It is clear that even at a relatively high load amplitude (35kN), the damage is controlled by the primary longitudinal fibre splits. The main area of delamination appears to occur in the longitudinal direction also and is mainly located within the ply interfaces of 0° and 45° plies. Some small transverse delamination damage is also evident. Figure 4.65 shows the proof loading induced damage distribution in a specimen with circular hole. This specimen is in fact the one shown in the third family of C-scans in figure 4.51. It appears that the overall damage distribution is very similar to that shown in figure 4.64. The interesting point in figure 4.65 is the initiation of final fracture from a point well away from the hole. Moreover, fracture has initiated in the stack of three 0° plies and it was transmitted into the adjacent 45° plies; see the first three sketches in figure 4.65.

(c) Scanning Electron Microscopy

This technique was employed in order to assess the state of the fibre/matrix interface as well as the matrix itself. At least one specimen per environmental condition was examined in this way.

Typical fractographs for the full range of environmental test conditions can be found in figure 4.66. It is evident that the fibre/matrix interface is attacked by moisture and/or heat. In the first fractograph (RT/dry) for example, all fibres are fully covered in matrix, whereas, in the rest, naked fibres can be seen, even at RT (second fractograph). Some degree of matrix plasticisation with moisture and/or elevated temperature can also be found; see for example the third fractograph, 90°C/dry case. Furthermore, the fourth and fifth fractographs suggest that both the state of the matrix and the fibre/matrix interface are very similar, in these two conditions. Such moisture/temperature equivalence has also been brought out by the notch tensile strength results; see section 4.3.2.

4.6 FINITE ELEMENT ANALYSIS

It has been shown through the damage evaluation techniques that environment affects damage development both under dynamic and proof loading. Any numerical indication of the stress distribution around the notches that can be substantiated by the observed behaviour may contribute to our understanding of the damage mechanisms. However, laminated composite are very complex materials and ordinary stress analysis methods, for example, the theory of orthotropic plates, are inadequate for the determination of the stress state near a stress concentration in a composite plate. Even a very thin composite will generate a three dimensional through-thickness stress state near a cut-out under in-plane loading. Furthermore, non-linear elastic properties, such as G_{12} constitute a further degree of complexity.

In the present study the task of a numerical evaluation of the stress state around the notches has been undertaken in a two part complementary programme. In the first part the elastic material constants, for the composite system used, were determined experimentally, see section 4.3.1. In the second part a three dimensional finite element analysis, FEA, was carried out, for both notch geometries and for both wet and dry material, at RT. It was the original intention that such analyses be carried out for elevated temperature conditions too. However, due to time constraints, this was not possible. For this analysis the Imperial College's standard finite element program "Finel" was used. A three dimensional, twenty node, isoparametric, brick element was chosen from the Finel element library. In order to apply this analysis efficiently to the composite material several assumptions were made:

(a) the laminated composite consists of homogeneous orthotropic layers,

(b) each orthotropic layer is linear elastic, under a generalised Hooke's law,

(c) the elastic properties of each orthotropic layer in tension are the same as the corresponding properties in compression,

(d) there exists a three plane symmetry that could allow the one eighth of the composite specimen coupon to be modelled,

(e) in the unloaded state the material is stress free (ie the residual curing stresses were not accounted for in the analysis) and,

(f) the sharp notch may be represented by an ellipse of tip radious of curvature equivalent to that of the sharp notch.

For an efficient use of computer time an appropriate mesh was designed so that an acceptable accuracy could be obtained from a minimum number of elements. The meshes for the sharp 10mm notch and the circular 5mm hole (of stacking sequence A) are shown in figures 4.67 and 4.68 respectively. In both cases, the area around the stress raiser was modelled with one through-thickness element per individual ply (or stack of identical plies). Loading was simulated by an applied unit displacement at the "free end" of the structure. The results were obtained in the form of nodal displacements as well as average nodal stresses; three displacement components and six stress components per node were obtained. In order to be able to compare the stress results directly from "wet", with the ones obtained from the "dry" model analysis, all stress results from the "wet" model were appropriately normalised (multiplied by a constant) so that the remote stress fields (at the loaded end) in both cases were made identical. The displacement results were also normalised in the same way. All distance values are in mm and the stress values are in GPa. However, in a linear elastic analysis such as this, it is the relative value of stress that matters rather than the actual calculated value. Therefore, in the presentation of the results below, no units of stress are quoted.

4.6.1 Sharp 10mm Notch.

The deformed shape for the "dry" sharp notch is shown in figure 4.69. The close-up view of the deformation indicates that the most severe deformations are related to the notch tip and the 0°/45° ply interfaces. Detailed examination of the deformed shape failed to reveal any significant differences between the "wet" and "dry" models. This is of course a direct result of the combined effect of;

(a) the small difference in the measured elastic constants between the wet and the dry materials, see table 3, and,

(b) the fact that a linear analysis does not take into account the large difference in G_{12}, between the wet and the dry material, which takes place at about 1% shear strain, see table 3.

Even so, some small differences in the peak (average) nodal stress values between "wet" and "dry" cases were observed near the notch tip. One of the most significant differences was a 2.3% reduction in the out-of-plane direct stress, σ_z, when the material was wet. This occurred at a point 0.05mm to the left of the notch tip line in the surface (top) layers, see figure 4.70. The variation in this particular peak

stress is thought to be significant since this is one of the main contributors to the observed delamination damage.

The through-thickness distribution of the stresses near the notch tip of a "dry" specimen is shown in figures 4.71 and 4.72. The direct components of stress σ_x, σ_y and σ_z are indicated by the letters A, B and C respectively; likewise, the shear stresses σ_{xy}, σ_{yz}, and σ_{xz} are indicated by the letters D, E, and F respectively. Furthermore, the abscissa of these plots corresponds to the direction (3), see figure 4.70. It is interesting to note that right at the notch tip a very large proportion of the applied stress, σ_x is carried by the 0° plies, figure 4.71. In contrast, at a very small distance away from the notch tip (towards the specimen's free edge), the 45° plies appear to carry a relatively larger proportion of σ_x, figure 4.72. In fact this figure can be misleading in suggesting that the 45° plies carry more longitudinal load than the 0° plies do; this is a result of the lack of a node in the middle of the element at that particular position (line through the thickness) of the plots; thus a peak value of stress occurring at the mid-point of the stack of three 0° plies will not be registered. Indeed figure 4.73 suggests a value of 28 units of stress in the middle of the stack of the three 0's, rather than the 6 units indicated by plot A of figure 4.72. In any case, figure 4.72 has been presented in order to show the dramatic changes in the distribution of σ_x which occur within a distance of only 0.05mm (less than half a ply thickness) from the notch tip.

The stress concentrating effect of the sharp notch is depicted in figures 4.73-4.80, each one demonstrating the variation of an individual component of stress for a given through-thickness location, along the plot directions (1) or (2), as defined in figure 4.70. Figures 4.73-4.75 for example, show the variation of σ_x with the distance from the notch tip. In all three cases a large value of stress at the tip is very rapidly reduced down to a more or less uniform value at about 2.5mm away from the notch tip. The rate of decrease of stress with increasing distance from the notch tip depends upon the fibre orientation in a particular ply. On some occasions the maximum value of σ_x is reduced to a near uniform value within a distance corresponding to less than a ply thickness, figure 4.73. In contrast figure 4.74 shows a smoother variation of σ_x with distance from the notch tip. This is thought to be due to the difference in the degree of anisotropy between the 0° and the stack of ±45° plies. Moreover, this phenomenon is thought to be responsible for the observed difference in the through-thickness distribution of σ_x which was demonstrated (above) by figures 4.71 and 4.72.

If a stress concentration factor, SCF, is defined as the ratio of the maximum value of a stress component (at the notch tip) to the value of the same stress component at a point away from the notch tip region where a uniform state of stress

exists, then a very rough estimate of the magnitude of this factor can be obtained from the plots of σ_x versus the nodal distance, corresponding to a particular stack of plies or a ply interface. Such estimates from the different plots are: 25 times for the stack of three 0° plies (figure 4.73); 25 times for the 45° plies (figure 4.74); and 20 times for the 45/0° ply interface (figure 4.75).

Examples of the other in-plane stress component variation around the notch tip area are shown in figures 4.76-4.78. Figures 4.79 and 4.80 show the variation of the out-of-plane component of stress, σ_z, along the directions (1) and (2) respectively (figure 4.70). These plots are situated in the second (from the top) 0/45° ply interface. It appears that a relatively large increase in stress occurs very close (within less than one half of a ply) to the notch tip. This behaviour was found to be typical of all through-thickness positions.

4.6.2 Circular 5mm Hole

The deformed shape for the "dry" circular hole, which is also typical of the "wet" case, is shown in figure 4.81. A close-up view of the "hole tip" indicates that unlike the sharp notch this area is relatively undeformed. Instead, the largest deformations have been recorded in the interior of the hole as indicated in the top half of figure 4.81. Likewise, some of the average peak values of stress occurred within the hole free edge rather than near the "hole tip".

An example of the through-thickness stress distribution for all stress components at the "hole tip" is shown in figure 4.82. On comparison with the corresponding figure for the sharp notch (4.71) it is made clear that in the case of the hole, σ_x is the only dominant stress. Furthermore, this is carried exclusively by the 0° plies: only a very small proportion of this stress is carried by the 45° plies. This is thought to be an important point since it implies that the large deformation observed near the tip of the sharp notch (figure 4.69) is a result of the complex loading, in the relatively flexible 45° plies, which consists of more than one, significant, component of stress (σ_x and σ_y), as figure 4.71 suggests.

Examples of the in-plane distribution of stress, for individual stress components, at a given through-thickness location are shown in figures 4.83-4.89. Figures 4.83 and 4.84 show the variation of σ_x, along the plot direction (1) (see figure 4.70 which applies to the circular hole as well as the sharp notch). It is apparent that there is a gradual reduction in stress from a peak value at the "hole tip" to a near uniform value at a distance of 5mm away from the tip. A rough estimate for the SCF is 4, for the 45°/0° ply interface (figure 4.83), and 4, for the 0° ply (at Z=0.00, see figure 4.70). Figures 4.85 and 4.86 show the variation of σ_y and

σ_{xy} respectively. It is interesting to note that the peak stress value does not occur at the "hole tip": instead it occurs at a point about 1mm away. This is in fact the point of intersection (in the plane of the specimen) of two mutually perpendicular tangents to the hole, oriented at ±45° to the loading direction.

The out-of-plane variation in stress (σ_z) is depicted in figure 4.87 for the plot direction (1) and 4.88-4.89 for the plot direction (2), see figure 4.70. Figure 4.87 shows the in-plane variation of σ_z which apart from the sign of the peak value, appears to be very similar to that obtained in the case of the sharp notch, figure 4.79. On the other hand, figures 4.88 and 4.89 show that the "tilde" like variation of the σ_z value along the hole interior is very much different in nature to that obtained in the case of the sharp notch, figure 4.80: in the case of the hole there are two peak values rather than one; one at the "hole tip" and the other at the "12 o'clock" point.

5. NEW MATERIALS

5.1 INTRODUCTION

It is well known that the mechanical behaviour of composites depends, amongst other factors, upon the behaviour of the individual constituent materials. Thus any experimental programme with the aim of understanding a certain mechanical behaviour should include more than one material system. In the present research work four material systems were included; one primary (XAS/914C), and three secondary.

The fatigue behaviour of the primary material system was thoroughly investigated in the main programme; the investigation included variation in stacking sequence, notch type, and level of moisture conditioning (see chapter 3). The fatigue behaviour of the secondary material systems is briefly investigated in a supporting (the present) programme. The objective of the present programme is to substantiate and enrich our understanding of the fatigue behaviour born by the study of the primary (standard) material system. Therefore, the secondary systems were so chosen, each one possesing at least one unique characteristic, hoping that an unforeseen behaviour could be brought about. The three new material systems are;

(1) Ciba Geigy 6376C-T400-5-34%, T400 carbon fibres in 6376 epoxy matrix: this is a thermoset system and is cured in a similar fashion to the standard (914C) system, thus expected to exhibit a similar residual stress state following curing. Furthermore, the hygrothermal behaviour of this system is thought to be similar to the standard one. The main qualities of this system are; toughened matrix, and high strain to failure fibres.

(2) ICI APC-2, AS4 carbon fibres in PEEK matrix: this is a thermoplastic-matrix system and requires a much higher moulding temperature than the thermoset based systems, thus expected to produce higher residual curing stresses: qualities include, environmental resistance, tough matrix, and high strain to failure fibres.

(3) BP R25/2-T300B, T300B carbon fibres in toughened bismaleimide matrix: this system has a thermoset matrix, which is cured at a rather higher temperature than the epoxies (195°C as compared with 175°C). This material is expected to be as sensitive to moist environment as the epoxies are. A major advantage of this system, over the other three, is the high (up to about 200°C) operating temperature. However, at lower temperatures this material is expected to be very brittle.

5.2 EXPERIMENTAL PROGRAMME

The experimental programme described in chapter 3 applies to the primary system only. However, the same apparatus and experimental techniques were utilised in the investigation of the fatigue behaviour of the new material systems. The tension-compression fatigue performance of all three material systems was briefly investigated in both the dry and the wet conditions. Half of the total amount of the available specimens (per system) was stored dry (see section 3.2.4) and the remainder wet. Only one "wet condition" was employed, 60°C/84% RH (see section 3.2.4). Specimens of stacking sequence A with sharp 10mm notches were investigated, in a selection of environmental combinations depending upon the individual material system and the number of available specimens in each case. In general specimens were fatigue tested at RT or 90°C, for 10^5 cycles at a cyclic load amplitude Ln (=20kN). Fatigue tests were usually followed by damage evaluation and residual strength determination; both the tensile and compressive residual strengths were evaluated for two test temperatures RT, and 130°C. At least two specimens were tested in each case.

Some damage evaluation techniques were employed in order to assess the fatigue damage and/or the state of the matrix material. These include C-scan, X-ray, and microscopic examination. As in the case of the standard material the C-scan technique was extensively used for an initial assessment of damage as well for the appropriate grouping of specimens prior to residual strength testing, see section 4.4.1. Based on the initial C-scan damage evaluation a typically damaged specimen per fatigue condition was then X-rayed. Non-destructive examination was also performed on specimens which were fatigue tested, at RT, beyond 10^5 cycles, usually 10^6 cycles; furthermore, on some occasions the effect of the load amplitude upon the damage development was also evaluated. Optical microscopy was very rarely used in this part of the programme. The most extensively applied destructive examination technique was fractography: pieces from fractured, statically tested, notched specimens were removed and examined under the SEM as described in section 3.6.2: at least one specimen per condition and material system was examined in this way. The deply technique was not used at all.

5.2.1 Toughened Epoxy Matrix

Thirty square metres of 6376C pre-preg was supplied by Ciba Geigy Plastics: 16 ply symmetric 2x300x530mm panels were layed-up in stacking sequence A; $(\pm 45°/0_3°/\pm 45°/0°)_S$. These were then cured and post-cured according to the manufacturer's recommended cycles: ten such panels were fabricated which

gave 100 notched (50x250mm) and 20 plain (25x250mm) specimens. The experimental programme was divided into two major parts the static and the fatigue tests which are briefly summarised in figure 5.1.

(a) Static Tests

Static tests were carried out on both plain and notched specimens. Plain specimens were tested in tension at RT, as described in section 3.3.1. However, notched specimens were tested in both tension and compression in a range of test temperatures, RT, 90°C and 130°C. Two notched specimens were tested in each case. A total number of 24 notched specimens were tested in this part of the programme.

(b) Fatigue Tests

Notched specimens were fatigue tested in tension-compression for 10^5 cycles at a load amplitude Ln (=20kN). Four environmental combinations were investigated; RT/dry, RT/wet, 90°C/dry, and 90°C/wet. At least nine specimens were fatigue tested in each condition. Residual strength tests were performed in tension and compression at RT, and 130°C. The remaining specimens were fatigue tested in tension-compression at RT to failure; several tests were interrupted and the fatigue damage assessed; a number of constant load amplitude cases were investigated.

5.2.2 Thermoplastic Matrix

Eight 2x300x300mm APC-2 panels of stacking sequence A were kindly supplied, free of charge, by the manufacturer, ICI. These were cut into 56 notched (50x250mm) and 14 plain (25x250mm) specimens. A summary of both static and fatigue tests can be found in figure 5.2.

(a) Static Tests

Unnotched static strength tests were performed in tension and at RT only. Notched specimens were tested both in tension and compression at RT, and 130°C. Due to specimen shortage, 130°C tests were performed only on dry specimens. A total of 12 notched specimens were tested in this part of the programme.

(b) Fatigue Tests

Notched specimens were fatigue tested for 10^5 cycles at the standard load amplitude Ln, in the environmental conditions; RT/dry, RT/wet, 90°C/dry, and

90°C/wet. At least nine specimens were fatigue tested in each condition. Residual strength tests were performed in tension and compression at RT, and 130°C.

It has been noted in the published literature that PEEK based composite materials are more strain-rate sensitive than epoxy based composites: therefore, a small complementary experimental programme was set up in order to investigate the effect of frequency upon fatigue damage development. In addition, a small number of zero-tension, and zero-compression fatigue tests were performed in order to establish the cause of a certain unique damage mechanism, which appeared during the tension-compression fatigue tests.

5.2.3 Bismaleimide Matrix

Forty square metres of R25 pre-preg was kindly supplied, free of charge, by the manufacturer, BP Advanced Composites. Initially a 16 ply 300x300mm unidirectional panel was layed-up and cured. Within the limitations (heating rate) of the autoclave the manufacturer's recommended cycles for temperature and pressure was followed as close as possible. Following postcuring, several test pieces were removed for RT ILSS tests. The results were compared with the manufacturer's quoted value of ILSS (for identical sized specimens), so that the curing quality could be assessed. The average result indicated that the measured ILSS was 4.7% lower than the manufacturer's corresponding quoted value which was thought to be acceptable. Following the preliminary test, six 2x460x530mm panels with stacking sequence A were fabricated. These panels were divided into 90 notched (50x250mm) and 20 unnotched (25x250mm) specimens. The test procedure for these specimens is briefly summarised in figure 5.3.

(a) Static Tests

Plain specimens were assessed in tension at RT only. Notched specimens were tested in both tension and compression at three test temperatures; RT, 130°C, and 200°C. Two notched specimens were evaluated in each case, resulting in a total of 24 specimens.

(b) Fatigue Tests

Notched specimens were fatigue tested in tension-compression for 10^5 cycles at a load amplitude Ln (=20kN). A total of four environmental combinations were investigated; RT/dry, RT/wet, 90°C/dry, and 90°C/wet. At least nine specimens were fatigue tested in each condition. Residual strength tests were performed in tension and compression at RT, and 130°C. Due to time constraints fatigue tests to

failure were not performed; however, the fatigue damage development has been assessed in tests involving fatigue cycles beyond 10^5 and/or load amplitudes other than Ln (=20kN).

5.3 EXPERIMENTAL OBSERVATIONS

The experimental results (static and residual strength values) for the new materials were reduced in the same way as the results for the standard system (see section 4). These are presented individually, for each material system, below.

5.3.1 Toughened Epoxy Matrix

(a) Moisture Conditioning

The moisture absorption characteristics of the 6376C system, under the hot/wet environment (60°C/84% RH) are shown in figure 5.4: the weight changes have been monitored through three traveller specimens, two 50mm wide and one 25mm wide. It appears that a 1.0%, by weight, equilibrium level was reached after about 6 months. As in the case of 914C, there is a difference in the moisture absorption characteristics between the 25mm and the 50mm wide specimens, due to the thickness difference between the two specimen geometries, (see section 4.2)

(b) Static Tests

The static tensile test results for the unnotched specimens are shown in table 38. These results appear to be in agreement with the equivalent results for the standard system; ie the wet specimens appear to be marginally stronger (3.6%) than the nominally dry specimens.

The notched static strength results for both tension and compression can be found in tables 39 and 40. In general, it appears that all the observations which applied to the standard system (914C), also apply to the toughened system: ie the tensile strength increases with temperature and/or moisture, whereas the contrary is true for the compressive strength.

The fractured surfaces appeared to be very similar in nature to those of the standard system, thus no further examples are presented here.

(c) Fatigue and Residual Strength Tests

Initially fatigue tests were performed in tension-compression at a normalised load amplitude Ln√(10/2a), where √(10/2a) is the normalisation factor (see section 4.3.1). For the dry material, this load amplitude corresponds to a remote strain amplitude of about 0.24%, see figure 5.5(a); this represents the adjusted value corresponding to an average specimen thickness of 2.14mm: five 2x25x250mm specimens were used for the determination of the stress-strain response. Following fatigue testing (for 10^5 cycles), specimens were then statically tested in tension or compression. The residual strength results can be found tabulated in tables 41-44, for both dry and wet specimens. These results are also summarised in the form of histograms of average strength against test condition in figure 5.6: for the purpose of comparison the notched static strength values are also included. The effect of fatigue loading on residual strength is depicted in figure 5.7, where the percentage variation in residual strength (from the corresponding static value) is shown for each test condition. It appears that fatigue loading had a largely beneficial influence on the residual strength: this is particularly true in the case of compression where a near 60% improvement in strength has been obtained in the 130°C test case.

Fatigue tests to failure were performed on both dry and wet notched specimens. The data from these tests can be found in tables 45 and 46 for nominally dry and wet specimens respectively; the results were reduced as described in section 4.3.2. The results are also presented in the form of S-N plots in figure 5.8. The corresponding average notched static compressive values are also included in the plots. Excluding the points which correspond to the static values, all other points per condition (dry or wet) appear to lie on a straight line. The basic difference between the dry and wet cases is that the line through the "wet points" is shallower than the one through the "dry points". This indicates that the long term fatigue behaviour of the wet material is marginally superior to the dry material.The superiority of the wet material becomes even more apparent in a plot of normalised stress amplitude, with respect to the static compressive strength, versus the fatigue life, figure 5.9.

(d) Damage Evaluation

Following the initial C-scan damage evaluation, typically damaged specimens were then X-rayed. Examples of the fatigue damage state and/or development can be found in the radiographs of figure 5.10. The fatigue damage, under the same conditions, in 6376C appeared to be similar in nature to that in the standard system, compare figure 5.10 with 4.54. The only difference is a suppression of matrix damage. This is not surprising since the 6376 is a tougher epoxy than the 914. Comparing the 10^6 cycle cases in figure 5.10 (third and sixth micrographs), it is made clear that a supression of matrix damage occurs when the material is wet. This

may be a result of residual stress reduction or a further matrix toughening due to moisture content or a combination of the two. In such cases the effect of the fibre/matrix interface must not be disregarded; any changes in the interface may be reflected as apparent matrix toughening: a poor fibre/matrix interface may obstruct the transfer of load from the fibres to the matrix thus reducing the matrix loading, and hence matrix damage. Figure 5.11 shows that indeed the fibre/matrix interface has been attacked by moisture (compare the top two fractographs): it also shows that at elevated temperatures, and in particular when the material is wet, the fibre/matrix interface is weakened even further.

5.3.2 Thermoplastic Matrix

(a) Moisture Conditioning

Figure 5.12 shows a plot of moisture content versus the square root of time. The weight was monitored through three traveller specimens, two 50mm wide and one 25mm wide. It appears that under an identical environment the thermoplastic system absorbed a negligible amount of water in comparison with the epoxies. A moisture equilibrium level of about 0.12% (by weight) was reached after about three months of conditioning under the hot/wet environment (60°C/84% RH). It is interesting to note that, unlike the epoxy based systems, the moisture level in the 25mm wide specimens appears to be marginally higher than the moisture level in the 50mm wide specimens. This is due to the fact that the actual 25mm wide traveller specimen had a larger average thickness than the 50mm wide traveller specimens.

(b) Static Tests

The static tensile tests results for the unnotched specimens are shown in table 38. As with the epoxy based systems, an increase (1.2%) in strength has been observed when the material was tested wet. This indicates that, no matter how small the moisture content may be, its effect is reflected in the material's mechanical strength.

The notched static strength results are summarised in tables 47 and 48. There are two points worth noting here. The first is the small but consistent (with the other material's observed behaviour) effect of moisture content upon strength. The second is the detrimental effect of heat (130°C) upon the tensile strength, see table 47. Note that, in the case of epoxy based systems there was an increase in the notched tensile strength, from RT to 130°C, of 8.5% and 26.1% for 914C and 6376C respectively: see tables 4 and 39.

Typical static tensile fractures, for both wet and dry specimens, are shown in the first two pictures of figure 5.13. Comparing these with the fracture modes in the epoxy system 914C, figure 4.10, it becomes immediately obvious that there is an equivalence in the fracture mode of the APC-2 specimen tested at RT and the epoxy specimens tested at either 130°C/dry or 90°C/wet. This indicates that the matrix in either system must be in a similar state: ie the APC-2 at RT is as plastic as the dry 914C at 130°C or the wet 914C at 90°C. A distinctively different failure mode was obtained when the APC-2 specimens were tested at 130°C; compare the second picture in figure 5.13 with the first picture in figure 4.19. It would appear that at this temperature the shear strength of the APC-2 is seriously degraded which resulted in a rather low tensile strength. Note that due to the relatively low failure load no delamination has initiated: an additional reason for the suppression of delamination damage may be due to the fact that the PEEK matrix is tougher than the ordinary epoxy, 914.

Examples of static compressive fracture modes are shown in the first two pictures of figure 5.14. It appears that even at RT the specimens fail without extensive delamination. This type of fracture compares very well with the one obtained during the high temperature testing of the epoxy systems, see figure 4.14: again, this indicates that the state of the PEEK matrix at RT is similar to the state of the 914 matrix at high temperatures.

(c) Fatigue and Residual Strength Tests

Tension-compression fatigue tests were performed at a normalised load amplitude Ln (=20kN), see section 4.3.1, for 10^5 fatigue cycles. For the dry material, Ln corresponds to a remote strain amplitude of about 0.26%, see figure 5.5(b); this represents the adjusted value corresponding to an average specimen thickness of 2.03mm: four 2x25x250mm specimens were used in the tests for the determination of the stress-strain curve. Residual strength tests were then carried out at RT or 130°C. The results from these tests for both tension and compression are summarised in tables 49-52. These are also plotted in the form of histograms of average strength versus test condition in figure 5.15: the static strength results are included also. The effect of fatigue loading on residual strength is demonstrated in figure 5.16, where the percentage variation in residual strength is plotted for each test condition. It is made clear, in figure 5.16, that fatigue loading (at the particular load amplitude, Ln, and number of fatigue cycles, 10^5) had a beneficial effect on both tensile and compressive residual strengths; increases in strength of 30% to 50% were recorded.

Typical tensile fracture modes of fatigue tested specimens are shown in figure 5.13. It is interesting to note the lines of plastic deformation on the surface of the hot tested specimen. Such damage has only been observed in APC-2 specimens. It appears that this was caused by excess matrix plasticity as a result of the high test temperature, compare the two last photographs of figure 5.13. A typical compressive failure mode of fatigue tested specimens is presented in the third photograph of figure 5.14: this shows that the fatigue damage had only a small effect on the final failure, compare the first with the third photograph of figure 5.14.

(d) Damage Evaluation

The radiographs of figure 5.17 show typical examples of the fatigue damage state and/or development in various environmental conditions: all tests were carried out in tension-compression at a constant load amplitude Ln (=20kN). There are three points worth noting in this figure: the first is the insensitivity of APC-2 to the hot/wet environment; the second is the slow rate of damage development, compare the first with the third radiograph; and the third is an additional, unique to APC-2, mode of damage. This occurred in the surface layers at right angles to the 45° fibres in the form of a line of plastic deformation (crease) which initiates at the notch tip and extends for about one specimen thickness. Such damage was typical of all fatigue conditions and it looks like the damage in the fourth specimen of figure 5.13. In the radiographs of figure 5.17, this damage appears as a 45° split.

So far as the insensitive behaviour of the material to the hot/wet condition is concerned, the drying out of moisture during the hot testing of the wet specimens should not be disregarded: It is only logical to assume that after a short period of fatigue testing at 90°C, the small amount of moisture (0.12%) present in the wet specimens would have dried out completely. Due to time constraint an assessment of the drying-out time could not be performed.

In order to establish the cause of the crease-like fatigue damage, a series of short tests were performed at RT. Initially two specimens were tested in either zero-tension (0-T) or zero-compression (0-C) at a load amplitude Ln (=20kN), at a frequency of 20 Hz, for 10^5 cycles. The resulting fatigue damage is shown in the two top radiographs of figure 5.18: it is apparent that neither of the two cases produced the crease-like damage mode.

In further tests, another two specimens were fatigue tested in either 0-T or 0-C, at a load amplitude Ln but, at a frequency of 30 Hz, for $2x10^5$ cycles. The purpose of these tests was to establish whether a peak shear stress was responsible for the observed crease-like damage. it was thought that if a peak shear stress

develops at every positive or negative applied maximum stress then, for every 10^5 tension-compression (T-C) fatigue cycles there are $2x10^5$ peaks of shear stress. Furthermore, it was anticipated that the cause of damage may be frequency related, thus the test frequency in the 0-T and 0-C was increased to 30 Hz so as to simulate a near similar rate of loading that occurs in the T-C case. The results from these tests are shown in the third and fourth radiographs of figure 5.18. Again there is no sign of the crease-like damage mode.

A further, brief, assessment of frequency has been carried out through fatigue testing in T-C at Ln for 10^5 cycles: two specimens were tested at a frequency of 0.3 Hz; subsequent damage examination revealed no difference in damage development between the 0.3 Hz and the 20 Hz (standard frequency) tested specimens, see the two bottom radiographs in figure 5.18.

From the above series of tests it has been established that the frequency is not responsible for the observed crease-like damage mode. Furthermore it has been shown that this unique damage is typical of reversed (T-C) fatigue loading alone: it would therefore appear that a shear stress reversal could be responsible for the observed damage. The answer to why the crease-like damage is unique to APC-2 will be presented in the next chapter, when a full comparison between the four material systems will be made.

Typical results from the fractographic analyses, of statically tested notched specimens, are shown in figure 5.19. These indicate that, under the same temperature conditions, the state of the fibre/matrix interface of the dry material is similar to that of the wet; compare the first two fractographs. The third fractograph shows a mild fibre/matrix interfacial degradation and the fourth shows the extensive plasticisation of the matrix at 130°C.

5.3.3 Bismaleimide Matrix

(a) Moisture Conditioning

The moisture absorption characteristics of the R25 system, under the 60°C/84% RH environment are shown in figure 5.20. The weight was monitored through three traveller specimens, two 50mm wide and one 25mm wide. It appears that an equilibrium level of just over 1.0%, by weight, was reached after about two months, although a moisture content of about 0.9% was reached after as little as two weeks.

(b) Static Tests

The static tensile test results for the unnotched specimens are shown in table 38. Of all four material systems, R25 exhibited the lowest plain tensile strength. Like the other three systems the wet R25 specimens were marginally stronger (2.2%) than the nominally dry specimens.

The notched static strength results for both tension and compression can be found in tables 53 and 54 for dry and wet specimens respectively: the R25, being a high temperature system, has also been evaluated at 200°C, the recommended maximum operating temperature. The trend of results, in the range of temperatures between RT to 200°C, appears to be similar to that of epoxies in the temperature range RT-130°C: ie the tensile strength increases with temperature and/or moisture, whereas the contrary is true for the compressive strength. It is important to note the detrimental effect of moisture and temperature on the notched compressive strength; at the maximum operating temperature of 200°C the compressive strength of the wet specimens has been reduced by as much as 53.6% when compared with the corresponding RT/dry value. The equivalent reduction in compressive strength for the epoxy systems, evaluated at their maximum operating temperature of 130°C, was 41.9% and 38.7% for 6376C and 914C respectively.

Examples of tensile fractures for notched specimens are presented in figure 5.21. A unique feature, to R25, is the excess fibre splitting. Even when tested wet at 200°C the material appeared to develop fibre splitting in the surface 45° plies: this may be contrasted to the behaviour of the other material systems; eg compare the fourth picture in figure 5.21 with the first and second pictures in figures 4.19 and 5.13 respectively. In general R25 exhibited a large fracture area which extended a long distance away from the vicinity of the notch. This indicates that extensive longitudinal fibre splitting must be responsible for blunting the notch and driving the damage in the longitudinal direction; note the 45° fibre fractures that lie on a longitudinal line which is approximately tangent to the notch tip, centre pictures in figure 5.21. Fibre splitting also developed during compression, figure 5.22. Even though there was some evidence of damage suppression with increasing test temperature, the straight line, clean type, of fracture that was previously obtained in the other material systems, was not observed; compare figures 4.14 and 5.14 with 5.22. It appears that, even in the 200°C/wet condition the R25 exhibits a brittle-like behaviour.

(c) Fatigue and Residual Strength Tests

Notched R25 specimens were fatigue tested in tension- compression at a normalised load amplitude Ln (=20kN), for 10^5 cycles. For the dry specimens, Ln

corresponds to a remote strain amplitude of 0.24%, see figure 5.5(c); this represents the adjusted value corresponding to an average specimen thickness of 2.25mm: four 2x25x250mm specimens were used for the determination of the stress-strain response. Subsequent residual strength tests were performed at RT and 130°C; the results, for both dry and wet specimens, can be found in tables 55-58. These are also plotted in the form of histograms of average strength versus test condition in figure 5.23. The effect of fatigue loading on residual strength is demonstrated in figure 5.24. It is evident that fatigue damage had a beneficial influence on tensile strength. In contrast, under several test conditions, a detrimental effect on compressive strength was recorded for the dry specimens.

Typical tensile fractures of fatigue tested specimens are shown in figure 5.25. It appears that in general, fatigue damage, had only a very small influence on the final failure since both fatigued and unfatigued specimens exhibited a similar mode of tensile fracture, compare figure 5.21 with 5.25. The same was also true in compression, figure 5.22, compare the first with the third specimen.

(d) Damage Evaluation

Typical examples of fatigue damage in the various environmental conditions are shown in the radiographs of figure 5.26. All tests were carried out in tension-compression at a constant load amplitude. It is obvious that so far as fatigue damage is concerned, the R25 material system is very sensitive to environmental changes. In general the nature of the fatigue damage appears to be similar to that observed in epoxy-based material systems. Perhaps the only basic difference between the R25 and the epoxy systems is the larger amount of fibre splitting, as well as damage area, in the R25 specimens.

Figure 5.26 shows that in general, the effect of moisture was to suppress the fatigue damage, compare the two radiographs on the left hand side; however, temperature had an opposite effect, compare the first two radiographs. Like in the case of epoxy systems, the combined effect of moisture and temperature was to cause a change in the overall fatigue damage mode, from a butterfly like shape to an oblong shape. The third micrograph suggests that the main effect of fatigue cycles was the promotion of multiple secondary longitudinal and off-axis fibre splitting. As in the case of 914C (figure 4.54), the effect of lower load amplitude was to encourage longitudinal damage propagation, see the last radiograph in figure 5.26.

Fractographic analyses of statically tested notched specimens revealed that the dry material had a good fibre/matrix interface, first picture in figure 5.27: however, the second picture shows that the matrix in the dry state is very brittle.

The third and fifth fractographs indicate that the fibre/matrix interface is degraded with increasing temperature; the fourth and sixth fractographs show that the same is true for the wet specimens, which appear to exhibit an increased degree of interface degradation; it is evident that at the limiting operating temperature, of 200°C, the fibre/matrix interface of the wet material is seriously degraded, see sixth fractograph.

6. DISCUSSION

6.1 INTRODUCTION

The chapters above have so far been of informative nature, with the intention of introducing the reader to the problem of fatigue in composites, the implications of the environment, and the objectives of the present work: such matters have been addressed in chapters 1 and 2. In chapter 3 the reader was guided through the experimental programme and methods, and in chapters 4 and 5 the results from the main and secondary programmes respectively were presented.

The ultimate objective of any research work dealing with the fatigue response of composite materials is the prediction of the long-term structural integrity of such materials. However, it would appear pointless to even attempt to predict the long-term response without the appropriate knowledge of the exact nature of damage mechanisms and their interaction with the operating environment which may seriously affect the residual strength and/or fatigue life.

In the present chapter the results from the various studies such as damage evaluation, strength determination, and computational analyses, will be linked together so as to form the foundation for a basic understanding and characterisation of the fatigue damage mechanisms in notched laminated fibre reinforced composites. Furthermore, an attempt will be made to identify a physical parameter which relates to a material's fatigue performance and internal microstructure. Based on this characteristic parameter a simple screening test will be proposed that would allow a fatigue tolerant material system and/or stacking sequence to be isolated from a number of possible candidate materials, using a single non-destructive examination technique.

For clarity, the results from the main and secondary experimental programmes will be discussed separately. Sections 6.2 to 6.4 are dedicated entirely to the standard material system, 914C. The new materials, 6376C, APC-2, and R25, will be discussed in the last section in which a brief comparison with the standard system will also be made.

6.2 DAMAGE STUDIES

Several damage evaluation techniques comprising, C-scan, X-ray, optical and scanning electron microscopy, and deply, were employed for a detailed fatigue damage characterisation. Based on the damage examination, a schematic overview of the fatigue damage state in notched CFRP, of stacking sequence A, is presented in figure 6.1(a) and (b) for the sharp notch and the circular hole respectively.

6.2.1 Sharp Notch

Figure 6.1(a) shows a two-stage fatigue damage development around a sharp notch. This kind of damage development is typical of most test cases at stress levels of approximately 20kN, with the exception of the hot/wet case. The most important features are; fibre splitting, indicated by the straight lines, fine lines for the secondary splitting; ply delamination, shown shaded; and 0° fibre fracture, indicated by the short, fat, transverse lines.

An early stage in fatigue damage development is depicted in the first picture of figure 6.1(a). It has been established, using optical microscopy, that damage initiates at the notch tips in the form of matrix microcracks (fibre splits) in both the 0° and the 45° directions. X-ray radiography suggested that, in the early stages of damage development, the SLS are associated with the off-axis splits: furthermore, it would appear that delamination damage occurs as a result of fibre splitting since it is often found in the areas of dense fibre splitting and in particular where 0° and 45° fibre splits intersect: this is especially true for the delamination in the net-section region of the specimen. Deply, as well as microscopic examination showed that, in general, damage initiates at the surface and then gradually propagates towards the mid-plane of the specimen with increasing fatigue cycles.

A later stage in fatigue damage development is depicted in the second picture of figure 6.1(a). Additional features are the increased delamination and the 0° fibre fracture: the darker shaded area represents delamination between three or more plies, and this is where fibre fracture is usually observed. Fibre fracture is thought to be the most important damage mode since it controls residual strength and/or fatigue life. It appears that extensive delamination and fibre splitting are responsible for promoting such failure, which is thought to occur by buckling during the compressive part of a fatigue cycle. Furthermore, it has been shown through the microscopic technique that such failures initiate in the outermost plies, see figure 4.59.

There are several factors that affect the fatigue damage development, including; environment, stacking sequence (and even more so, lay-up), and load amplitude. The effect of environment became particularly evident during the hot (90°C) fatigue testing of wet specimens, in which case a complete deviation from the above described typical damage development occurred: the off-axis fibre splitting had been suppressed which resulted in the confinement of damage within the PLS, figure 4.54.

A more subtle deviation in damage development has been observed with the change in stacking sequence: in the case of stacking sequence B the damage development, in all test cases, appears to be superficially similar to that in stacking sequence A. However, under the same test conditions, fibre fracture, in B, occurs much earlier, which results in shorter fatigue lives, for example see figure 4.59. Such behaviour is particularly true in the hot/wet case, see figure 4.47.

Fatigue damage development has also been found to depend upon the fatigue load amplitude, see figure 4.54: at high load amplitudes (higher than 20kN) delamination and fibre fracture become evident very early on, during the course of a fatigue test. It is anticipated that under very high load levels, fibre fractures may occur during the compressive as well as the tensile part of a fatigue cycle. In contrast, at low load levels (lower than 20kN) fibre splitting and in particular longitudinal fibre splitting constitute the primary modes of fatigue damage. A major difference between high and low stress levels appeared to be in the preferred direction of damage propagation: lateral and longitudinal for high and low load levels respectively. This is one of the most important observations and it will be shown, later on, that such behaviour can be correlated with the fatigue response of the notched specimens.

6.2.2 Circular Hole

A two-stage schematic diagram of fatigue damage development around a circular hole is shown in figure 6.1(b): this is typical of stacking sequence A and it is representative of all test conditions examined. The first picture shows that, in the early stages, fatigue damage is confined mainly within the PLS and POS. Deply damage examination revealed that delamination occurs in all 45°/0° ply interfaces, see figure 4.64, and X-ray radiography revealed that this delamination is not associated with any fibre splitting, ie is a direct result of the stress state in the region.

The second picture in figure 6.1(b) shows a further stage in damage development: damage propagates primarily in the longitudinal direction, although, strictly speaking, the actual rate of propagation along a certain direction (longitudinal or lateral), for a given load amplitude, depends upon the environment;

compare figures 4.45 and 4.46. In any case, the main effect of increasing number of fatigue cycles is to promote multiple secondary splits both in the 0° and 45° plies as well as to increase the length of the primary splits. In the event of secondary 0° and 45° fibre splits being intersected some delamination may initiate as a result in the net-section region of the specimen: this is marked by the light shaded regions.

Although it is not the objective of the present study to compare the sharp notch with the circular hole, one cannot help noticing the fact that, for the cases examined, the damage development around a sharp notch is much more sensitive to factors such as load amplitude, and hygrothermal exposure.

So far as the the examination techniques are concerned, it would appear that none of the five techniques employed is adequate, alone, for providing an integral view of the state of damage that could be used in a life or residual strength prediction. This is a twofold problem which relates (a) to the lack of a standard parameter or behaviour that a researcher would specifically search for (during the course of a damage examination) and use in the correlation with residual strength and/or fatigue life; and (b) the complexity of the material's internal microstructure which promotes a wide range of damage modes.

6.3 COMPUTATIONAL STUDIES

The complex problem of determining the three-dimensional stress field around the notches has been tackled by a relatively simple finite element analysis, where a number of questionable assumptions had to be made, see section 4.6. Such assumptions have often been employed in the past by a number of researchers, eg see (93-95), and they are a consequence of the complexity of the material and the stress field near a cut-out. So far as the present work is concerned, inaccuracies as a result of approximations are expected mainly due to the combination of two factors: the non-linearity of the material, and element distortion, both of which are a direct result of computer power, time and/or capacity limitations.

In theory the non-linearity of the material could be taken care of by running a series of linear jobs incorporating appropriate consecutive changes in the input stiffness matrix and using the output displacements as input load displacements for the next analysis. The accuracy of such analysis would then depend on the number of computer runs. Such a quasi-non-linear method can substitute a more expensive "truly" non-linear analysis, where a complex theory has to be incorporated into the program. Element distortion is a finite element method related problem surfacing, at present, as a characteristic limitation in the modelling of thin three dimensional structures like the fibre reinforced plies in a composite laminate. On such occasions

a large number of elements is the only solution to the problem. In the present study this problem was partly overcome by an appropriate design of a through-thickness graduating mesh. In this way the three dimensional mesh was restricted to the area of expected high stress concentration only. An approximate solution to the problem can be achieved by incorporating similar adjacent plies, like ±45°, into a single orthotropic lamina, eg see (95). The penalty for such procedure is the loss of information on the interlaminar stress distribution within the angle plies.

It is widely believed that the assumption of homogeneity of fibre reinforced plies should result in inaccurate rates of change of stress near a discontinuity. This problem has been investigated by Rybicki and Pagano (96) who found that the validity of the above assumption depends upon the fibre diameter. Their findings would suggest that the smaller the fibre diameter the more valid the assumption is. Thus so far as CFRP composites are concerned the assumption of homogeneity should be a reasonable one.

The objective of the present section is the understanding of the nature of the stress concentration around the notches. Such understanding is limited to RT conditions and undamaged state however, an attempt will be made to comment on the anticipated behaviour in the presence of notch blunting and/or environmental changes.

6.3.1 Sharp Notch

It has been established through proof load testing that a major difference between the behaviour of the wet and dry specimens is in the direction of damage propagation prior to final failure. In the wet specimens damage propagation is confined within the PLS, whereas, in the dry specimens damage tends to propagate in the lateral direction, see figure 4.57. This characteristic behaviour was also identified by the FEA: ie the magnitude of σ_z in the "dry model" was found to be marginally larger in the net section region of the specimen, compared to the "wet model". However, the analysis was proved to be far too simple to produce any useful information on the different nature of the stress concentration between the dry and wet specimens.

A rough estimate on the overall stress concentrating effectiveness of the sharp notch could be obtained by comparing the notched tensile (net-section) and the unnotched strengths. Such comparison for the RT/dry case of stacking sequence A indicates a reduction in tensile strength, as a result of the presence of the notch, of about 50%. The FEA suggested a SCF, in σ_x, in the vicinity of the notch tip of the order of 20-25, see section 4.6.1. This signifies that a blunting effect must have

been responsible for a stress redistribution prior to final failure which reduces the overall effective stress concentration down to a value of about 2: this is only a very rough indication of the SCF, based on strength, and may vary from ply to ply or ply interface, as well as component of stress. The X-ray radiographs of proof-loaded specimens, figure 4.57 show that such notch blunting does indeed take place in the form of primary fibre splitting which is particularly evident under the hot/wet conditions.

6.3.2 Circular Hole

So far as the circular hole is concerned, the most important point brought about by the FEA is the in-plane position of the peak stresses within the ±45° plies. These appear to occur at a point 1mm away from the hole boundary, along the lateral direction. It would appear that so far as the ±45° plies are concerned, the boundary of the stress concentrator is defined by four mutually perpendicular tangents to the hole which are at 45° to the loading direction. This is an important finding since it predicts the position from which 45° fibre splitting is expected to initiate. Such splitting, under cyclic loading, may eventually develop into lateral growth of delamination damage which in turn may promote fibre microbuckling and hence fatigue failure. Such lateral development of fibre splitting and delamination may also have a negative effect upon the residual compressive strength.

So far as the tensile strength is concerned, the overall stress concentrating effectiveness of the circular 5mm hole for the RT/dry case may be calculated by comparing the net-section strength with the plain strength of stacking sequence A. Such calculation indicates a reduction in strength, due to the presence of the hole, of about 37%. Based on strength, this value suggests an overall stress concentration factor of about 1.6. A value for the SCF based on the σ_x variation locally to the hole, as determined by the FEA, is about 4, see section 4.6.2. As in the case of the sharp notch this indicates that some kind of notch blunting effect is responsible for the apparent lower overall SCF, based on strength.

Typical variations in the direct stress σ_x, near the notch tips, are shown in figures 6.2 and 6.3 for 0° and ±45° plies respectively. Figure 6.2 shows a schematic presentation of the stress concentration as determined by the FEA. Shown superposed, is the anticipated effective (reduced) stress concentration, as a result of notch blunting: this has been approximately deduced from the SCF based on plain and net-section strengths. It is clear that, under a given environmental condition, the notch blunting efficiency of the sharp notch is much greater than that of the circular hole. The nature of the stress concentration in the ±45° plies is demonstrated in figure 6.3. The basic difference between the notch and the circular hole is the position of the

peak stress. In relation to figure 6.2, the stresses in figure 6.3 are shown magnified by a factor of about 1.5. It is anticipated that any reduction in the shear stiffness G_{12} will effectively reduce the direct load carrying cabability of the ±45° plies thus reducing the σ_x stress concentration in the 45° plies. As a consequence, the 0° plies would then be expected to carry more load.

6.4 STRENGTH STUDIES

Strength studies were carried out on both plain and notched specimen coupons. Tests on notched specimens were divided into two major categories: the static and the fatigue tests. Notched specimens are of special importance to the present research study and thus more emphasis will be placed upon tests involving such specimens.

In the present section the observed proof load induced damage is correlated with notched static strength and the fatigue damage is correlated with residual strength and/or fatigue life. Furthermore, as a result of damage observation and examination, a physical parameter will be pointed out which is related to the material's fatigue performance and more importantly it can be evaluated from a small number of specimens using a single NDE technique.

6.4.1 Static

Notched static tests were performed in both tension and compression under a range of environmental conditions; RT/dry, 90°C/dry, 130°C/dry, RT/wet, 90°C/wet and 130°C/wet: complementary proof load tests and subsequent damage examination were also carried out. Because of the distinctively different modes of failure involved in tension and compression, these subjects will be discussed separately.

(a) Tension

The bulk of results for both the sharp notch and the circular hole showed that, in general, the notched tensile strength tends to increase with increasing temperature and/or moisture content. Such behaviour is very well supported by the observed damage development in proof loaded specimens. Figure 4.57 shows that, under a tensile load and prior to failure, a dry specimen with a sharp notch developed damage which is mainly located in the net-section area of the specimen. However, an otherwise identical wet specimen, tested in the same fashion, developed damage which is confined within the notch tips: furthermore, the PLS in the wet specimen are at least twice as long as the equivalent ones in the dry specimen. Clearly the blunting of the notch in the wet specimens should be more efficient: indeed the average strength

of the wet specimens (at 130°C) was 12.3% higher than the equivalent dry value, see tables 4 and 5.

A large difference in the behaviour between the sharp notch and the circular hole has been observed in the hot/wet case. Unlike the sharp notch, an unexpected decrease in tensile strength took place in the wet specimens, with holes, tested at 130°C; compare figure 4.8 with 4.15. In general, a levelling out followed by a reduction is to be expected since the strength cannot rise indefinitely with increasing temperature and/or moisture content. However, in this particular case, the reduction in strength in one type of specimen alone (under the same conditions) appeared to be rather surprising. The above behaviour can only be explained by an interaction of two or more mechanisms that have an opposite effect on tensile strength, the most possible of which are: the blunting of the notches (the beneficial one) and the state of the matrix which may deteriorate as a result of excess moisture content and/or heat. The actual existence of such mechanisms is supported by a number of observations, for example; the blunting of the notches due to the development of PLS prior to failure, the trend of tensile strength results for the unnotched specimens, and the moisture/temperature equivalence effect which has been demonstrated by the failure modes of the notched specimens, see section 4.3.2.

It has been shown (table 1) that a moderate amount of moisture (1.4%) had a beneficial effect on plain tensile strength. However, a reduction in strength (from the maximum value, at 1.4% wet) took place when the moisture content was increased to 2.0%. The point at which the tensile strength of a group of specimens, notched or unnotched, reaches a maximum, will, from now on, be referred as the *tensile limit*: ie for the plain specimens of stacking sequence A, tested ar RT, the *tensile limit* occurs when the specimens are 1.4% wet. So far as the plain specimens (of the same stacking sequence) are concerned the tensile limit should approximately coincide with a point at which the state of the matrix is optimum. An optimum state in a wet epoxy matrix has also been observed by Dickson et al (44): they related this effect to resin plasticisation and reductions in the thermal residual stresses. Apparent matrix strengthening in epoxy resins, following moisture absorption, has also been reported by Hoa (79) and Hojo et al (80).

Moisture/temperature equivalence was made evident as a result of the failure modes in notched specimens. It appeared that dry specimens tested under elevated temperature conditions exhibited the same failure mode as otherwise identical wet specimens tested at a lower temperature. It is thought that such equivalence occurs when the state of the matrix in the two cases is similar. A well known moisture effect in epoxy matrices is the lowering of the Tg. Indeed Wright (1) suggested a rough rule of thumb involving a 20°C reduction in Tg for every 1.0% moisture content in the

matrix. Volume fraction tests carried out by RAE on present sample specimens of XAS/914C showed a matrix content of about 31% by weight: thus assuming all the moisture in the composite is taken up by the matrix, the 1.4% moisture content in the composite can be translated into 4.5% moisture content in the resin. Applying Wright's rule of thumb gives a 90°C reduction in Tg for the 1.4% wet specimens and a 130°C reduction in the Tg for the 2.0% wet specimens. Strictly speaking, when the moisture/temperature equivalence refers to strength, the Tg of the matrix is not the only relevant property that is altered by moisture: swelling related effects, such as the suppression of the residual stresses or matrix microcracking, can be equally important.

It would be reasonable to assume that the blunting mechanism is a function of the length of the PLS; longer splits drive the final fractures away from the notch along the longitudinal direction, thus promoting an increase in strength. It is equally reasonable to suggest that the presence of POS will have an opposite effect, driving the damage towards the free edges of the specimen, thus effectively extending the notch. It has been shown by the proof loading induced damage examination that dry specimens tend to develop both PLS and POS: ie, the beneficial effect provided by the longitudinal splits will be partly offset by the simultaneous development of off-axis splits. The degree of compensation depends upon the environment. At 130°C the 1.4% wet specimen, in figure 4.57, develops PLS only; thus the longitudinal splits should offer a 100% benefit, so far as the blunting of the notch is concerned. Likewise, when a notched specimen is tested dry at RT, the beneficial effect by the longitudinal splits may be completely eliminated by the off-axis splits.

Bearing in mind the above observed features of each mechanism a schematic presentation for both the wet and the dry specimens is produced, which briefly explains the observed behaviour of notched tensile strength: see figures 6.4 and 6.5 for the sharp notches and 6.6 for the circular hole. The average notched strength variation from the RT/dry value is plotted against test condition: the schematic effect of notch blunting and moisture (state of the matrix) are also plotted. It has been assumed that a moisture/temperature equivalence, between dry and wet specimens, takes place at 90°C/dry, RT/wet and 130°C/dry, 90°C/wet. Furthermore, it has been assumed that blunting and moisture effects are the only variable mechanisms which influence the notched strength: thus the sum of the two effects constitutes a measure of the apparent tensile strength variation; this implies that the strength of the fibres is assumed to remain constant under all environmental conditions.

Figure 6.4 shows the strength variation in a stacking sequence A specimen with a 10mm notch. It appears that within the range of temperatures RT-90°C, the effect of notch blunting is minimum. Within the same range of conditions the state of

the matrix contributes a small but negative effect due to the residual stresses, which are thought to be maximum in the RT/dry material. On increasing the temperature or moisture level, the matrix reaches an optimum value, at 90°C/dry or RT/1.4% wet; in this condition the effect of the notch blunting must also be rather low, since there is only a very small increase in the average strength: it is believed that the overall effect of notch blunting at low temperatures is small (a) due to the suppression of PLS by the well coupled ±45° plies and (b) by the development of POS. At higher temperatures, and beyond the matrix optimum conditions, notch blunting is increased, aided by the development of PLS and the suppression of POS, thus resulting in higher tensile strength.

The suppression of POS with increasing temperature and/or moisture content is thought to be a result of stiffness losses in the 45° plies. Hyer et al (97) have presented data for T300/5208 carbon epoxy, which suggests a reduction in G_{12} of about 17% and an increase in E_{11} of about 4%, in the range of test temperatures between RT and 130°C. If these results are translated into multidirectional laminate elastic behaviour, it would appear that, as the test temperature is increased, the load carrying cabability of the 45° plies is reduced: thus a larger proportion of the load, both direct and transverse, has to be borne by the 0° plies. As a result relatively more matrix damage (PLS) is sustained by the 0° plies.

The effect of hygrothermal environment upon the notched static strength of stacking sequence B is illustrated in figure 6.5. It appears that stacking sequence B exhibits a higher rate of strength increase than A: it follows that, if the state of the matrix due to moisture effects, in B, is the same as in A, then the apparent large rate of increase in strength with environment must be attributed to the notch blunting effect. Moreover, since the most basic difference between stacking sequence A and B is thought to be in the ply constraints, it follows that ply coupling effects must be responsible for the observed larger rate of increase in notch blunting in stacking sequence B, compared to A. If the ply constraints are relaxed by exposure to hygrothermal environments, it would be reasonable to suggest that the effect of such relaxation would, initially at least, be more pronounced in the relatively unconstrained outer, 0°, plies of stacking sequence B, which could then be made susceptible to fibre splitting.

A similar interaction between the two mechanisms (the notch blunting and matrix degradation) must take place in the specimens with circular holes. The effect of moisture and/or temperature was assumed to be identical to that described above. However, in order to match the observed trend in strength, the blunting mechanism had to be completely different, see figure 6.6. Initially the rate of increase of blunting of a hole, with environment, appears to be similar to that observed in the

notch, figure 6.4: but as the test temperature and/or moisture content is increased the blunting of the circular hole becomes much more effective.

A basic difference between the blunting mechanisms in the specimens with holes and sharp notches is the plateau reached at 130°C/dry or 90°C/wet: this condition is eventually reached when a specimen with a circular hole is effectively divided in to two plain specimens and there can be no more blunting. Consequently the begining of a plateau in the blunting mechanism, signals the (notched) material's *tensile limit.* Beyond this condition, the net section strength of the specimen appears to be controlled by the state of the matrix alone.

Based on the above observations, it would appear that every type of specimen, plain or notched, reaches a *tensile limit* when tested in a range of environmental conditions. The conditions under which such a limit is reached depend upon the specimen's geometrical features: ie in the case of the plain specimens a *tensile limit* was observed at RT/1.4% wet condition, and in the specimens with circular 5mm holes at 130°C/dry or 90°C/1.4% wet. It is anticipated that, in specimens with sharp notches, a *tensile limit* will eventually occur at some condition beyond 130°C/1.4% wet, see figure 6.4 and 6.5.

Since the residual stress state in a laminated composite is bound to have some influence on tensile strength, it would appear that any factors which can affect the residual stress state will also have an influence on the *tensile limit:* such factors are, lay-up, and/or manufacturing processes. Likewise, since notch blunting or more generally, notch sensitivity, is one of the controlling factors of notched tensile strength, it would be reasonable to assume that the *tensile limit* would depend upon the stacking sequence and even more so upon lay-up.

(b) Compression

Unlike tensile strength, a consistent reduction in compressive strength was observed with increasing temperature and/or moisture content, see figure 6.7.

Proof loading and subsequent damage examination failed to reveal any detectable matrix damage prior to final failure. This signifies that notch blunting equivalent to that observed in tension does not exist in compression. This behaviour may be attributed to one possible cause; the lower strain loading of the matrix. It is possible that during compressive loading the fibres fail before their full extensional capacity is reached. Premature fibre failure may occur as a result of microbuckling as well as macrobuckling. Microbuckling is thought to be sensitive to matrix lateral support and shear stress state, see for example (53). Macrobuckling is thought to be

sensitive to factors such as lay-up, stacking sequence, and method of testing. Furthermore, so far as the compressive strength is concerned, the apparent matrix degradation which occurs at high temperatures and/or moisture contents (as seen above) is further deteriorated by additional factors which in general do not affect the tensile strength; eg weakened fibre/matrix interface, and matrix softening.

The observed trend of results in compression, figure 6.7, may be explained simply by imagining an interaction of two or more negative mechanisms such as matrix and fibre/matrix interface deterioration, stress raising due to the notches, and perhaps specimen macrobuckling.

It has been shown that the fibre/matrix interface is indeed attacked by moisture and/or heat, see figure 4.66. Moreover, results suggested that under very high test temperature conditions the matrix, and in particular the wet matrix, becomes soft and plastic, see for example figure 4.19 or the fourth specimen in figure 4.29. The combination of a weak fibre/matrix interface and a soft matrix is expected to promote fibre microbuckling and hence poor compressive performance. These effects, all being matrix related, are bound to have an equal influence upon all specimen types ie, sharp notch, stacking sequence A or B and circular hole, under the same test conditions. Thus the difference in the observed compressive behaviour between the different types of specimens, figure 6.7, must be attributed to other factors such as notch sensitivity, ply coupling, and perhaps specimen bending stiffness.

An interesting point brought about by the comparison of specimens with sharp notches and circular holes is that the (compressive) stress raising effectiveness of the sharp notch appears to remain more or less constant within the whole range of environmental test conditions: such behaviour is demonstrated in figure 6.7 by the relatively shallow rate of decrease in strength. In contrast, specimens with circular holes exhibited a notch insensitive behaviour at low temperature and/or moisture content conditions and a notch sensitive behaviour at higher temperature and/or moisture test conditions: as a result of such dramatic changes in the notch sensitivity by the hole, a very high rate of decrease in strength was observed in the hot/wet conditions, see figure 6.7. Further supporting evidence is provided in figure 6.8: it is shown that at high temperature and/or moisture regimes the compressive strength, calculated on a net-section stress basis, is independent of stacking sequence and, more importantly, notch geometry. Thus in the hot/wet condition a circular hole is effectively as bad as a sharp notch. In simple terms the above behaviour suggests that the hot/wet notched compressive strength of laminated composites is determined by the net-section area of the load carrying material.

Bearing in mind that stacking sequence B has a greater bending stiffness ($E_{xx}I$) than A, due to the fact that it has a bigger effective second moment of area I, the lower compressive strength attained by B is rather surprising. Furthermore, it should be noted that when ply coupling is maximum, ie RT/dry case, the difference in compressive strength between the two stacking sequences A and B is greatest, compare figures 4.12 and 4.13. A similar behaviour has also been observed by Potter and Purslow (53): notched (circular holes) laminates with blocked plies exhibited higher compressive strengths compared to laminates with well distributed plies: however, when tests were performed in a hot/wet condition the effect of stacking sequence had disappeared. The only possible explanation for such behaviour is a ply coupling effect, responsible for promoting 0° fibre failure, possibly through the influence of a high shear stress. If such a ply coupling effect does occur it must be more pronounced in stacking sequence B where a lower strength value was obtained. The fact that the influence of stacking sequence upon the compressive strength disappears at high temperature and/or moisture content (see figures 4.12 and 4.13) tends to support the argument for the existence of a ply coupling effect.

A point of concern is born out by the observations of Collings and co-workers (42), who suggested that when a moisture gradient is present it is probable that the notched compressive strength is largely governed by the moisture content at the free edge. Such moisture gradients, however small, must clearly have been present during the hot testing of the wet specimens, even though the heating up time was kept to a minimum, see section 3.2.2. Furthermore, it should be noted that any results involving compression depend upon the particular anti-buckling fixtures used and therefore great care should be exercised when comparisons with data from other experimental set ups are made.

6.4.2 Fatigue

The basic understanding and the arguments relating strength to the state of the matrix and stress concentration which were developed as a result of the relatively simple study of the notched static behaviour will now be employed in the present section dealing with the more complex behaviour of fatigue and the implications of environment.

Two types of tension-compression fatigue tests were performed: fatigue tests at a predetermined load amplitude and number of cycles; and fatigue tests to failure. Specimens belonging to the first type of tests were fatigued at RT or 90°C and subsequently tested in static tension or compression in a range of environmental conditions; RT/dry, 90°C/dry, 130°C/dry, RT/wet, 90°C/wet and 130°C/wet. Fatigue tests to failure were carried out at RT only.

(a) Residual Strength Tests

An overview of fatigue damage development around notches has been presented in the section 6.2 and a schematic presentation of the fatigue damage development was shown in figure 6.1. Several factors responsible for the observed damage were isolated, some of which are; environment, stacking sequence, and the magnitude of the cyclic load amplitude. In the present section an attempt will be made to answer a single question: what is the effect of observed fatigue damage upon residual strength and/or fatigue life? Before such an attempt is made it is necessary to define and classify fatigue and/or environmental damage according to their anticipated effect upon residual strength. This is achieved through a schematic presentation in figure 6.9. It is believed that there are three major factors which control the residual strength:

(a) notch blunting, which depends upon the relative amount of longitudinal and off-axis fibre splitting,

(b) fibre degradation, which depends upon the cyclic stress amplitude, number of fatigue cycles and ply delamination and,

(c) matrix degradation, which depends upon the test temperature and/or moisture content. In the case of compression, the state of the fibre/matrix interface should also be incorporated.

It has to be pointed out that, during the course of a fatigue test, factors (a), (b) and (c) may interact and influence the development of one another. Furthermore, some of these factors may be affected by variables such as notch geometry, load regime, lay-up and/or stacking sequence. However, for a given fatigue damaged specimen, these can be considered to have an independent influence upon residual strength.

In figure 6.9, an arrow pointing away from a particular box signifies a negative effect and vice versa. Each box is thought of as a reservoir and the arrows indicate the direction of "flow" between the different reservoirs. The relative rate of "flow" between the reservoirs is indicated by the arrow thickness. For example, the residual strength reservoir, is "supplied" by notch blunting and is "drained" by the degradation of the matrix and the fibres. Likewise the notch blunting reservoir is "supplied" by longitudinal splitting and is "drained" by off-axis splitting. If at any point in a specimen's lifetime the influence of factor (a) is greater than the combined effects of (b) and (c), the specimen is said to be in a state of "wear in". Thus the

expected residual strength will be higher than the corresponding static value, see (98-100). As damage accumulates during further loading, the influence of factor (a) may be counterbalanced by the sum of (b) plus (c). At this stage the specimen is said to have reached a state of "wear out". From this point onwards only a reduction in residual strength is possible.

It may be worthwhile pointing out the generality of the schematic model in figure 6.9. For example, if the notch blunting effect is omitted the model should predict the residual strength of a plain specimen where in general a residual strength degradation is expected. Likewise, if fibre degradation alone is omitted the model should predict the notched static strength: in this case the model is represented by the simple diagrams of figures 6.4-6.6. Finally, if in addition to the fibre degradation, notch blunting is also omitted, then the model should predict the unnotched strength where the strength is controlled by the state of the matrix alone, see section 6.4.1.

If as a result of low cyclic stress level and/or fatigue cycles, fibre failure is not observed and the development of lateral delamination damage is small, the only active damage mechanisms (in the model of figure 6.9) will be notch blunting and matrix degradation. This represents a relatively simple case since it is similar in nature to the notched static case. Thus a schematic model similar to that in 6.4 or 6.6, can be employed to demonstrate the effect of notch blunting and matrix degradation upon tensile residual strength. This kind of damage was observed in most fatigue cases considered, apart from stacking sequence B specimens which, after 10^5 cycles, developed fibre fractures in the outer plies.

For example, suppose that a dry specimen with a sharp notch has developed a certain degree of notched blunting as a result of fatigue loading, which may be represented by a point on the "blunting effect" curve in figure 6.4; say point 1a. If the specimen is statically tested in tension at an elevated temperature, say 130°C, then the state of its matrix would be identified by the point 2a on the "moisture effect" curve. Furthermore, additional blunting, prior to failure, may occur as a result of tensile loading. Consequently the effective notch blunting, prior to final failure, may "move" slightly to the right, up the "blunting effect" curve, say point 1b. The specimen's expected tensile residual strength variation would then be the difference between notch blunting and matrix degradation, identified by the point 3a. It should be noted that, in this particular example, the specimen's tensile residual strength would be slightly lower than the corresponding static tensile strength. On the other hand if the same specimen was tested at 90°C instead of 130°C, its expected residual strength, point 4a, would have been higher than the corresponding static value. It is believed that the specimen's compressive strength could also be benefited

by notch blunting, as a result of fatigue loading, since this serves as a stress relief and redistribution mechanism. However, strictly speaking the compressive residual strength should also depend upon the state of the fibre/matrix interface, and matrix softening.

It is believed that lateral development of delamination will in general have a minor effect on the tensile residual strength. On the other hand severe delamination may promote local fibre buckling and hence low compressive residual strength. Thus if severe lateral delamination develops as a result of fatigue loading, see for example the fourth and fifth radiographs in figure 4.54, it is expected to have a negative effect upon the residual compressive strength. Such a severe form of delamination has not been observed in the fatigue cases (load amplitudes Ln or Lh) examined. However, on some occasions (ie see figure 4.34) a large reduction in compressive residual strength has been observed, even though delamination or fibre fractures were not detected. Moreover, it has been observed that these reductions in residual compressive strength occurred when the specimens were fatigue tested for a very small number of cycles, ie 10^3 and disappeared after a larger number of fatigue cycles, ie 10^5. The only explanation for this behaviour is the promotion of delamination by the 45° fibre splits prior to final failure.

It has been shown by the FEA that, in the case of a circular hole, the high stress concentration point in the ±45° plies (in the undamaged state) occurs 1mm ahead the hole boundary (tip). It is therefore possible that very fine matrix cracking initiates in the 45° plies ahead of the hole tip during the first few hundreds of fatigue cycles and before the blunting effect of the PLS takes effect. It is then possible that, during the residual strength test, the cracks in the 45° plies impose a high shear stress concentration upon the 0° plies. If the load is compressive, fibre microbuckling is promoted (eg see 53) and hence a low strength is attained. However, if as a result of longer fatigue loading, large enough PLS develop, the effect of the off-axis splitting is counterbalanced by notch blunting.

Fibre fracture, as a result of fatigue loading, is another negative contributing factor so far as the residual strength is concerned, which affects both the tensile and compressive strengths. Once fibre fracture develops it is much more difficult to visualise the actual process of final failure during a residual strength test, because of the interaction between the larger number of damage mechanisms. Obviously, the more fibre fracture a specimen contains the nearer it is to its fatigue life, and therefore a low residual strength is expected. Fibre fracture can be promoted by either a relatively low cyclic stress amplitude after a high number of fatigue cycles or by a high cyclic stress amplitude after a low number of fatigue cycles, eg see the fourth and fifth radiographs in figure 4.54. Since the same state of damage (fibre

fracture) can be reached by a number of different combinations of stress amplitude and number of fatigue cycles, Simonds and co-workers (101) have seen the need of introducing the concept of "percentage of life": ie they defined the damage state of a composite material for a given stress amplitude by one parameter alone; how close a specimen is from its fatigue life.

Simonds et al (101) presented tension-compression results for notched (circular hole) qausi-isotropic laminates which show that, for a given percentage of life, the magnitude of the residual strength depends upon the stress amplitude. Furthermore, specimens which were fatigued at a low stress amplitude exhibited "wear in" up to about 90% of their life. However, specimens which were fatigue tested at high stress amplitudes exhibited "wear out" throughout their lifetime. This is an important point indicating that above a certain stress amplitude the residual strength of a composite is governed by delamination and fibre failure, whereas at a lower stress amplitude the composite's residual strength response is controlled by fibre splitting (notch blunting).

The stress amplitude at which the behaviour of a notched composite undergoes a transition, will, from now on, be referred to as the *transition stress,* S_t. The transition of damage from primarily lateral delamination to primarily longitudinal fibre splitting is very well demonstrated by the last two radiographs in figure 4.54: the fourth radiograph, in the same figure, appears to approximately correspond to S_t; ie lateral delamination and longitudinal fibre splitting appear to co-exist and propagate simultaneously. Furthermore, comparing the fatigue behaviour of stacking sequences A and B, eg figures 4.47, 4.54 and 4.59, it would appear that under the same fatigue conditions, fibre fracture and hence poorer fatigue performance occurs in stacking sequence B specimens. This indicates that almost definitely the magnitude of S_t for stacking sequence A must be higher than that for B. Furthermore, Stinchcomb et al (75) have shown that, for the same stacking sequence and load regime, damage in notched polymer matrix composites developed predominantly in the longitudinal direction: in contrast,in otherwise identical, metal matrix composites damage developed laterally. This indicates that the magnitude of S_t is also sensitive to the properties of the constituent materials. Moreover, if the magnitude of S_t depends upon factors such as stacking sequence, and/or material system it is reasonable to assume that it will also depend upon lay-up and/or notch geometry.

It has been established that the residual strength of notched composites depends upon three major factors: notch blunting, contributor to "wear in" and fibre and matrix degradation, contributors to "wear out". Moreover, it has been shown that whether "wear in" or "wear out" will dominate the residual strength response of a notched specimen depends upon the applied cyclic stress amplitude. Above a

characteristic value, S_t, the residual strength is governed by "wear out" whereas below S_t, the residual strength is governed by "wear in". This implies that, in the case of a variable applied stress amplitude the residual strength response would depend on the sequence of applied stress. For example if an applied cyclic stress lower than S_t is followed by a cyclic stress higher than S_t, the specimen may exhibit a residual strength response governed by "wear in", since the initial development of notch blunting may considerably delay delamination and hence fibre fracture. On the other hand if a higher than S_t stress amplitude is followed by a lower than S_t cyclic stress, the specimen will most probably exhibit a tendency for "wear out". In general, for obvious reasons, the problem of variable stress amplitude has received very little attention, even though it is the most representative of real load situations.

The above arguments applicable to the residual strength response should in principle, at least, apply to the problem of fatigue life, since this is a special case of where the residual strength is equal to the maximum applied stress amplitude.

(b) Fatigue Tests to Failure

Fatigue tests to failure were carried out on both wet and dry stacking sequence A specimens at RT. Both notch geometries were investigated, see figures 4.39 and 4.41 for sharp notches and circular holes respectively. It would appear that in all test cases considered, a straight line would approximately fit the experimental points. Furthermore, the slopes of these straight lines appear to depend upon the environment used: in general, the wet conditioned specimens exhibited flatter lines. Due to the fact that composite materials in general do not exhibit a true "fatigue limit" analogous to that in steels for example, the usefulness of the S-N plots has often been questioned, see (62).

It is thought that as a result of the "compressed" nature of the fatigue life axis, details such as the damage transition stress, in notched composites, are masked. However, it has been observed that if an S-N curve is plotted in a linear fashion, two distinct slopes emerge, see figure 6.10. Furthermore, it has been observed that the y-coordinate of the point of intersection of the two lines corresponds to the magnitude of S_t, the damage transition stress. There are three important points which can be identified from the "linear S-N plots" of figure 6.10:

(1) the slope of the first of the two lines is highly dependent upon the environment,

(2) the slope of the second line appears to be more or less common to all environmental conditions considered and,

(3) the magnitude of S_t appears to be unaffected by the wet environment.

At this stage it has to be stressed that the second line does not represent a fa[illegible]e limit, it is just a very shallow slope and it marks a ceiling line below which e[illegible]y notched specimen undergoes extensive longitudinal fibre splitting and hence r[illegible]h blunting: ie a region of expected "wear in".

The region immediately below the first line (and above S_t), figure (f[illegible]), marks the area where the specimen's performance is governed by delaminati[illegible]d hence fibre fracture: the actual rate of accumulation of damage is indicated b[illegible]e slope of the first line. It would then appear that the effect of the wet environm[illegible]ts considered is effectively to toughen the matrix thus reducing the rate of delamin[illegible]n damage accumulation.

The fact that the magnitude of S_t is more or less independent of the[illegible]t environment suggests that S_t is related to the properties of the fibres likel[illegible]e longitudinal stiffness of the load bearing, 0°, plies or perhaps the relative loadin[illegible]f the 0° plies compared to the ±45° plies: ie if the stiffness of the 0° plies rem[illegible]s more or less unaffected by the wet environment then, for a given applied load, t[illegible]e percentage load carried by the 0° plies would be unaffected by the environmenta[illegible]d hence the percentage load carried by the ±45° will also remain approxima[illegible]y constant, provided that the shear stiffness of the wet material is not reduced t[illegible]o much. Furthermore, a comparison of figure 6.10 with figure 6.11 indicates that t[illegible]e magnitude of S_t depends on the geometry of the stress concentrator: ie it w[illegible]d appear that S_t is a function of the stress field local to the notch tip. For the sha[illegible]p notch S_t appears to be approximately 200 MPa as compared to 327 MPa for t[illegible]e circular hole, see figures 6.10 and 6.11.

It has been observed through the FEA that a major difference between t[illegible]e nature of the stress concentration around a sharp notch and a circular hole is in t[illegible]e relative amount of maximum stress carried by the 0° and the ±45° plies at the no[illegible]h tips; ie compare figures 4.71 and 4.82: for simplicity the ratio of maximum str[illegible]s σ_x in the 0° plies divided by the maximum σ_x in the ±45° plies, will be referred [illegible]o as R_{ms}. In the case of the sharp notch the ratio R_{ms} is about 2.8 (figure 4.71). [illegible]n the other hand, the value of R_{ms} for the circular hole appears to be 9.1 (figu[illegible]e 4.82). However, strictly speaking the ratio R_{ms} for the circular hole should [illegible]e lower than 9.1, since the peak σ_x stress in the ±45° plies does not occur at the ho[illegible]e tip but approximately 1mm ahead, see figure 6.3. Thus a more representative val[illegible]e of R_{ms} for the hole, based on the absolute maximum value of σ_x, in the ±45° plies [illegible]s 4.9. Therefore, it appears that the magnitude of S_t for a given notched specim[illegible]n

depends upon the ratio R_{ms}, ie the relative amount of load borne by the 0° plies compared to the ±45° plies. If somehow the ratio R_{ms} is altered, eg by the notch geometry, the magnitude of S_t will also change accordingly: the higher the R_{ms} the higher the S_t appears to be. Based on a very rough calculation it would appear that, for a given stacking sequence, the ratio S_t/R_{ms} remains more or less constant regardless of the notch geometry. For example the ratio S_t/R_{ms} for the sharp notch is about 71 MPa compared to 67 MPa for the circular hole. In order to establish a reliable relationship between S_t and the ratio R_{ms}, a much more detailed study of the exact nature and magnitude of the stress concentration around the notches is needed: in particular under more complex loading such as biaxial loading.

For the particular lay-up considered in the present research work, R_{ms} has been defined as the ratio of the maximum direct stress in the 0° plies divided by the maximum direct stress in the ±45° plies. In a more general situation, say a quasi isotropic $(0°/\pm45°/90°)_s$ laminate, R_{ms} should be related to the ratio of the maximum stress in the longitudinal plies divided by the maximum direct stress in the weakest plies, ie the 90° plies.

It has been established that the physical parameter, S_t, can be identified from a linear plot of stress amplitude versus fatigue life. It has been shown that the magnitude of S_t, for a given stacking sequence and notch geometry remained approximately constant under the wet environments considered. Furthermore, it has been shown that for a given stacking sequence the ratio S_t/R_{ms} may also be a constant regardless of the notch geometry. Moreover, it has been established that the x-coordinate of the point S_t, on the cyclic stress versus fatigue life plot, depends upon the state of the matrix. Therefore, the point S_t appears to be a unique characteristic parameter that may be used in a life prediction model provided that it is well understood and firmly established that it can be easily identified for any material system, lay-up, load regime, environment, and specimen geometry.

Results from the present research work have shown that at least for the wet environments considered, which included both accelerated conditioning and natural weather conditioning for approximately 2.5 years, the magnitude of S_t remained more or less constant. This was attributed to the rather insensitive behaviour (including strength and stiffness) of the carbon fibres to the wet environment. This behaviour may in general be true for most inorganic fibres: however, organic fibres like "kevlar" may be more susceptible to environmental influence since they absorb a large amount of moisture (44). Thus the above statement may no longer be valid. Furthermore, based on the assumption that the insensitivity of S_t, to the wet environment, is related to the insensitivity of the 0° plies, it would be reasonable to assume that in the case of a lay-up which is not dominated by the 0° plies, eg a

quasi-isotropic, the environment may have a greater influence upon S_t compared with a 0° dominated lay-up, like a (0°/±45°) type.

In the present work, the influence of temperature upon the magnitude of S_t has not been studied directly due to time and experimental set-up limitations. If it is accepted that the magnitude of S_t depends upon the stiffness of the 0° and ±45° plies through the influence of the ratio R_{ms}, then it would be reasonable to assume that temperature will have a greater influence upon S_t than moisture does. Hyer et al (97) have presented data for a carbon/epoxy system which suggests a reduction in G_{12} of about 17% and an increase in E_{11} of about 4% in the range of temperatures between RT and 130C. Clearly, such large changes in stiffness will have a considerable effect upon R_{ms} and hence S_t. In fact in cases where other factors, such as matrix softening (fibre support) for example, are not important, an increase in R_{ms} should occur since some of the load originally carried by the ±45° plies (at RT) will be transferred onto the 0° plies (at say 130°C). Indeed, the first radiograph of figure 4.54 suggests that the value of S_t for the hot/wet case of stacking sequence A, may be marginally higher than that of the RT conditions since lateral development of damage at the load level Ln (=20kN) under the hot/wet condition appears to be minimal. On the other hand the third micrograph in figure 4.54 suggests that, under otherwise identical conditions, stacking sequence B developed lateral damage, including fibre fracture. This indicates that for stacking sequence B, S_t must be lower than 200 MPa (200MPa ≈ 20kN).

The lower S_t value in stacking sequence B compared with A, has been attributed to the detrimental effect of compressive loading upon stacking sequence B: the relatively unsupported outer 0° plies, once split or delaminated are prone to microbuckling and hence premature fracture, particularly at very high temperatures and/or moisture levels in which case the matrix offers a minimum support to the fibres. Another example, demonstrating the detrimental effect of extreme environment, stems from the hot testing of 2.0% wet specimens containing circular holes. Figure 6.11 suggests an S_t value, for RT wet and dry specimens, of about 327 MPa: however, table 11 shows that the static hot/wet (90°C/2.0%) compressive strength of these specimens is less than the magnitude of RT S_t. This means that at this particular condition the hot/wet value of S_t (if there is any) for the specimens with circular holes must be less than 317.7 MPa.

The effect of lay-up upon the magnitude of S_t has not been examined experimentally at present, but evidence implies that it should depend upon the lay-up. A reasonable question then arises: can S_t be identified from a "linear S-N curve" for any lay-up? Without solid evidence in hand it is difficult to answer such a question, but it is anticipated that, whether S_t can easily be identified or not would

depend upon the relative slopes of the two parts of a "linear S-N plot": the larger the difference between the slopes the more accurate the identification will be. In fact, since the slope of the second part of the curve is very nearly zero, a large initial slope would be an adequate requirement. The present results suggest that the slope of the first part of the plot depends upon the geometry of the notch. For example the magnitude of the initial slope of the "linear S-N plot" for the dry specimens with sharp notches (figure 6.10) is about 45 MPa/(million cycles) compared to 30 MPa/(million cycles) for the corresponding specimens with circular holes (figure 6.11). Therefore, for a given lay-up, an appropriate notch geometry could be used to identify an S_t with the minimum amount of effort, ie short test periods. For example in the case of a 0° dominated lay-up a sharp notch would be a more suitable stress concentrator, whereas in the case of a quasi-isotropic or a cross-ply lay-up a circular hole may be more appropriate.

So far as the identification of S_t is concerned, the effect of the difference in slope between the two parts of the "linear S-N plot" for the sharp notch and the circular hole is demonstrated in figures 4.54 and 4.55. It is apparent that when the difference in slopes is large, eg in the case of the sharp notch, a rough estimate for S_t can be made by a comparison of the damage development under different load amplitudes, for example compare the last three radiographs in figure 4.54. However, if the difference in the two slopes is relatively small, eg in the case of circular hole, S_t can no longer be identified by damage examination alone, see the last three radiographs of figure 4.55. Thus whether the damage transition can be detected by damage evaluation or not depends upon the initial slope of the "linear S-N plot" which in turn depends upon the notch geometry, lay-up, and the resistance of the matrix to delamination.

In order to examine the validity of the statements made above, tension-compression fatigue data for a notched (circular hole) quasi-isotropic lay-up for two carbon fibre reinforced systems, taken from reference (101), were plotted in a "linear S-N curve" fashion, see figure 6.12. It is apparent that an S_t value for both material systems can be identified. There are two points worth noting; the first is the reasonable magnitude of the initial slope for each material system, which is approximately 50 MPa/(million cycles): the steep initial slope suggests that a circular hole is indeed an appropriate notch for the determination of S_t, for this particular lay-up. The second, is the difference in magnitude of S_t for the two material systems, which is thought to be due to the different type of reinforcing fibre in either system: the 5208 matrix was reinforced with T300 fibres, whereas the PEEK matrix was reinforced with AS4 fibres. Note that in the actual paper it is stated that the PEEK matrix is reinforced with T300 fibres: however, it was later established that the reinforcing fibres were in fact AS4.

It has so far been established that the magnitude of S_t depends upon the stacking sequence, lay-up, notch geometry, and most importantly material system. Thus if S_t represents a measure of fatigue performance then it can be employed as a screening parameter for optimum fatigue response, by isolating:

(1) the best stacking sequence, for a given lay-up and,

(2) the best material system, for a given stacking sequence.

It has been shown, figure 4.54, that a rough indication of the magnitude of S_t may be obtained by means of non-destructive examination. Thus for the purpose of comparison, in a screening programme, fatigue tests to failure are not really necessary unless an exact value for S_t is needed. For example, suppose that it is required to identify the most fatigue resistant material system from a number of candidate systems, for a given lay-up. The usual approach is a vast amount of fatigue tests to failure per system and stacking sequence combination. However, using the proposed *damage transition method* a small number of appropriately notched specimens, say a maximum of five, may be fatigue tested under a given load mode, for a predetermined number of cycles, eg 10^5, at a range of maximum amplitudes. An indication of S_t per specimen case could be obtained by subsequent damage examination, for example X-ray radiography. In this way one or more specimen types with the highest S_t value may be identified. Further fatigue tests to failure on the selected few specimen types could then be carried out for a more accurate determination of S_t through a "linear S-N plot". Furthermore, since the magnitude of S_t appears to be independent of the wet environments, the proposed method may be carried out for dry material only, at least for the 0° dominated lay-ups. However, in any case, the effect of temperature must not be disregarded.

Before such a proposed method of screening can be employed successfully a number of questions need to be answered which are beyond the objectives of the present research work, some of which are:

(1) does the superior fatigue performance of a notched composite translate to a superior performance in the unnotched state?

(2) What is the effect of changing the loading mode? For example, if a certain specimen has been chosen for its superior fatigue behaviour under a given loading mode, say R=-1 constant frequency and amplitude cyclic load, would a superior performance also be expected under different loading modes?

(3) Can the superior behaviour of the laboratory size specimens be reflected into the performance of a full size structure? And for that matter how does the relative size of the notch to the specimen's width affect the magnitude of S_t and/or its identification?

Finally, if a stage in time is reached when the above questions are reliably answered, S_t may become the key parameter in the definition of a standard fatigue test that would reliably describe the fatigue properties of a given composite material.

6.5 NEW MATERIALS

All sections above have so far dealt with the fatigue response of the main material system, Ciba Geigy 914C-XAS-5-34%. The present section is dedicated to the fatigue performance of the new materials, from the secondary programme, which were presented in chapter 5. The objective of this section is to discuss and compare the fatigue behaviour of each new material with that of the standard system, thus evaluating the wider applicability of certain observed behaviour and ideas which were developed as a result of the comprehensive study of the main system. The performance of the new materials was briefly examined; including static and residual strength tests. Only one type of notch geometry and stacking sequence were evaluated: sharp 10mm notch in stacking sequence A. The three new material systems were;

(a) Ciba Geigy 6376C-T400-5-34%,

(b) ICI PEEK-AS-4 (APC-2) and,

(c) BP R25/2-T300B

6.5.1 Toughened Epoxy Matrix

Of the three new materials examined, this was the most widely investigated. Tests included, static, fatigue at a predetermined number of cycles (at a load amplitude Ln=20kN) followed by residual strength tests, and fatigue to failure. Both dry and wet specimens were evaluated.

In general the static as well as the fatigue behaviour of 6376C was found to be very similar to that of 914C. The plain tensile strength of the wet specimens was higher than that of the dry specimens, the notched tensile strength increased with temperature and/or moisture content, the notched compressive strength decreased with increasing temperature and/or moisture content, and the fatigue damage development appeared to be very similar in nature to that in 914C. The only major

difference between the two material systems was less fatigue damage at equivalent loads, and much less lateral delamination compared to 914C, compare figure 4.54 with 5.10. As expected the absence of lateral delamination resulted in a generally higher compressive residual strength increase compared with the corresponding fatigue cases in 914C, compare figure 4.24 with 5.7.

Fatigue tests were also carried out on a small number (five) of stacking sequence B specimens with sharp notches. Subsequent damage examination verified the inferior performance of stacking sequence B, compared with A. Even in this toughened matrix material system, lateral damage developed after as little as 10^5 cycles at a cyclic load amplitude Ln (=20kN). As with 914C such damage was mainly confined in the outer 0° plies. However, in the case of 6376C no fibre fracture, equivalent to that in 914C, was observed.

In a recent review Curtis and Dorey (71) mentioned that the fatigue behaviour of improved composite systems, relative to their static strength, has not been as good as expected. One of these improved composites is 6376C and indeed in comparison with the standard system 914C it does not appear to be as superior as one would expect, especially in the wet condition, see figure 6.13. In these plots the cyclic stress amplitude has been normalised with respect to the corresponding RT notched static compressive strength.

According to Curtis (54) the hot/wet notched compressive strength has currently become one of the key parameters in the design of military aircraft. Thus normalising the stress amplitude with respect to the hot/wet compressive strength, instead of the RT static compressive strength, may be of more practical significance since most advanced composites are destined for military aircraft applications. Such a normalised S-N plot with respect to the corresponding hot/wet (130°C/equilibrium under 60°C/84% RH) compressive strength is shown in figure 6.14. It is apparent that both in the dry as well as in the wet state, 6376C is superior to 914C: in the case of 6376C no fatigue failures were observed below the "design line", $S/S_{HW}=1$.

The superior fatigue performance of 6376C over the standard system 914C is also demonstrated by the higher S_t value, figure 6.15. If it is indeed accepted that the slope of the first part of a "linear S-N plot" is a measure of matrix toughness then, in the dry state at least, 6376C does not appear to be tougher than 914C. A similar behaviour was also noted in figure 6.12, in the comparison between AS4/PEEK and T300/5208. It is well known that under static conditions the fracture toughness of PEEK matrix is higher than that of the standard epoxy 5208. However, the superior behaviour with respect to toughness evaluated under dynamic load conditions has

often been questioned, see (101). It should perhaps be pointed out that strictly speaking the apparent toughness (resistance to matrix fracture) of a composite, particularly under fatigue loading, should also depend upon the relative properties of the constituent materials as well as the properties of the fibre/matrix interface. The fact that the AS4/PEEK system does not appear to be as tough as its matrix would suggest, may be due to the fact that the AS4 fibres fail at a higher strain compared to the T300 fibres: the T300 fibres are classified as high strength low strain to failure (1.2% strain) whereas the AS4 fibres are classified as intermediate strain to failure fibres (1.5% strain). Thus due to the difference in the fibre strain to failure, both matrices may suffer the same relative damage, particularly at high strains: ie at fatigue amplitudes greater than S_t.

At least two important observations can be made from figure 6.15. The first stems from the difference in magnitude of S_t for the two materials. In the case of 914C, the standard load amplitude Ln happened to corespond to S_t. However, the magnitude of S_t for 6376C is approximately 240 MPa, much higher than the cyclic load amplitude Ln, which is equivalent to about 200 MPa. Therefore, it is not surprising that for the same load amplitude, and judged by the fatigue damage development, 6376C appeared to be tougher than 914C, compare figure 4.54 with 5.10. The second point is the change in slope, of the first part of the curves for wet specimens. This behaviour appeared to be consistent for both material systems as well as notch geometries, see also figure 6.11. Furthermore, damage examination revealed that the observed slope reduction is always accompanied by a consistent suppression of the fatigue damage in the wet specimens when compared with the dry equivalent: see for example figures, 4.55 (compare the second and third specimens) and 5.10 (compare the third and sixth specimens). Thus it would appear that the slope of the first part of a "linear S-N plot" is a measure of the material's toughness under dynamic loading. Factors such as the relaxation of the residual stresses, matrix plasticisation, and weakening of the fibre/matrix bond may be positive contributors to the observed toughening.

The process of residual stress relaxation by moisture swelling is well understood. Provided that moisture does not cause a stress reversal by excess swelling, its effect on matrix toughness is usually beneficial. The effect of matrix plasticisation should also be beneficial so far as matrix toughening is concerned. It is thought that a certain degree of weakening in the fibre/matrix interfacial bond may also have a beneficial effect on the onset of delamination. If a fibre/matrix interface is too strong, then delamination will almost definitely initiate in the matrix. However, as the matrix is toughened by plasticisation, and the fibre/matrix interface is weakened by moisture content, a point must be reached at which the

composite's resistance to delamination is at a maximum. At such an optimum state, delamination is equally likely to initiate in the matrix as well as in the interface.

6.5.2 Thermoplastic Matrix

Due to a limited number of available specimens, the fatigue behaviour of APC-2 system was only very briefly examined. Tests included plain tensile strength determination, notched static strength evaluation, and residual strength assessment following fatigue testing, at a load level Ln (=20kN).

A major difference between APC-2 and the other three material systems was observed in the amount of absorbed moisture. Under an identically controlled moist environment, 60°C/84% RH, APC-2 gained 0.12% of moisture by weight compared to at least 1.0% in the other material systems. In fact the measured value of moisture gain may have been underestimated since APC-2 was the only material which was not fabricated in house. It is therefore possible that a certain amount of moisture was already present in the material on delivery. In any case results by Curtis (54), on a similar material conditioned in a controlled environment of 70°C/84% RH, indicate an equilibrium value of 0.21% by weight, which compared to the moisture level of the other three material systems appears to be negligible.

So far as the notched static strengths are concerned, there is one point worth noting: the detrimental effect of heat (130°C) upon the tensile strength. This behaviour suggests that a low *tensile limit*, for APC-2, below 130°C was reached possibly due to matrix deterioration which promoted shear failure, see figure 5.13. The failure modes in figure 5.13 indicate that even at 130°C the plies were well coupled at failure. Therefore, one would expect a shear failure in the 45° plies to be efficiently transmitted into the 0° plies thus promoting an overall shear failure.

As a result of the small moisture content, APC-2 exhibited an insensitive behaviour to the wet and/or hot environments so far as fatigue damage development is concerned. Unlike the epoxy based systems, under the hot/wet environment, APC-2 did not develop the typical rectangular damage; for example compare figure 5.17 with 4.54 and 5.10. This is another example demonstrating the good ply coupling in APC-2 which appears to have remained intact even under the hot/wet environment.

The effect of fatigue loading upon the residual strength of APC-2 was demonstrated in figure 5.16. A comparison with figure 4.24, for 914C, or 5.7, for 6376C, suggests that in general, and for the cases considered, APC-2 exhibited the largest increases in compressive residual strength. This improvement in residual compressive strength was attributed to a relatively large amount of fibre splitting

and a negligible amount of lateral delamination. It appears that the material has the ability to split but due to the toughness in the matrix it does not delaminate. This unique behaviour suggests that there exists an additional mechanism in APC-2 that contributes to excessive primary splitting, compared to the epoxy systems. Such a mechanism can only arise from the exceptionally high moulding temperature for APC-2: 380°C compared to typically 170°C for the epoxies.

An approximate indication on the magnitude and nature of the residual stresses can be obtained from a lamination theory analysis for a thermally loaded laminate. Results from such an analysis indicated that the largest thermally induced stress is in-plane shear (σ_{xy}) in the ±45° plies. The actual magnitude of this shear stress depended of course upon the applied thermal loading and it was approximately 2.5 times greater in APC-2 compared with 914C. In practice, the ratio of the residual shear stress in APC-2 divided by the residual shear stress in 914C, should be greater than 2.5, since the residual stresses in the thermoset system may be partly relieved by postcuring. In any case, the important point is that the residual shear stress in the ±45° plies of APC-2, at RT, is approximately 80% of the shear strength of these plies. This was calculated using the manufacturer's quotation for the tensile strength of the ±45° plies: it has been assumed that the shear strength is one half of the tensile strength of the ±45° plies, see (102). An equally important high residual stress, σ_y, was also found in the 0° plies. This stress was found to be approximately 78% of the manufacturer's quoted value for strength. Both of these stresses (σ_{xy} and σ_y) are thought to be the prime contributors to the observed fibre splitting.

It is thought that the exceptionally high residual stress in APC-2 is also responsible for the unique fatigue induced crease-like damage at the tip of the notches. Furthermore, it has been shown, figure 5.18, that the crease-like damage as well as the excessive fibre splitting are typical of tension-compression fatigue loading. Thus it would appear that the effect of the residual stresses and in particular that of shear, becomes important under a fully reversed loading situation.

6.5.3 Bismaleimide Matrix

The Bismaleimide matrix system, T300/R25, was chosen for the present research programme for its high operating temperature cababilities. Both static and fatigue tests were carried out. Static tests included plain tensile strength determination, and notched strength evaluation in both tension and compression. Fatigue tests were performed at a load amplitude Ln (=20kN) and were followed by residual strength assessment.

Of the four material systems examined R25 exhibited the lowest plain tensile strength. So far as the notched strengths are concerned, R25 showed an analogous behaviour to that of the epoxy systems. The notched tensile strength tends to increase with temperature and/or moisture content, and the compressive residual strength decreased with increasing temperature and/or moisture content.

In fatigue, R25 also behaved like the epoxy systems: ie it appeared to be sensitive to the environmental test conditions. Perhaps the most basic difference between R25 and the epoxy systems is the larger amount of fatigue damage, compare figure 5.26 with 4.54 and 5.10. The fatigue damage consisted of both extensive fibre splitting and lateral delamination. Compared with the APC-2, under identical test conditions, R25 exhibited a generally larger amount of fibre splitting and in particular secondary splitting which indicates the fatigue sensitive behaviour of its brittle matrix.

Judging by fatigue damage development alone, R25 appears to be the only material, of the four considered, to have an S_t value marginally below the cyclic load amplitude Ln. The effect of fatigue damage upon the residual strength was demonstrated in figure 5.24. As in the cases of the other three material systems, the tensile residual strength of R25 was generally improved by the presence of fatigue damage: this is connected with the fact that no fibre failures were observed in the test cases considered. However, compared to the other material systems, figures 4.24, 5.7 and 5.16, the compressive residual strength response has not been as good. This is of course a result of the existence of lateral delamination, which in general counterbalances the beneficial effect of notch blunting, thus reducing the compressive strength.

As a result of the comparison of different materials there appears to be a problem in the choice of an appropriate cyclic load amplitude. In the beginning of this research work there were two logical methods of choosing the cyclic load (or stress) amplitude: (a) by means of constant strain, and (b) by means of a constant load for all materials considered. Choice (a) meant that due to the expected difference in longitudinal stiffness, each material system could have been tested under a different standard load (Ln). The second choice which was eventually adopted, meant that each material system was tested under a different maximum strain, as figures 4.21 and 5.5 suggest. Looking at the results above, it would perhaps seem more appropriate, for the sake of comparison as well as the sake of extracting the maximum information, to test each material system at a load level corresponding to each material's S_t value. In this way the comparison of the damage development could reveal a more representative information of the fatigue performance of each material.

A good example, demonstrating the advantage of testing at a load amplitude corresponding to S_t, arises from a comparison between the amount of information gained from testing specimens with sharp notches and circular holes. In the case of sharp notches, Ln , corresponded to S_t. However, in the case of the holes , Lh, happened to correspond to a stress amplitude lower than S_t. Clearly, more information on the effect of environment upon the fatigue damage development, has been gained by the study of sharp notches compared with the circular holes.

Finally for the purpose of a general comparison, the static and residual strength results for all four material systems, are summarised in figures 6.16 and 6.17, for dry and wet specimens respectively.

7. CONCLUSIONS AND FURTHER WORK

7.1 CONCLUSIONS

The objective of the present section is to classify and summarise the most important findings and observations made as a result of the experimental study of notched composite laminates under a range of environmental conditions and load regimes.

7.1.1 Static Strength Studies

Static strength studies were carried out on both plain and notched specimens. Tests on plain specimens were restricted to the ambient temperature tensile load regime. Notched specimens were more widely investigated. Tests included tension and compression under a range of hygrothermal environments.

(a) Plain Specimens

In general, an increase in static tensile strength of plain specimens, was observed with increasing moisture content until a maximum strength was reached. The maximum strength point has been defined as the *tensile limit*. Further increase in moisture content resulted in strength deterioration. The increase in tensile strength with moisture content was confirmed by all material systems examined. The strength increase with moisture was attributed to a combination of two factors:

(1) residual stress relaxation and,

(2) matrix toughening by plasticisation.

The strength reduction following a large moisture content was attributed to matrix deterioration: possibly by matrix cracking due to excess swelling.

(b) Notched Specimens

With the exception of very few cases, the tensile strength of notched specimens showed a consistent increase with increasing temperature and/or moisture content. This behaviour was attributed to an interaction of two mechanisms:

(1) notch blunting and,

(2) the state of the matrix.

The effect of the two mechanisms responsible for the notched tensile strength variation were successfully incorporated in a schematic presentation. The exact influence of each mechanism upon strength was isolated. Finally, it has been shown through the schematic diagrams that, like plain specimens, notched specimens also reach a *tensile limit* when tested in a range of hygrothermal environments. The conditions under which such a limit is reached depends upon the specimen's geometrical features.

It was found that the rate of increase of the blunting mechanism with respect to temperature and/or moisture, was much greater in specimens with circular holes compared to specimens with sharp notches.

It has been observed that dry specimens tested under elevated temperature conditions exhibited the same failure mode as otherwise identical wet specimens tested at a lower temperature. This phenomenon was referred to as the moisture/temperature equivalence. For 914C such equivalence was observed between two sets of conditions: 90°C/dry, RT/1.4%wet, and 130°C/dry, 90°C/1.4%wet.

Unlike tensile strength, a consistent reduction in compressive strength was observed with increasing temperature and/or moisture content. Several factors responsible for the observed behaviour were isolated the most important of which are:

(1) state of the fibre/matrix interface,

(2) matrix lateral support and,

(3) ply coupling.

It has been observed that under a hot/wet environment both the effect of the notch geometry as well as stacking sequence disappear. In other words, the hot/wet notched compressive strength of laminated composites is determined by the net-section area of the load carrying material.

(c) Computational Studies

As a result of the finite element analyses, at least two important points were identified:

(1) the ratio R_{ms} for a circular hole is higher than that for a sharp notch and,

(2) in the case of the specimens with circular holes, the stress concentration in the ±45° plies occurs ahead of the hole boundary at the point of intersection of two mutually perpendicular tangents to the hole boundary, oriented at ±45° to the loading axis.

7.1.2 Fatigue Studies

Two types of tension-compression fatigue were performed: fatigue tests at a predetermined load amplitude and number of fatigue cycles, and fatigue tests to failure. The first type of fatigue test was usually followed by residual strength evaluation under a range of hygrothermal environments.

(a) Damage Evaluation

Several damage evaluation techniques comprising C-scan, X-ray, optical and scanning electron microscopy, and deply, were employed for a detailed fatigue damage characterisation.

A typical fatigue damage development around a notch consisted of fibre splitting and ply delamination. More rarely and under situations of high stress amplitudes or after a very large number of fatigue cycles, fibre fracture was also evident.

The fatigue damage development was found to depend upon several factors such as:

(1) notch geometry,

(2) stacking sequence,

(3) cyclic stress amplitude,

(4) environment and,

(5) material system.

Based on damage examination, a physical parameter related to the damage development was isolated. This parameter was defined as the damage transition stress, denoted S_t. It has been shown that the magnitude of S_t may constitute a measure of the fatigue performance of a particular material system. Some of the most important observations made in relation to the characteristic parameter S_t, are:

(1) S_t may be identified from a "linear S-N plot",

(2) the ratio S_t/R_{ms} , for the cases examined, appears to be independent of the notch geometry,

(3) the magnitude of S_t depends upon factors such as; material system, lay-up and stacking sequence. Furthermore, it is anticipated that the magnitude of S_t may also depend upon the loading regime; eg axial, biaxial, bending etc,

(4) for the range of wet environments examined, it was found that for a particular material system, the magnitude of S_t remained approximately constant,

(5) the slope of a "linear S-N plot" is an indication of a material's resistance to delamination under cyclic loading and,

(6) depending upon the lay-up and notch geometry combination S_t may be identified by means of non-destructive damage examination.

As a result of the unique behaviour of the parameter S_t, a simple screening method for fatigue insensitive composite laminates was proposed.

(b) Residual Strength Tests

As a result of an extensive residual strength study, under a wide range of hygrothermal conditions, a schematic model was developed which demonstrates the effect of several factors upon residual strength. The contributing factors have been incorporated into three major categories:

(1) notch blunting

(2) fibre degradation and,

(3) matrix degradation.

It is thought that, although during the progress of a fatigue tests the above mechanisms may interact and influence the development of one another, for a given damaged specimen, these can be consider to have an independent influence upon residual strength.

7.2 FURTHER WORK

This research work concentrated upon understanding the fatigue damage processes and their relation to environmental exposure. It is hoped that as a result of this study, a small contribution has indeed been made to the development of a basic understanding of the complex behaviour of composite materials. However, at the same time a number of unanswered questions were also developed, some of which are:

(1) is the ratio S_t/R_{ms}, for a given stacking sequence, constant for a wider choice of notch geometries?

(2) does the superior fatigue performance of a notched composite, based upon the transition stress screening method, translate to a superior performance in the unnotched state? If not, what is the significance of unnotched specimen testing with respect to structural design limits?

(3) what is the effect of changing the loading mode upon the magnitude of S_t?

(4) how do specimen geometrical parameters affect the magnitude of S_t.

(5) can the superior behaviour of the laboratory size specimens be reflected into the performance of a full size structure?

Unless a reliable answer to the above questions is obtained, the value of the characteristic parameter S_t, may never be realised. Therefore, it is suggested that any further work along the lines of the present programme is directed towards answering some of these questions.

REFERENCES

1) Wright W.W. "A review of the influence of absorbed moisture on the properties of composite materials based on epoxy resins", RAE Tech. Memo. MAT 324, 1979.

2) Komorowski J.P. "Hygrothermal effects in continuous fibre reinforced composites. Part I: Thermal and moisture diffusion in composite materials", Aeronautical note, NAE-AN-4, NRC Canada, 1983.

3) Komorowski J.P. "Hygrothermal effects in continuous fibre reinforced composites. Part II: Physical properties", Aeronautical note, NAE-AN-10, NRC Canada, 1983.

4) Komorowski J.P. "Hygrothermal effects in continuous fibre reinforced composites. Part III: Mechanical properties 1, Static tests, Aeronautical note, NAE-AN-11, NRC Canada, 1983.

5) Komorowski J.P. "Hygrothermal effects in continuous fibre reinforced composites. Part IV: Mechanical properties 2, Fatigue and time-dependent properties", Aeronautical note, NAE-AN-12, NRC Canada, 1983.

6) Hiel C.C. and Adamson M.J. "Durability of composites", Proc. ICCM-VI & ECCM 2, Vol.4, pp. 172-179, London, 1987.

7) Eckstein B.H. "Moisture absorption by epoxy laminating resins", American Chemical Society, Org. Coatings. Plast. Chem. Preprints, 38, p. 503, 1978.

8) Piggott M.R. "Water absorption in carbon and glass fibre composites", Proc. ICCM VI & ECCM 2, Vol.4, pp. 180-189, London, 1987.

9) Dewas J.N. and Favre J.P. "Prevision of CFRP moisture absorption from data on neat resin", Proc. ICCM-V, pp. 1059-1069, San Diego, 1985.

10) Shen C.H. and Springer G.S. "Moisture absorption and desorption of composite materials", J. Composite Materials, Vol.10, pp. 2-20, 1976.

11) Jackson S.P. and Weitsman Y. "Moisture effects and moisture induced damage in composites", Proc. ICCM-V, pp. 1435-1452, San Diego, 1985.

12) Hertz J. "Moisture effects on spacecraft structures", 24th National SAMPE Symposium, 1979.

13) Grayson M.A. and Wolf C.J. "Diffusion of water in carbon epoxy composites", Proc. ICCM-V, pp. 1463-1473, San Diego, 1985.

14) Carter H.G. and Kibler K.S. "Rapid moisture characterization of composites and possible screening applications", J. Composite Materials, Vol.10, pp. 355-370, 1976.

15) Harper B.D., Staab G.H. and Chen R.S. "A note on the effects of voids upon the hygral and mechanical properties of AS4/3502 graphite/epoxy", J. Composite Materials, Vol.21, pp.280-289, 1987.

16) Apicella A. and Nicolais L. "Environmental aging of epoxy resins: Synengistic effect of sorbed moisture, temperature and applied stress", Industrial Engineering Chemistry Production Research Development, Vol.20, PP.138-144, 1981.

17) Curtis P.T. and Moore B.B. "The effect of environmental exposure on the fatigue behaviour of CFRP laminates", RAE TR 84027, 1984.

18) Edge E.C. "The implications of laboratory acceleratedconditioning of carbon fibre composites", AGARD-CP-288, 1980.

19) Carter H.G. and Kibler K.G. "Langmuir-type model for anomalous moisture diffusion in composite resins", J. Composite Materials, Vol.12, pp.118-131, 1978.

20) Tajima Y.A. and Sandorff P.E. "Experimental determination of moisture distribution and diffusion parameters in graphite-epoxy laminates", ASCE annual convention, Chicago, 1978.

21) Murayama T. "Dynamic mechanical analysis of polymeric material, Elsevier Scientific Publishing Company, pp. 201-202, 1978.

22) Putter S., Buchanam D.L. and Rehfield L.W. "Influence of frequency and environmental conditions on dynamic behavior of graphite/epoxy composites", ASTM STP 787, pp. 414-424, 1982.

23) Museux F., Surrel Y., Vautrin A. and Verchery G. "Characterization of the mechanical behaviour of T300/914 laminates using the local viscoelastic response", Proc. ICCM VI & ECCM 2, Vol.4, pp. 252-261, London, 1987.

24) Gillatt O. and Broutman L.J. "Effect of an external stress on moisture diffusion and degradation in a graphite-reinforced epoxy laminate", ASTM STP 658, pp.61-83, 1978.

25) Collings T.A. and Stone D.E.W. "Hygrothermal effects in CFC laminates part II - Damaging effects of temperature moisture and thermal spiking", RAE TR 84003, 1984.

26) Pritchard G. and Stansfield K. "The thermal spike behaviour of carbon fibre reinforced plastics", Proc. ICCM VI & ECCM 2, Vol.4, pp. 190-199, London, 1987.

27) Neumann S. and Marom G. "Stress dependence of the coefficient of moisture diffusion in composite materials" Polymer Composites, Vol.6 no.1, pp.9-12, 1985.

28) Fahmy A.A. and Hurt J.C. "Stress dependence of water diffusion in epoxy resin", Polymer Composites, Vol.1 no.2, pp.77-80, 1980.

29) Hiel C., Cardon A., Adamson M. and Nelson H. "The combined effects of stress and moisture on the structural integrity of composites", Proc. ECCM 1, pp. 193-198, Bordeaux, 1985.

30) Neumann S. and Marom G. "Prediction of moisture diffusion parameters in composite materials under stress", J. Composite Materials, Vol.21, pp.68-80, 1987.

31) Blikstad M., Sjoblom P.O.W. and Johannesson T.R. "Long-term moisture absorpion in graphite/epoxy angle-ply laminates", J. Composite Materials, Vol.18, pp.32-46, 1984.

32) Kelly F.N. and Bueche F. "Viscosity and glass transition temperature relations for polymer-diluent systems", J. Polymer Science, Vol.50, pp.549-556, 1961.

33) Carter H.G. and Kibler K.S. "Entropy model for glass transition in wet resins and composites", J. Composite Materials, Vol.11, pp.265-275, 1977.

34) Barton J.M. and Greenfield D.C.L. "The use of dynamic mechanical methods to study the effect of absorbed water ontemperature-dependent properties of an epoxy resin-carbon fibre composite", British Polymer Journal, Vol.18, no.1, pp. 51-56, 1986.

35) Marchetti M., Maura G., Pauri M. and Veniali F. "Effect of moisture on thermal properties of composite materials for aerospace applications", Proc. ECCM 1, pp. 201-206, Bordeaux, 1985.

36) Danieley N.D. and Long E.R. "Effects of curing on the glass transition temperature and moisture absorption of a neat epoxy resin", J. Polymer Science, Vol.19, pp. 2443-2447, 1981.

37) Allred R.E. "The effect of temperature and moisture content on the flexural response of kevlar/epoxy laminates: Part II. (±45/0/90) filament orientation", J. Composite Materials, Vol.15, pp.117-132, 1981.

38) Adamson M.J. "Thermal expansion and swelling of cured epoxy resin used in graphite/epoxy composite materials", J. Material Science, Vol.15, pp.1736-1745, 1980.

39) Harper B.D. "The effects of moisture induced swelling upon the shapes of anti-symmetric cross-ply laminates", J. Composite Materials, Vol.21, pp.36-48, 1987.

40) Henriksen M.S., Arthur P.D. and Pardoen G.C. "Thermal cycling and vacuum baking effects on the thermal expansion of graphite fiber reinforced composite laminates", Proc. Composite Structures 2, pp. 349-363, Paisley, 1983.

41) Loos A.C. and Springer G.S. "Moisture absorption of graphite-epoxy composites immersed in liquids and in humid air", Carbon Reinforced Epoxy Systems Part II. Vol.8, Materials Technology Series, Technomic Publishing Co; pp.165-181, 1982.

42) Collings T.A., Mead D.L. and Stone D.E.W. "The effects of high temperature excursions on environmentally exposed CFC", RAE TR 85074, 1985.

43) Morgan R.J., O'Neal L.E. and Fanter D.L. "The effect of moisture on the physical and mechanical integrity of epoxies", J. Material Science, Vol.15, pp.751-762, 1980.

44) Dickson R.F., Jones C.J., Adam T., Reiter H. and Harris B. "The environmental fatigue behaviour of reinforced plastics", Final Report Agreement no. 2112/034 XR/MAT, University of Bath, School of Materials Science, 1983.

45) Kunz S.C. "Thermomechanical characterization of graphite/polyimide composites", ASTM STP 768, PP.33-53, 1982.

46) White R.J. and Phillips M.G. "Environmental stress-rupture mechanisms in glass fibre/polyester laminates", Proc. ICCM-V, pp. 1089-1099, San Diego, 1985.

47) Joshi OM K. "The effect of moisture on the shear properties of carbon fibre composites", Composites, Vol.14 no.3, pp. 196-200, 1983.

48) Porter T.R. "Environmental effects on composite fracture behavior", ASTM STP 734, pp. 396-410, 1981.

49) Bishop S.M. "Effect of moisture on the notch sensitivity of carbon fibre composites", Composites, Vol.14 no.3, pp. 201-205, 1983.

50) Ellis R.E. and Mason A.J. "The in-service flight testing of some carbon fibre-reinforced plastic components", Composites, Vol.14 no.3, pp. 233-236, 1983.

51) Garg A.C. "Hygrothermal influence on fracture behavior of graphite/epoxy laminates", The American Society of Mechanical Engineers, Winter annual meeting, 85-WA/Mats-14, 1985.

52) Grimes G.C. "Experimental study of compression-compression fatigue of graphite/epoxy composites", ASTM STP 734, pp.281-337, 1981.

53) Potter R.T. and Purslow D. "The environmental degradation of notched CFRP in compression", Composites, Vol.14 no.3, pp. 206-224, 1983.

54) Curtis P.T. "An investigation of the mechanical properties of improved carbon fibre composite materials", RAE TR 86021, 1986.

55) Scola D.A. "The status of Bismaleimides for composites", Proc. ICCM-V, pp. 1601-1621, San Diego, 1985.

56) Belend S., Komorowski J.P. and Roy C. "Hygrothermal influence on the interlaminar fracture energy of graphite/bismaleimide modified epoxy composite (IM6/5245C)", Proc. ICCM VI & ECCM 2, Vol.3, pp. 305-316, London, 1987.

57) McKague L., Reynolds J.D. and Fruit J. "Mechanical characteristics of T300-6K/V378A graphite/polyimide", ASTM STP 787, pp. 73-84, 1982.

58) Barrie J.A., Sagoo P.S. and Johncock P. "The sorption and diffusion of water in bismaleimide resin", J. Applied Polymer Science, Vol.33, pp. 2253-2258, 1987.

59) Cogswell F.N. and Hopprich M. "Environmental resistance of carbon fibre-reinforced polyether etherketone", Composites, Vol.14 no.3, pp. 251-253, 1983.

60) Hartness J.T. "Polyether etherketone matrix composites", Proc. SAMPE, Atlanta, 1982.

61) Dew-Hughes D. and Way J.L. "Fatigue of fibre-reinforced plastics: a review", Composites, pp. 167-173, July 1973.

62) Harris B. "Fatigue and accumulation of damage in reinforced plastics", Proc. SEE fatigue Group, pp. 1-15, London, 1977.

63) Stinchcomb W.W. and Reifsnider K.L. "Fatigue damage mechanisms in composite materials: a review", ASTM STP 675, PP. 762-787, 1979.

64) Hahn H.T. "Fatigue behavior and life prediction of composite laminates", ASTM STP 674, pp. 383-417, 1979.

65) Reifsnider K.L. "Fatigue behavior of composite materials", International Journal of Fracture, Vol.16, pp. 563-583, 1980.

66) Harris B. "Fatigue testing of fibre composites", AGARD-LS-118, 1981.

67) Harris B. "Monitoring of damage in fibre composites", AGARD-LS-118, 1981.

68) Reifsnider K.L. "The mechanics of fatigue in composite laminates", Proc. Japan-U.S. Conference, Tokyo, 1981.

69) Gerharz J.J. "Mechanisms of fatigue damage and fatigue testing", AGARD-LS-124, 1982.

70) Hwang W. and Han K.S. "Cumulative damage models and multi-stress fatigue life prediction", J. Composite Materials, Vol.20, pp.125-153, 1985.

71) Curtis P.T. and Dorey G. "Fatigue of composite materials", Proc. Institute of Mechanical Engineers, pp. 297-305, 1986.

72) Lucas J.J. and Sainsbury-carter J.B. "Effects of specimen geometry on fatigue strength of boron and glass epoxy composites", Journal of Materials, JMLSA, Vol.7, no.4, pp. 586-589, 1972.

73) Wang A.S.D., Law G.E. and Warren W.J. "An energy method for multiple transverse cracks in graphite epoxy laminates", Modern Development in Composite Materials and Structures, Ed. Vinson J.R., P.17, 1979.

74) Beaumont P.W.R. and Harris B. "The effect of environment on fatigue and crack propagation in carbon-fibre-reinforced epoxy resin", Plastics & Polymers, Proc. Carbon Fibres Their Composites and Applications, no.5, pp. 283-291, London 1971.

75) Stinchcomb W.W., Reifsnider K.L., Williams R.S. and Marcus L.A. "Failure modes in composites II, Eds. Fleck J. and Mehan R., Metallurgical Society of the American Institute of Mining Engineers, PP. 3-15, 1975.

76) Stinchcomb W.W., Reifsnider K.L., Yeung P. and Masters J. "Effect of ply constraint on fatigue damage development in composite material laminates", ASTM STP 723, pp. 64-84, 1981.

77) Whitcomb J.D. "Experimental and analytical study of fatigue damage in notched graphite/epoxy laminates", ASTM STP 723, pp. 48-63, 1981.

78) Sumsion H.T. and Williams D.P. "Effects of environment on the fatigue of graphite-epoxy composites" ASTM STP 569, pp. 226-247, 1975.

79) Hoa S.V. "Effects of liquids on the stress-rupture lives of fiber glass-reinforced plastics", ASTM STP 734, pp. 411-419, 1981.

80) Hojo M., Tanaka K., Gustafson C. G. and Hayashi R. " Effect of water environment on propagation of delamination fatigue cracks in CFRP", Proc. ICCM VI & ECCM 2, Vol.4, pp. 222-231, London, 1987.

81) Rotem A. and Nelson H.G. "Fatigue behavior of graphite-epoxy laminates at elevated temperatures", ASTM STP 723, pp. 152-173, 1981.

82) Ryder J.T., Walker E.K. "The effect of compressive loading on the fatigue lifetime of graphite/epoxy laminates", AFML-TR-79-4128, 1979.

83) Black N.F. and Stinchcomb W.W. "Compression fatigue damage in thick, notched graphite/epoxy laminates", ASTM STP 813, PP. 95-115, 1983.

84) Kellas S. "Tension-compression fatigue performance of notched orthotropic CFRP laminates", MSc Thesis, Imperial College, Department of Aeronautics, 1984.

85) Morton J. and Praulitis E. "Compression behaviour of GRP laminates", MoD (PE) Agreement no. 2037/0259 XR/MAT, Imperial College, Department of Aeronautics, Progress report, 1985.

86) Kretsis G. "Mechanical characterisation of hybrid glass/carbon fibre-reinforced plastics" PhD Thesis, Imperial College, Department of aeronautics, 1987.

87) Sottos N.R. and Hodgkinson J.M. "A practical comparison of standard test methods using carbon fibre-reinforced epoxy", Proc. ICCM-VI & ECCM 2, Vol.1, pp. 310-320, London, 1987.

88) British Standard Methods of Testing, BSI, BS 2782; Pt 3; Methods 320A to 320F, 1976.

89) Owens G.A. "The material development, component manufacture and post-service evaluation of RB 211-524 cowl doors utilising carbon fibre composite materials", Proc. Composite Structures 3, pp. 83-99, Paisley, 1985.

90) Jamison R.D. and Reifsnider K.L. "Advanced fatigue damage development in graphite epoxy laminates", AFWAL-TR-82-3103, VPI & SU, Interim report, 1982.

91) Rummel W.D., Tedrow T. and Bunkerhoff H.D. "Enhanced stereoscopic NDE of cmposite materials", AFWAL-TR-80-3053, 1980.

92) Freaman S.M. "Characterization of lamina and interlaminar damage in graphite-epoxy composites by the deply technique", ASTM STP 787, pp. 50-62, 1982.

93) Bar-Yosph P. and Arrashi J. "Interlaminar stress analysis for laminated plates containing a curvilinear hole", Computers & Structures Vol.21, No.5, pp. 917-932, 1985.

94) Lucking W.M., Hoa S.V. and Sankar T.S. "The effect of geometry on interlaminar stresses of $[0/90]_S$ composite laminates with circular holes", Journal of Composite Materials, Vol.17, pp. 188-198, 1984.

95) Rybicki E. F. and Schmveser D.W. "Effect of stacking sequence and lay-up angle on free edge stresses around a hole in alaminated plate under tension", Journal of Composite Materials, Vol.12, pp. 300-313, 1978.

96) Rybicki E.F. and Pagano N.J. "A study of the influence of microstructure on the modified effective modulus approach for composite laminates", Proc. ICCM 1975, Published by the Metallurgical society of AIME, New York, Vol.2, pp.149-156, 1975.

97) Hyer M.W., Herakovich C.T., Milkovich S.M. and Short JR. J.S. "Temperature dependence of mechanical and thermal expansion properties of T300/5208 graphite/epoxy", Composites, Vol.14 no.3, pp. 276-280, 1983.

98) Kulkarni S.V., McLaughlin P.V., Jr., Pipes R.B. and Rosen B.W. "Fatigue of notched fiber composite laminates: analytical and experimental evaluation", ASTM, STP 617, pp. 70-92,1977.

99) Chang F. H., Gordon D.E. and Gardner A.H. "A study of fatigue damage in composites by nondestructive testing techniques",ASTM STP 636, pp. 57-72, 1977.

100) Reifsnider K.L., Stinchcomb W.W. and O' Brien T.K. "Frequency effects on a stiffness-based fatigue failure criterion in flawed composite specimens", ASTM STP 636, pp. 171-184, 1977.

101) Simonds R.A., Bakis C.E. and Stinchcomb W.W. "Effects of matrix toughness on fatigue responce of graphite fiber composite laminates", Presented at: 2nd ASTM Symposium on Composite Materials: Fatigue and Fracture Cincinnati, Ohio, 1987.

102) Chiao C.C., Moore R.L. and Chiao T.T. "Measurement of shear properties of fibre composites. Part I: Evaluation of test methods" Composites pp. 161-169, 1977.

103) Collings T.A. and Copley S.M. "On the accelerated ageing of CFRP", Composites, Vol.14, no.3, pp. 180-188, 1983.

104) Whitney J.M. and Browning C.E. "Some anomalies associated with moisture diffusion in epoxy matrix composite materials" ASTM STP 658, 1978.

105) Fahmy A.A. and Hurt J.C. "Stress dependence of water diffusion in epoxy resin", Polymer Composites, Vol.2, no.2, pp. 77-80, 1980.

106) Neumann S. and Marom G. "Free-volume dependent moisture diffusion under stress in composite materials", Journal of Material Science, Vol.21, no.1, pp. 26-30, 1986.

107) Rosen B.W. "A simple procedure for experimental determination of the longitudinal shear modulus of unidirectional composites", Journal of Composite Materials, Vol.6, pp. 552-554, 1972.

APPENDIX I

MOISTURE ABSORPTION PREDICTION MODELS

In order to evaluate a composite structure's long term integrity, it is often required to predict the moisture content and/or distribution throughout the structure's service lifetime. The most widely used models for such predictions are based on Fick's first and second laws of moisture diffusion which are analogous to thermal conduction. Fick's first law states that the rate of transfer of matter, F, through a unit area is proportional to the concentration gradient normal to the section;

$$-F_i = D_{ij} \frac{\partial c}{\partial x_i}$$

Fick's second law, in its generalised form may be written as;

$$\frac{\partial c}{\partial t} = \frac{\partial}{\partial x_i} \left[D_{ij} \frac{\partial c}{\partial x_j} \right]$$

where: c -Moisture concentration
D_{ij} -Diffusion coefficient (tensor)
x_i -Co-ordinate axis
t -time.

If it is assumed that the diffusion coefficient D_{ij} does not vary significantly with moisture content, which appears to be true for reinforced epoxy composites, (103), the equation above may be written as;

$$\frac{\partial c}{\partial t} = D_{ij} \frac{\partial^2 c}{\partial x_i \partial x_j}$$

or according to Collings and Copley (103) a more useful form, for the one dimensional diffusion problem, the equation above becomes;

$$\frac{\partial M}{\partial t} = D \frac{\partial^2 M}{\partial x^2}$$

where M is the moisture content, expressed as a percentage of the dry weight, and D is the diffusion coefficient. Methods of solution of the equation above are described in references (2) and (103).

A number of expressions for calculating the diffusion coefficient, D, can be found in the literature some of which are;

for a single ply, $D_{11} = (1-v_f)D_r$ and,

$$D_{22} = [1-2\sqrt{(v_f/\Pi)}]D_r$$

(NB; for an orthotropic ply, such as a unidirectional layer, $D_{33}=D_{22}$)

where: D_{11} -Diffusion coefficient along the fibre direction
D_{22} -Diffusion coefficient transverse to the fibres
D_r -Diffusion coefficient of the resin
v_f -Fibre volume fraction.

The above expressions were presented in reference (2), and may be used provided that the moisture diffusivity of the fibres or the interface are negligible compared to the diffusivity of the resin. Furthermore, the material has to be stress free.

Collings and Copley (103) have presented an expression for the one dimensional diffusion coefficient, D, which for a particular composite material may be obtained experimentally from;

$$D = \frac{\Pi h^2}{16M_\infty^2}\left(\frac{M_2-M_1}{\sqrt{t_2}-\sqrt{t_1}}\right)^2$$

where M_1 and M_2 are the moisture contents after time t_1 and t_2 respectively, expressed as percentage weight gain, and taken from the linear portion of the M versus $\sqrt{t}$ plot. M_∞ is the expected moisture content at equilibrium and h is the laminate thickness. The above equation does not take into account the geometrical features of a specimen. A correction factor has been presented by Shen and Springer (10);

$$D_{cor.} = D(1+h/w+h/l)^{-2}$$

where: w -laminate width
l -laminate length
h -laminate thickness.

In many cases (103), it may be assumed that D is independent of the relative humidity of exposure, and depends upon the absolute temperature alone. In this case the relationship between the temperature of exposure T and the diffusion coefficient, D, is given by;

$$\log_e D \propto \frac{1}{T}$$

Whitney and Browning (104) showed that, above a certain humidity and/or temperature of exposure, the process of moisture diffusion may deviate from that defined by Fick's equations. Furthermore, Fickian diffusion does not account for changes in the diffusion process due to stresses in the material, for example. This problem has been examined by, amongst others, Fahmy and Hurt (105). They found an exponential dependence of D upon a dilatational stress $\sigma(z,t)$;

$$D_{(z,t)} = D_0 e^{-A\sigma(z,t)}$$

where: D_0 -Diffusion coefficient for $\sigma=0$
A -Stress sensitivity factor
t -Time
z -Axis perpendicular to the plane of the specimen.

For small stresses, such as swelling induced stresses, the above expression may be written as;

$$D_{(z,t)} = D_0[1+A\sigma(z,t)]$$

Piggot (8) has presented an approximate expression for D, for a composite ply, which takes into account the diffusion properties of the polymer matrix, the fibres, and the interface, but **not** the voids in the matrix;

$$D = D_p\left[\frac{D_p}{D_p-D_f}\left\{\frac{2}{\sqrt{1-c^2}}\tan^{-1}\sqrt{\frac{1+c}{1-c}}-\frac{\Pi}{2}\right\}+\frac{D_p t}{D_p(a-t)+D_i t}+\frac{a-r-t}{a}\right]^{-1}$$

where;

$$c = r(D_p - D_f)/[\,D_p(a-t)+ D_i t]$$

a -Size of the square unit cell considered; thus $v_f=4a^2/\Pi r^2$
v_f -Fibre volume fraction
D_p -Diffusion coefficient of the polymer matrix
D_f -Diffusion coefficient of the fibres
D_i -Diffusion coefficient of the interfacial region

$2r$ -diameter of the fibres

t -thickness of the interfacial region.

Neumann and Marom (30) have listed a number of free-volume based theories for diffusion processes in which the voids in the material are accounted for: ie for a polymer;

$$D = A\exp(-\gamma\upsilon^*/\upsilon_f) \quad \text{- Cohen/Turnbull equation}$$

where: υ^* -Critical void volume

A,γ -Constants

υ_f -Free volume per molecule.

The free volume is defined here as the difference between the measured volume of a polymer and the occupied volume, which is the volume occupied by the actual mass of a molecule plus the volume it occupies because of thermally dependent vibration.

For a composite under an in-plane stress, σ_x, where only the matrix is assumed to absorb moisture, the diffusion coefficient D_σ may be obtained from the equation below, reference (30);

$$\log_e\left(\frac{D_\sigma}{D_o}\right) = \frac{a}{v_m}\,\frac{(\Delta V/V_o)_m}{\upsilon_{fo}\left[\upsilon_{fo}+(\Delta V/V_o)_m\right]}$$

where: D_σ -Diffusion coefficient of the stressed material

D_o -Diffusion coefficient of the unstressed material

$(\Delta V/V_o)_m$ -Volume strain in the matrix: an expression for the volume strain in terms of the applied in-plane stress, σ_x, can be found in reference (106).

υ_{fo} -Free volume per molecule for $\sigma=0$

v_m -Matrix volume fraction.

The moisture absorption capacity M_∞, for a composite ply under an applied in-plane stress σ_x, is given by;

$$(M_\infty)_\sigma = (M_\infty)_o + (\Delta V/V_o)_m \frac{\rho_w}{\rho_c} v_m$$

where: $(M_\infty)_\sigma$ -Moisture content at equilibrium for a stressed material

$(M_\infty)_o$ -Moisture content at equilibrium for $\sigma_x=0$

ρ_w -Water density

ρ_c -Composite density.

Carter and Kibler (19) have presented evidence of anomalous moisture diffusion in epoxy matrices which under a prolonged exposure did not obey the Fickian diffusion theory. Some of these anomalies are: following a long term exposure, under constant environmental conditions, the moisture gain plotted against $\sqrt{t}$ tends to rise above an equilibrium plateau. In some cases a secondary equilibrium level was also evident. Another anomaly relates to a history dependence of saturation level, or equilibrium moisture content (M_∞). A model in which anomalies can be accounted for has been presented by Carter and Kibler (19). An expression for the moisture content after time t, m_t, is given by;

$$m_t = M_\infty \left[1 - \frac{8}{\Pi^2} \sum_{i=1}^{\infty\,(odd)} \frac{r_i^+ e^{-r_i^- t} - r_i^- e^{-r_i^+ t}}{i^2 \left(r_i^+ - r_i^- \right)} + \frac{8}{\Pi^2} \left(\frac{k\beta}{\gamma+\beta} \right) \sum_{i=1}^{\infty\,(odd)} \frac{e^{-r_i^- t} - e^{-r_i^+ t}}{r_i^+ - r_i^-} \right]$$

where;

$$r_i^{\pm} = \frac{1}{2} \left[\left(kc^2 + \gamma + \beta \right) \pm \sqrt{\left(kc^2 + \gamma + \beta \right)^2 - 4k\beta c^2} \right]$$

and,

$$k = \Pi^2 D_\gamma / (2\delta)^2$$

An approximate solution may be obtained if 2γ and 2β are both small compared to k:

$$m_t \approx M_\infty \left[\frac{\beta}{\gamma+\beta} e^{-\gamma t} \left(1 - \frac{8}{\Pi^2} \sum_{i=1}^{\infty\,(odd)} \frac{e^{-ki^2 t}}{i^2} \right) + \frac{\beta}{\gamma+\beta} \left(e^{-\beta t} - e^{-\gamma t} \right) + \left(1 - e^{-\beta t} \right) \right]$$

where: i -Odd integer

β -Probability per unit time that a bound H_2O molecule becomes mobile

γ -Probability per unit time that an H_2O molecule becomes bound

δ -Specimen half thickness

k -Characteristic diffusion constant, $k=\Pi^2 D_\gamma/(2\gamma)^2$

D_γ -Diffusion coefficient for mobile H_2O molecules.

APPENDIX II

EVALUATION OF THE ELASTIC CONSTANTS

For a three dimensional stress analysis of an orthotropic material, such as a unidirectional ply, the stress-strain relationship is given by;

$$\begin{bmatrix} \sigma_{11} \\ \sigma_{22} \\ \sigma_{33} \\ \sigma_{23} \\ \sigma_{13} \\ \sigma_{12} \end{bmatrix} = \begin{bmatrix} \frac{1-\nu_{23}\nu_{32}}{E_{22}E_{33}\Delta} & \frac{\nu_{12}+\nu_{32}\nu_{13}}{E_{11}E_{33}\Delta} & \frac{\nu_{13}+\nu_{12}\nu_{23}}{E_{11}E_{22}\Delta} & & & \\ \frac{\nu_{12}+\nu_{32}\nu_{13}}{E_{11}E_{33}\Delta} & \frac{1-\nu_{13}\nu_{31}}{E_{11}E_{33}\Delta} & \frac{\nu_{23}+\nu_{21}\nu_{13}}{E_{11}E_{22}\Delta} & 0 & & \\ \frac{\nu_{13}+\nu_{12}\nu_{23}}{E_{11}E_{22}\Delta} & \frac{\nu_{23}+\nu_{21}\nu_{13}}{E_{11}E_{22}\Delta} & \frac{1-\nu_{12}\nu_{21}}{E_{11}E_{22}\Delta} & & & \\ & & & G_{23} & & \\ & 0 & & & G_{13} & \\ & & & & & G_{12} \end{bmatrix} \begin{bmatrix} \varepsilon_{11} \\ \varepsilon_{22} \\ \varepsilon_{33} \\ \varepsilon_{23} \\ \varepsilon_{13} \\ \varepsilon_{12} \end{bmatrix}$$

Where;

$$\Delta = \frac{1-\nu_{12}\nu_{21}-\nu_{23}\nu_{32}-\nu_{31}\nu_{13}-2\nu_{21}\nu_{32}\nu_{13}}{E_{11}E_{22}E_{33}}$$

E -Young's modulus
G -Shear modulus
and ν -Poisson's ratio.

The subscripts 1, 2, 3, represent a set of orthogonal axes: 1 and 2 being the in-plane axes with 1 along the fibre direction.

In order to describe the 6x6 stiffness matrix, shown above, six independent elastic constants are required; E_{11}, E_{22}, G_{12}, G_{23}, ν_{12}, and ν_{23}. E_{11} and ν_{12} were determined from the stress-strain relationship of a unidirectional specimen, loaded in tension along the fibre direction, direction 1. A similar method of approach was followed in the calculation of E_{22} and ν_{23} using specimens type

number 3, see figure 3.12. G_{12} was evaluated from a 10° off-axis specimen test using the equation;

$$\frac{1}{E_{xx}} = \frac{1}{E_{11}}\cos^4\theta + \left(\frac{1}{G_{12}} - \frac{2\nu_{12}}{E_{11}}\right)\sin^2\theta\ \cos^2\theta + \frac{1}{E_{22}}\sin^4\theta$$

which may be rearranged to;

$$G_{12} = \frac{E_{xx}E_{11}E_{22}\sin^2\theta}{4E_{xx}\left(\frac{1}{2}\nu_{12}E_{22}\sin^2 2\theta - E_{22}\cos^2\theta - E_{11}\sin^2\theta\right) + E_{11}E_{22}}$$

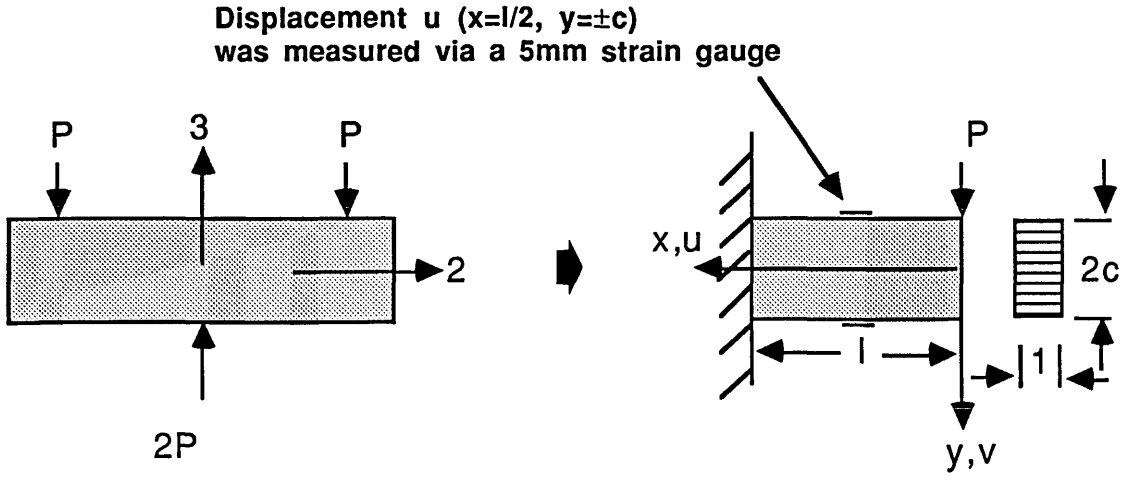
where: θ -Angle between the loading and the fibre directions (=10°)
E_{xx} -Stiffness along the loading direction (the measured stiffness).

For comparison G_{12} was also evaluated from a ±45° test, in which case G_{12} may be determined approximately from;

$$G_{12} = \frac{\sigma_x}{2(\varepsilon_x - \varepsilon_y)}$$

where the shear stress $\tau_{12} = \sigma_x/2$, and the shear strain $\gamma_{12} = \varepsilon_x - \varepsilon_y$; see Rosen (107).

The shear stiffness G_{23}, has been evaluated from a three-point-bend test, and using the theory of elasticity for the bending of a cantilever beam.



where;

$$u(x,y) = -\frac{Px^2y}{2E_{22}I} - \frac{\nu_{23}Py^3}{6E_{22}I} + \frac{Py^3}{6IG_{23}} + \left(\frac{Pl^2}{2E_{22}I} - \frac{Pc^2}{2IG_{23}}\right)y$$

or,

$$u_{x=l/2,\ y=-c} = \frac{Pl^2c}{8E_{22}I} + \frac{\nu_{23}Pc^3}{6E_{22}I} - \frac{Pc^3}{6IG_{23}} - \frac{Pl^2c}{2E_{22}I} + \frac{Pc^3}{2IG_{23}}$$

$$= \frac{Pc^3}{3IG_{23}} - \frac{3Pl^2c}{8E_{22}I} + \frac{\nu_{23}Pc^3}{6E_{22}I}$$

$$= \text{gauge length} \times \varepsilon_x$$

Thus by measuring ε_x or P/ε_x, G_{23} may be obtained. In fact P/ε_x was found to be linear for all values of P. However, due to a difference between the tensile E_{22} (at y=-c) and the compressive E_{22} (at y=+c) two different P/ε_x slopes were obtained: an average value was used in the evaluation of G_{23}.

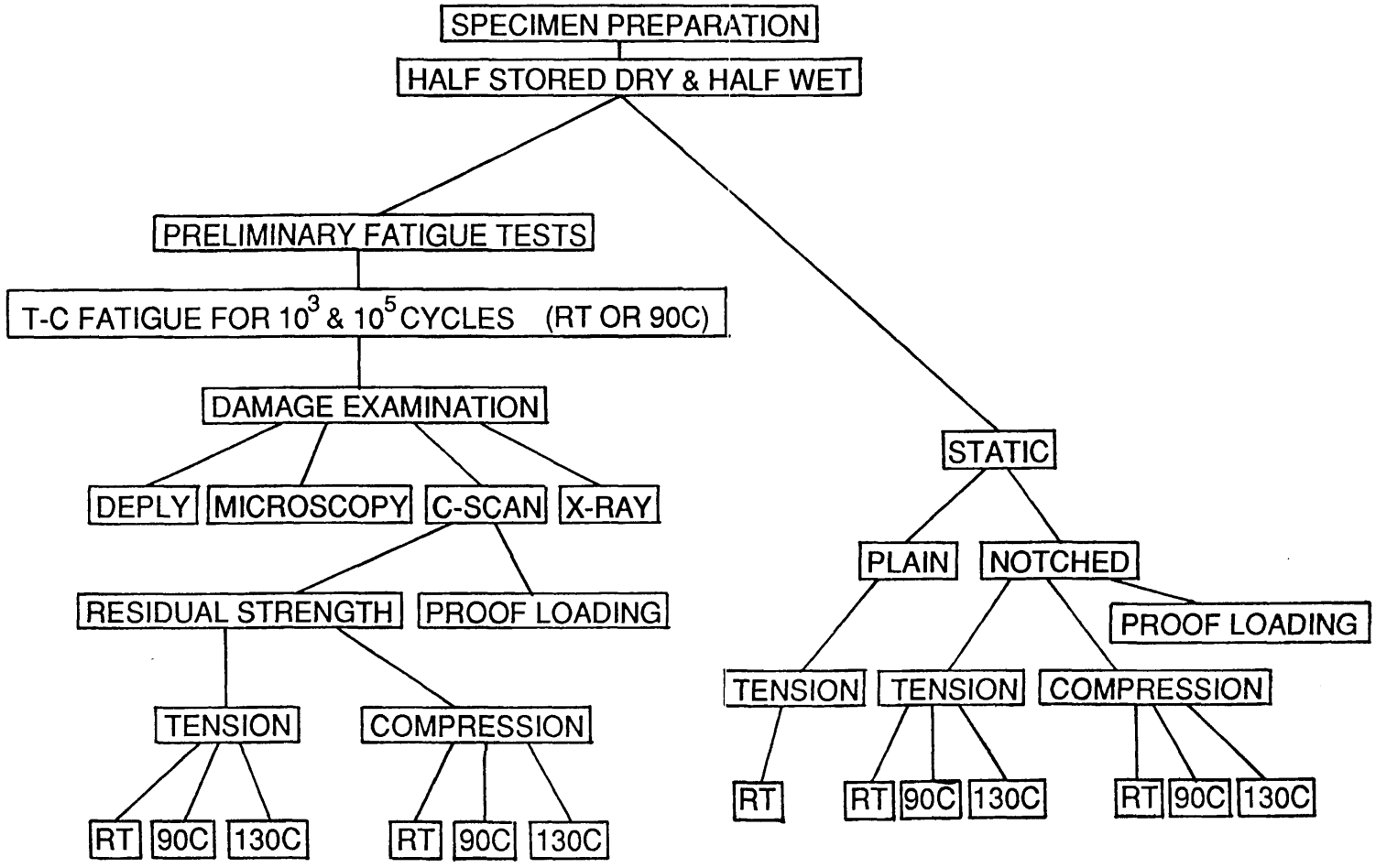


Fig. 3.1: Summary of the main experimental programme for the stacking sequence A, as applied to the environmental conditions; nominally dry, and 1.4% wet. Both specimens with10mm notches and 5mm circular holes were considered.

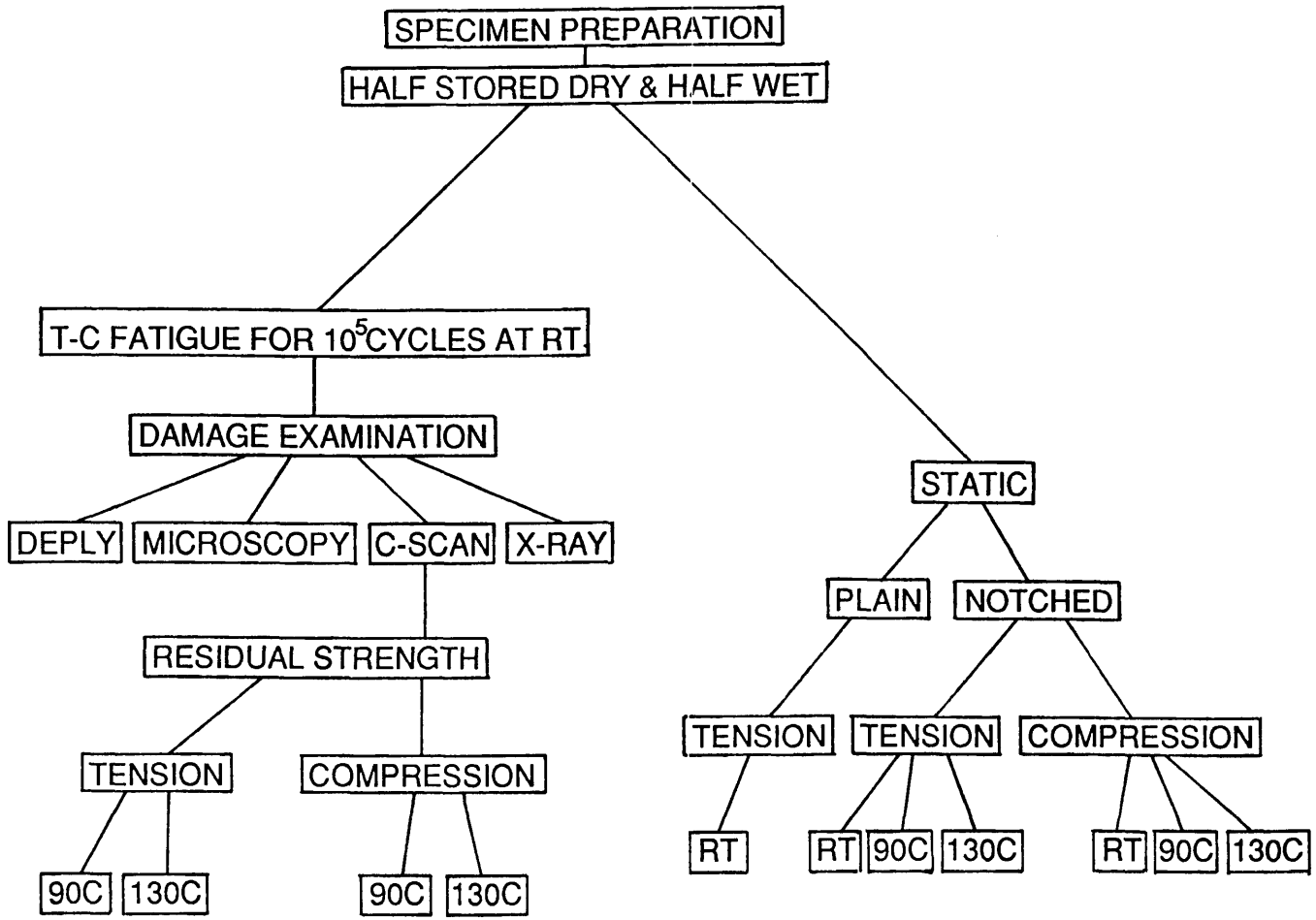
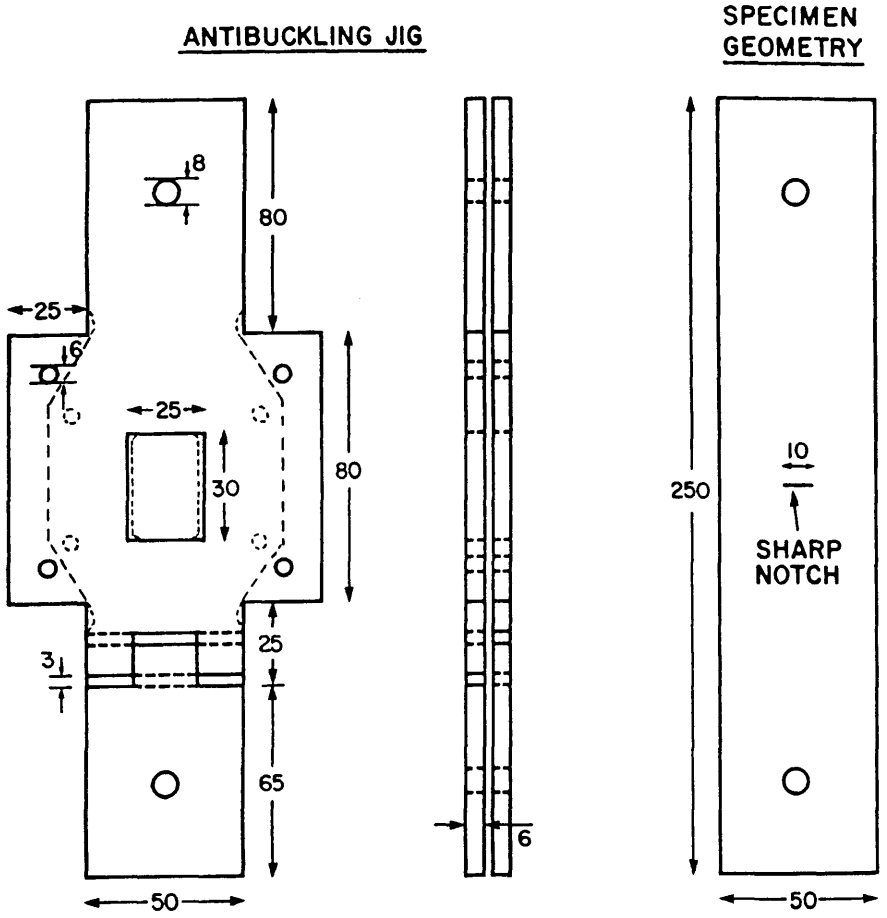


Fig. 3.2: Summary of the main experimental programme for the stacking sequence B, as applied to the environmental conditions; nominally dry, and 1.4% wet. Specimens with 10mm notches were considered only.



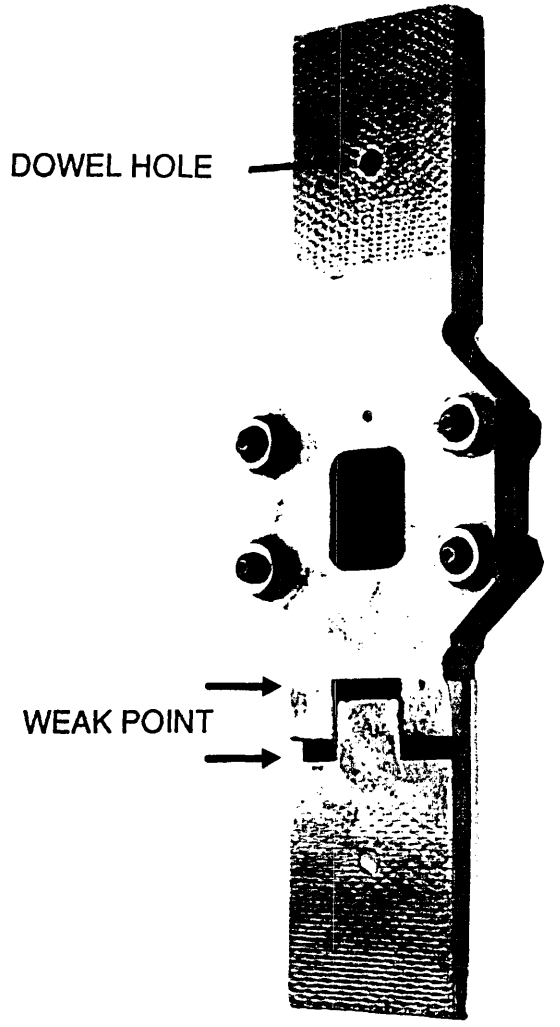


Fig. 3.3: On the left, a drawing of the anti-buckling guide together with the specimen geometry. The modifications are shown by the dotted lines. On the right, a picture of the antibuckling guide containing a notched specimen.

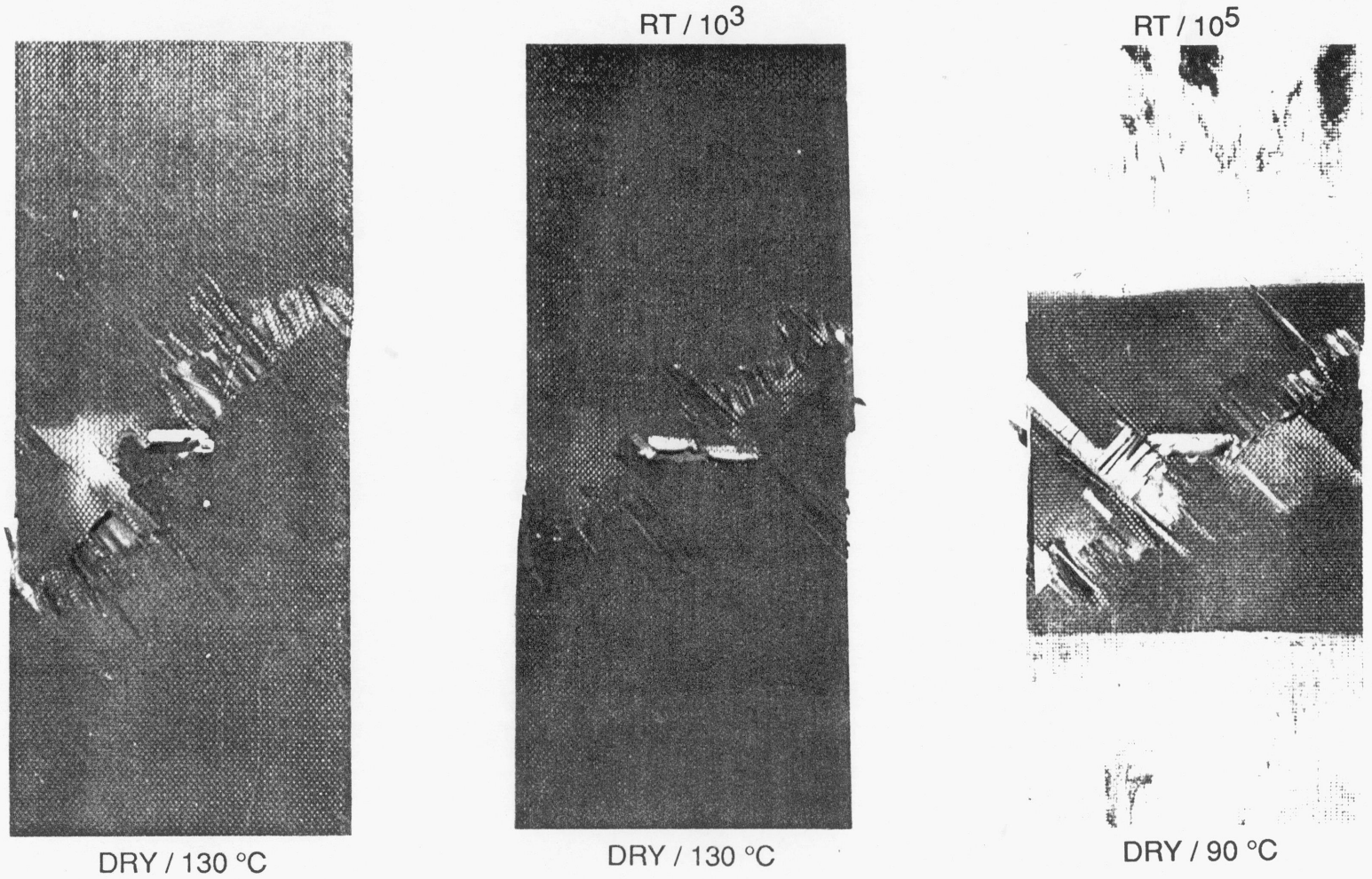


Fig. 4.26: A comparison of tensile fracture modes in dry specimens of sequence A with sharp notches: the fatigue condition is shown at the top and the static condition at the bottom of each picture.

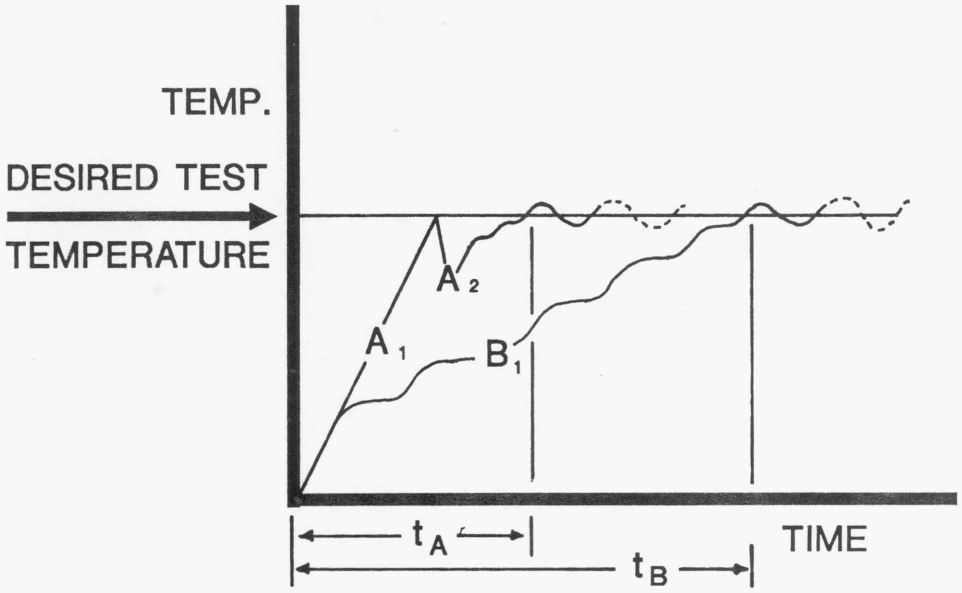


Fig.3.5: A schematic representation of the heating-up procedure, showing the time saving when a twofold controller adjustment (A_1 and A_2) is employed, instead of a single (B_1).

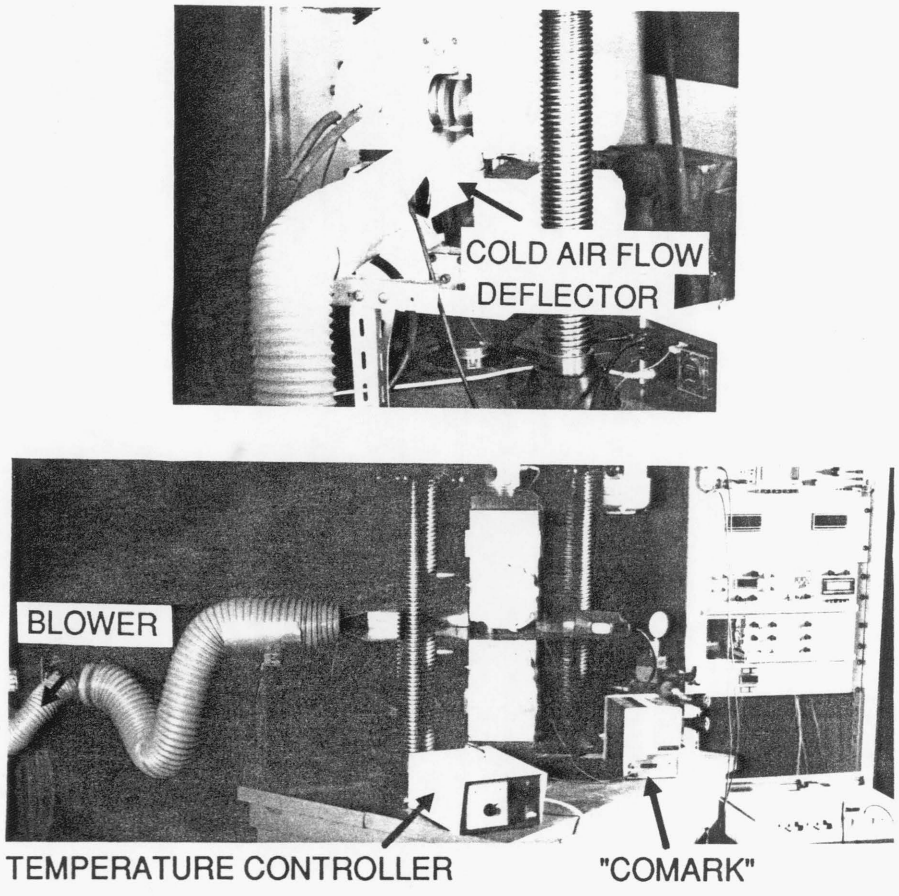
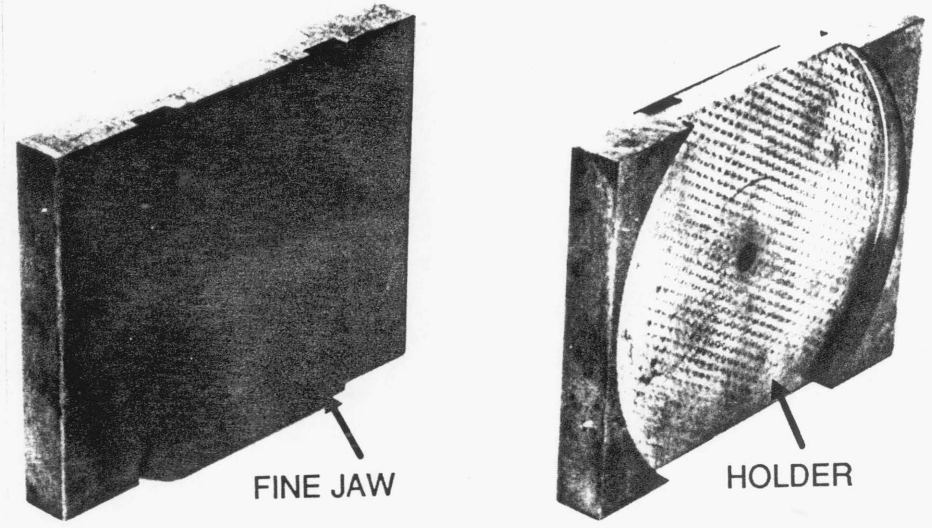


Fig. 3.6: Pictures of the experimental set-up showing the use of the grip-cooling apparatus in conjunction with the specimen-heating apparatus.



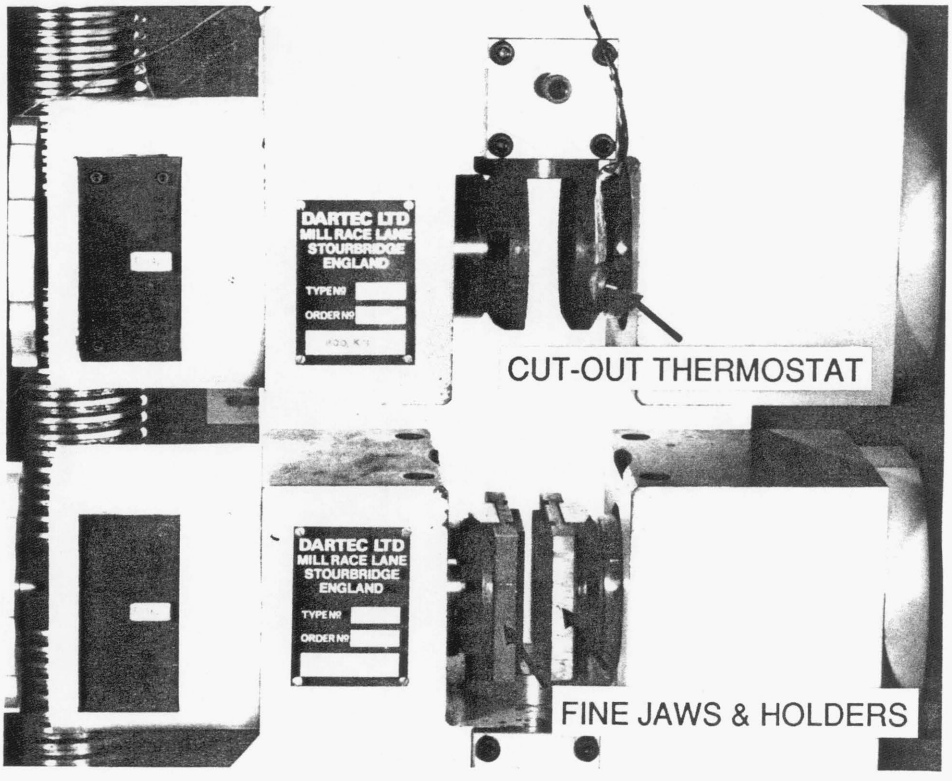


Fig. 3.7: Above, a close-up photograph of the fine jaw and holder arrangement which was used during plain (unnotched) specimen testing. Below, a close-up view of the hydraulic grips.

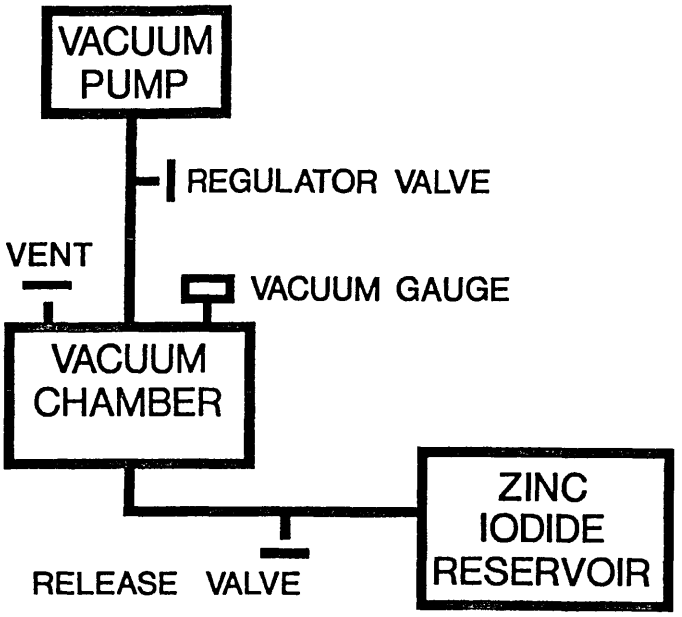


Fig. 3.8: A schematic representation of the vacuum apparatus used for the penetrant introduction into the damaged areas prior to X-raying.

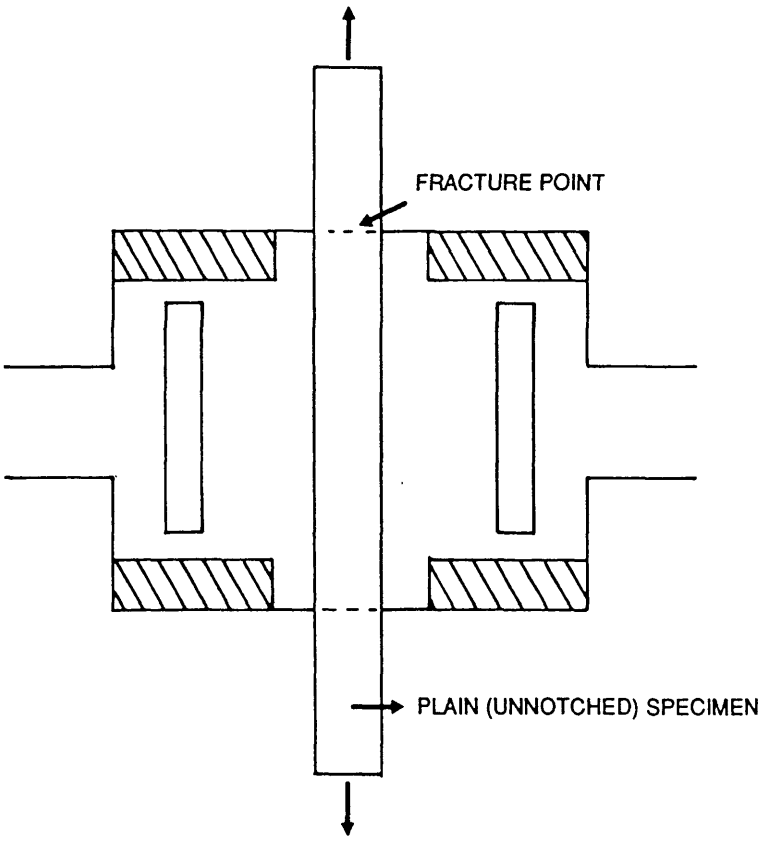


Fig. 3.9: A schematic representation of the plain specimen arrangement during elevated temperature testing.

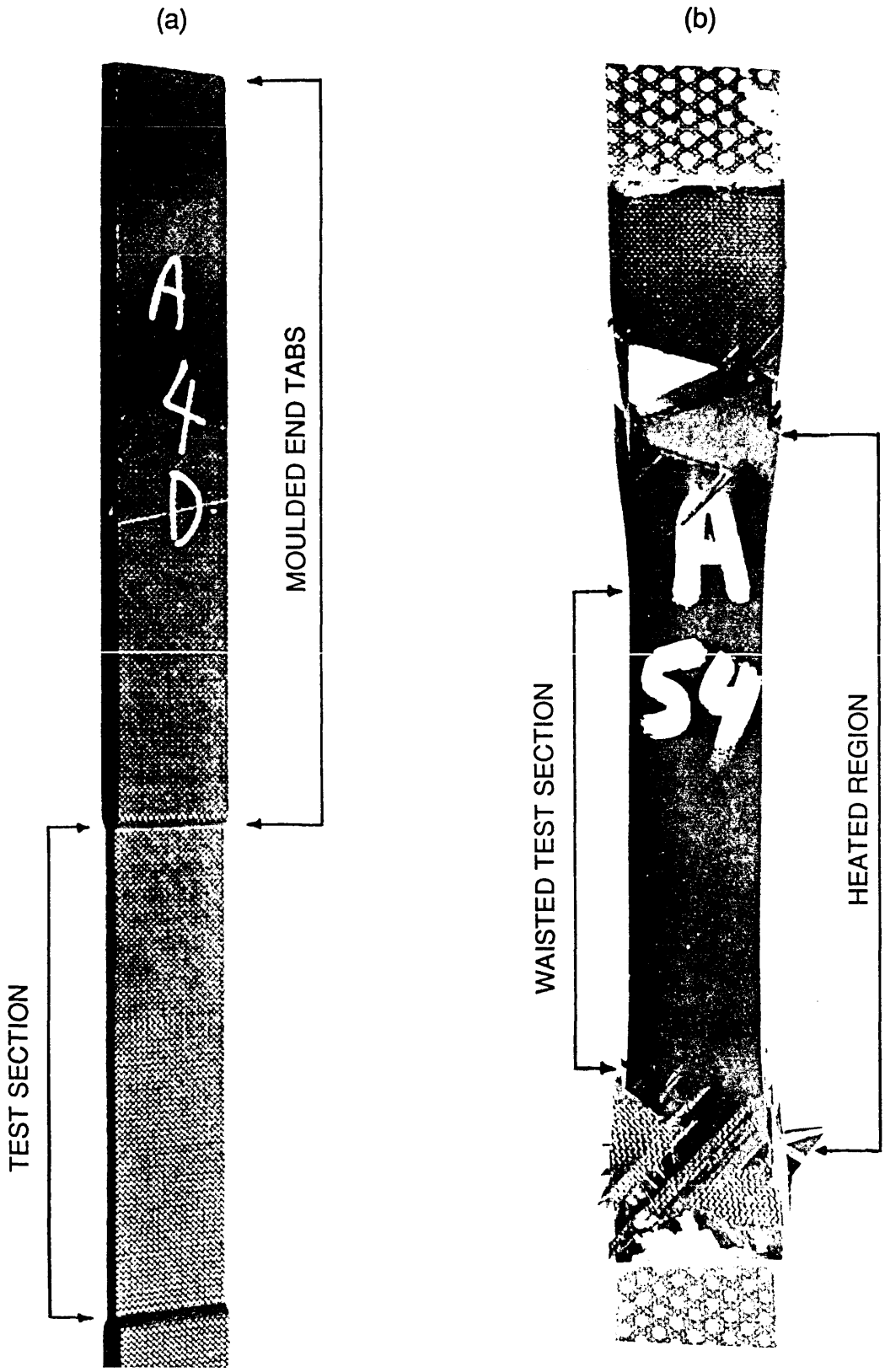


Fig.3.10: Photographs of specially designed (plain) specimens for elevated temperature testing; (a) a parallel sided specimen with long moulded end tabs ; and (b) a specimen with a waisted test section.

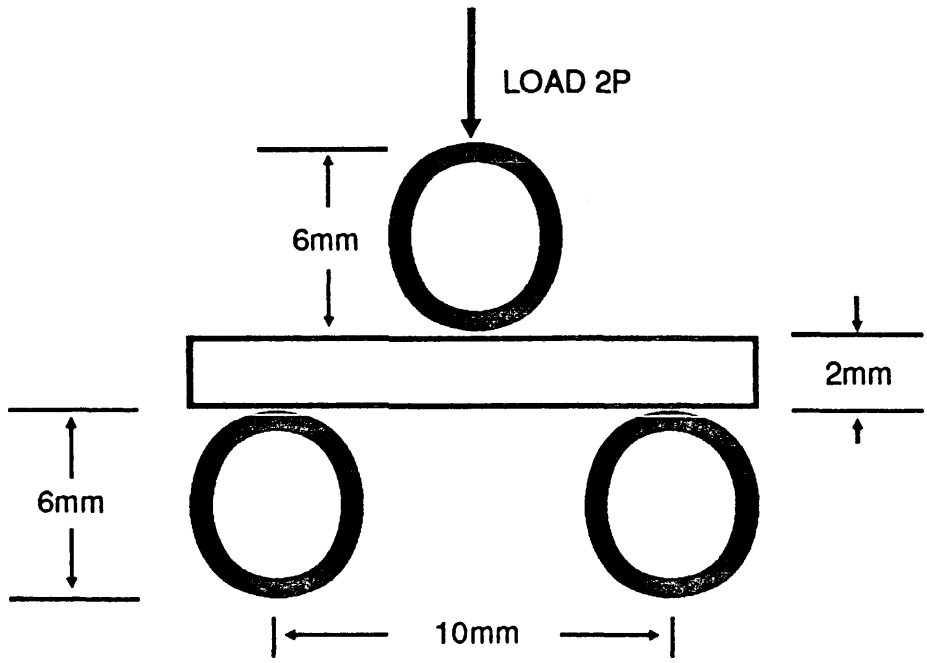


Fig.3.11: The three-point-bend loading fixture (and specimen) which was used in the ILSS evaluation tests.

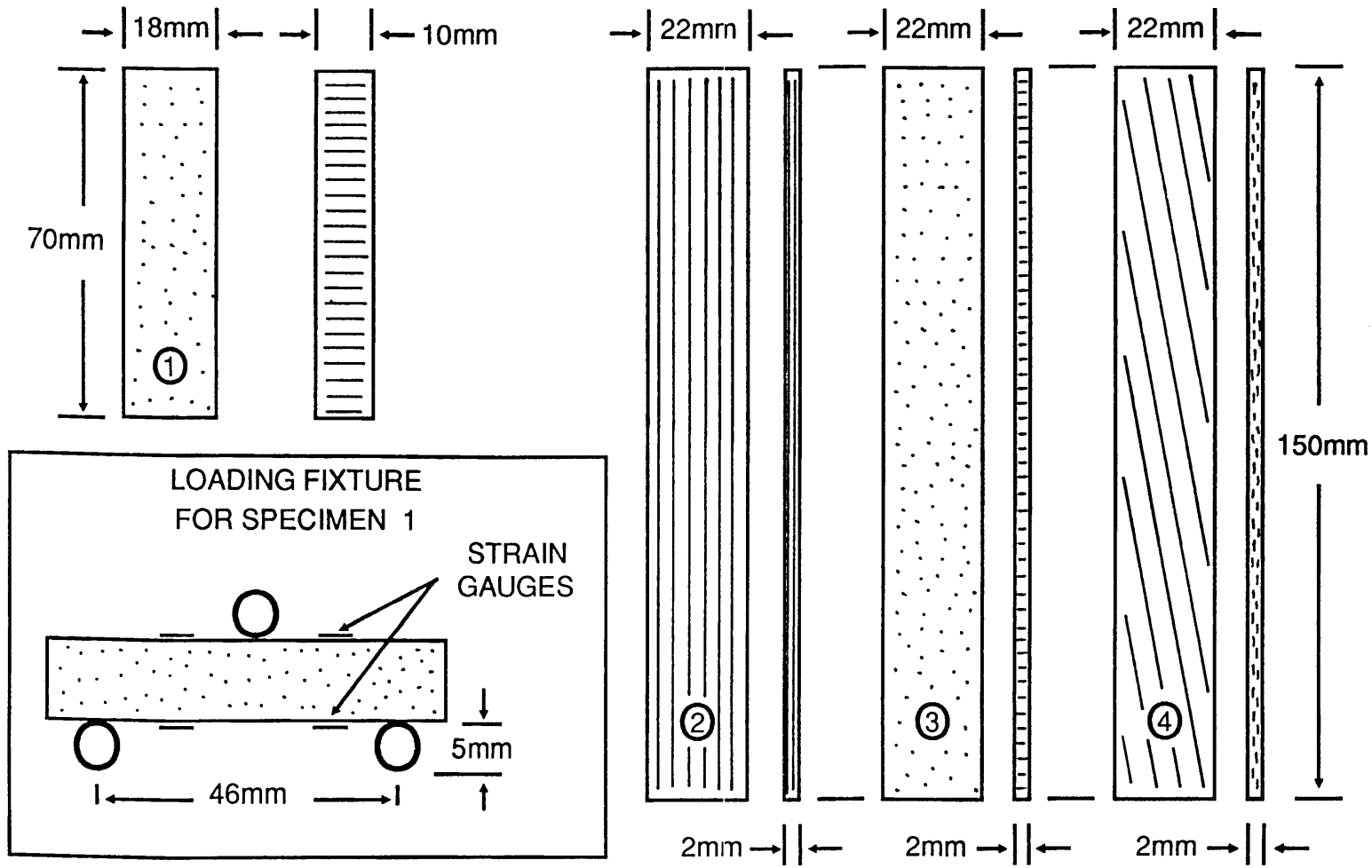


Fig. 3.12: Geometries of the specimens used for the experimental determination of the elastic material properties. The specimen mumber 1 was loaded in three point bending in order to obtain G_{23}; the rest of the specimens were loaded in tension in order to obtain E_{11} & ν_{12}, E_{22} & ν_{23}, and G_{12} from specimens 2, 3, and 4 respectively.

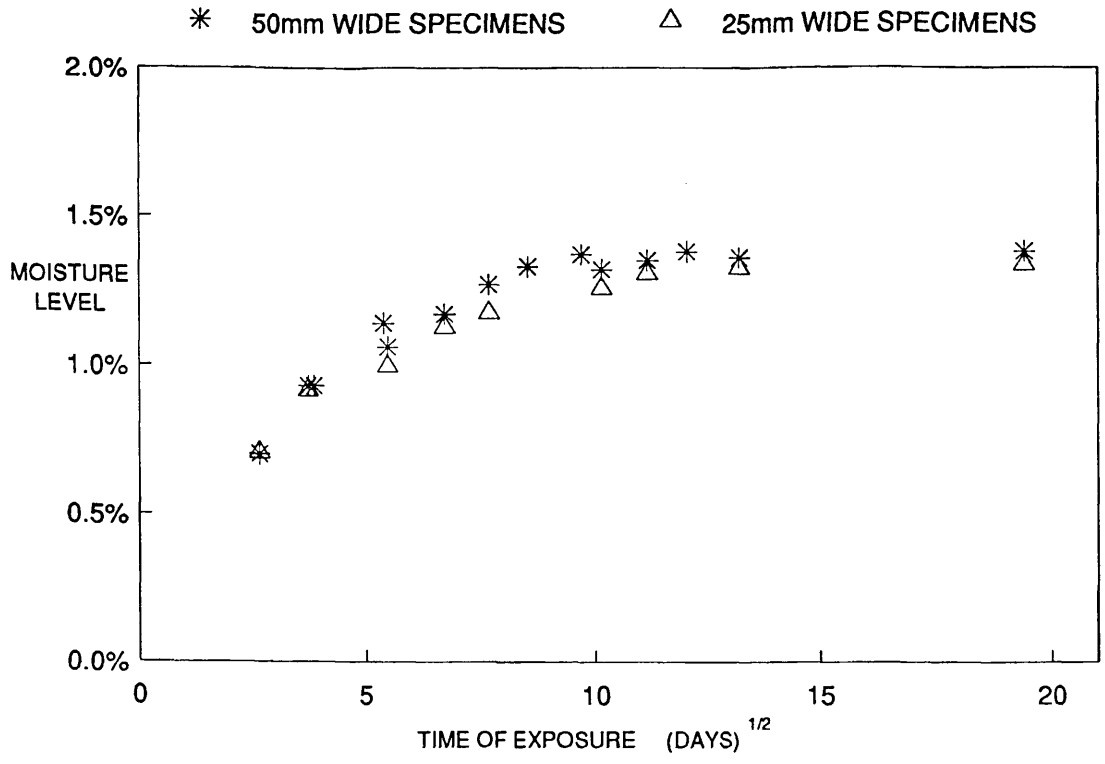


Fig. 4.1: Moisture pickup in 914C following environmental exposure at 60°C and 84% RH.

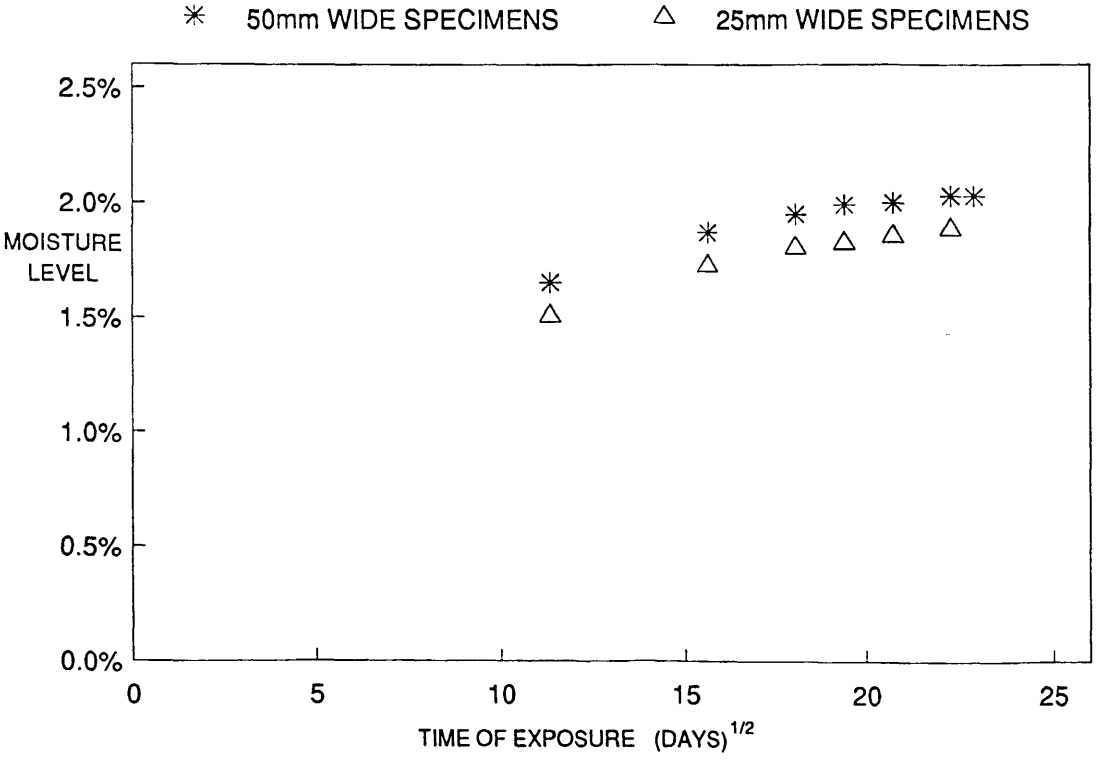


Fig. 4.2: Moisture pickup in 914C following environmental exposure at room temperature (RT) and 100% RH.

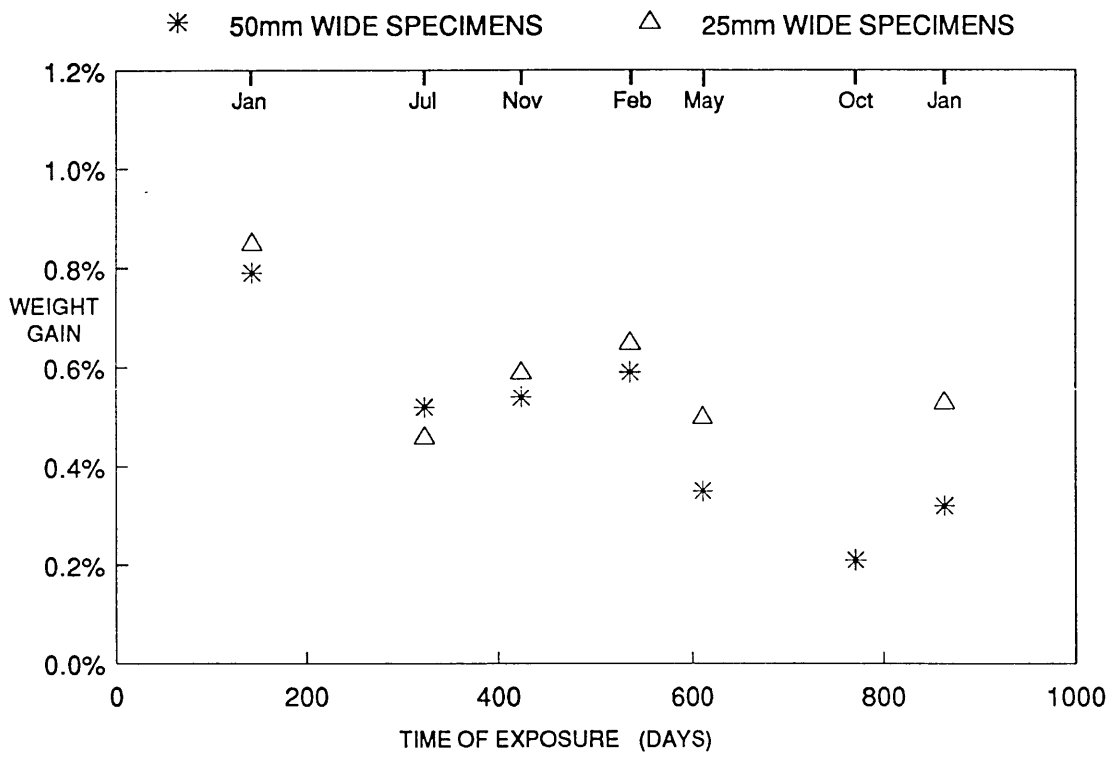


Fig. 4.3: Moisture pickup in 914C following natural weather exposure.

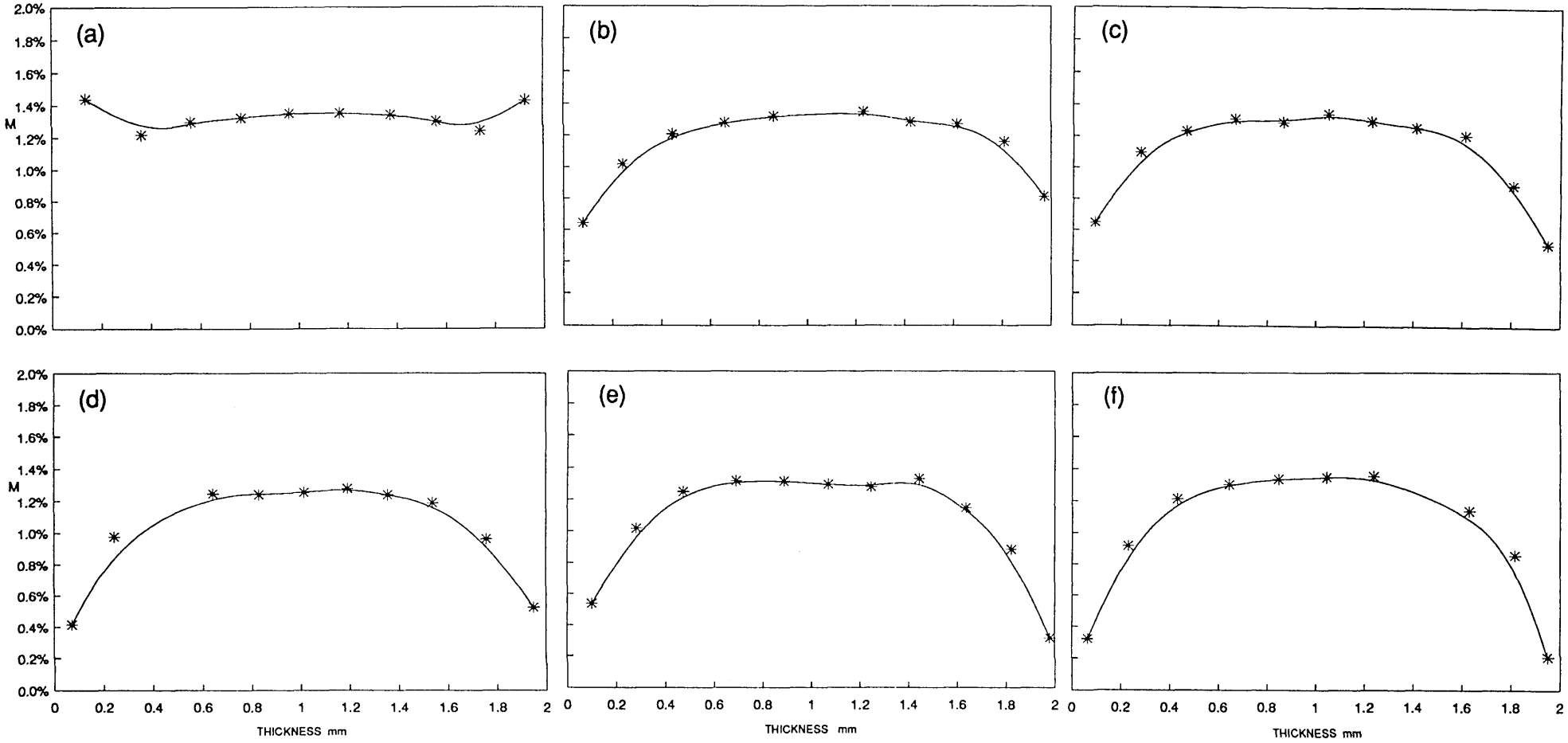


Fig. 4.4: Through-thickness moisture distribution in unidirectional XAS/914C, after different intervals of drying out time, t, at 90°C: plots (a), (b), (c), (d), (e) & (f) represent time intervals of 0, 30, 60, 90, 120 & 150 minutes respectively.

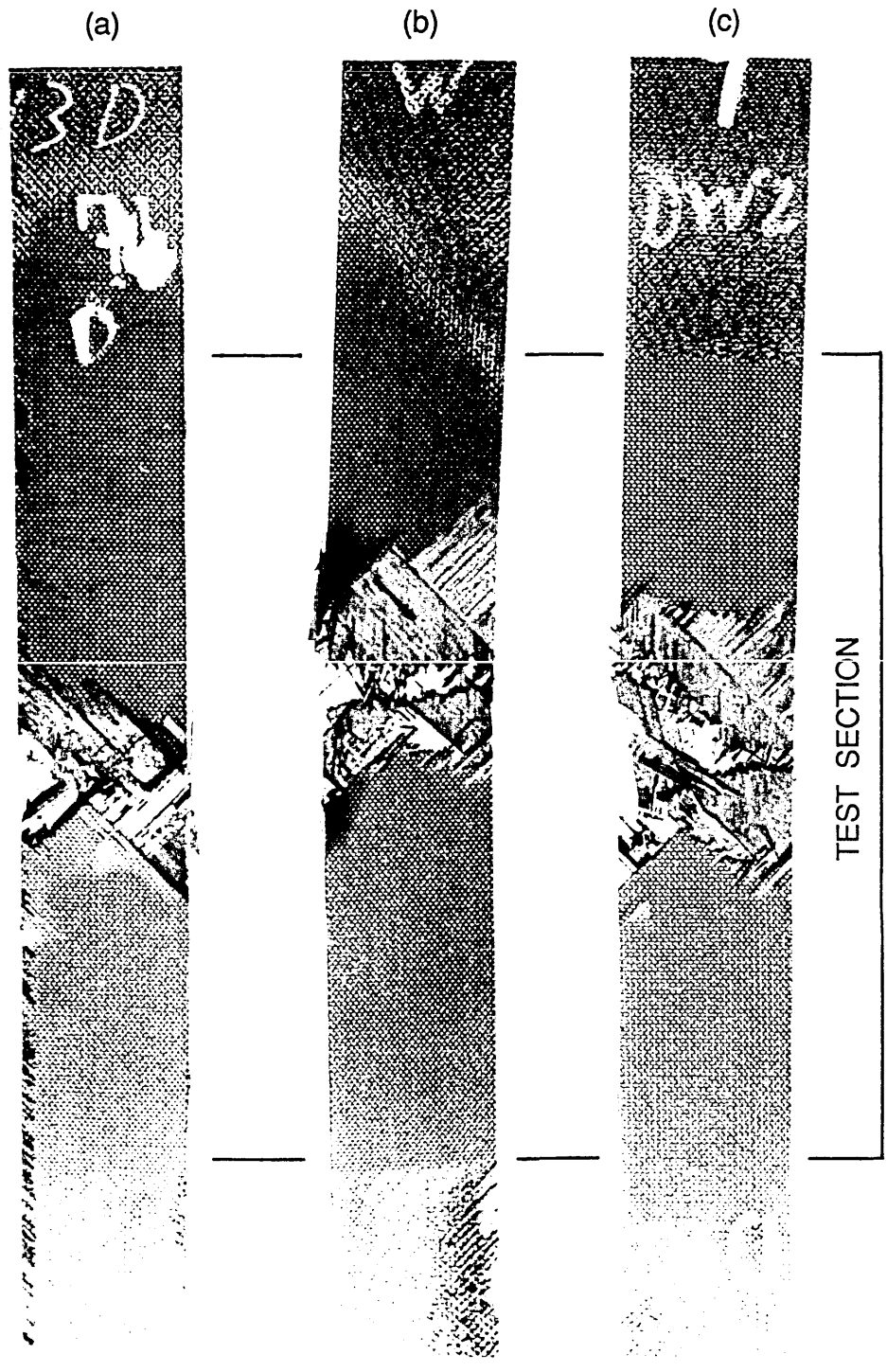


Fig. 4.5: Photographs of tensile fracture modes in plain specimens; (a) nominally dry; (b) 1.4% wet; and (c) 2.0% wet.

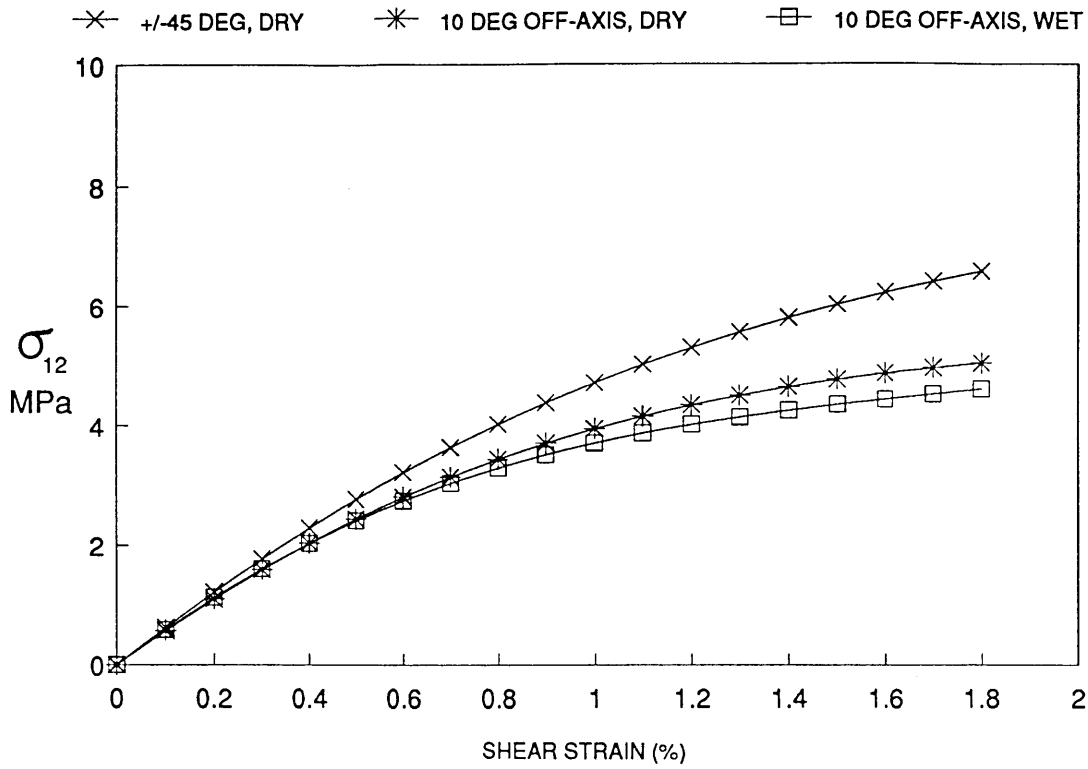


Fig. 4.6: Plots of shear stress σ_{12} versus shear strain ε_{12} for wet and dry 914C. The effect of the test method is also demonstrated for the dry material.

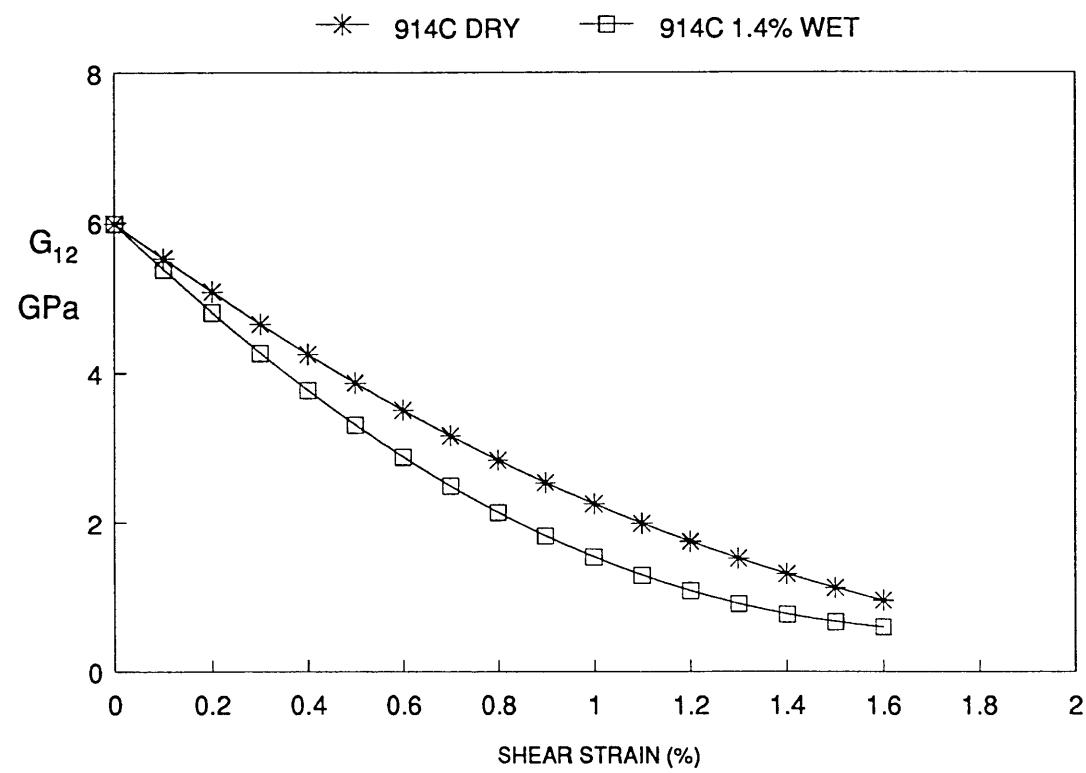


Fig. 4.7: The shear stiffness (G_{12}) variation with shear strain ε_{12} for wet and dry 914C.

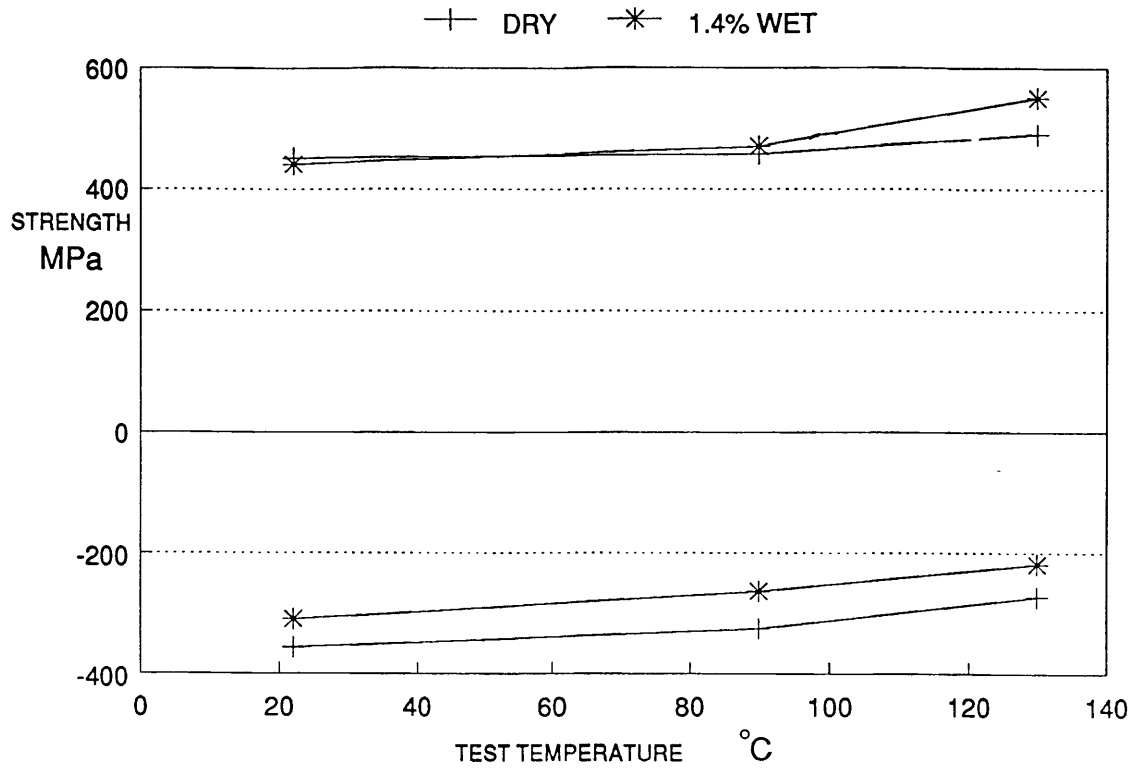


Fig. 4.8: Notched static strength variation with test temperature for specimens with sharp notches of stacking sequence A: both tensile and compressive values are plotted. Note the approximate equivalence in strength between wet and dry specimens tested at 90°C and 130°C respectively.

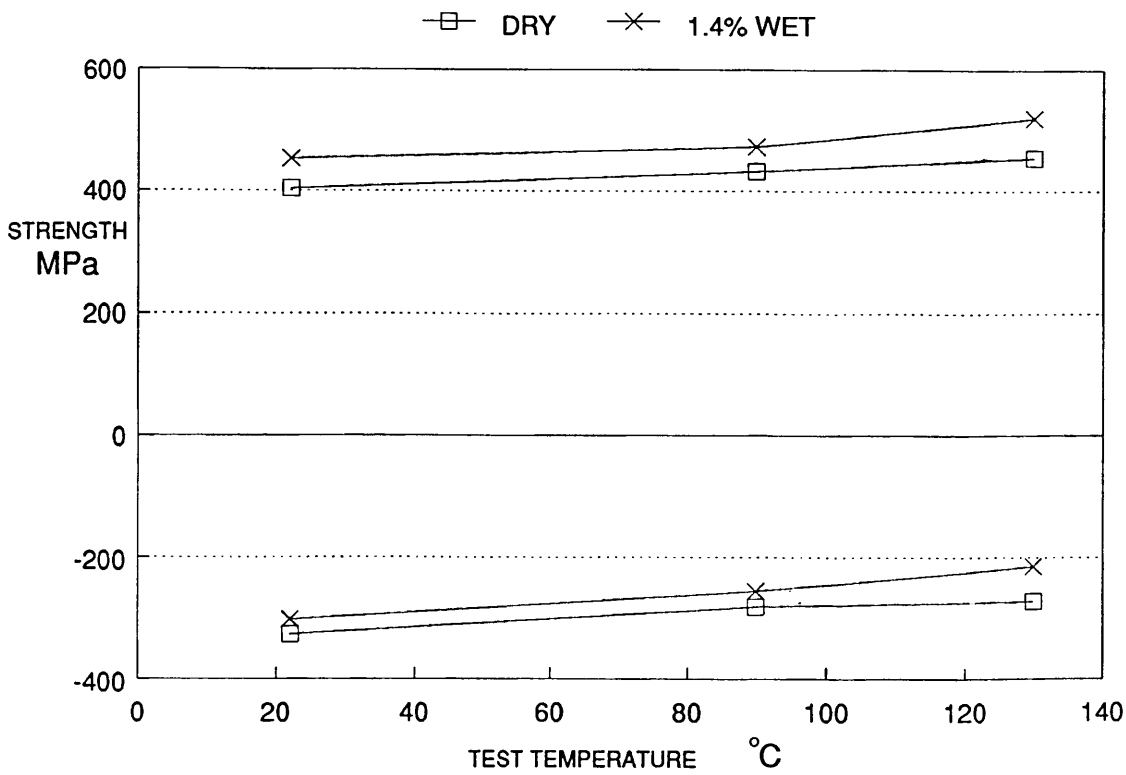


Fig. 4.9: Notched static strength variation with test temperature for specimens with sharp notches of stacking sequence B: both tensile and compressive values are plotted. Note the approximate equivalence in strength between wet and dry specimens tested at 90°C and 130°C respectively.



Fig. 4.10: Tensile fracture modes of dry and 1.4% wet specimens with sharp 10mm notches of stacking sequence A. Note the similarity in fracture between dry and wet specimens tested at 130°C and 90°C respectively.

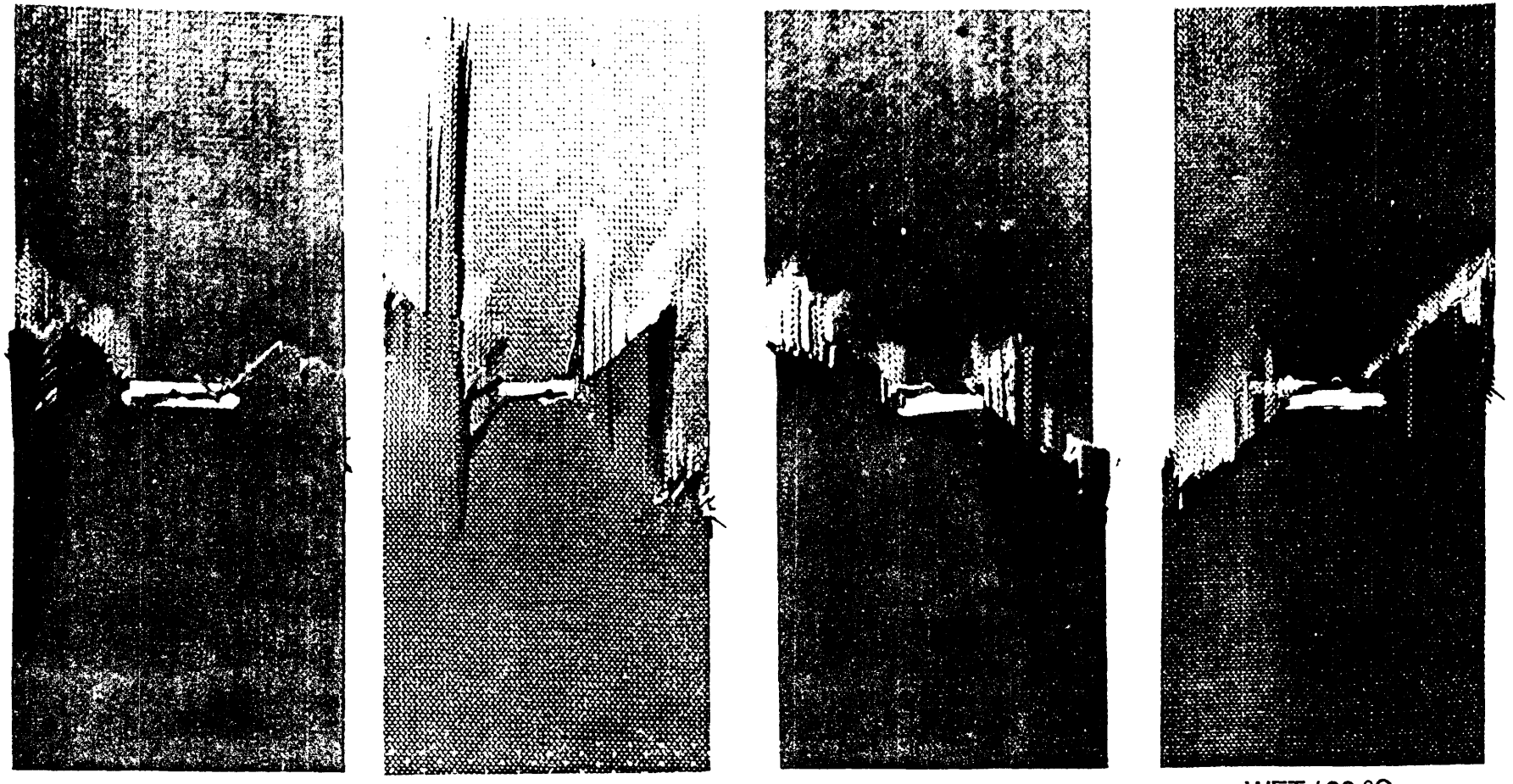


Fig. 4.11: Tensile fracture modes of dry and 1.4% wet specimens with sharp 10mm notches of stacking sequence B. Note the similarity in fracture between dry and wet specimens tested at 130°C and 90°C respectively.

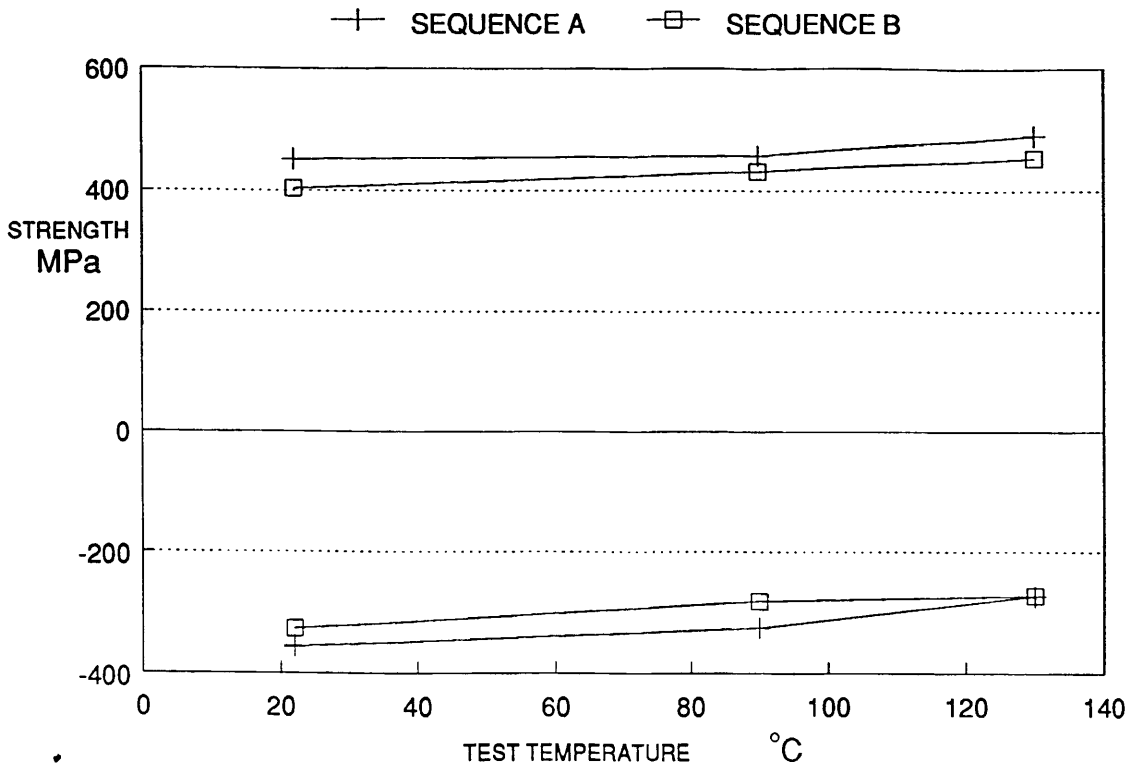


Fig. 4.12: A comparison of "dry" notched static strengths between the stacking sequence A and B. Both tensile and compressive strengths are plotted as a function of test temperature.

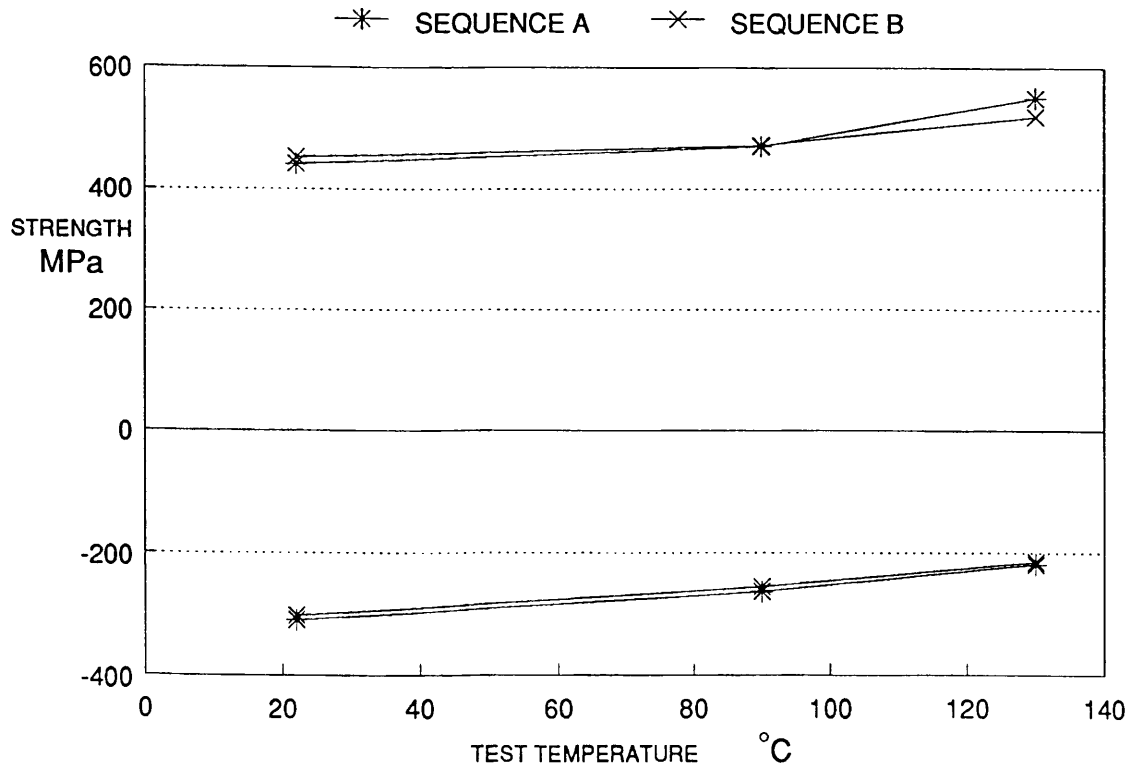


Fig. 4.13: A comparison of "wet" notched static strengths between the stacking sequence A and B. Both tensile and compressive strengths are plotted as a function of test temperature.

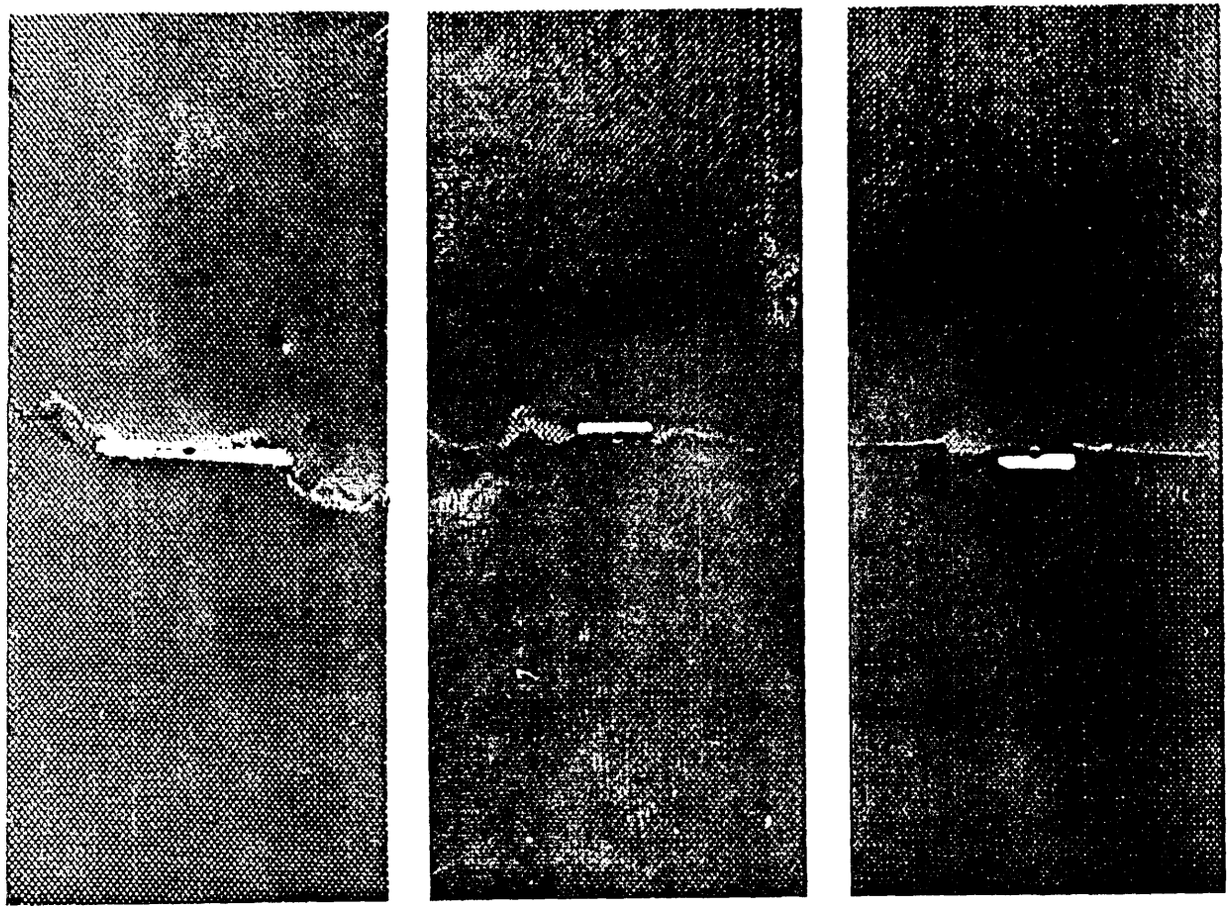


Fig. 4.14: Compressive fracture modes of 1.4% wet specimens with sharp 10mm notches. Note the change in fracture mode with increasing test temperature.

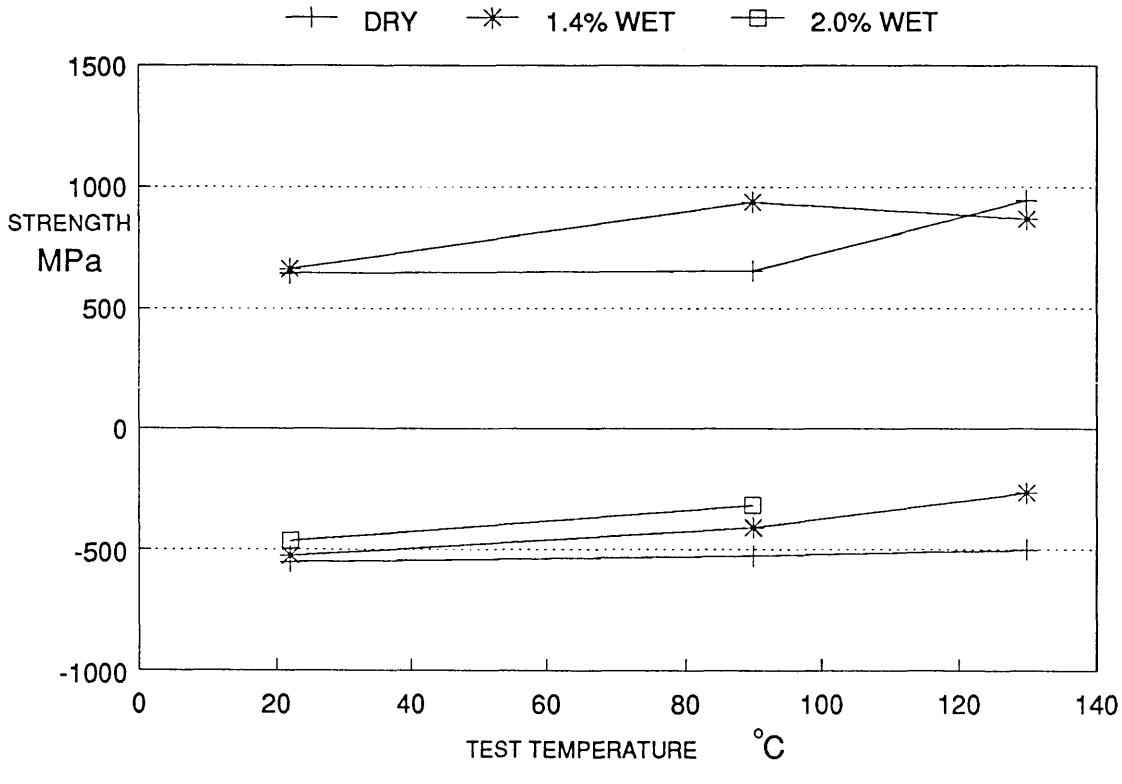


Fig. 4.15: Notched static strength variation with test temperature for specimens with circular holes (stacking sequence A): both tensile and compressive values are plotted. Note the approximate equivalence in tensile strength between (1.4%) wet and dry specimens tested at 90°C and 130°C respectively.

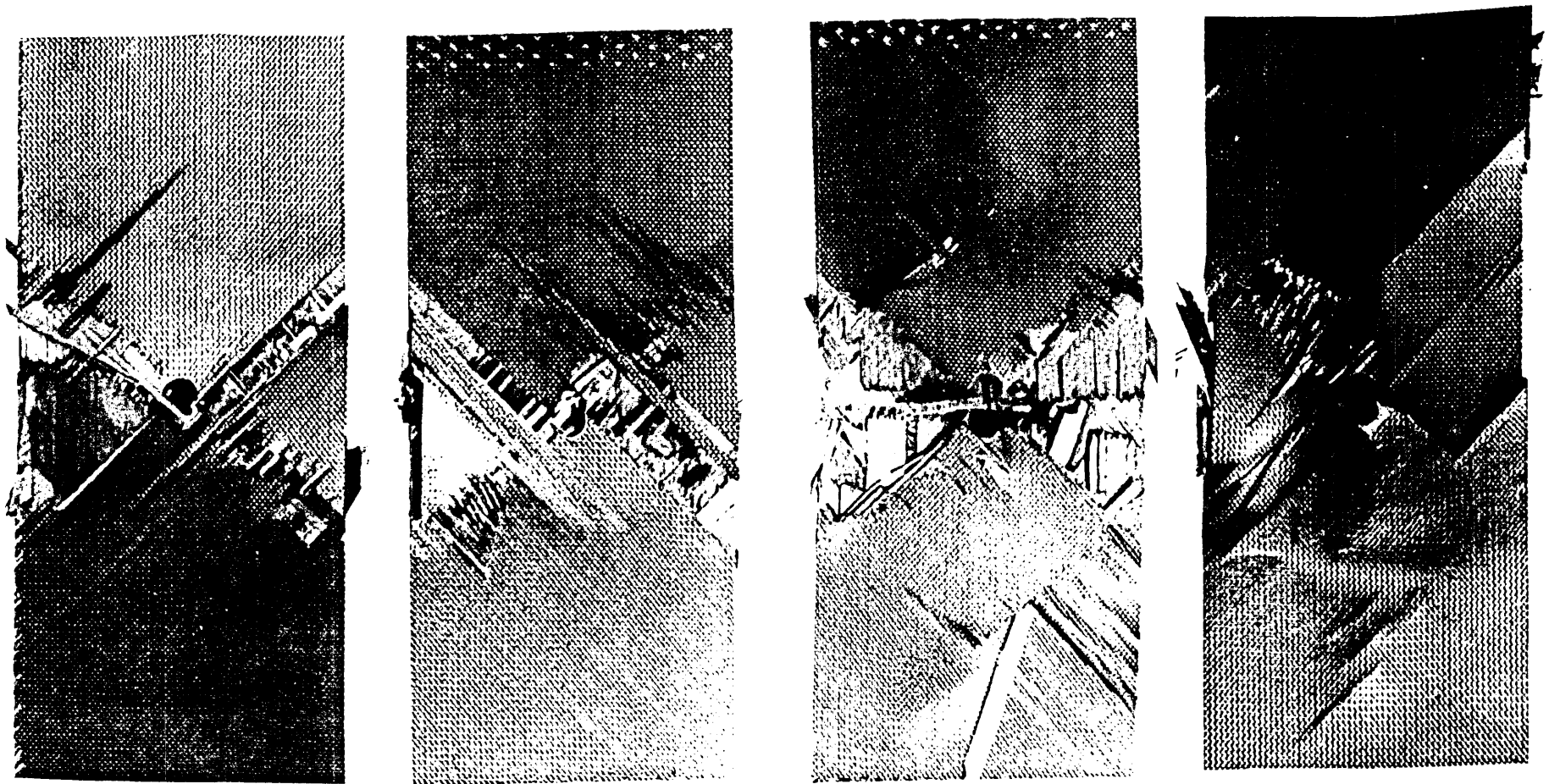


Fig. 4.16: Tensile fracture modes of dry and 1.4% wet specimens with circular 5mm holes (stacking sequence A). Note the similarity in fracture between dry and wet specimens tested at 90°C and RT respectively: likewise for dry and wet specimens tested at130°C and 90°C respectively.

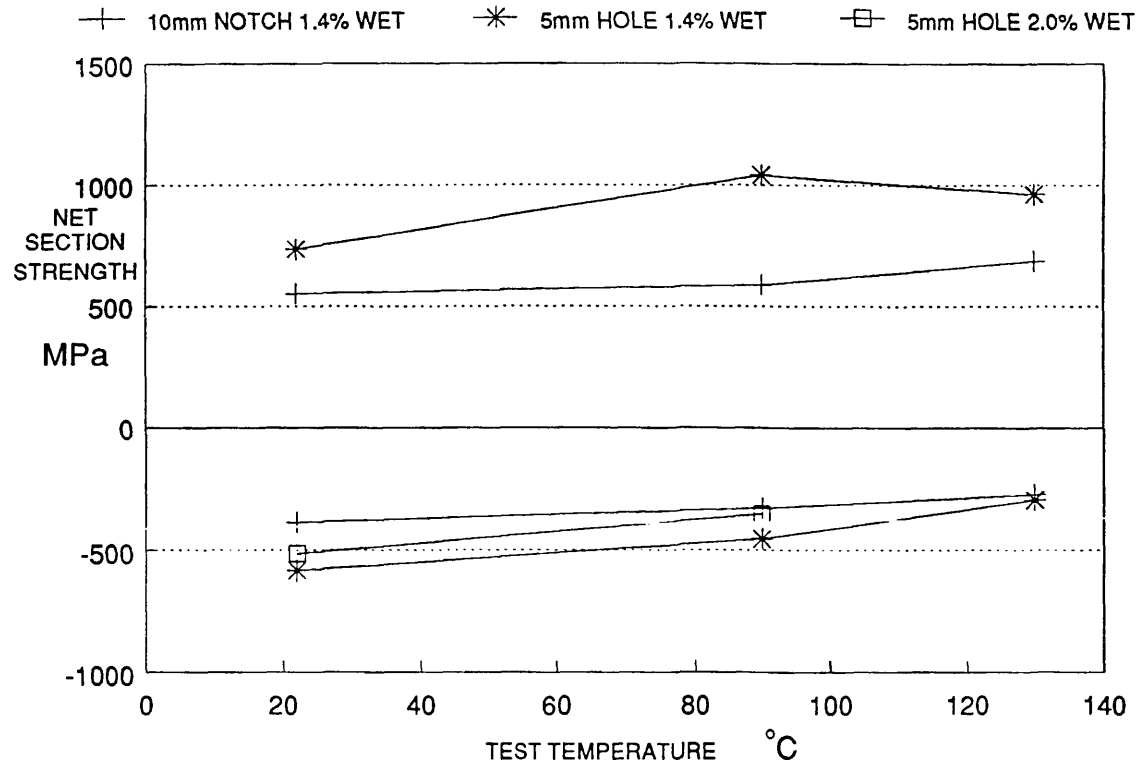


Fig. 4.17: A comparison of net-section strength between wet specimens with sharp notches and circular holes. Both tensile and compressive strengths are plotted as a function of test temperature.

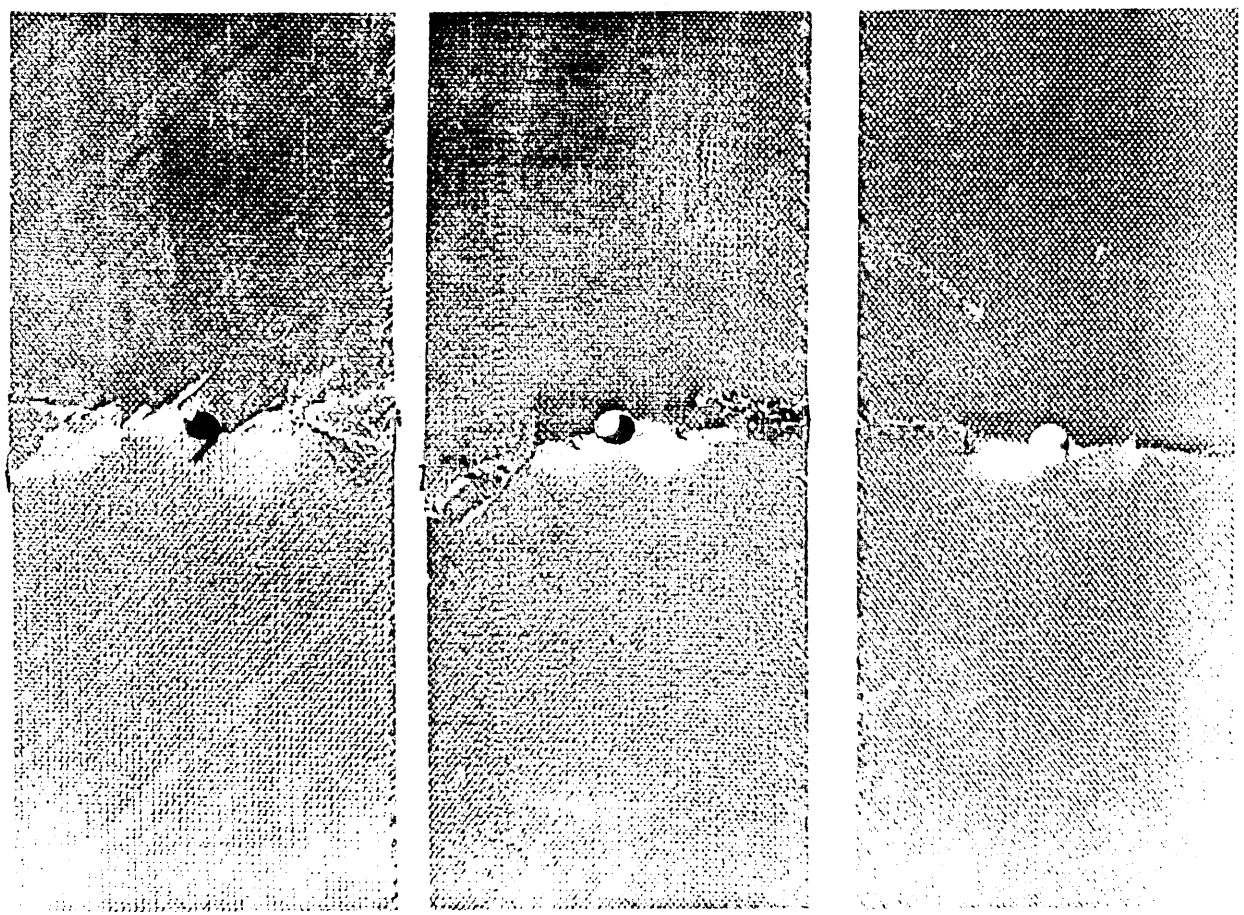


Fig. 4.18: Compressive fracture modes of 1.4% wet specimens with circular 5mm holes. Note the change in fracture mode with increasing test temperature.

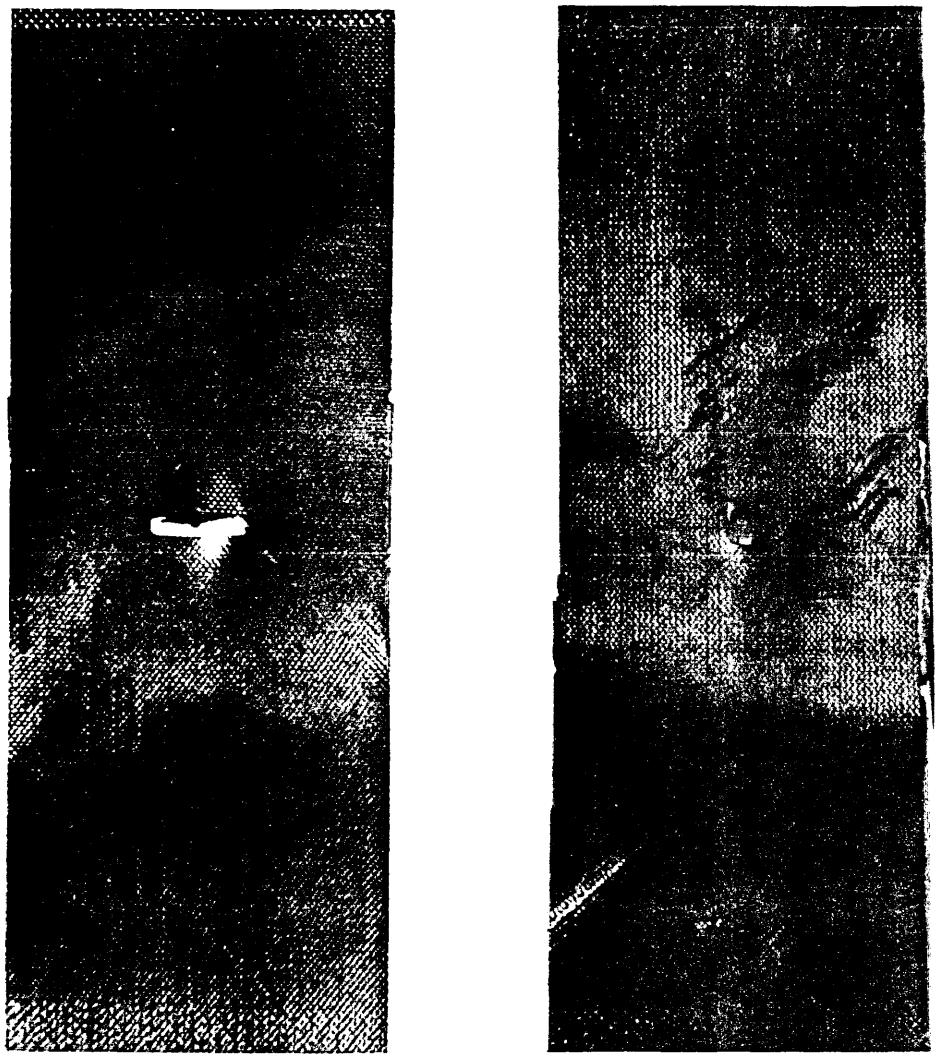


Fig. 4.19: A comparison between the tensile fracture modes of notched specimens tested at 130°C while wet. Note the plastic deformation in the surface 45° plies.

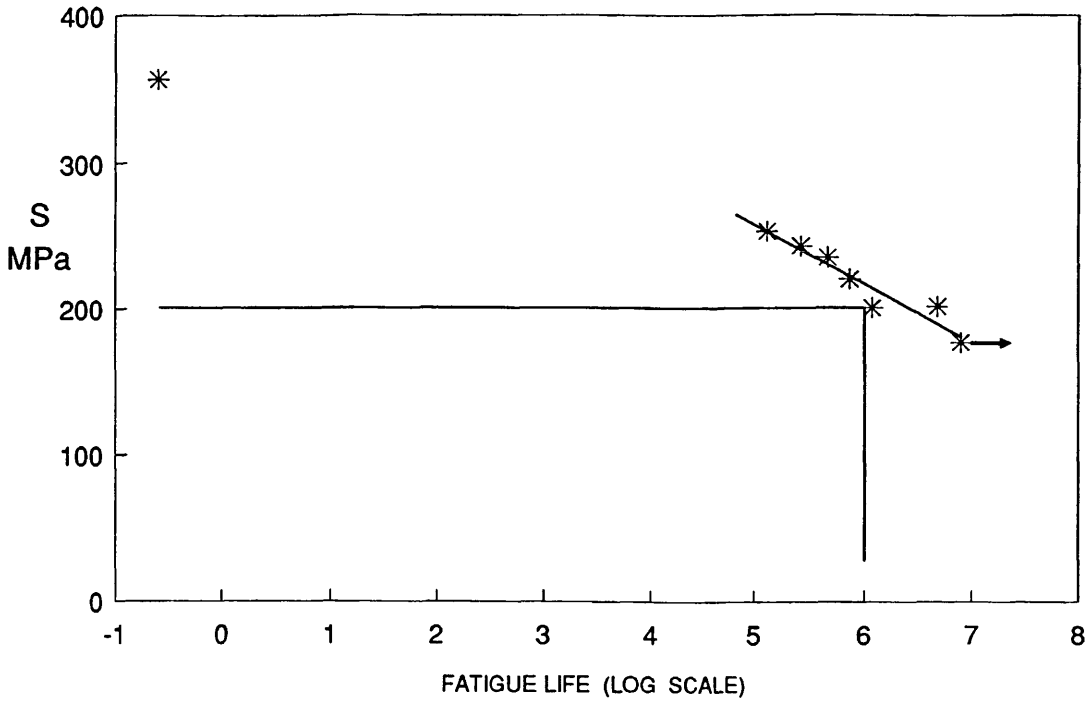


Fig. 4.20: A plot of cyclic stress amplitude versus fatigue life for dry specimens with sharp notches; all tests were performed in tension-compression at RT. The arrow indicates higher than marked (expected) life.

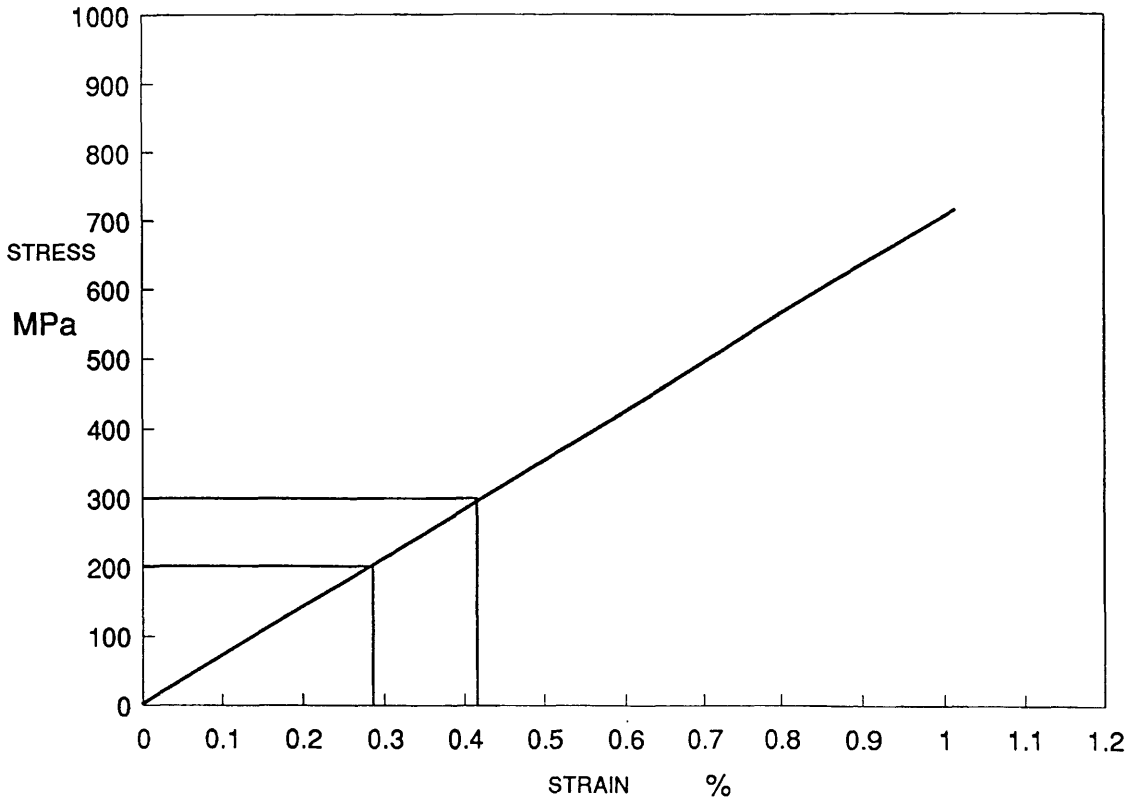


Fig. 4.21: Stress-Strain behaviour of plain (914C) dry specimens of stacking sequence A. The line represents a best fit to the average data from three specimens (2x25x250mm). The strain measurement was obtained via an extensometer with a gauge length of 100mm.

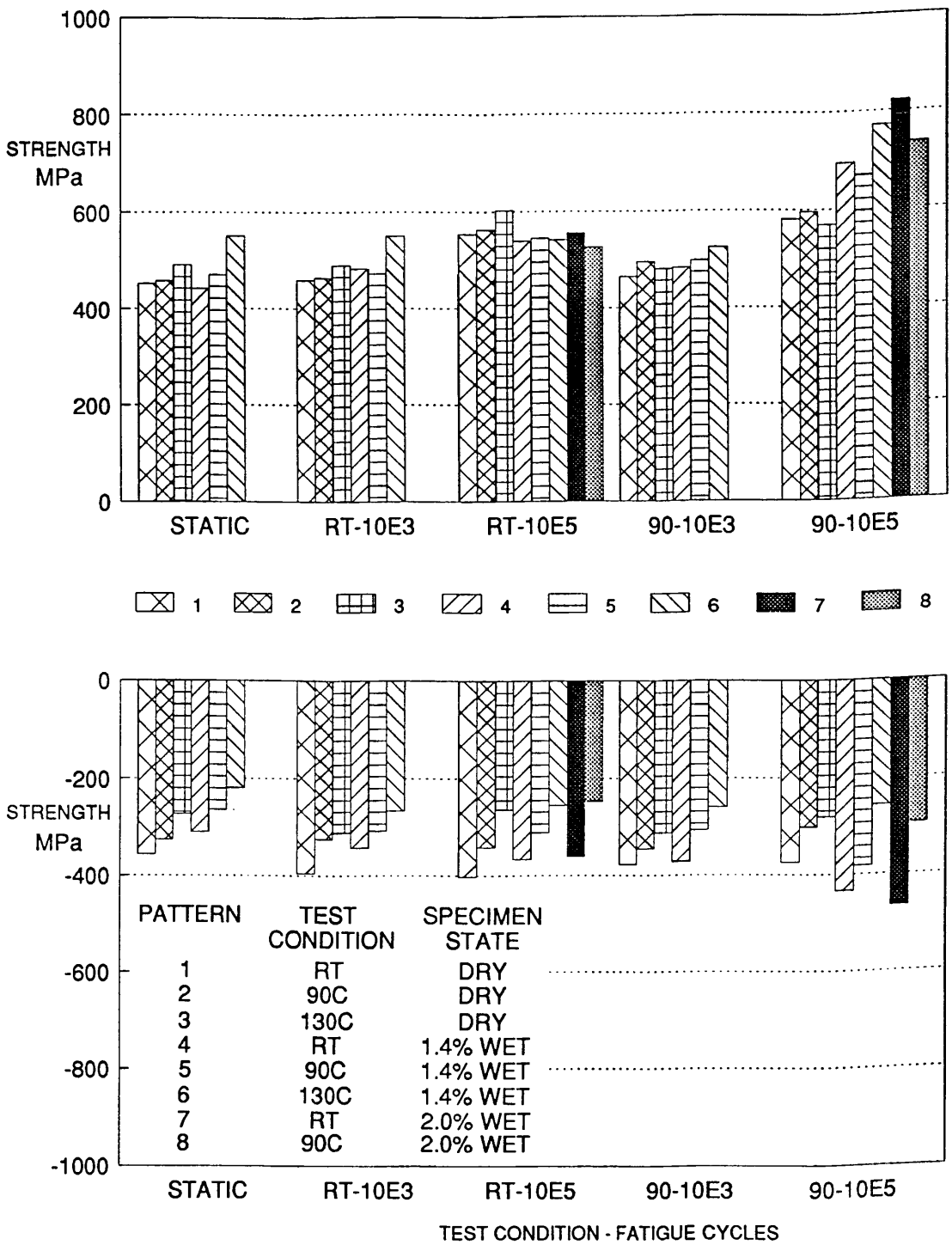


Fig. 4.22: Above, the tensile residual strength results for the dry and wet (914C) specimens with sharp notches, of stacking sequence A: below, the compressive residual strengths. The notched static strength results are also included.

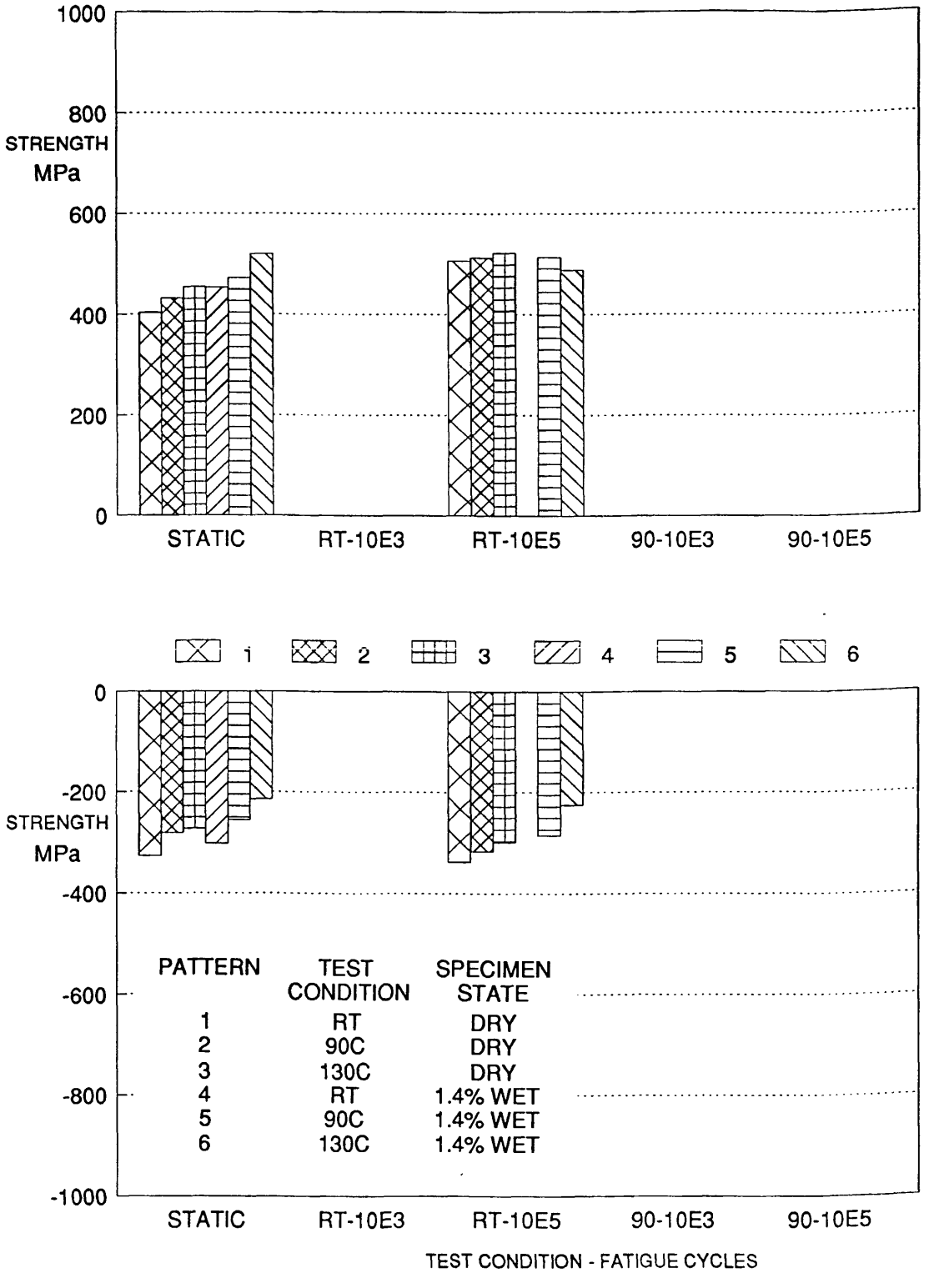


Fig. 4.23: Above, the tensile residual strength results for the dry and wet (914C) specimens with sharp notches, of stacking sequence B: below, the compressive residual strengths. The notched static strength results are also included.

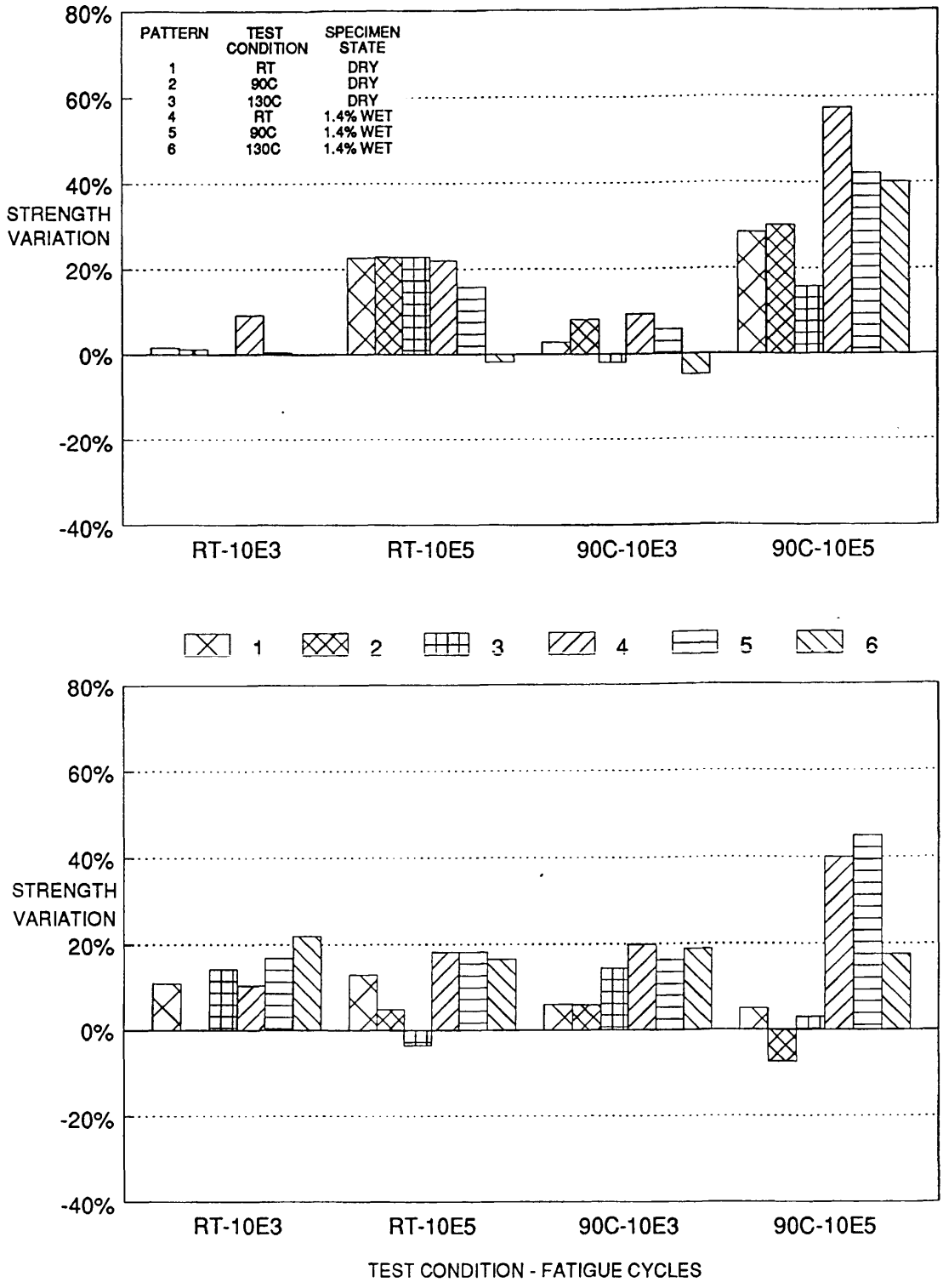


Fig. 4.24: Above, variation of the tensile residual strength with respect to the corresponding static value, for dry and wet specimens with sharp notches, of stacking sequence A: below, variation of the compressive residual strength.

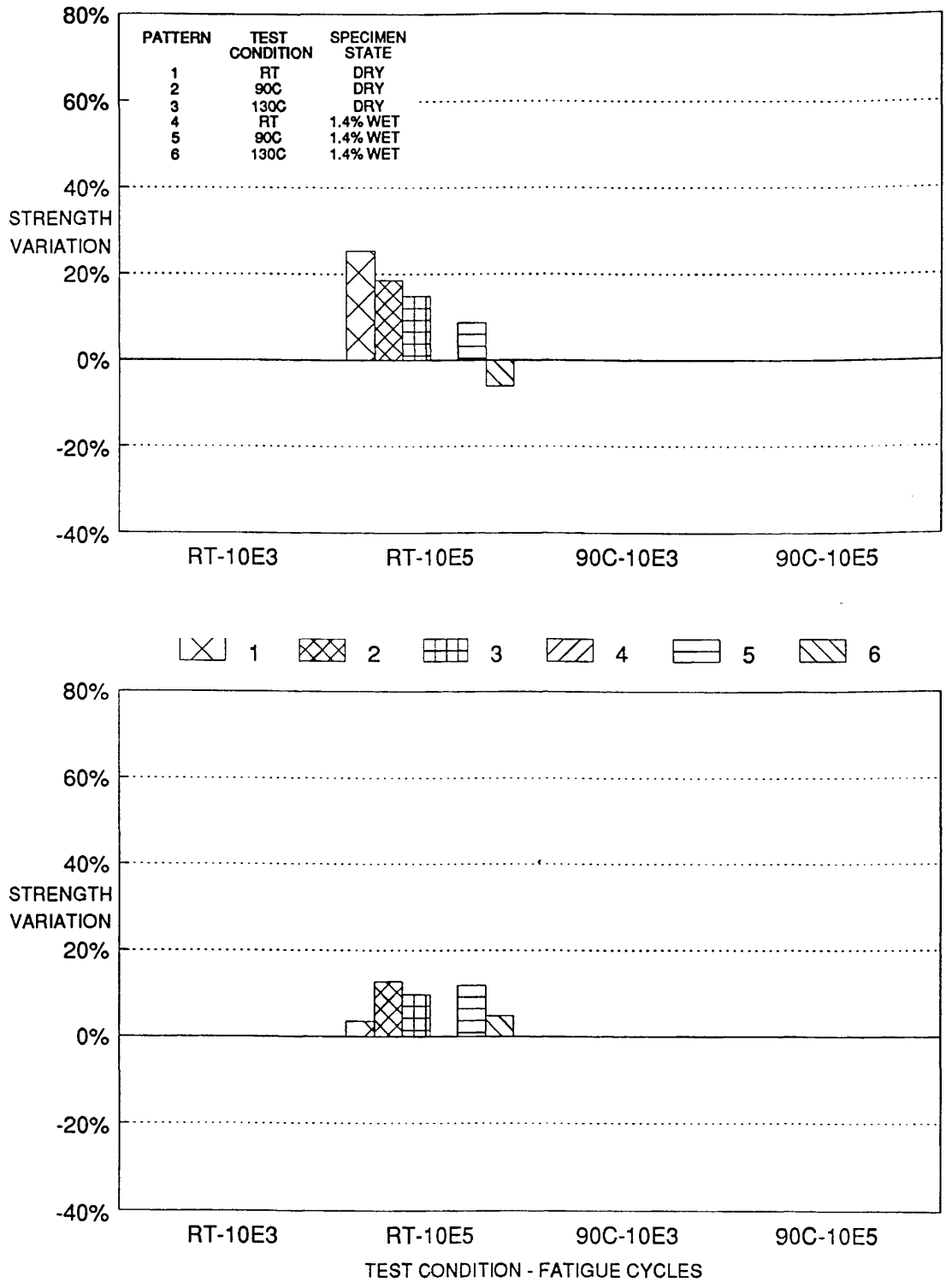


Fig. 4.25: Above, variation of the tensile residual strength with respect to the corresponding static value, for dry and wet specimens with sharp notches, of stacking sequence B: below, variation of the compressive residual strength.

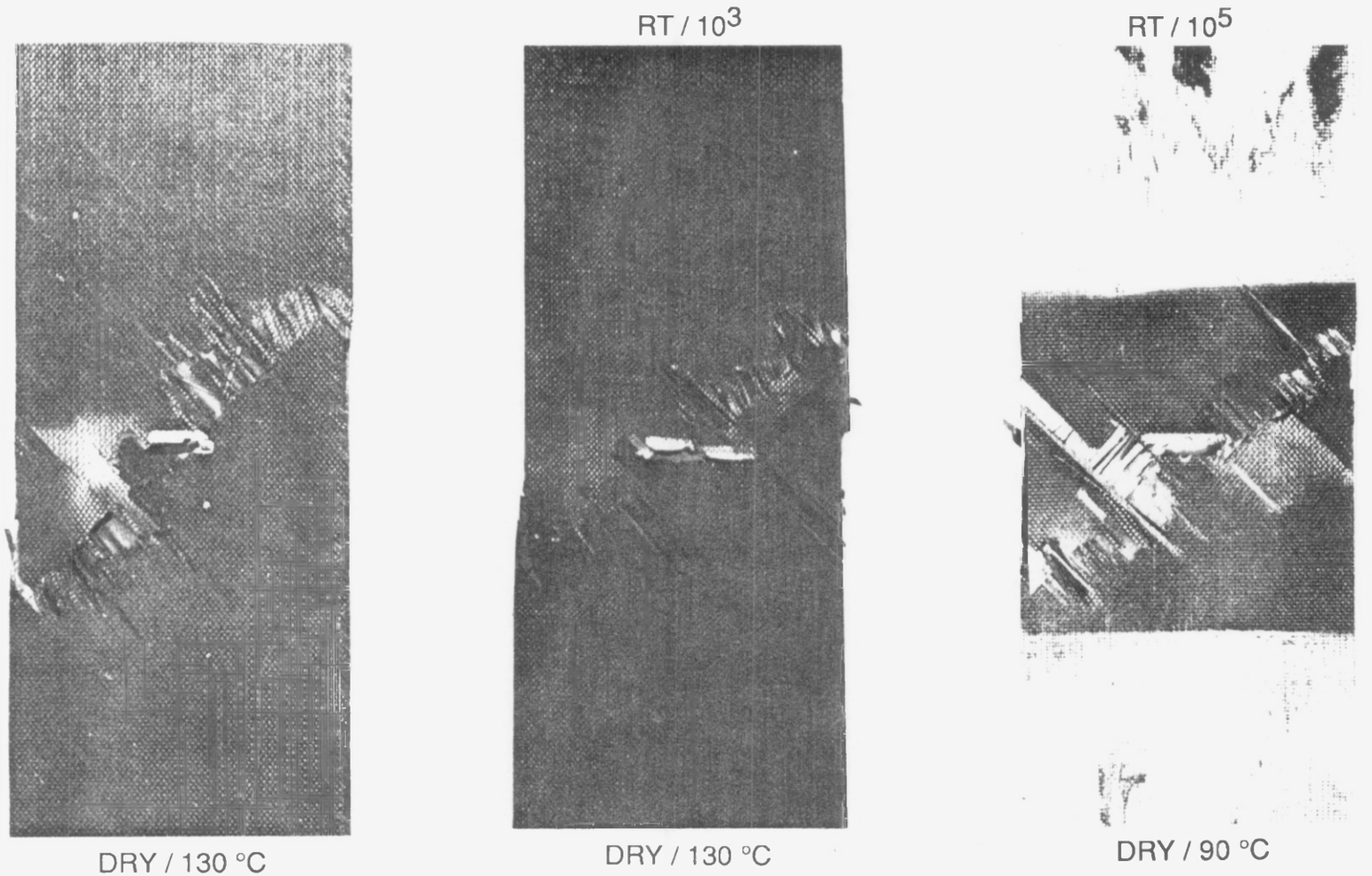


Fig. 4.26: A comparison of tensile fracture modes in dry specimens of sequence A with sharp notches: the fatigue condition is shown at the top and the static condition at the bottom of each picture.

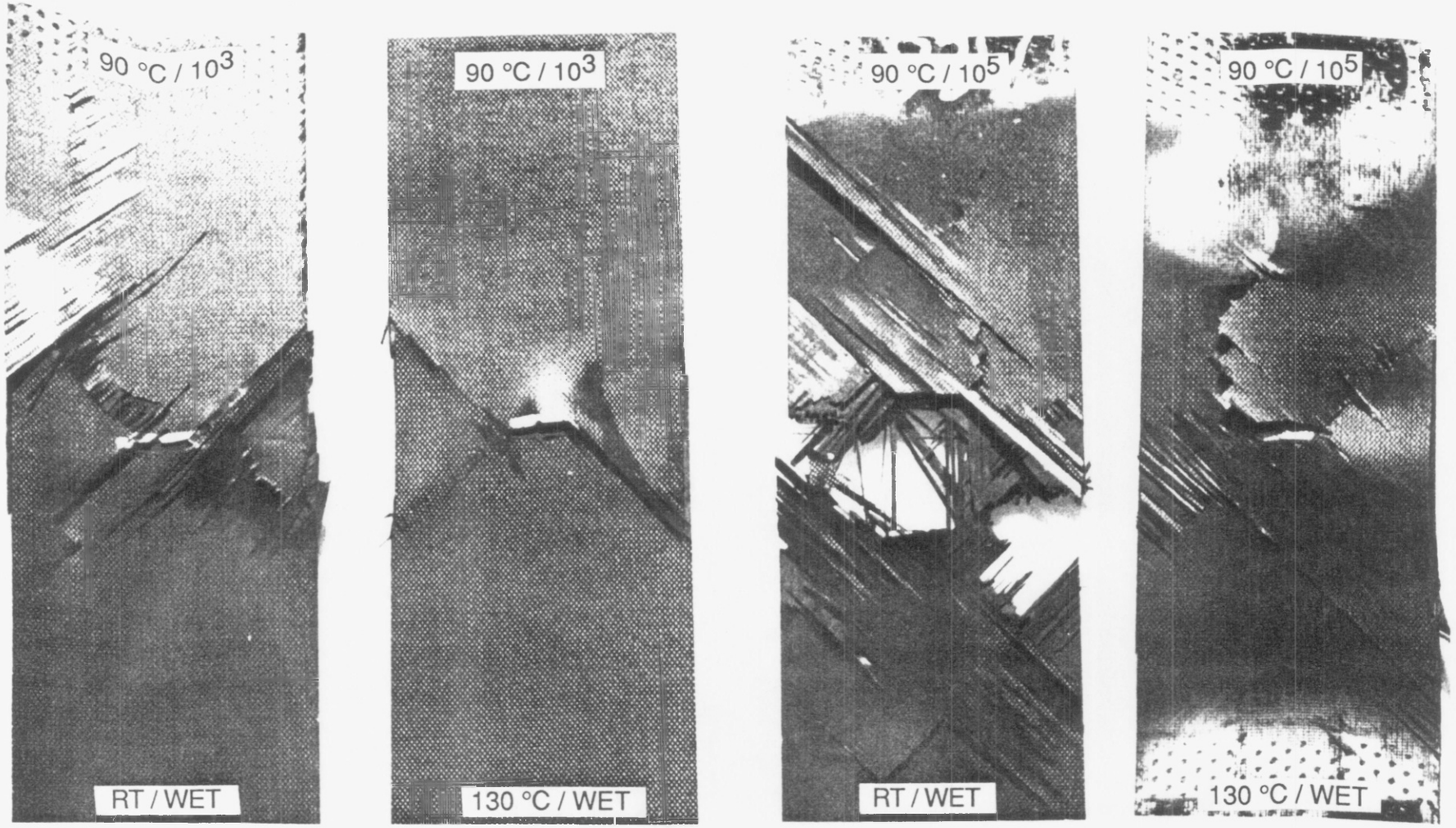


Fig. 4.27: A comparison of tensile fracture modes in wet specimens of sequence A with sharp notches: the fatigue condition is shown at the top and the static condition at the bottom of each picture.

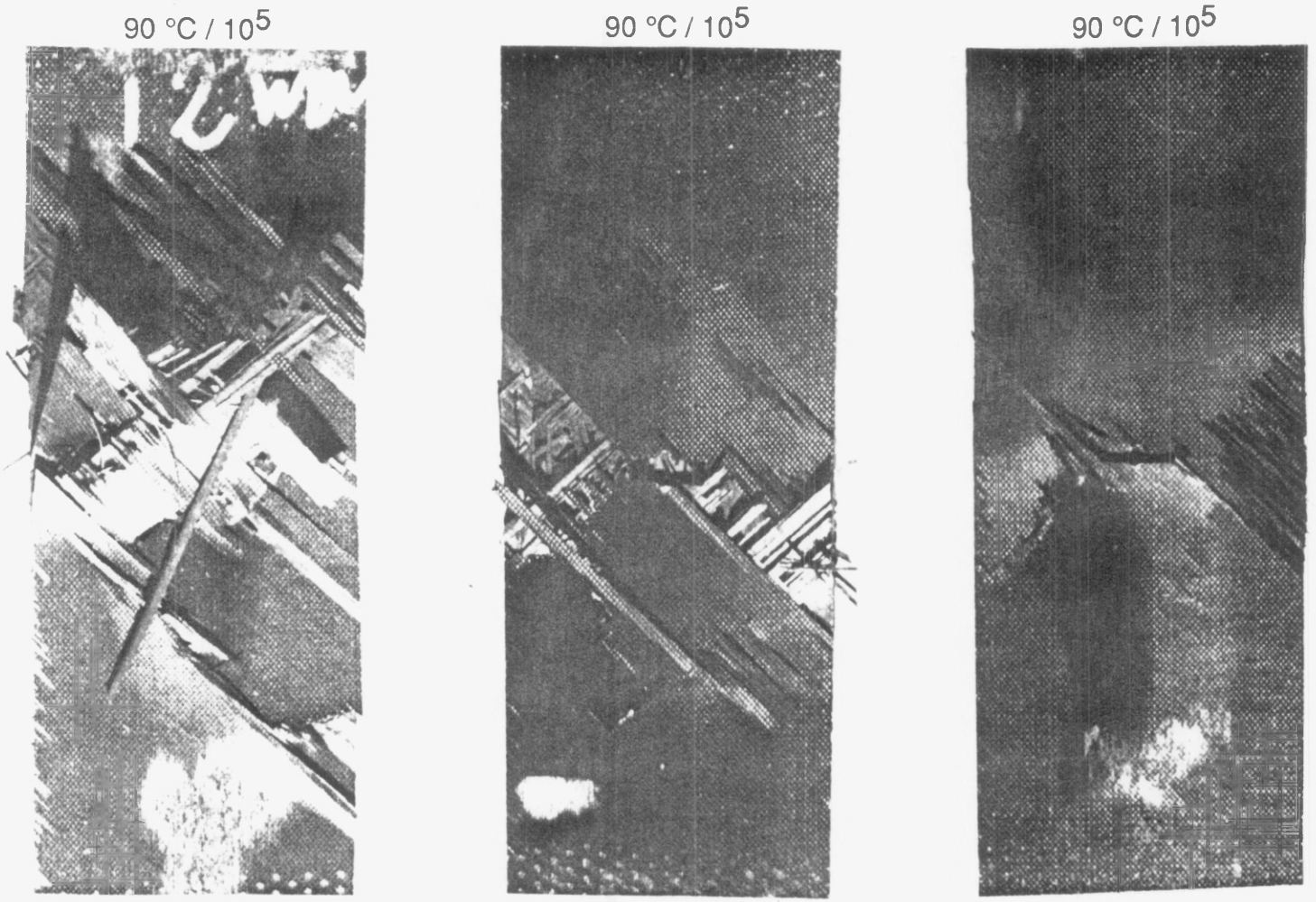


Fig. 4.28: A comparison of tensile fracture modes in wet specimens of sequence A with sharp notches. Note that for specimens in the same condition, the reduction in strength is accompanied by a smaller amount of damage: the fatigue condition is shown at the top and the static condition at the bottom of each picture.

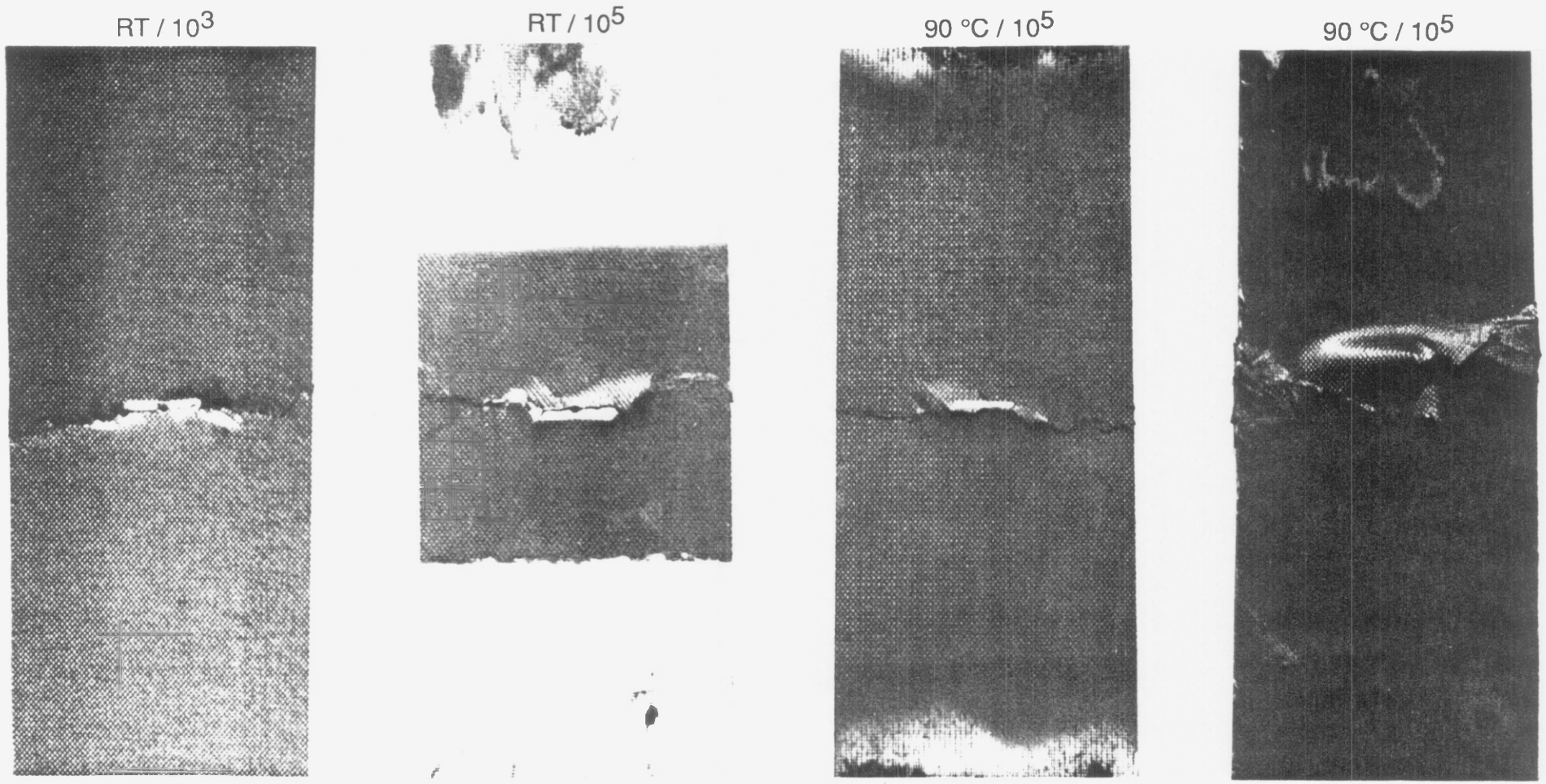


Fig. 4.29: A comparison of compressive fracture modes in wet and dry specimens of stacking sequence A with sharp notches: the fatigue condition is shown at the top and the static condition at the bottom of each picture.



Fig. 4.30: A plot of cyclic stress amplitude versus fatigue life for dry specimens with circular holes; all tests were performed in tension-compression at RT.

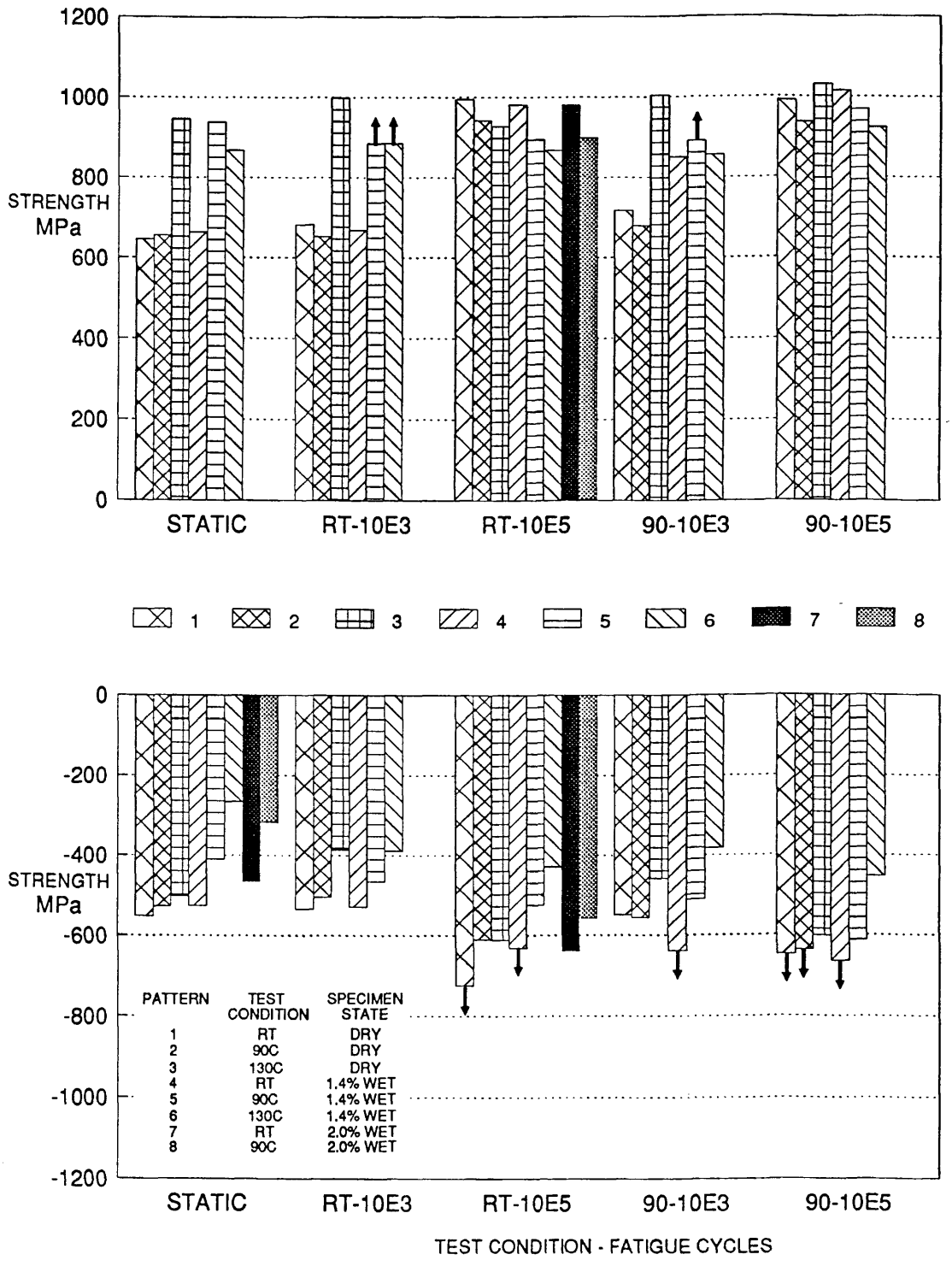


Fig. 4.31: Above, the tensile residual strength results for the dry and wet (914C) specimens with circular holes, (stacking sequence A): below, the compressive residual strengths. The notched static strength results are also included. The arrows indicate higher than marked (expected) strength.

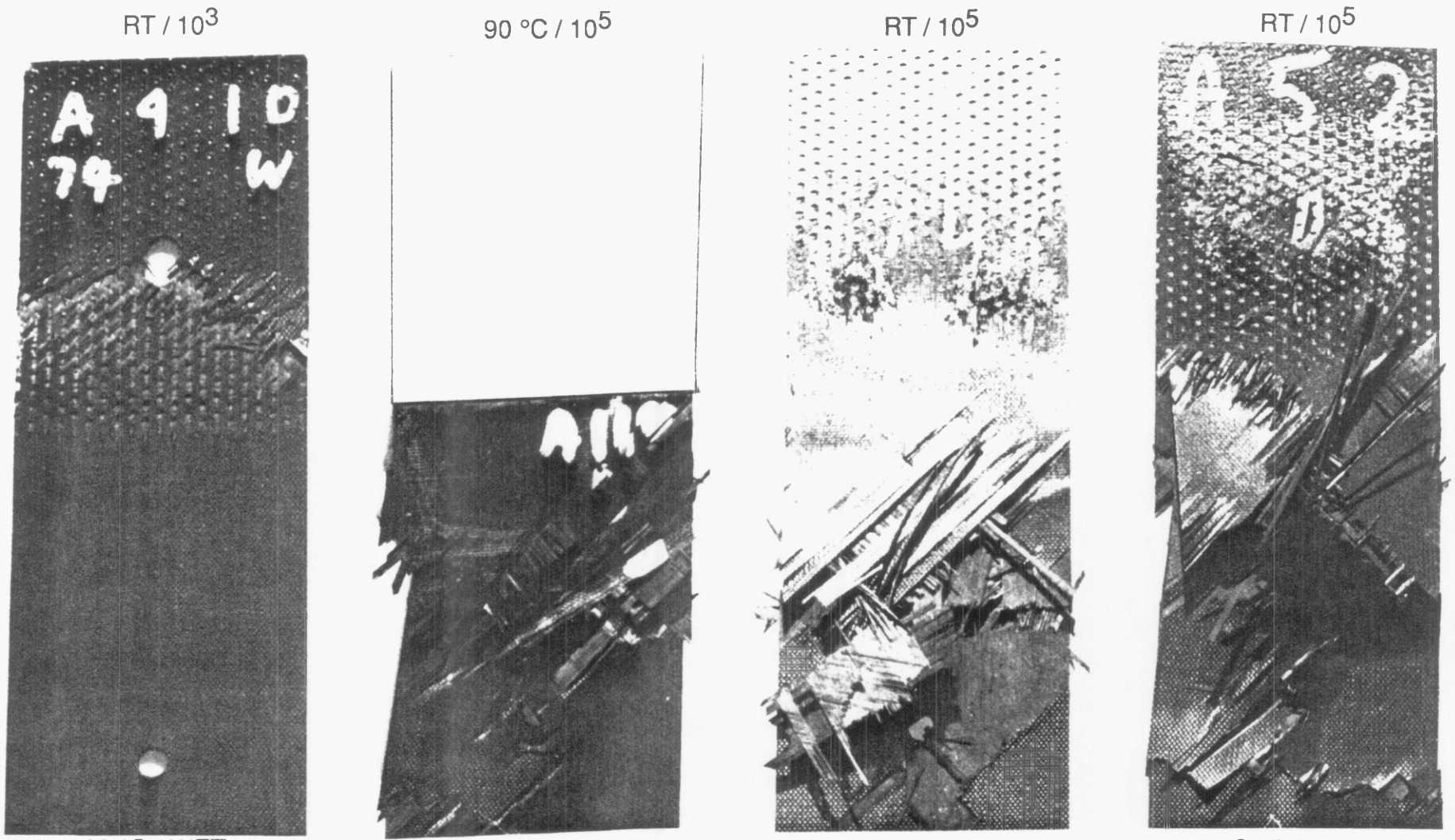


Fig. 4.32: A comparison of tensile fracture modes in wet and dry specimens with circular holes: Note the dowel hole fracture and the end tabed specimen, first and second pictures respectively: the fatigue condition is shown at the top and the static condition at the bottom of each picture.

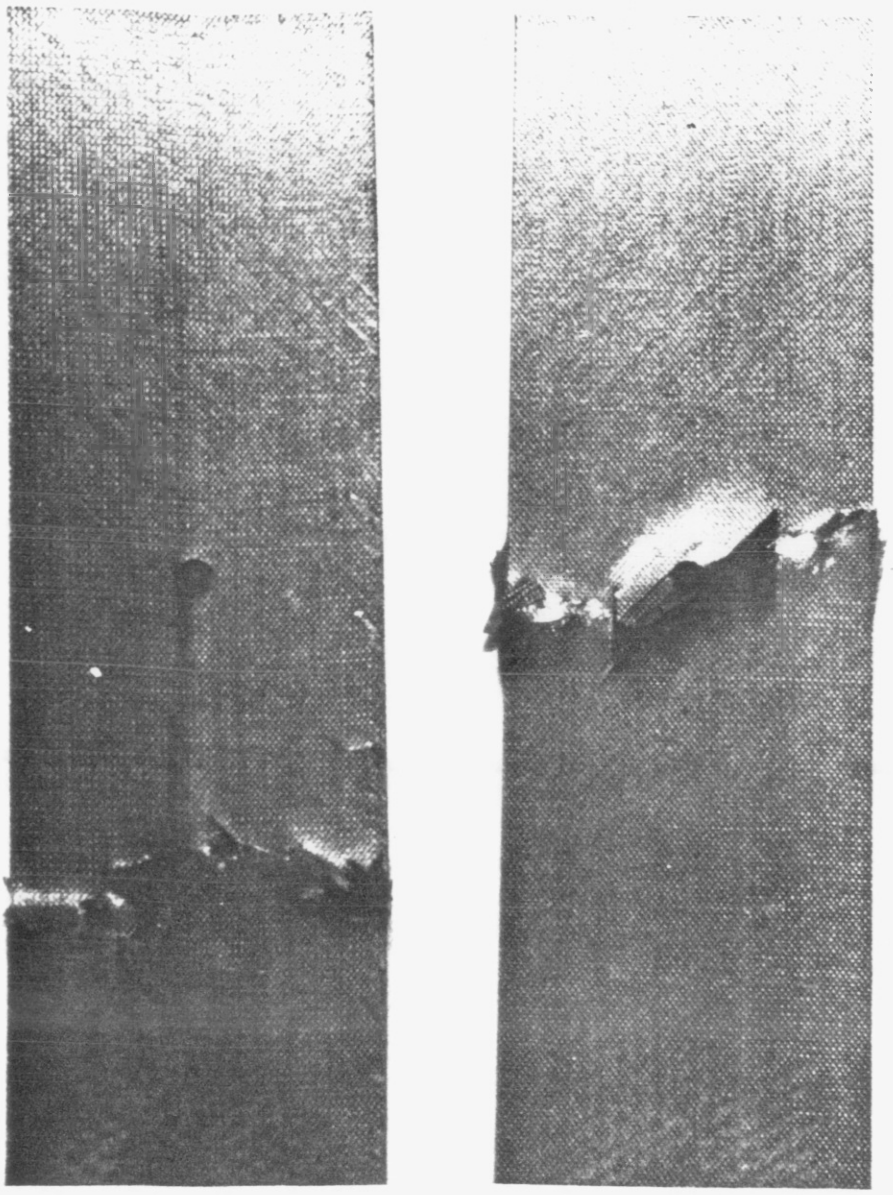


Fig. 4.33: "Premature" and "valid" compressive fracture modes, first and second specimens respectively: both specimens have been fatigue tested for 10^3 cycles at 90°C: both specimens were then statically tested at RT.

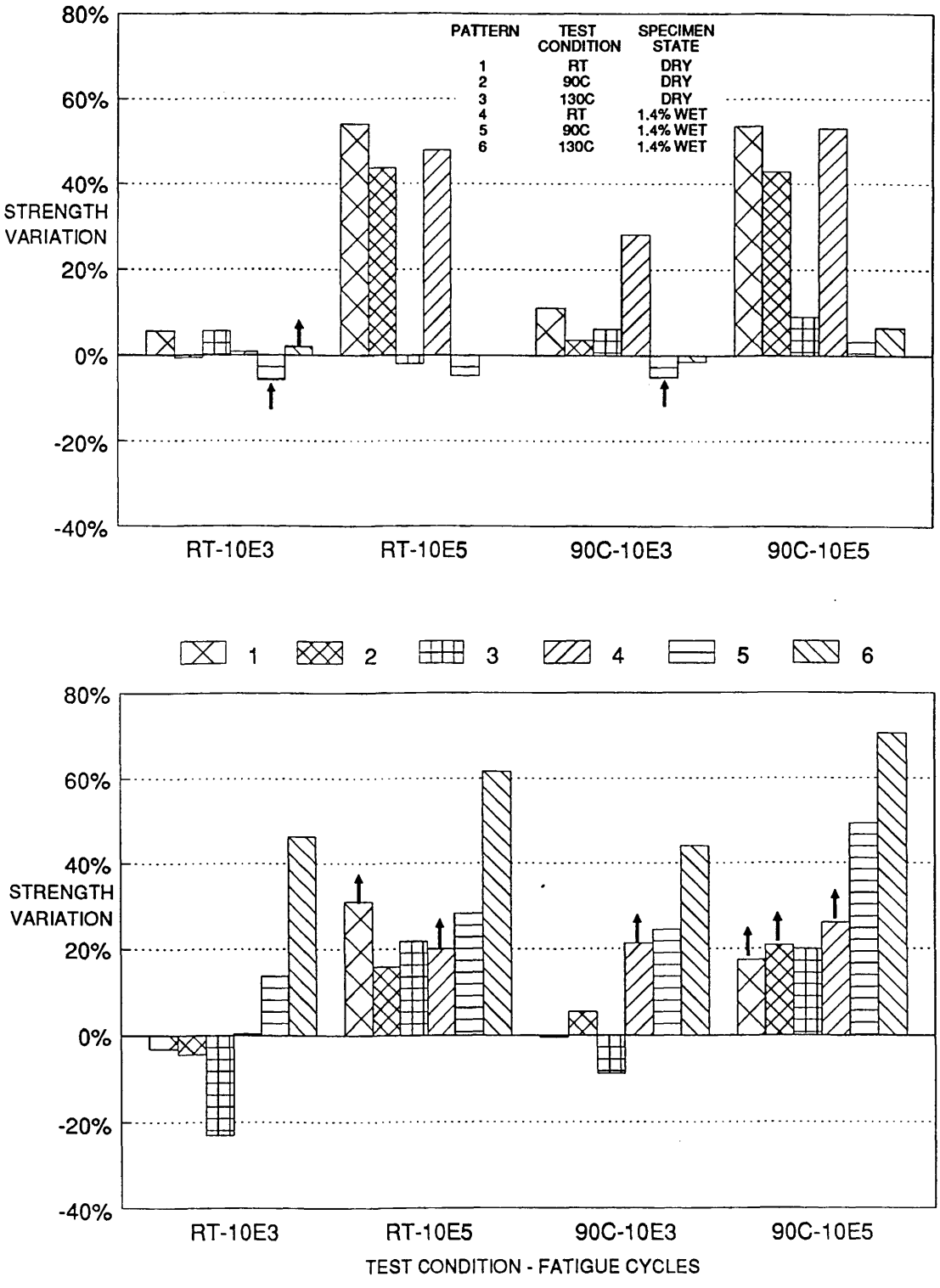


Fig. 4.34: Above, variation of the tensile residual strength with respect to the corresponding static value, for dry and wet specimens with circular holes, (stacking sequence A): below, variation of the compressive residual strength. The arrows indicate higher or lower than marked (expected) variation.

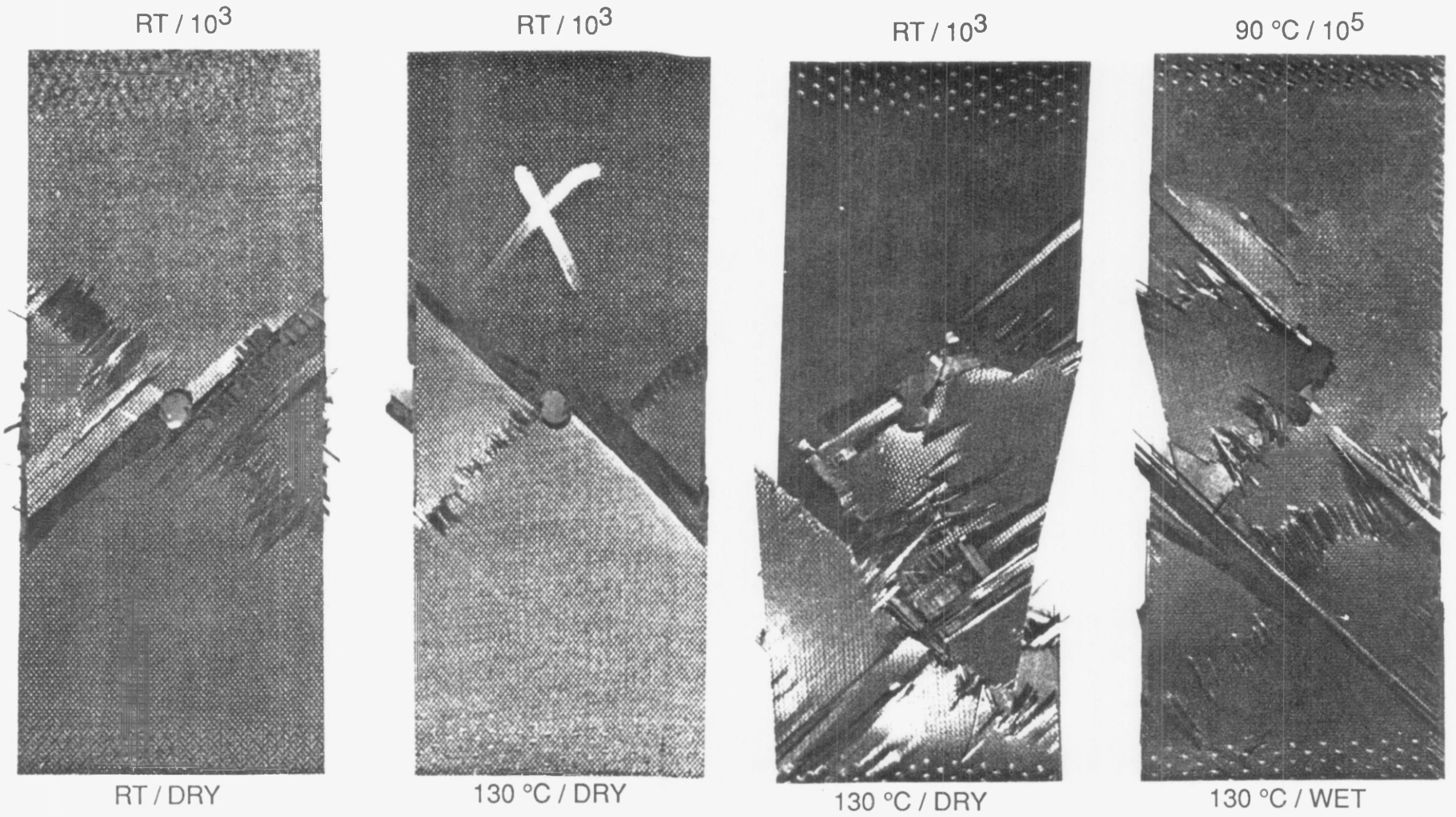


Fig. 4.35: A comparison of tensile fracture modes in wet and dry specimens with circular holes. Note the difference in fracture mode between the second and the third specimen: the fatigue condition is shown at the top and the static condition at the bottom of each picture.

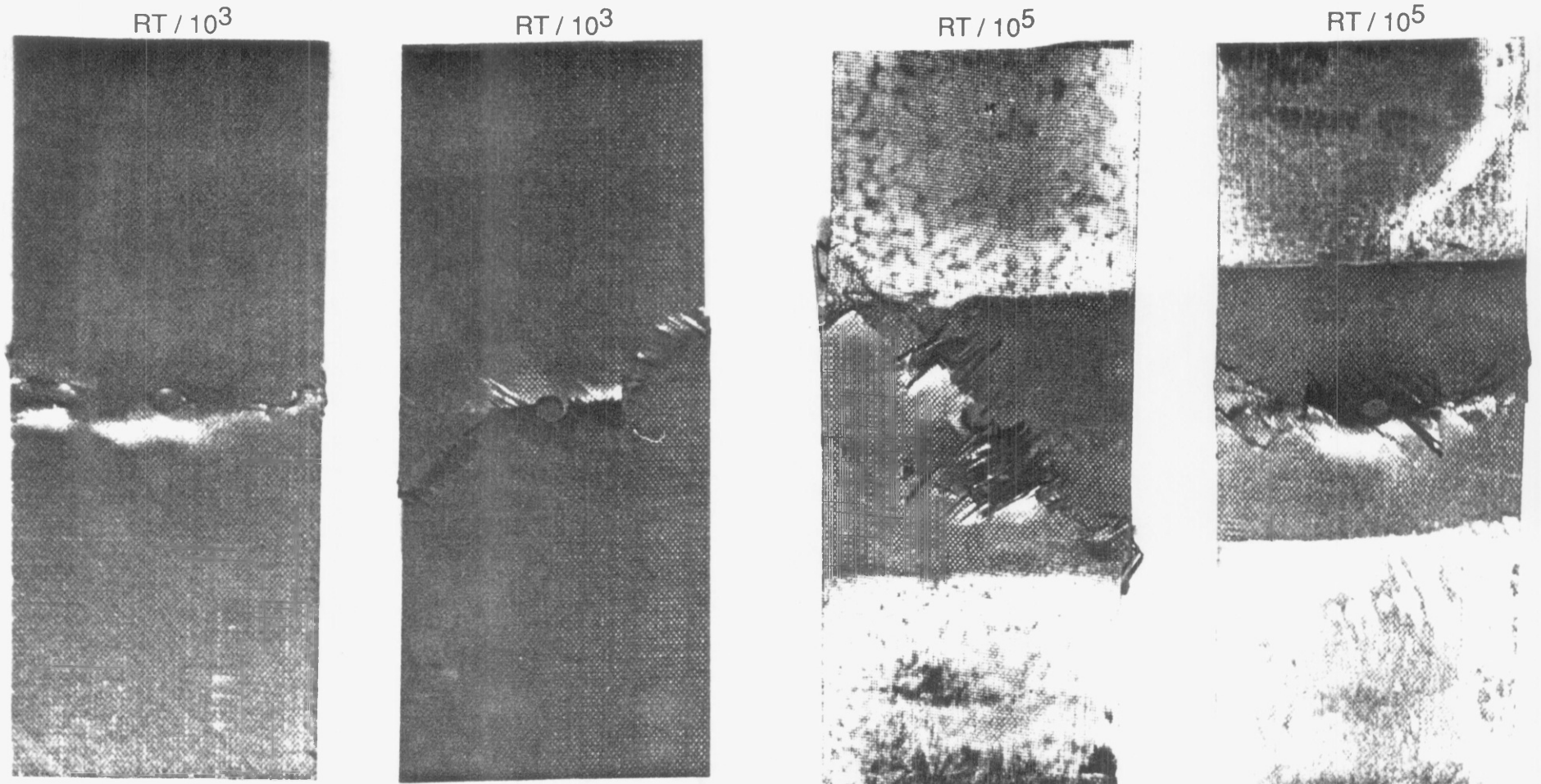


Fig. 4.36: A comparison of compressive fracture modes in dry specimens with circular holes. Note that for specimens in identical conditions, a difference in strength is accompanied by a change in fracture mode: the fatigue condition is shown at the top and the static condition at the bottom of each picture.

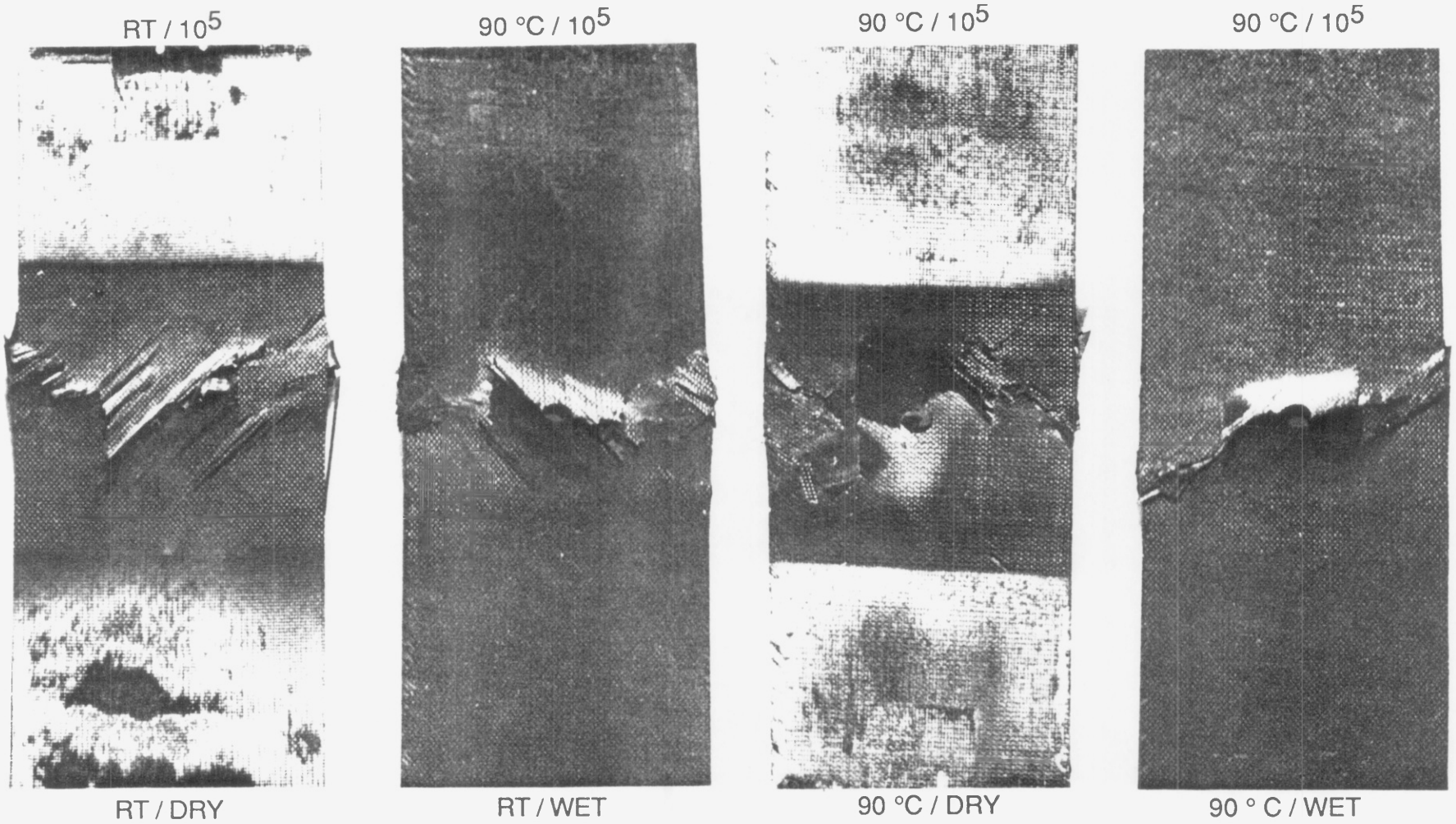


Fig. 4.37: A comparison of compressive fracture modes in wet and dry specimens with circular holes: the fatigue condition is shown at the top and the static condition at the bottom of each picture.

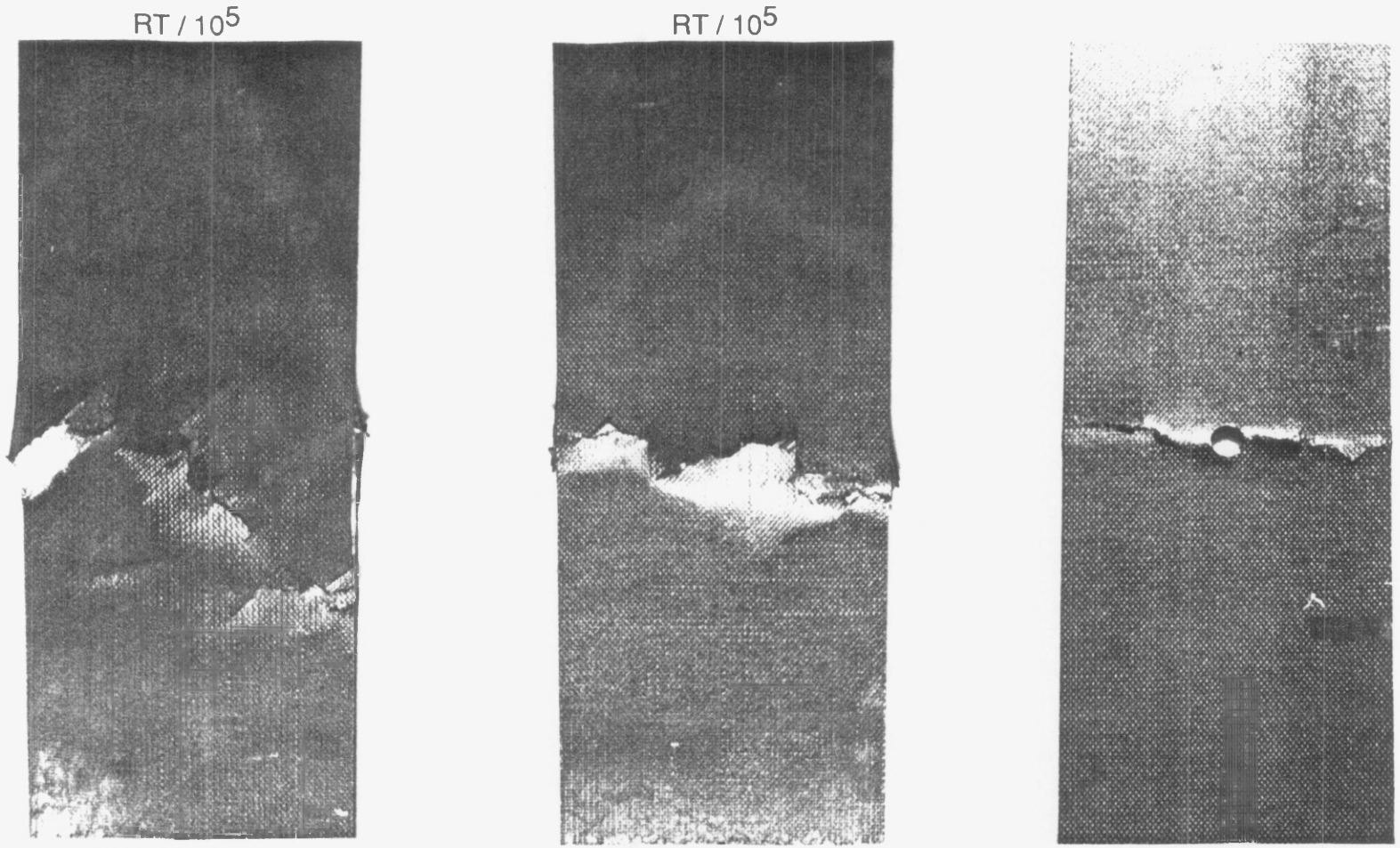


Fig. 4.38: A comparison of compressive fracture modes in 2.0% wet specimens with circular holes: the fatigue condition is shown at the top and the static condition at the bottom of each picture.

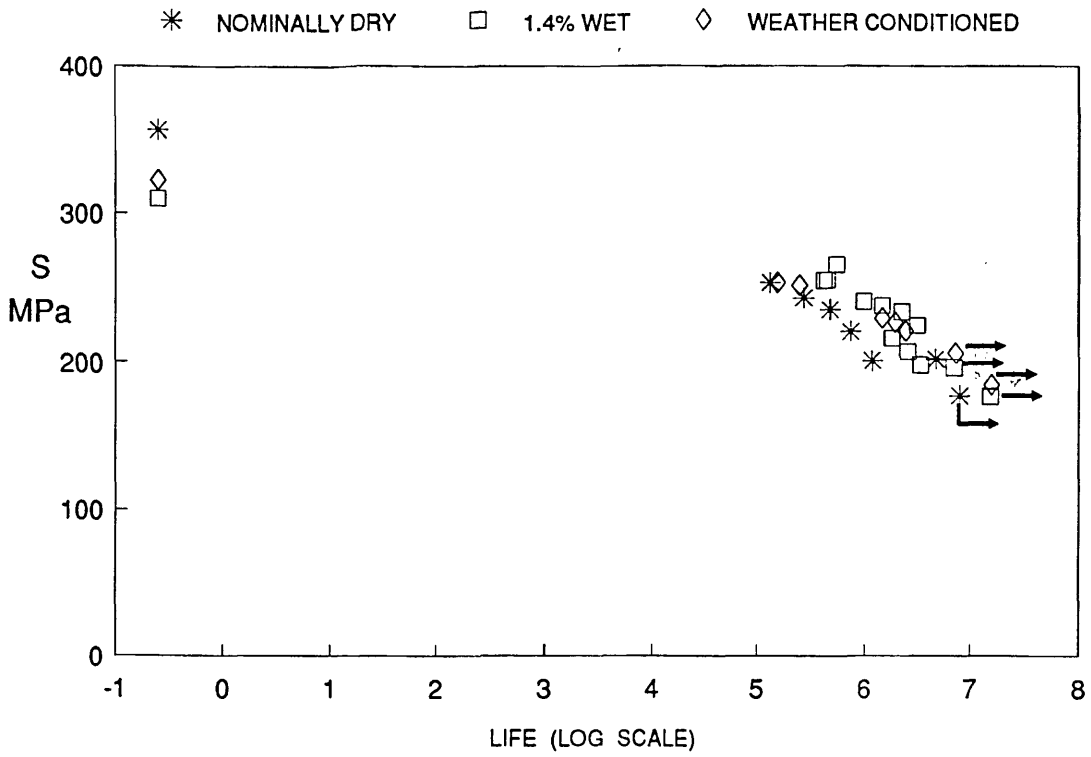


Fig. 4.39: Cyclic stress amplitude versus fatigue life: a comparison between dry and wet specimens of stacking sequence A with sharp notches: all tests were performed in tension-compression at RT. The arrows indicate higher than marked (expected) life.

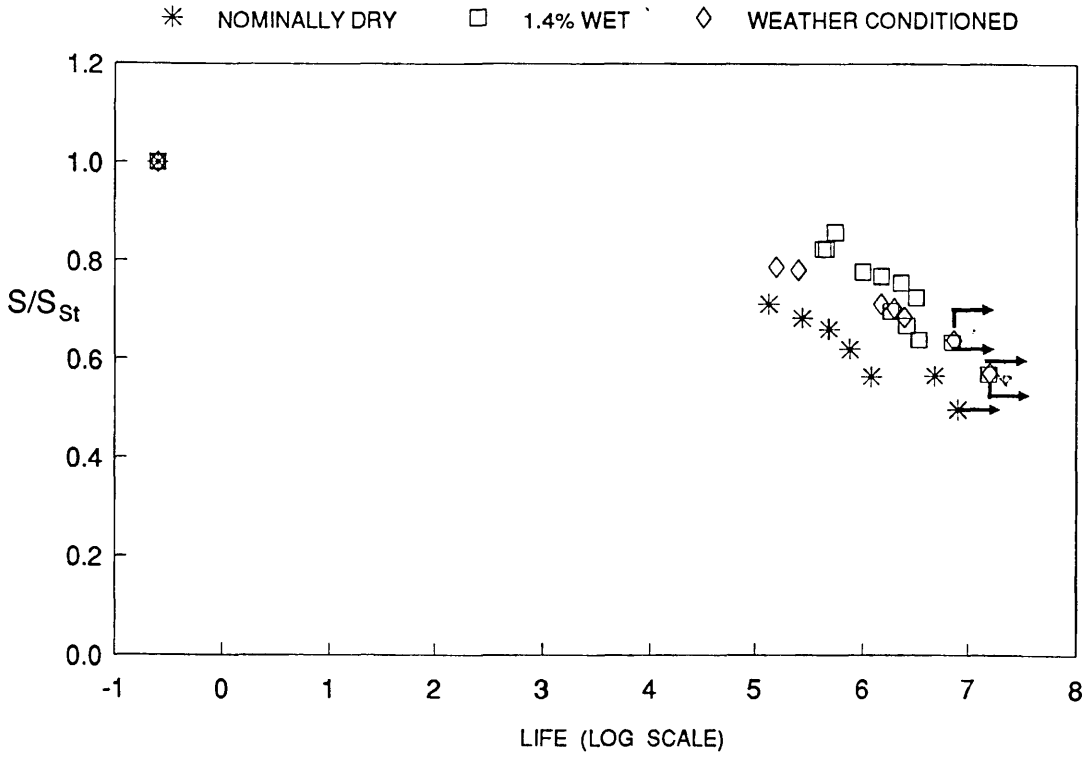


Fig. 4.40: Normalised cyclic stress amplitude versus fatigue life: the cyclic stress has been normalised with respect to the corresponding compressive value: tests include dry and wet specimens with sharp notches: all tests were performed in tension-compression at RT. The arrows indicate higher than marked (expected) life.

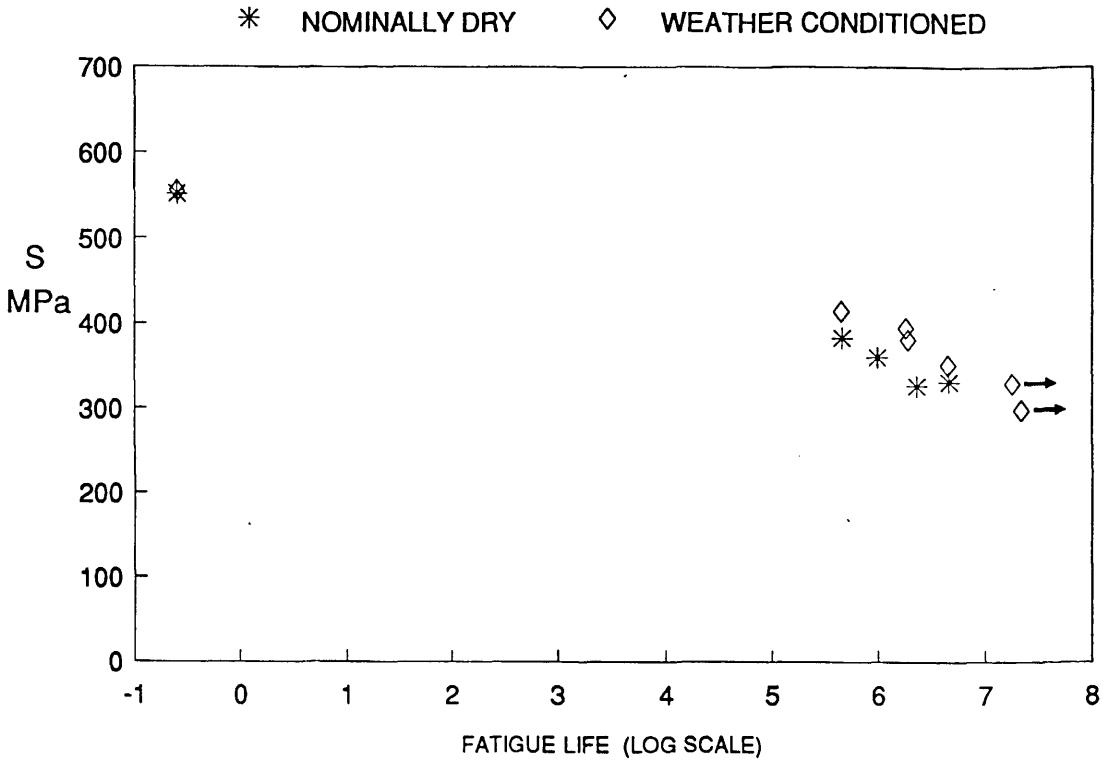


Fig. 4.41: Cyclic stress amplitude versus fatigue life: a comparison between dry and wet specimens (stacking sequence A) with circular holes: all tests were performed in tension-compression at RT. The arrows indicate higher than marked (expected) life.

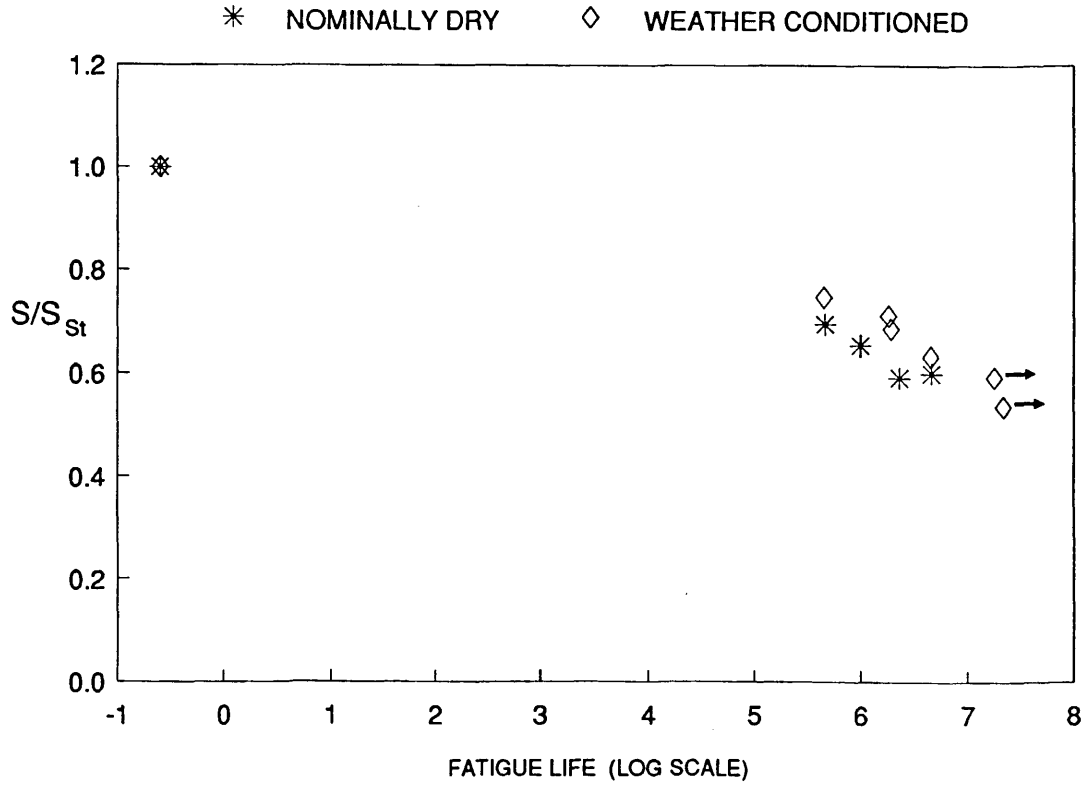


Fig. 4.42: Normalised cyclic stress amplitude versus fatigue life: the cyclic stress has been normalised with respect to the corresponding compressive value: tests include dry and wet specimens with circular holes: all tests were performed in tension-compression at RT. The arrows indicate higher than marked (expected) life.

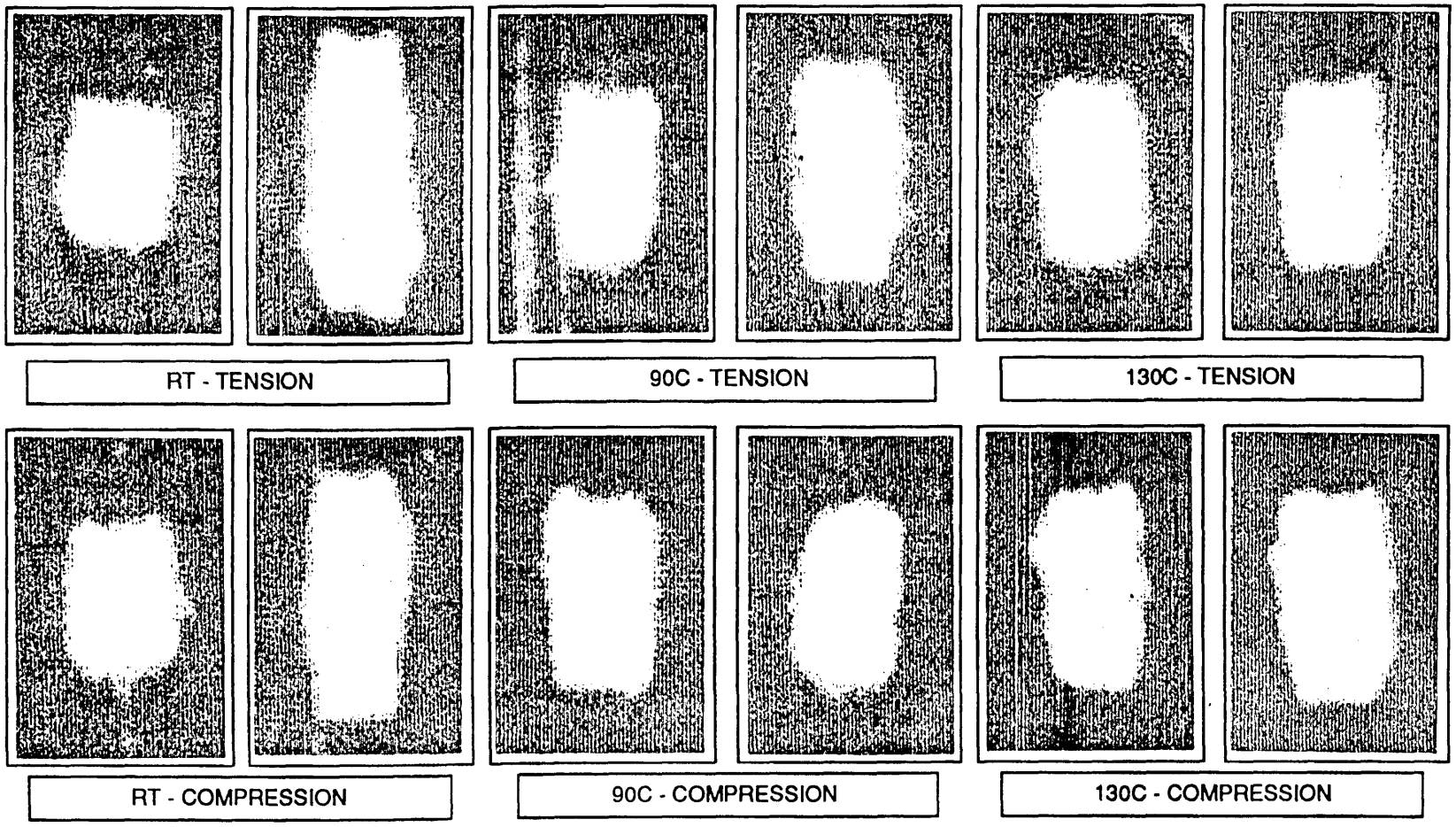


Fig. 4.43: A set of C-scans indicating the fatigue damage in wet specimens of stacking sequence A with sharp notches: test were performed in tension-compression at 90°C for 10^5 cycles at a load amplitude Ln (=20kN). The specimens were selected in pairs (as shown) for subsequent residual strength testing.

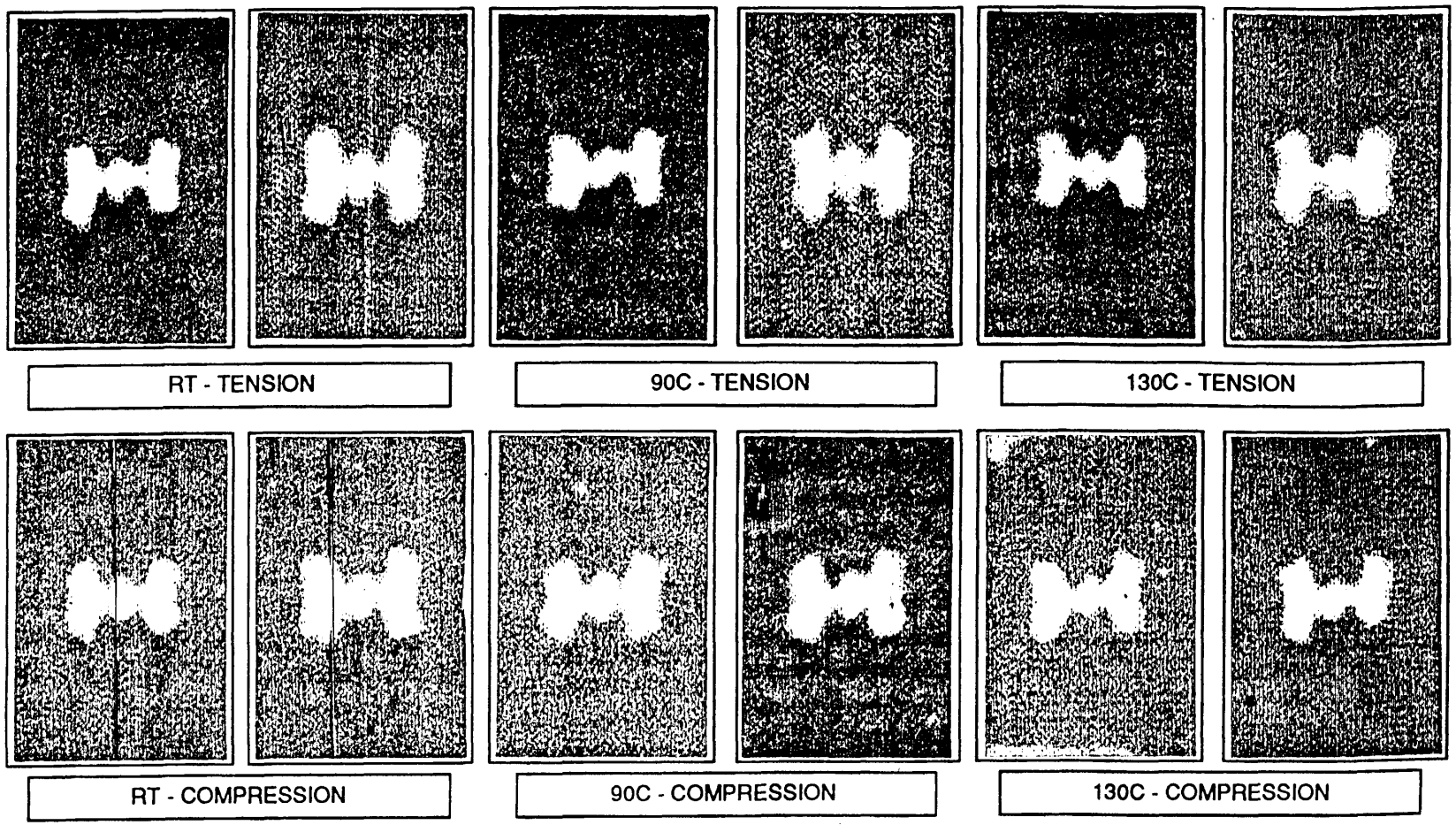


Fig. 4.44: A set of C-scans indicating the fatigue damage in dry specimens of stacking sequence B with sharp notches: test were performed in tension-compression at RT for 10^5 cycles at a load amplitude Ln (=20kN). The specimens were selected in pairs (as shown) for subsequent residual strength testing.

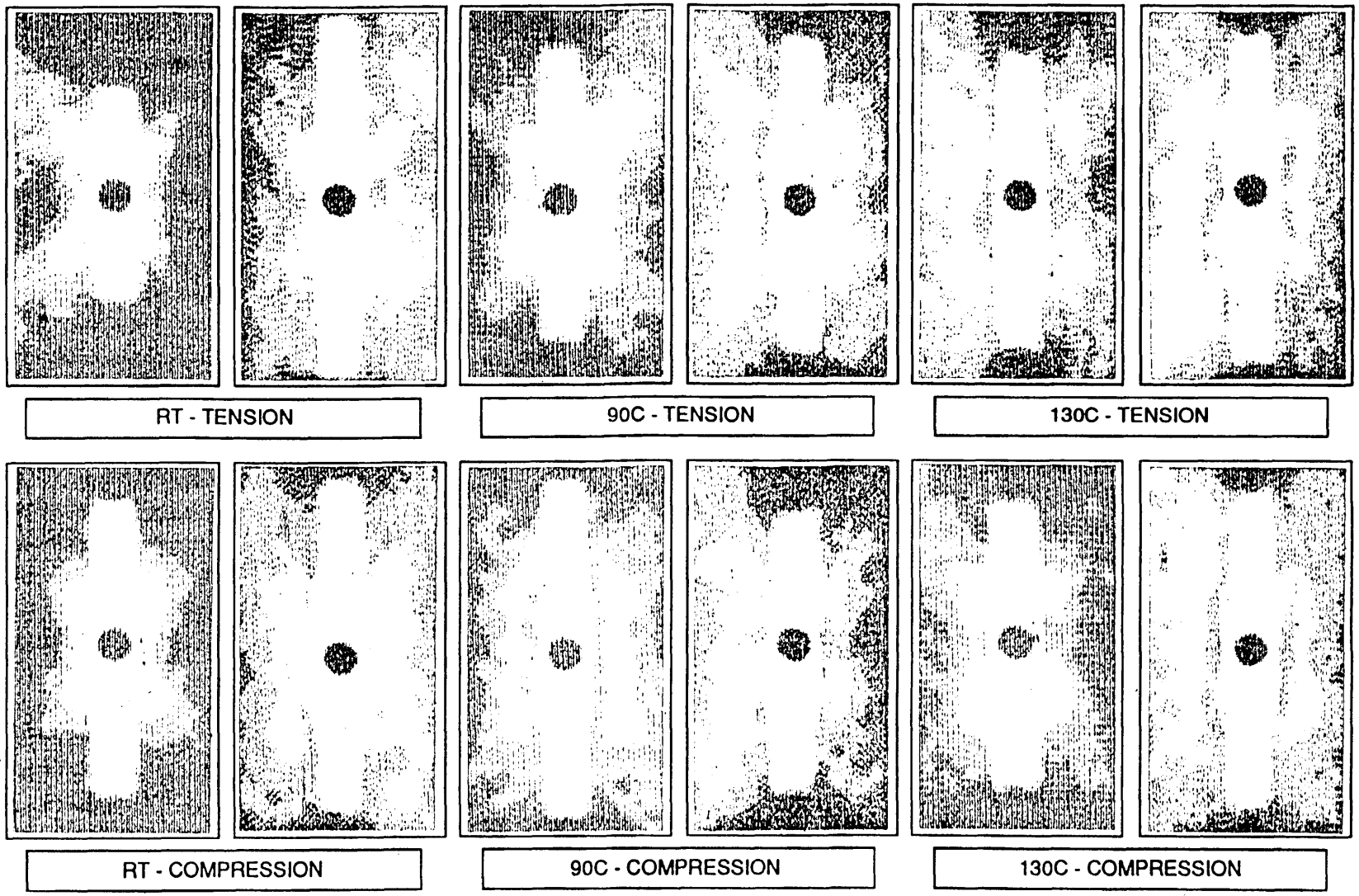


Fig. 4.45: A set of C-scans indicating the fatigue damage in dry specimens with circular holes: test were performed in tension-compression at RT for 10^5 cycles at a load amplitude Lh(=30kN). The specimens were selected in pairs (as shown) for subsequent residual strength testing.

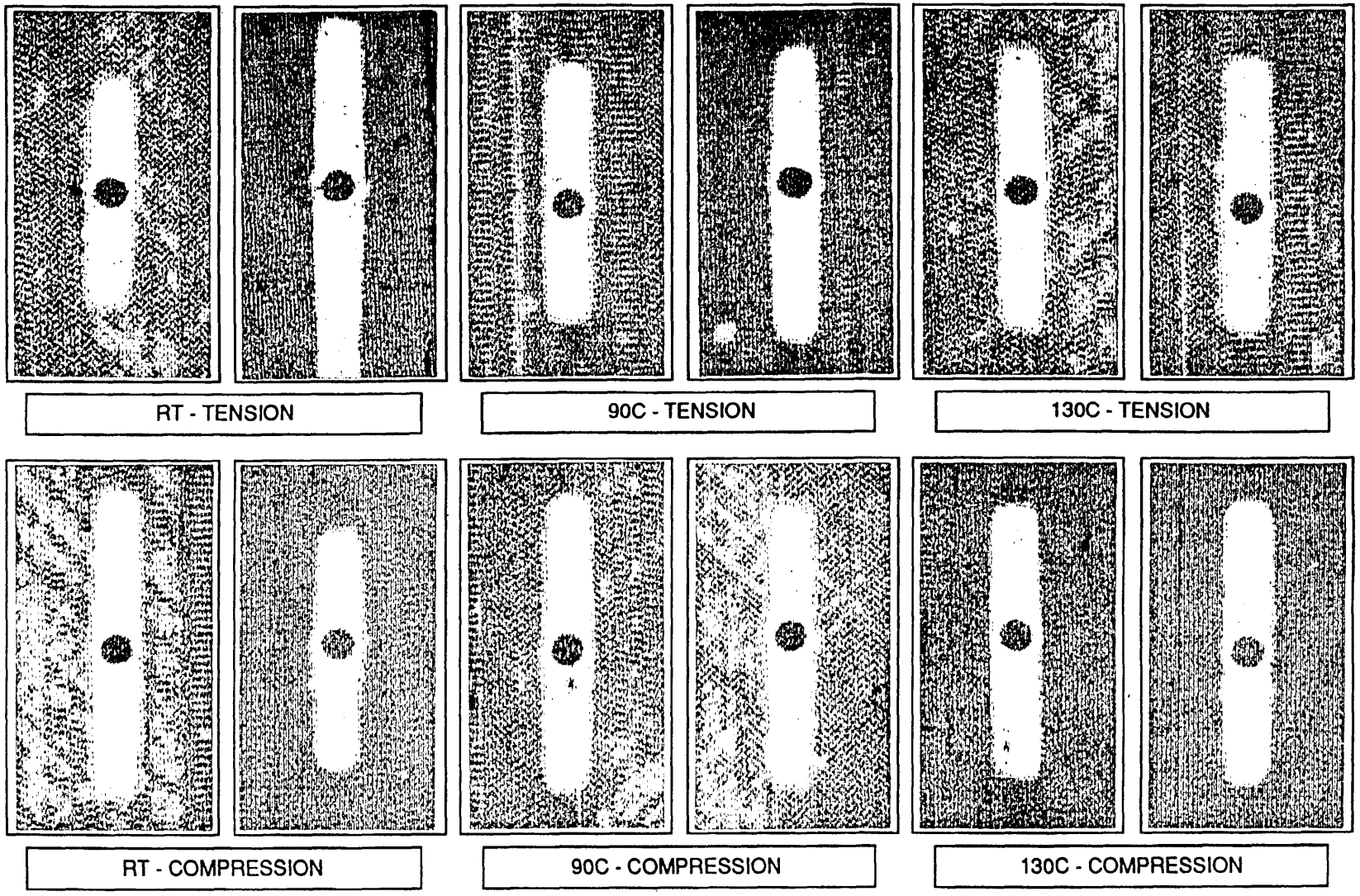
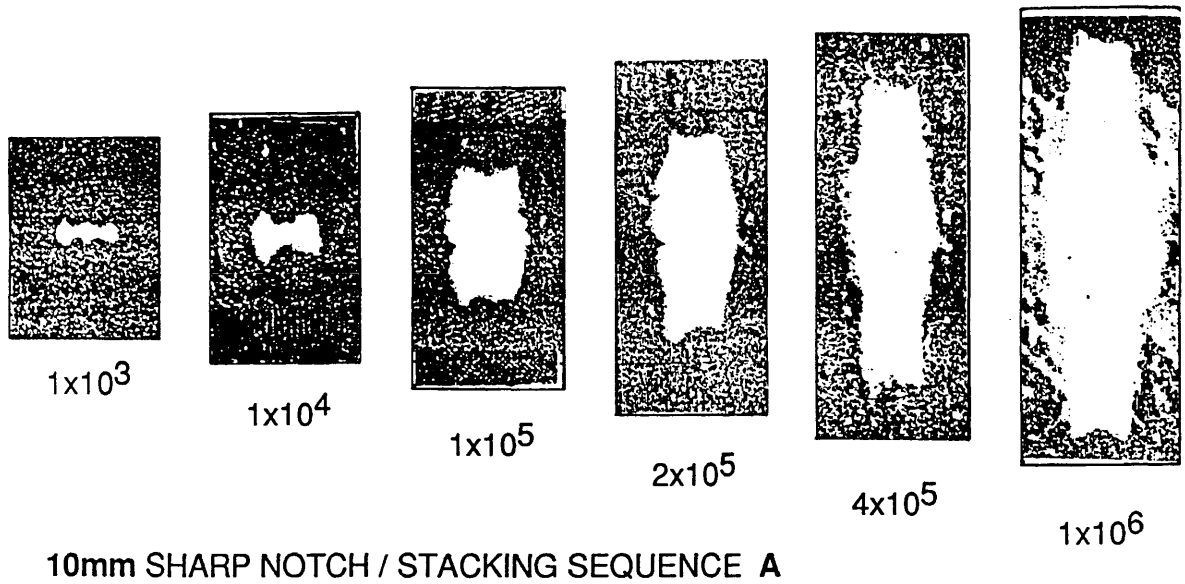
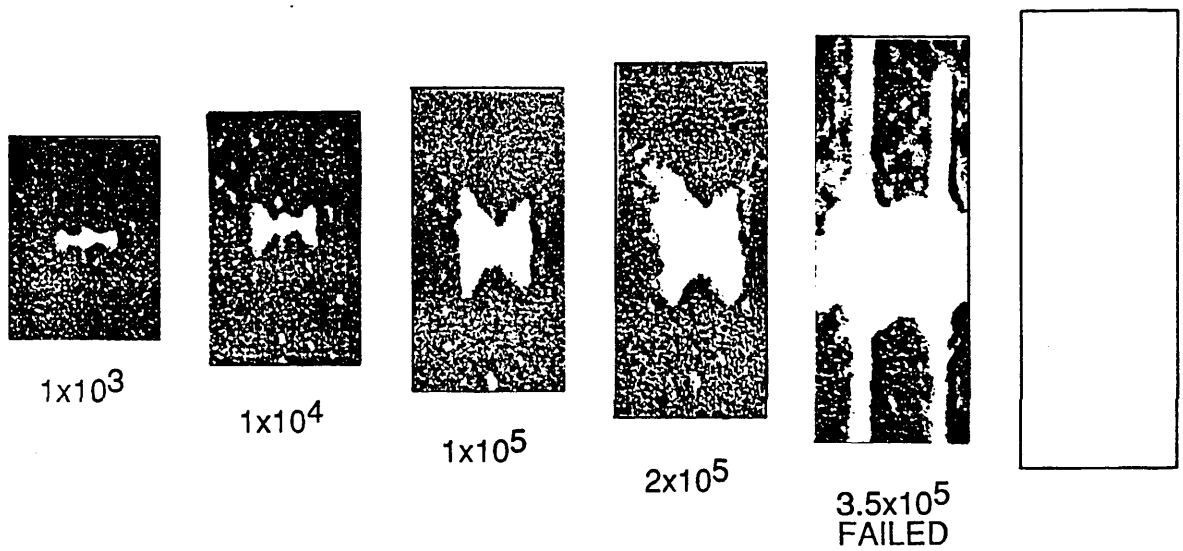


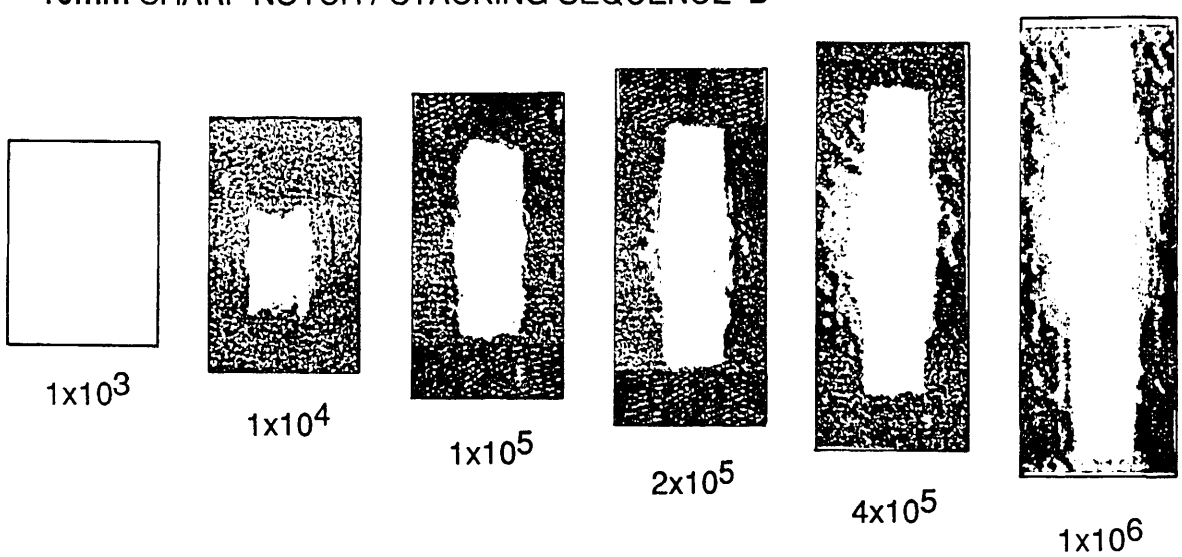
Fig. 4.46: A set of C-scans indicating the fatigue damage in wet specimens with circular holes: test were performed in tension-compression at RT for 10^5 cycles at a load amplitude Lh(=30kN). The specimens were selected in pairs (as shown) for subsequent residual strength testing.



10mm SHARP NOTCH / STACKING SEQUENCE **A**



10mm SHARP NOTCH / STACKING SEQUENCE **B**



10mm CIRCULAR HOLE

Fig. 4.47: C-scan damage development in wet specimens with (a) 10mm sharp notch of **stacking sequence A** (above), (b) 10mm sharp notch of **stacking sequence B** (middle) and (c) **10mm circular hole** (below): tests were performed in tension- compression at 90°C at a load amplitude Ln (=20kN). Note that the box width does not represent the specimens full width.

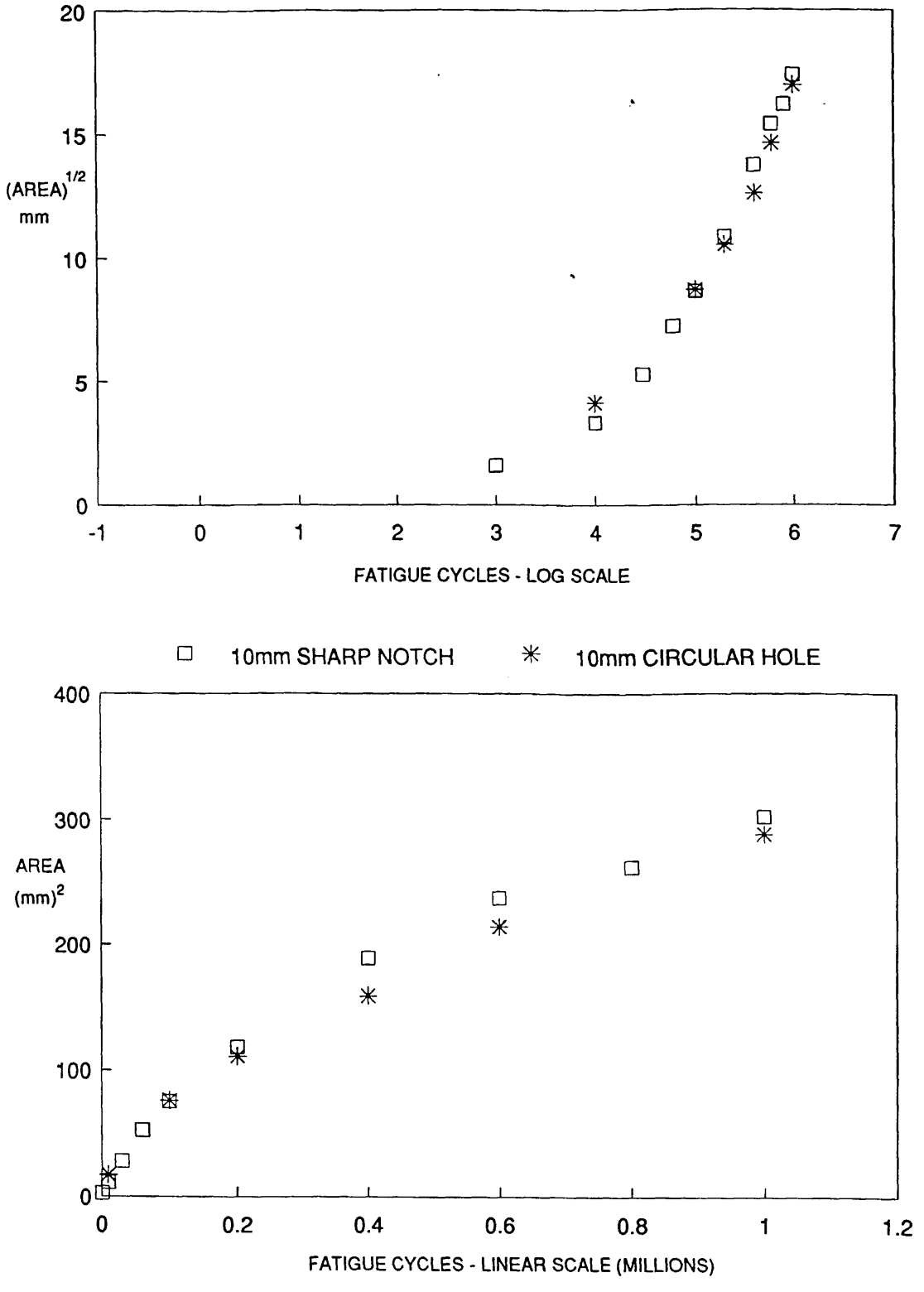


Fig. 4.48: C-scan damage area (see figure 4.47) versus number of fatigue cycles for 10mm notch and 10mm hole of stacking sequence A: (a) log cycle scale and (b) linear cycle scale.

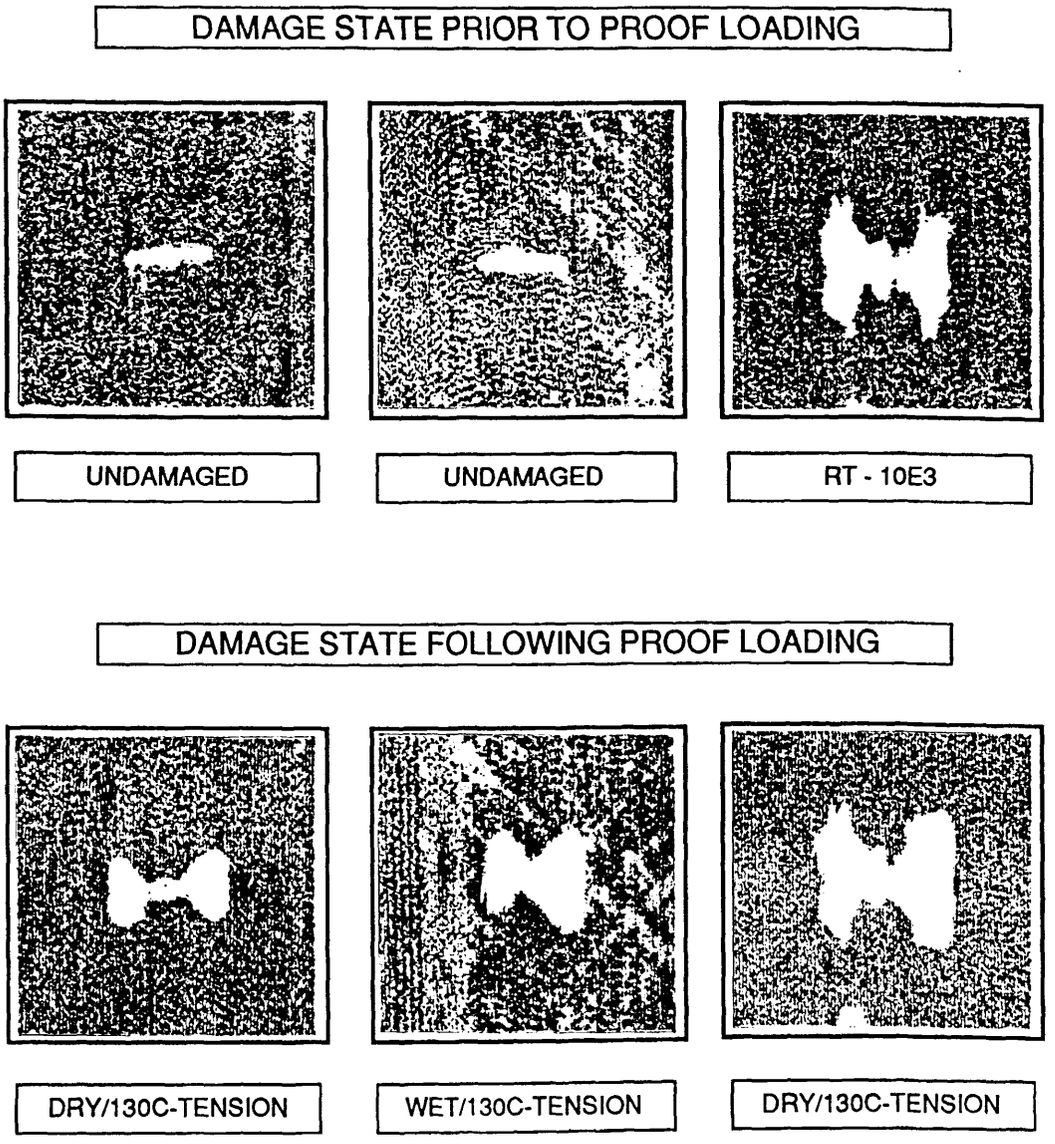


Fig. 4.49: C-scan damage development in dry and wet specimens of stacking sequence A with sharp notches, following proof loading in tension.

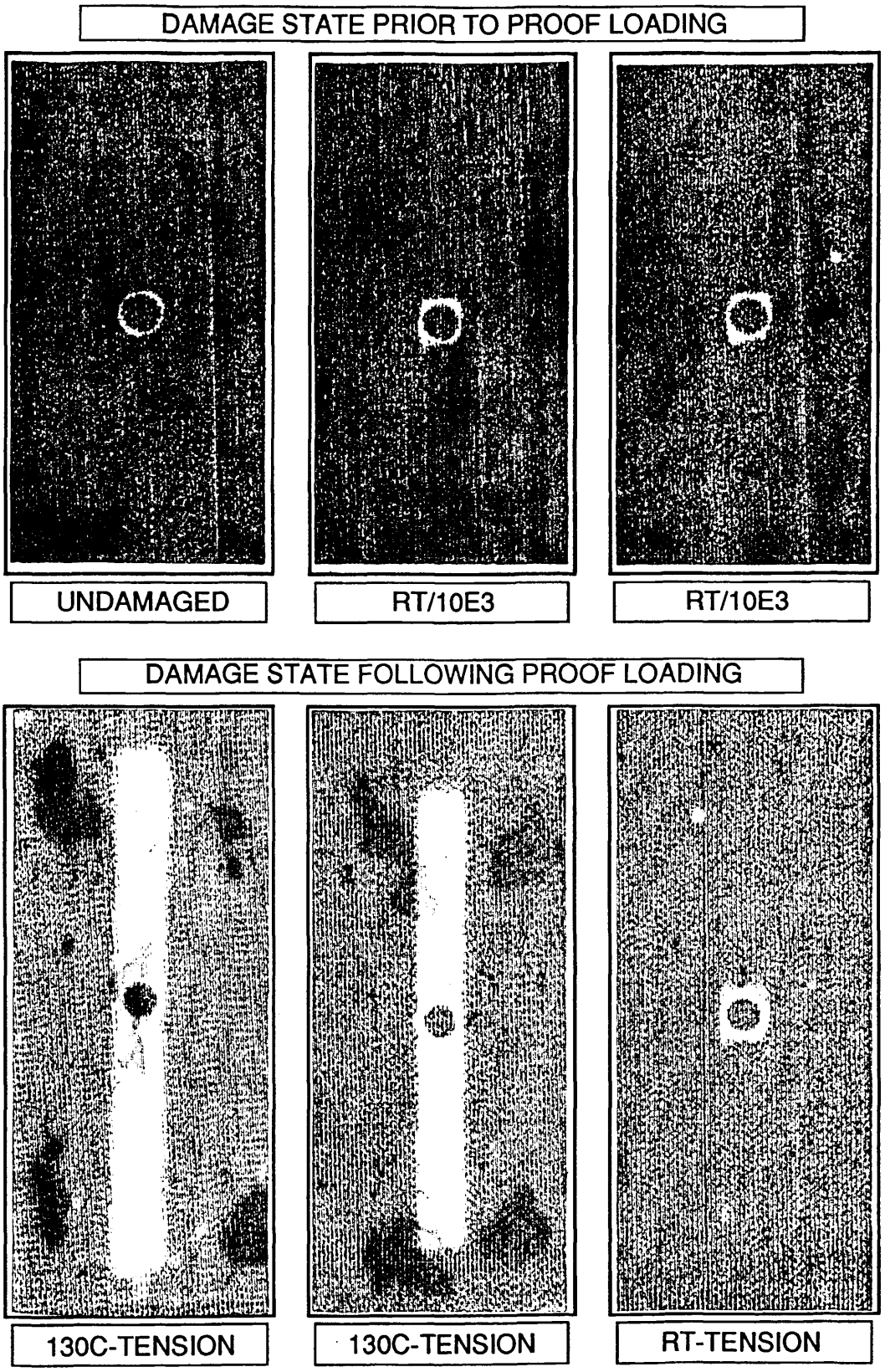


Fig. 4.50: C-scan damage development in dry specimens (stacking sequence A) with circular holes, following proof loading in tension.

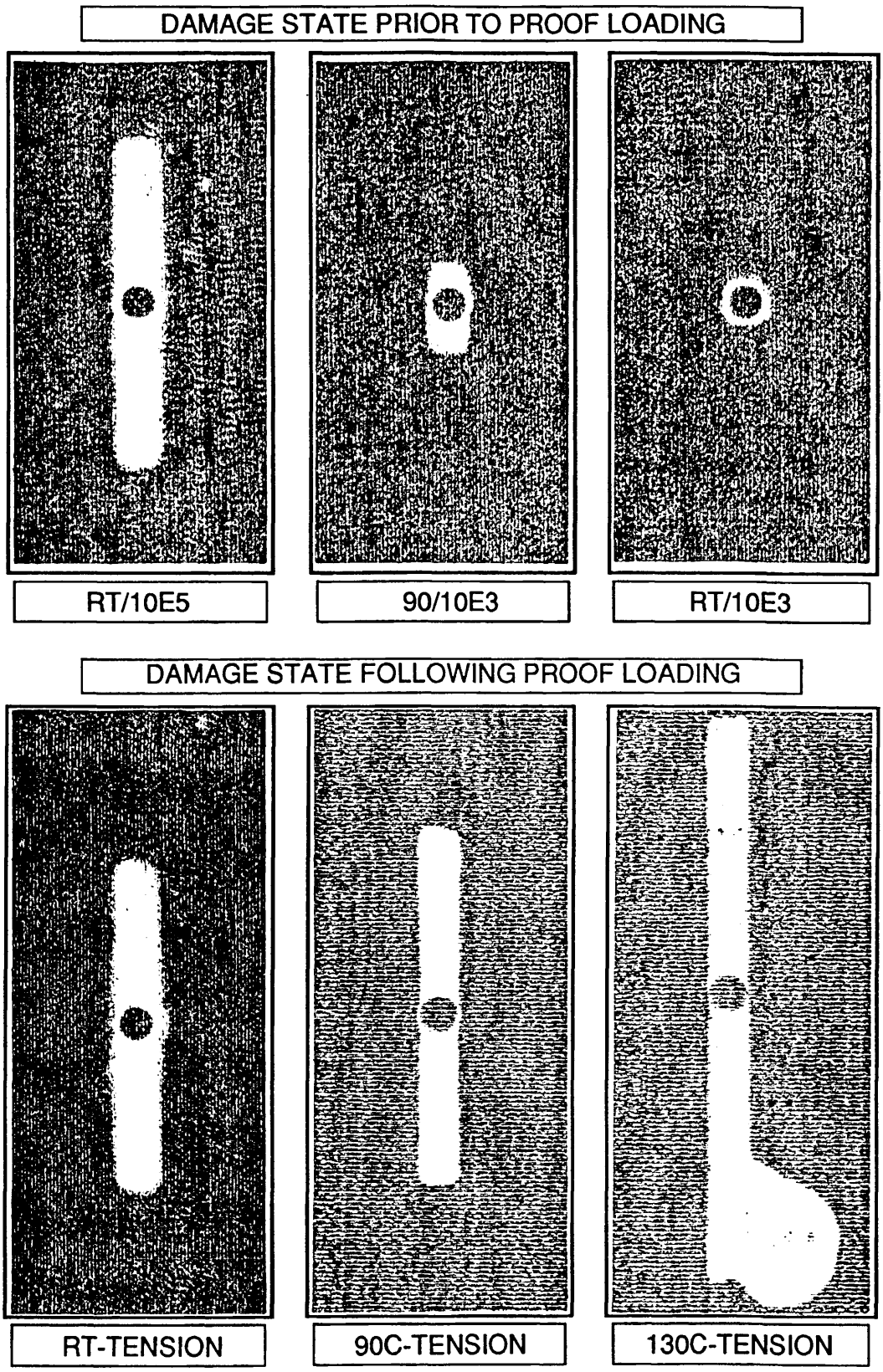


Fig. 4.51: C-scan damage development in wet specimens (stacking sequence A) with circular holes, following proof loading in tension.

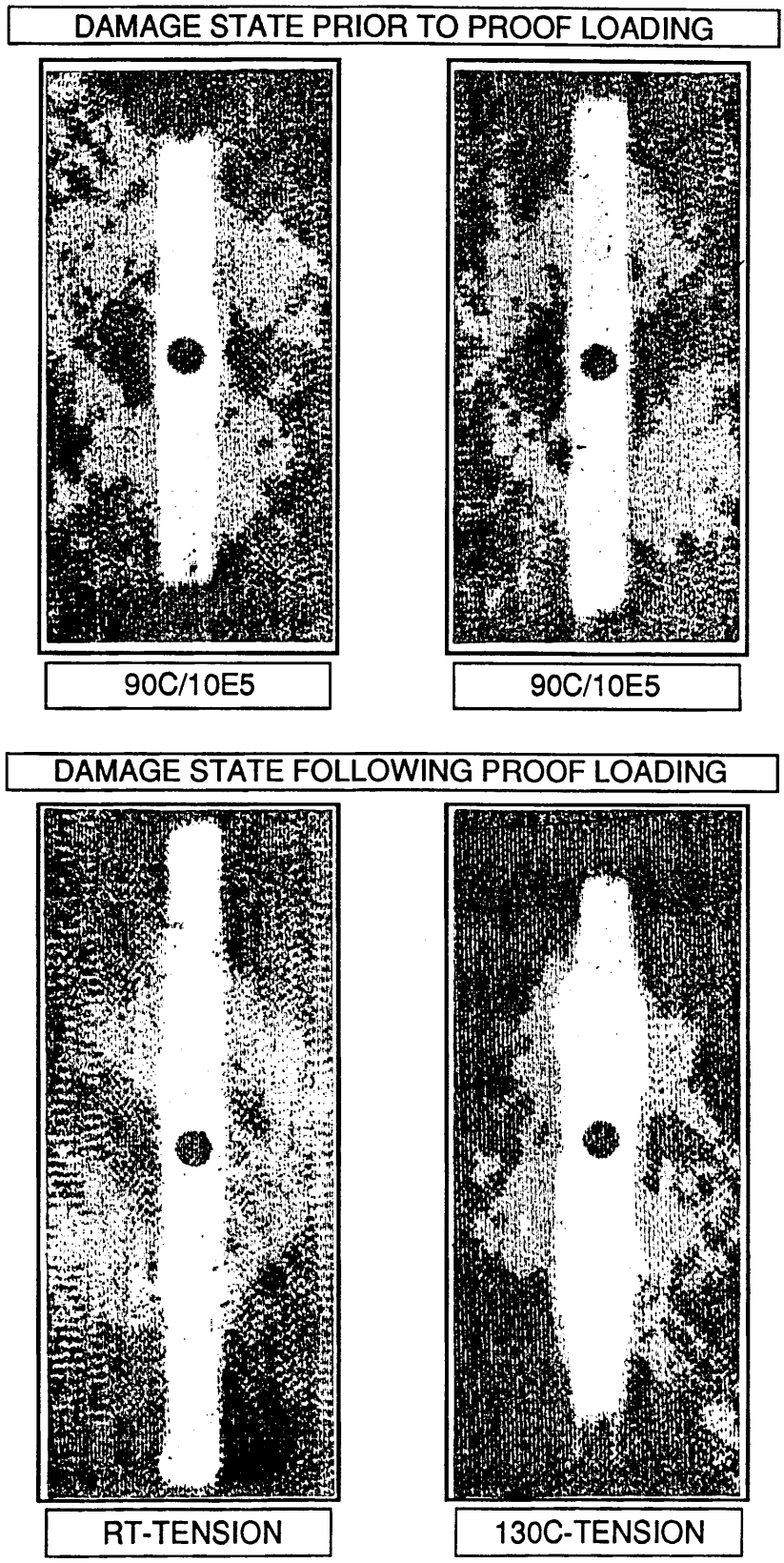


Fig. 4.52: C-scan damage development in dry specimens (stacking sequence A) with circular holes, following proof loading in tension.

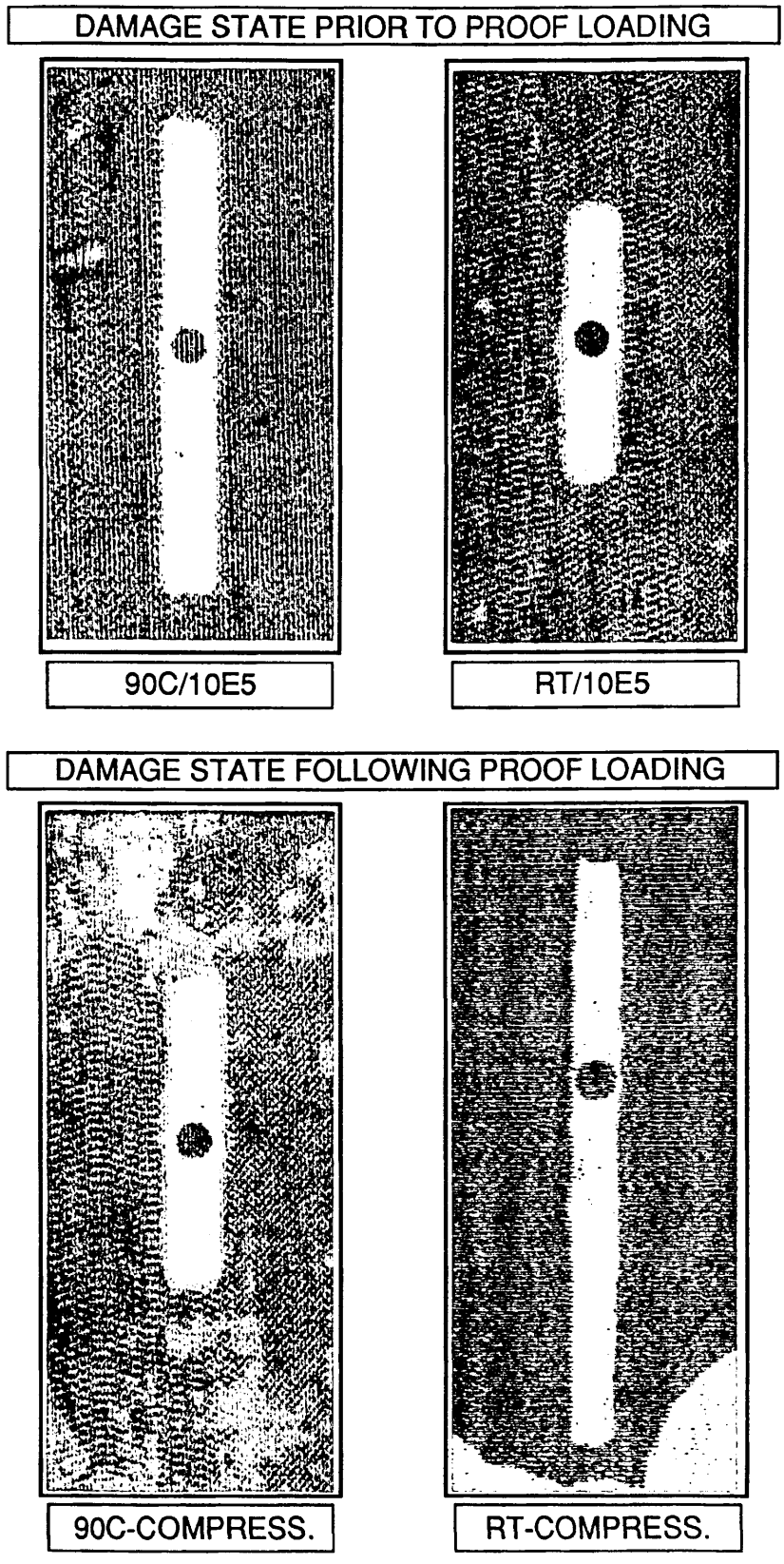


Fig. 4.53: C-scan damage development in dry (left) and wet specimens (stacking sequence A) with circular holes, following proof loading in compression.

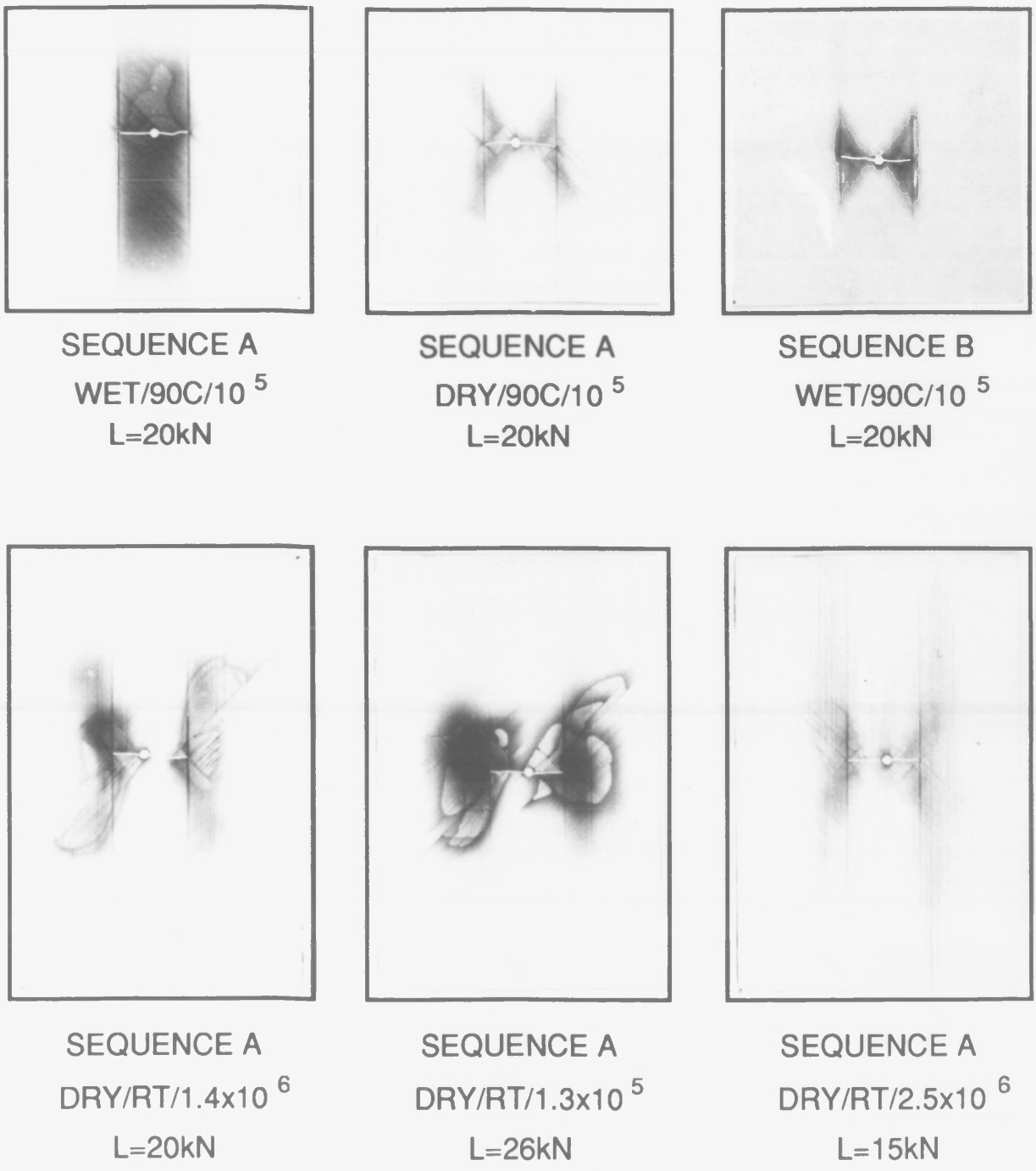


Fig. 4.54: X-ray radiographs of typical fatigue damage development under various environmental conditions in specimens with sharp notches: the load amplitude is denoted L.

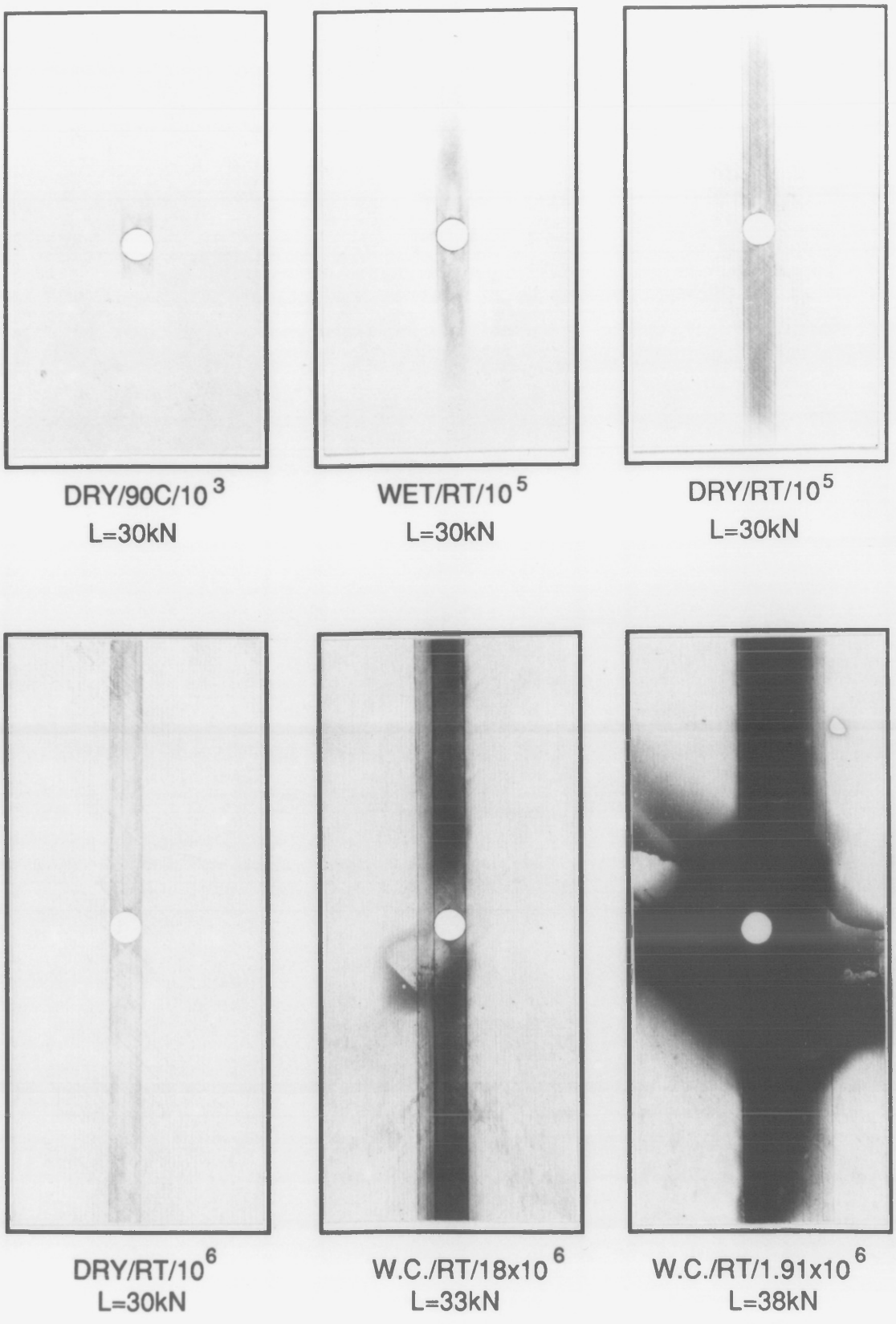


Fig. 4.55: X-ray radiographs of typical fatigue damage development under various environmental conditions in specimens with circular holes: the load amplitude is denoted L.

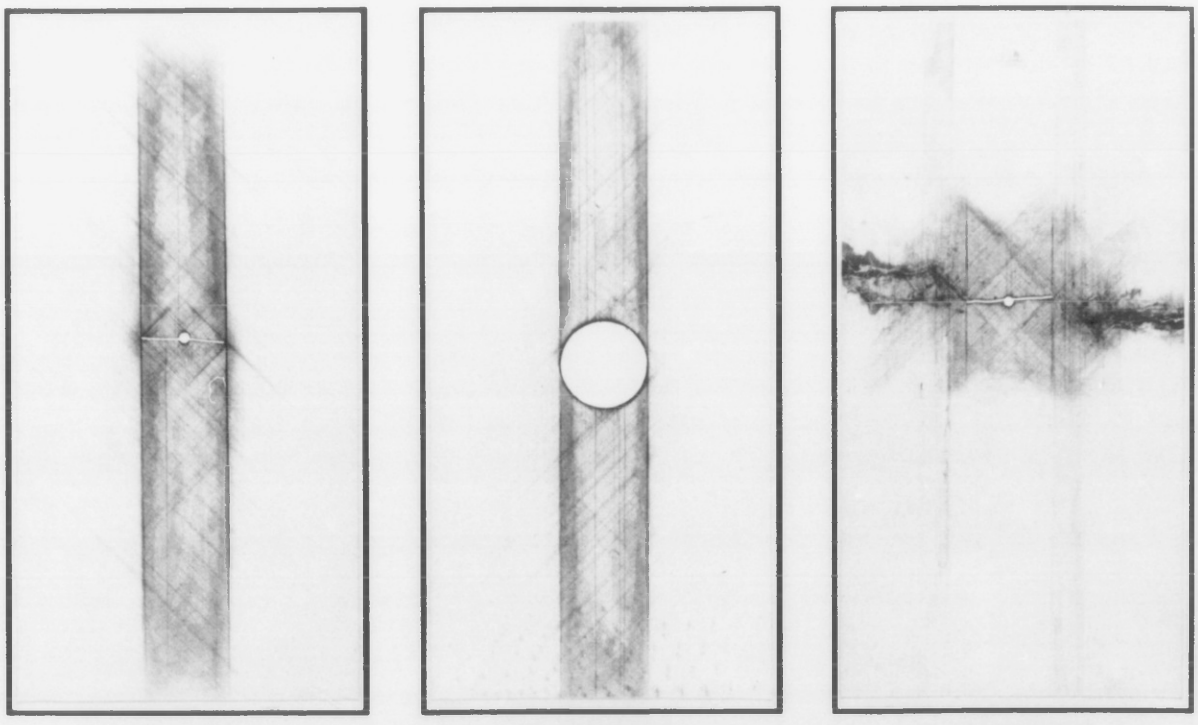


Fig. 4.56: X-ray radiographs of wet specimens, fatigue tested at 90°C in tension-compression at a load amplitude Ln (=20kN): the damage development in these particular specimens is shown in figure 4.47.

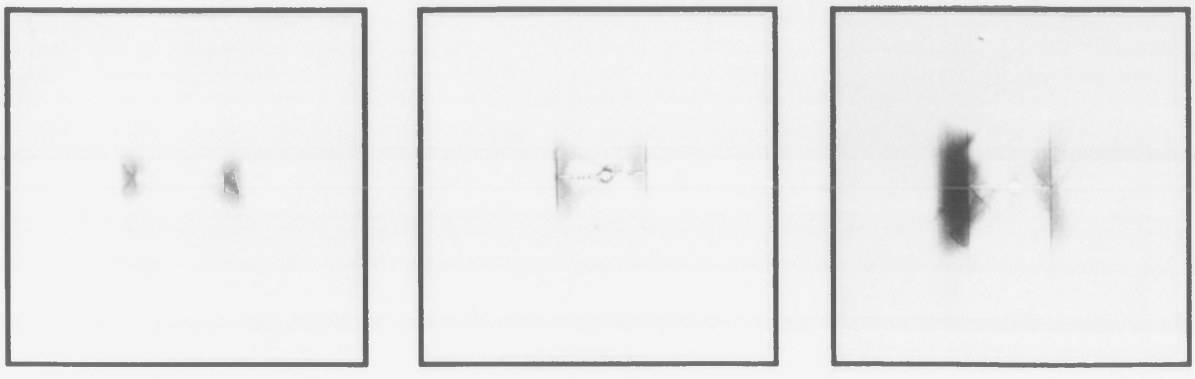


Fig. 4.57: X-ray radiographs of damage development in dry and wet specimens of stacking sequence A with sharp notches, following proof loading in tension.

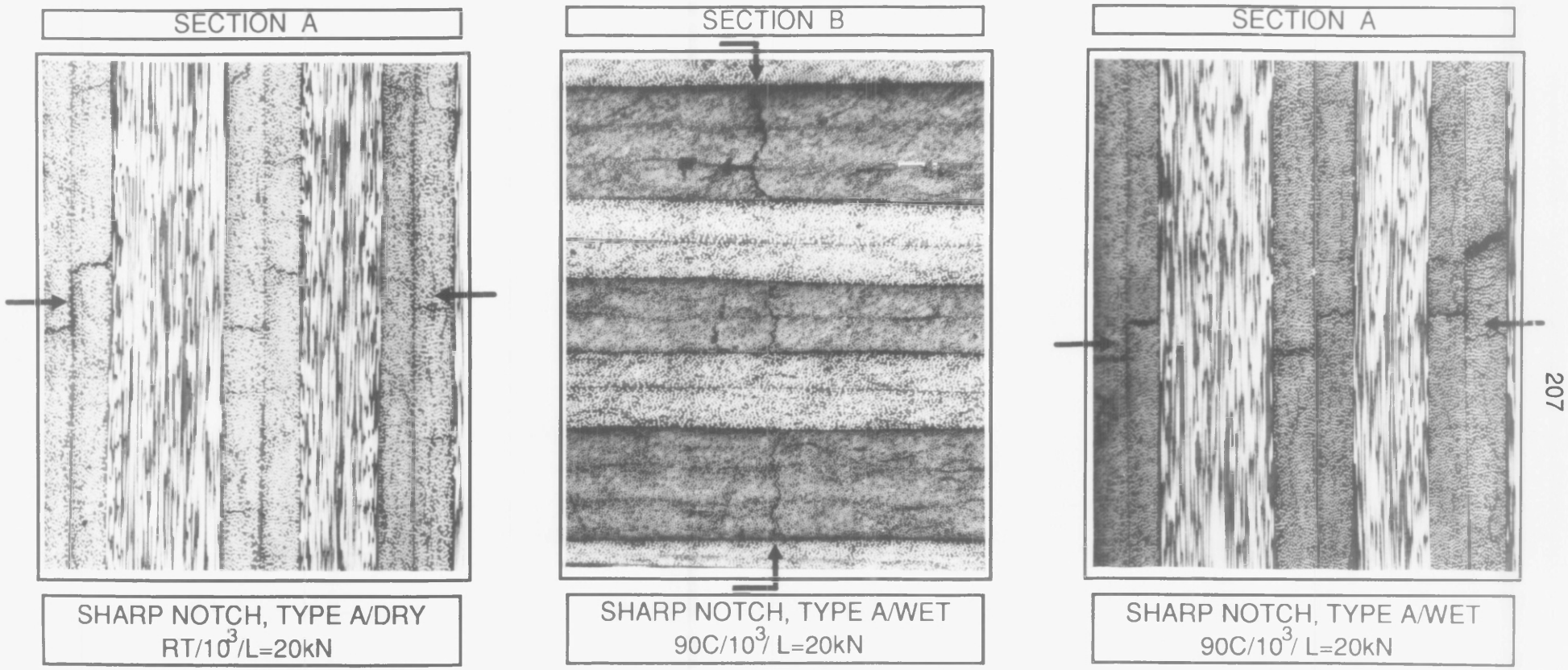


Fig. 4.58: Micrographs of the fatigue damaged region near the sharp notch tip of specimens with stacking sequence A: tests were performed in tension-compression at a load amplitude Ln (=20kN) for 10^3 cycles: the arrows indicate the location of the "notch tip line": in the case of sections A , the surface plies are located at the left hand side of the micrographs.

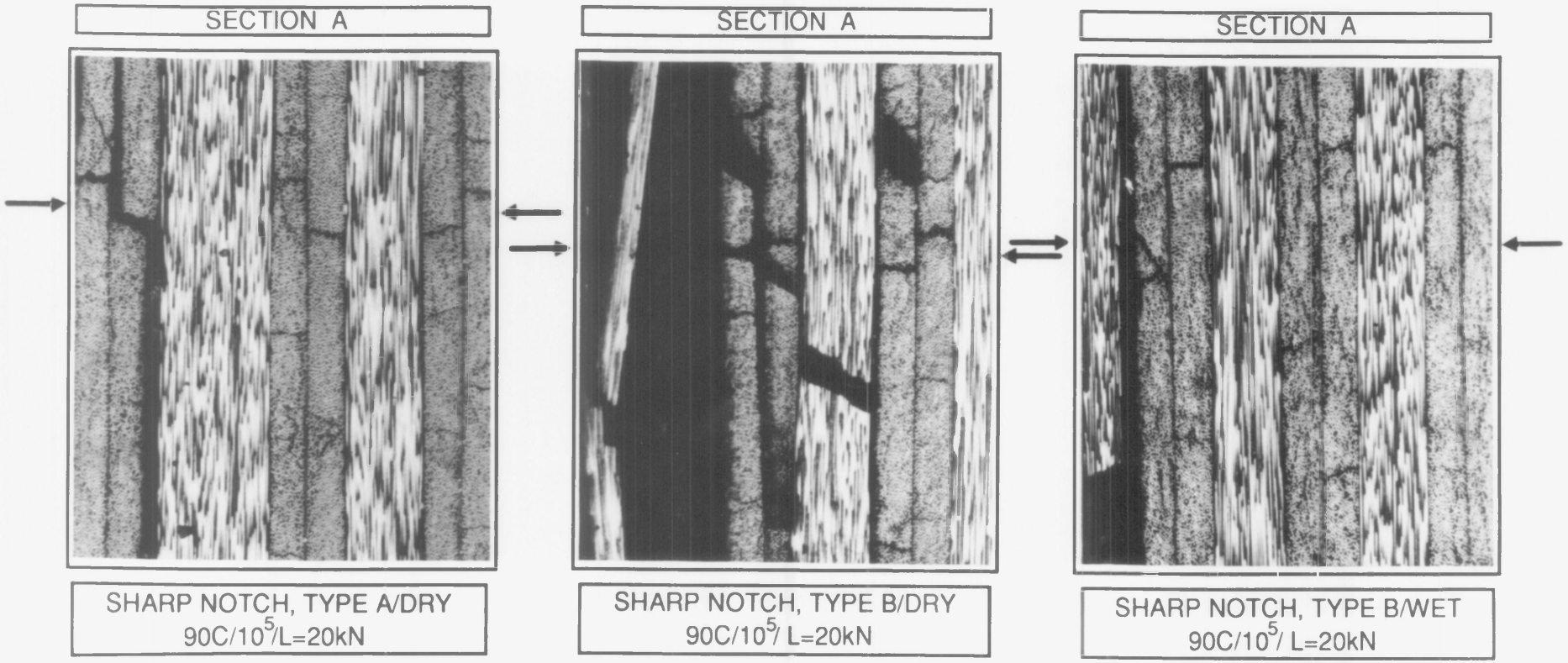


Fig. 4.59: Micrographs of the fatigue damaged region near the sharp notch tip of specimens with stacking sequence A or B: tests were performed in tension-compression at a load amplitude Ln (=20kN) for 10^5 cycles: the arrows indicate the location of the "notch tip line": the surface plies are located at the left hand side of the micrographs. Note the surface 0° fibre fractures in the B type specimens.

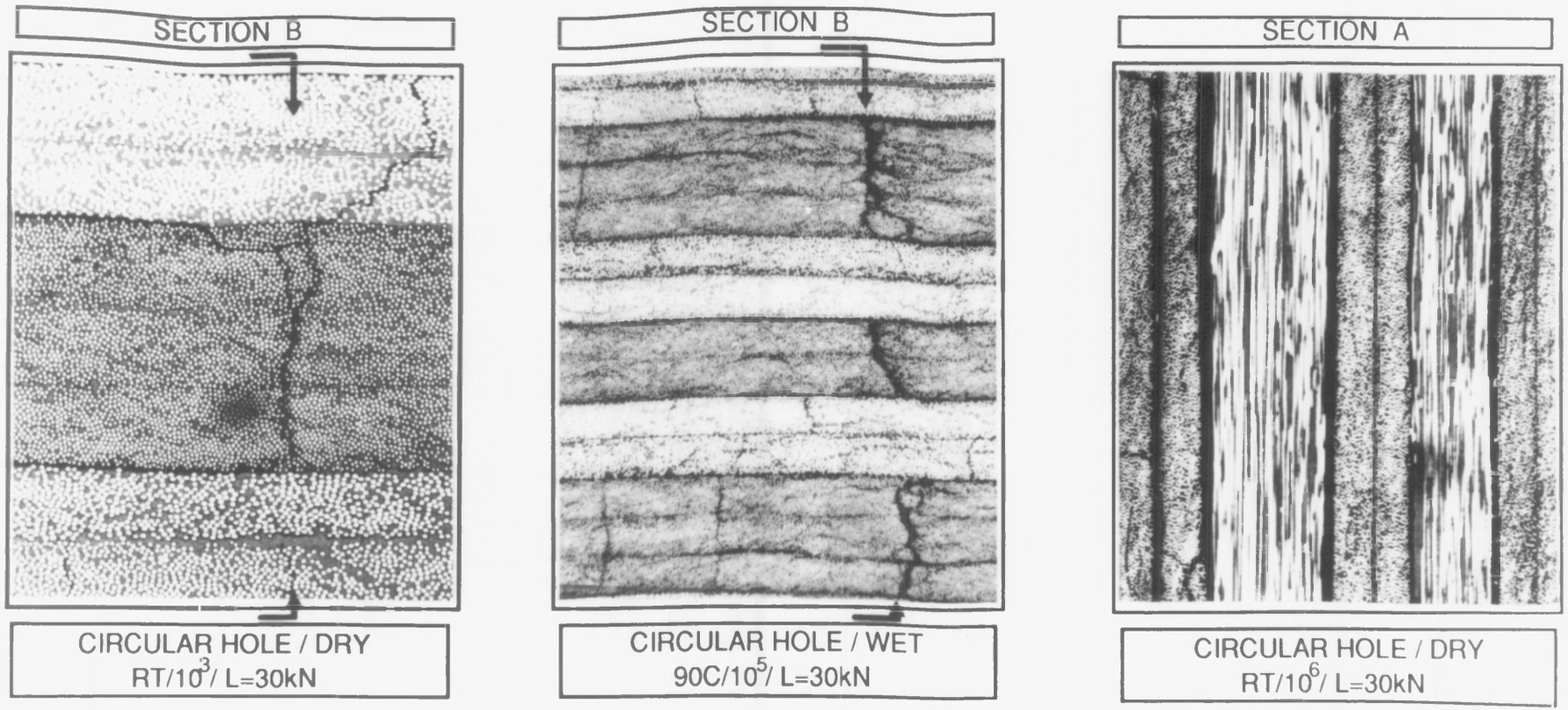


Fig. 4.60: Micrographs of the fatigue damaged region near the circular hole: tests were performed in tension-compression at a load amplitude Lh (=30kN): the arrows indicate the location of the "hole tip line": in the case of section A (third micrograph) the surface plies are located at the left hand side of the micrograph: in the case of sections B the surface plies are located at the top of the micrographs.

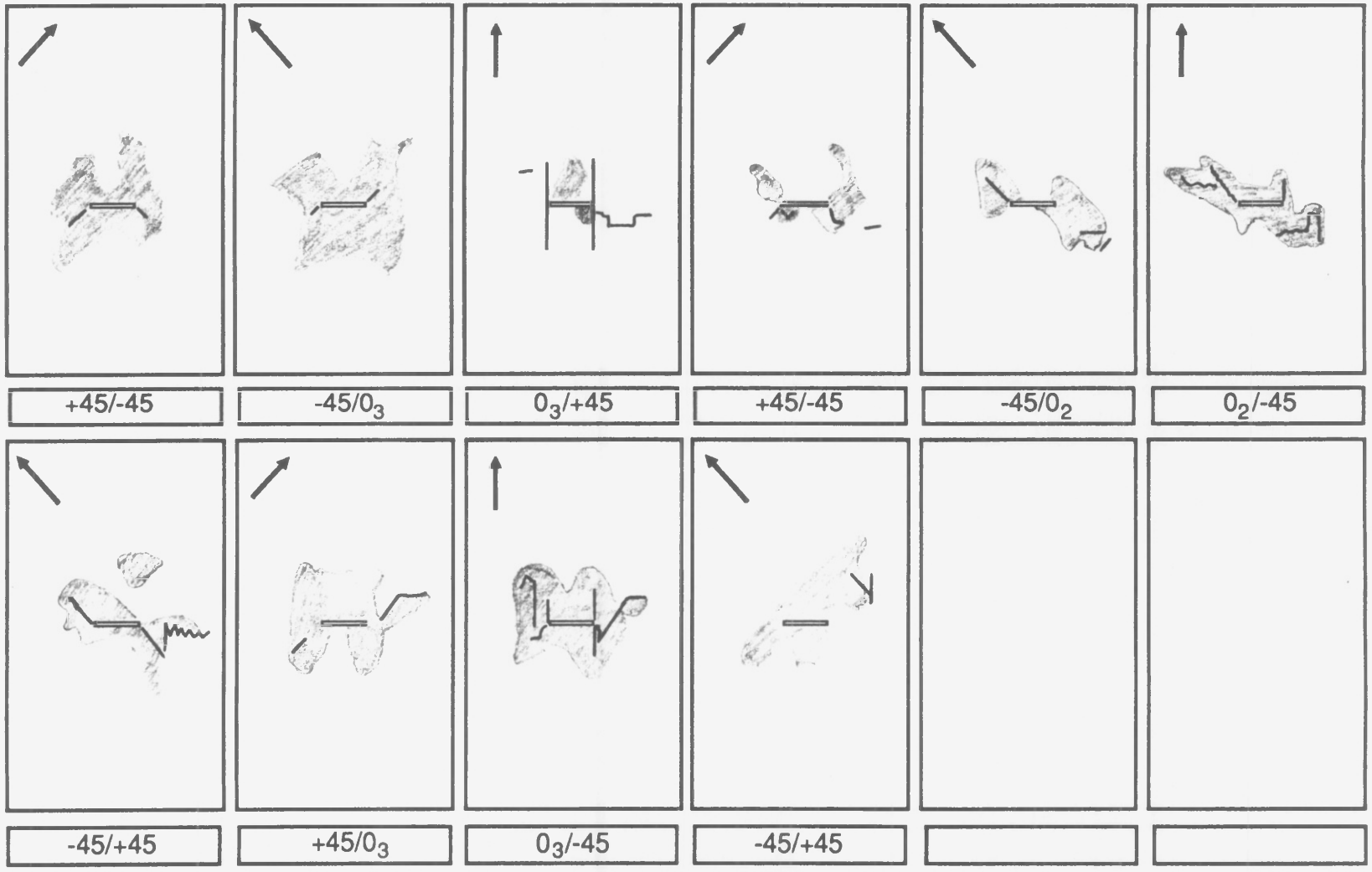


Fig. 4.61: Through-thickness damage development as seen by the deply technique for a dry specimen of stacking sequence A (sharp notch): the specimen was fatigue tested in tension-compression at RT at a load amplitude slightly higher than Ln (=21kN) for $2x10^6$ cycles.

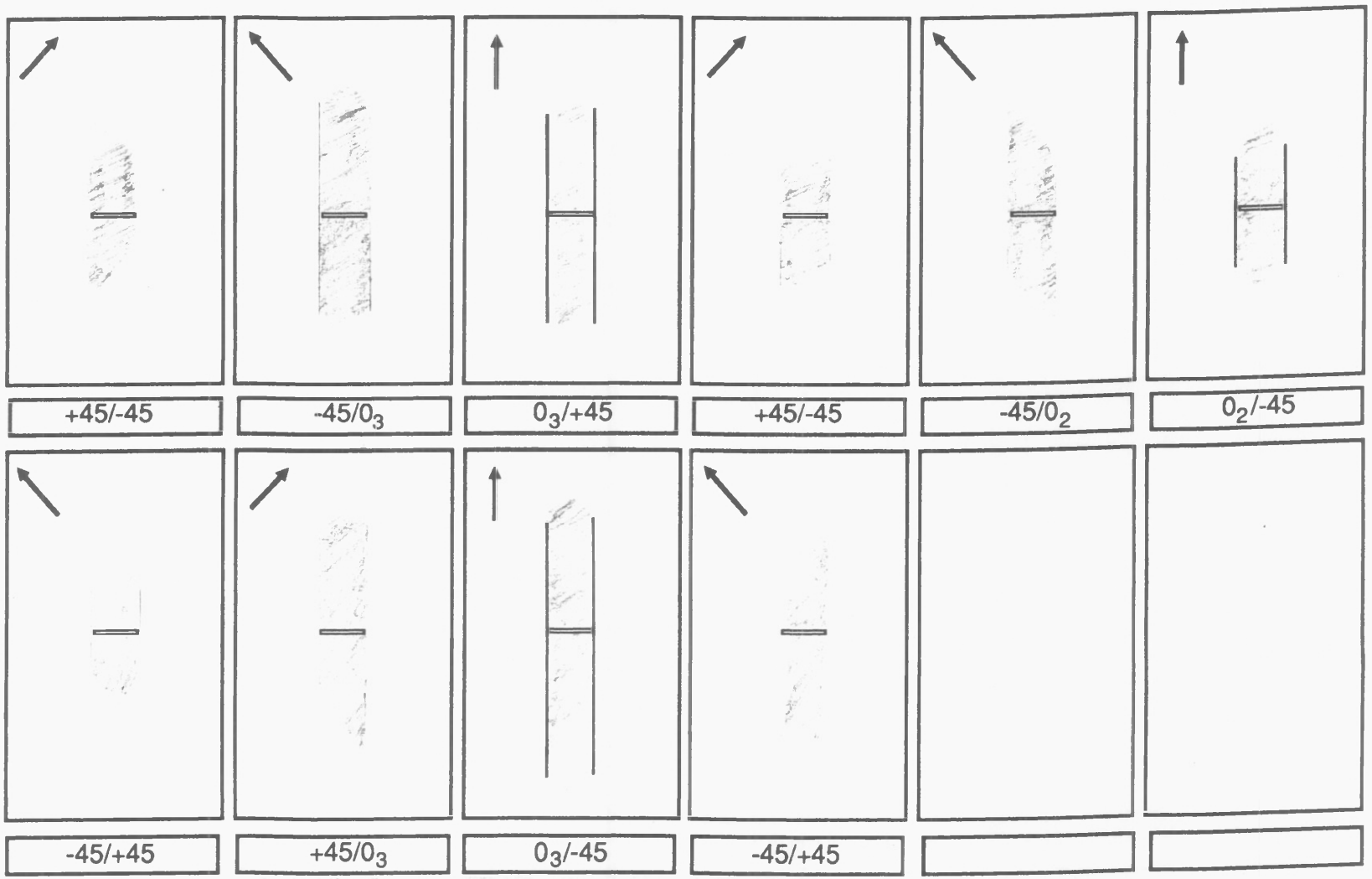


Fig. 4.62: Through-thickness damage development as seen by the deply technique for a wet specimen of stacking sequence A (sharp notch): the specimen was fatigue tested in tension-compression at 90° C at a load amplitude Ln (=20kN) for 10^6 cycles.

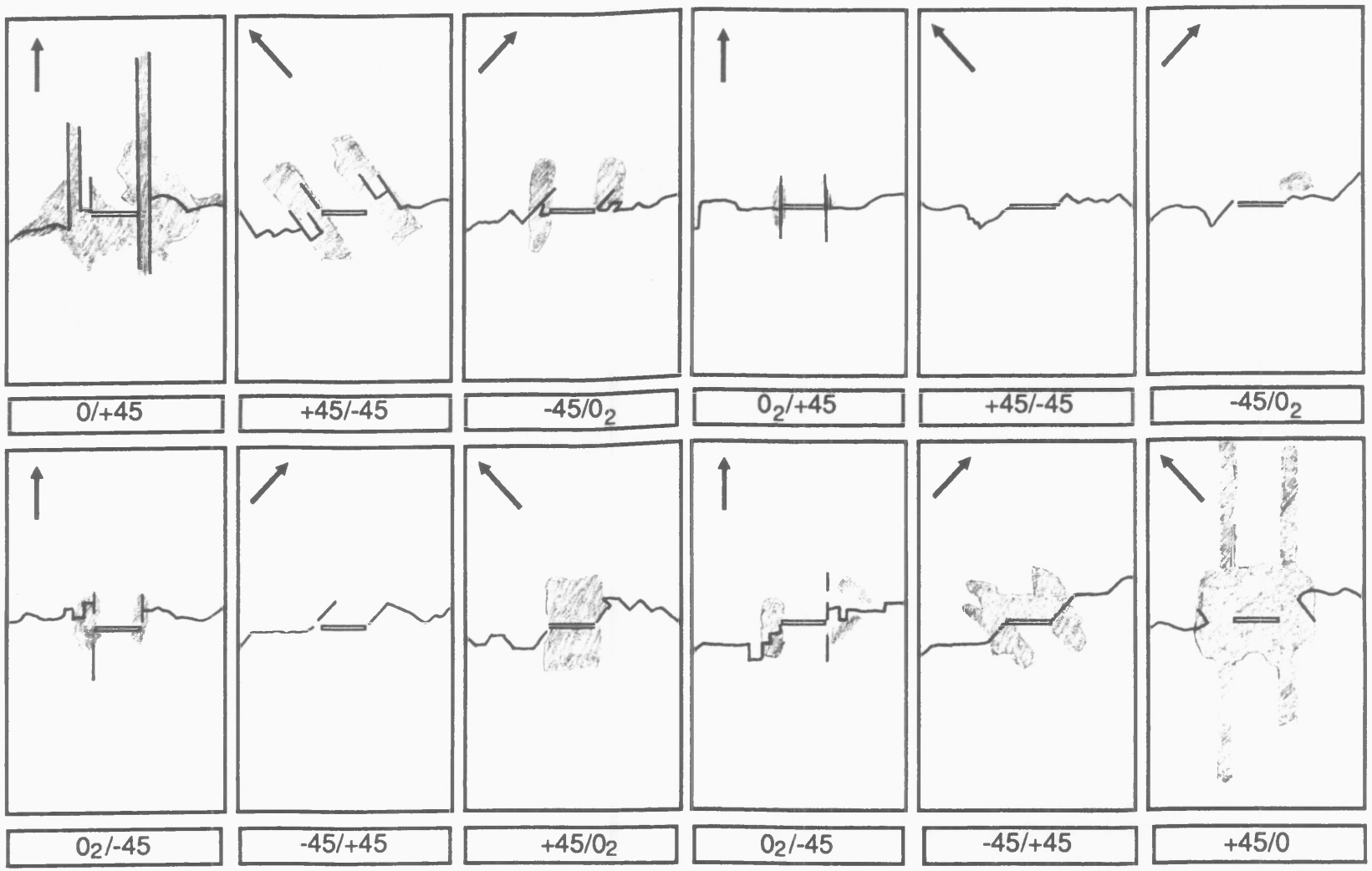


Fig. 4.63: Through-thickness damage development as seen by the deply technique for a wet specimen of stacking sequence B (sharp notch): the specimen was fatigue tested (to failure) in tension-compression at 90° C at a load amplitude Ln (=20kN) for 3.5×10^5 cycles.

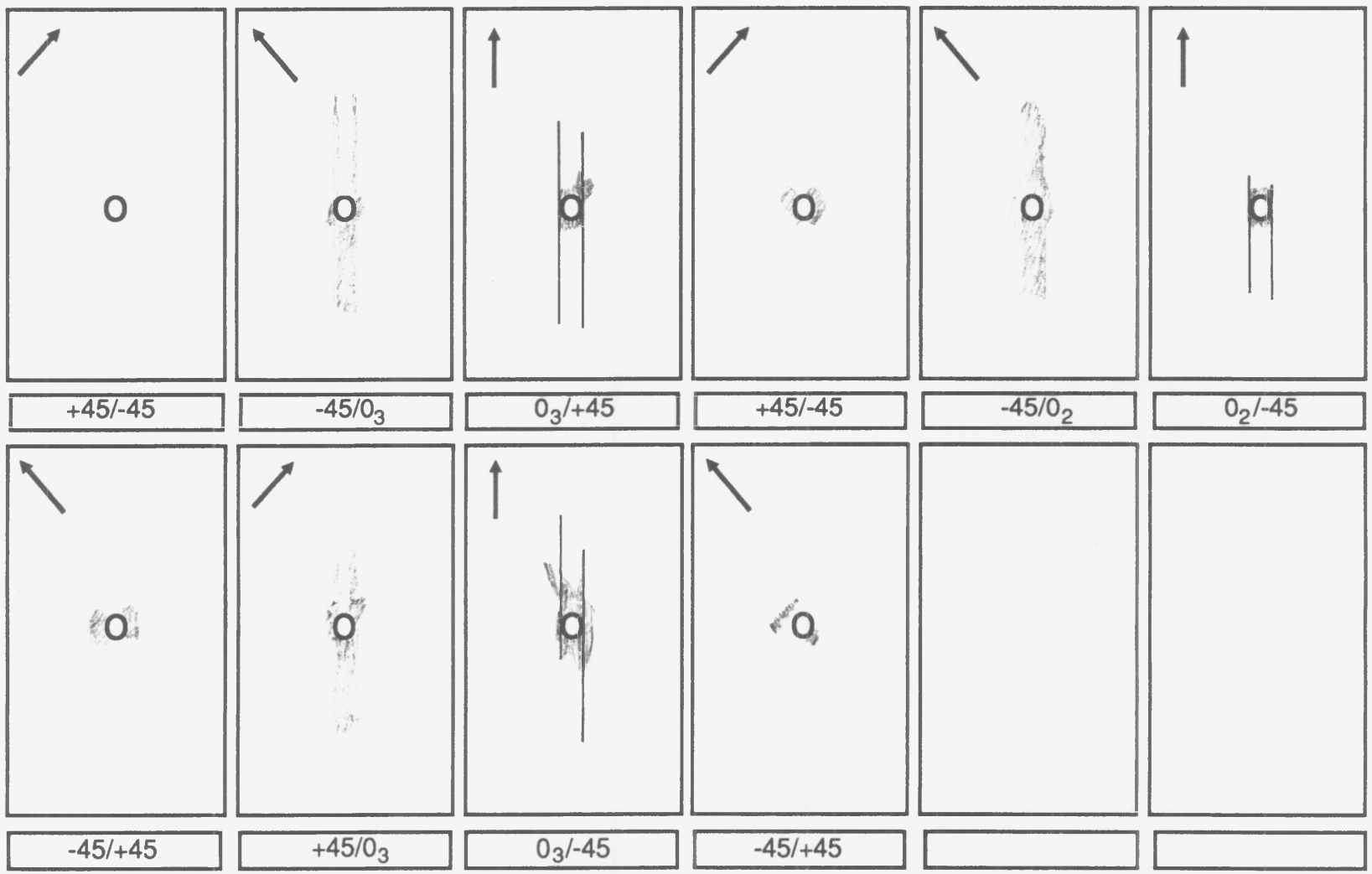


Fig. 4.64: Through-thickness damage development as seen by the deply technique for a dry specimen with circular hole: the specimen was fatigue tested in tension-compression at RT at a load amplitude of 35kN for $4x10^4$ cycles.

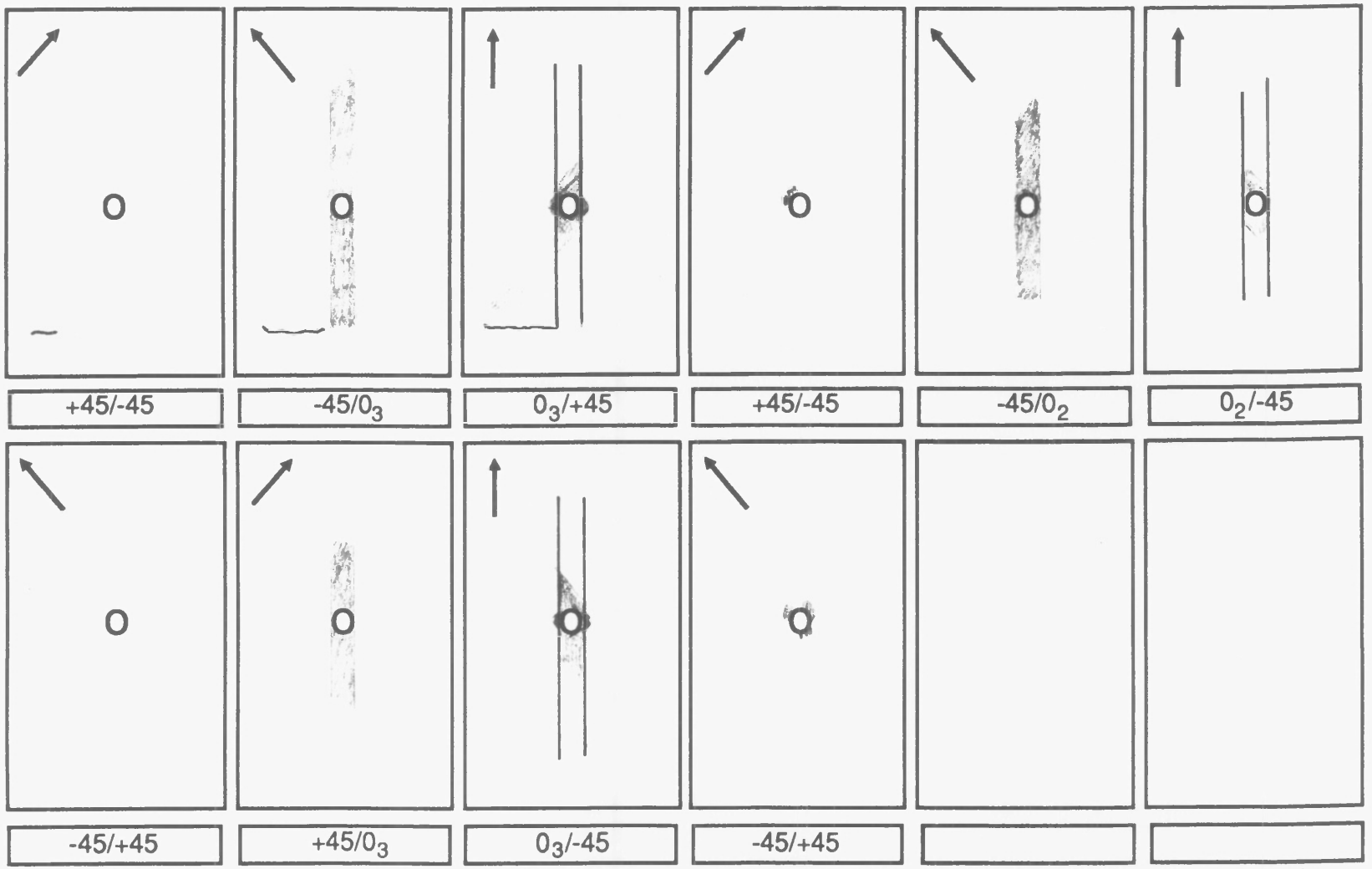


Fig. 4.65: Deply of proof loading induced damage for a wet specimen with circular hole: the specimen was initially fatigue tested at RT at a load amplitude Lh (=30kN) for 10^3 cycles, it was then proof loaded in tension at 130 °C. Note the initiation of final failure in the 0° plies (third box from the top).

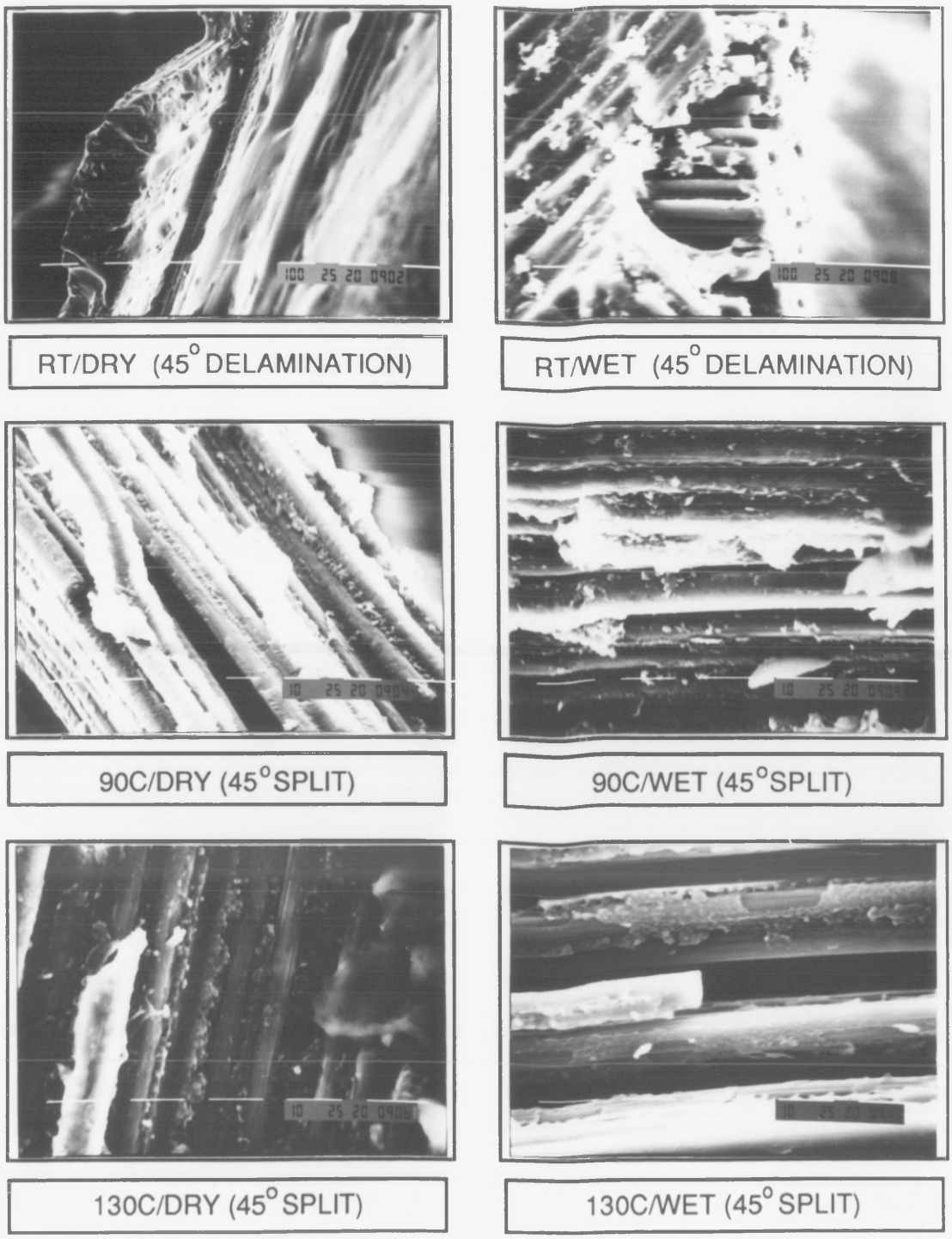


Fig. 4.66: Typical fractographs of delamination or fibre splitting under a range of test temperatures, for both dry and wet (914C) specimens.

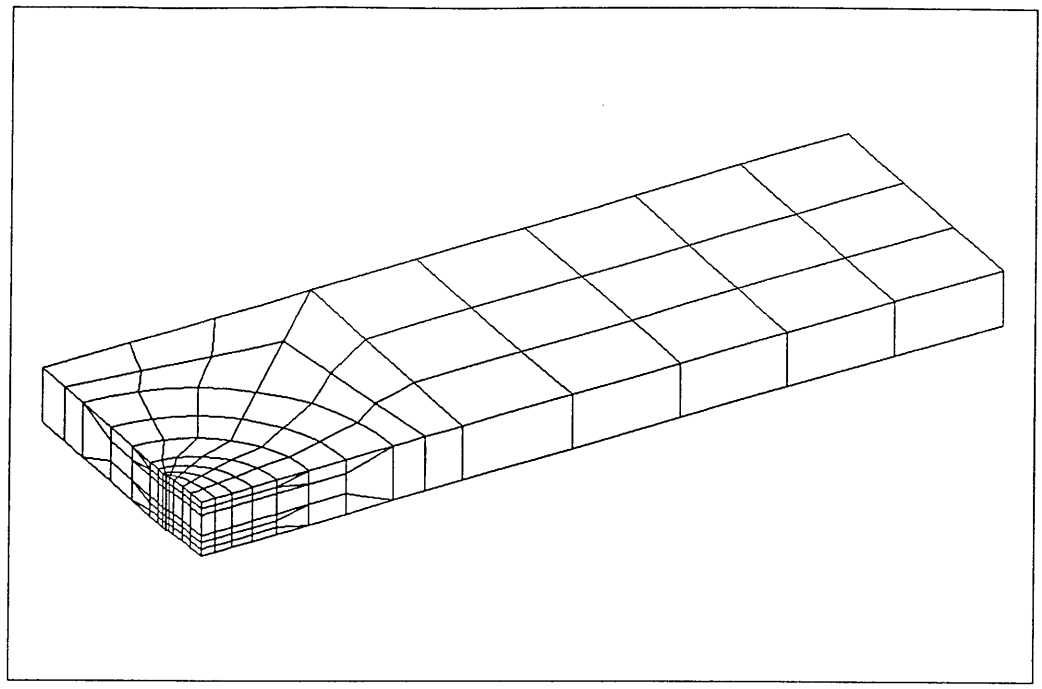


Fig. 4.67: Finite element mesh for the sharp 10mm notch of stacking sequence A; the scale is X=1, Y=1 and Z=5, where Z is the through-thickness direction.

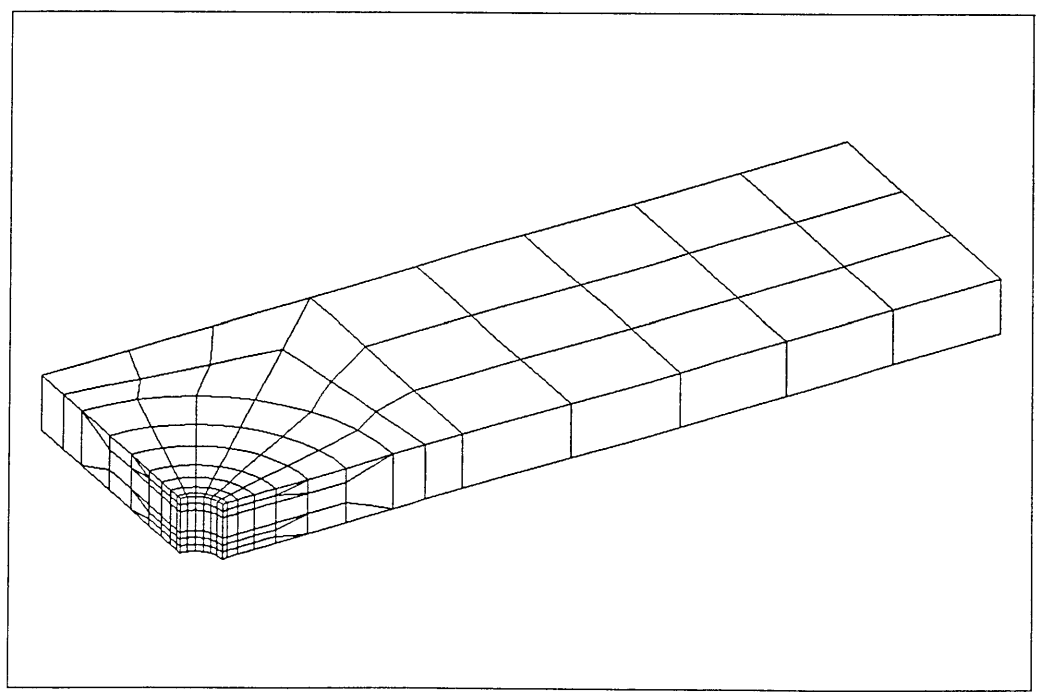
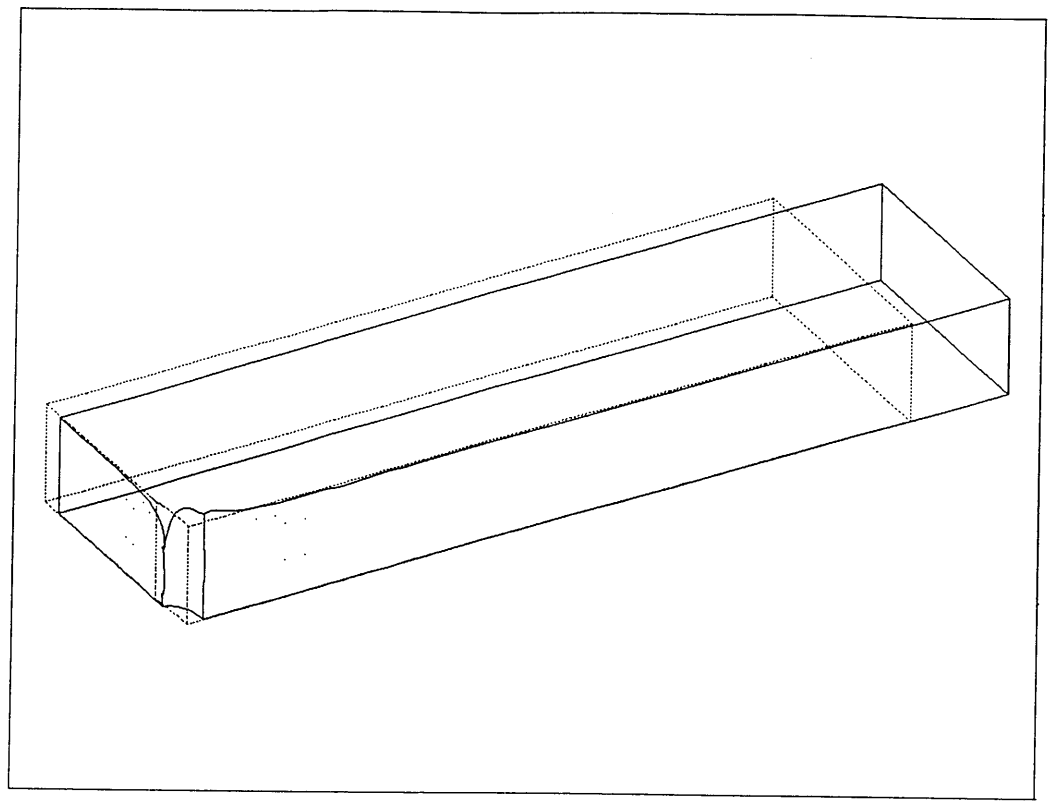


Fig. 4.68: Finite element mesh for the circular 5mm hole (stacking sequence A); the scale is X=1, Y=1 and Z=5, where Z is the through-thickness direction.



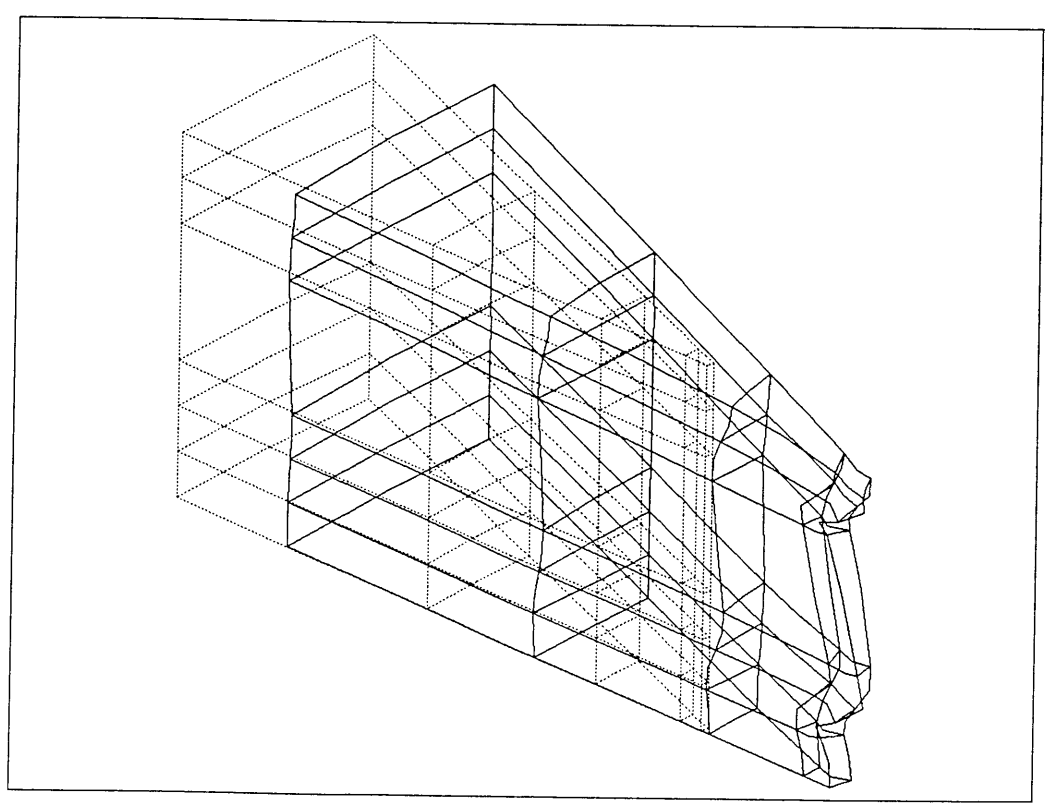
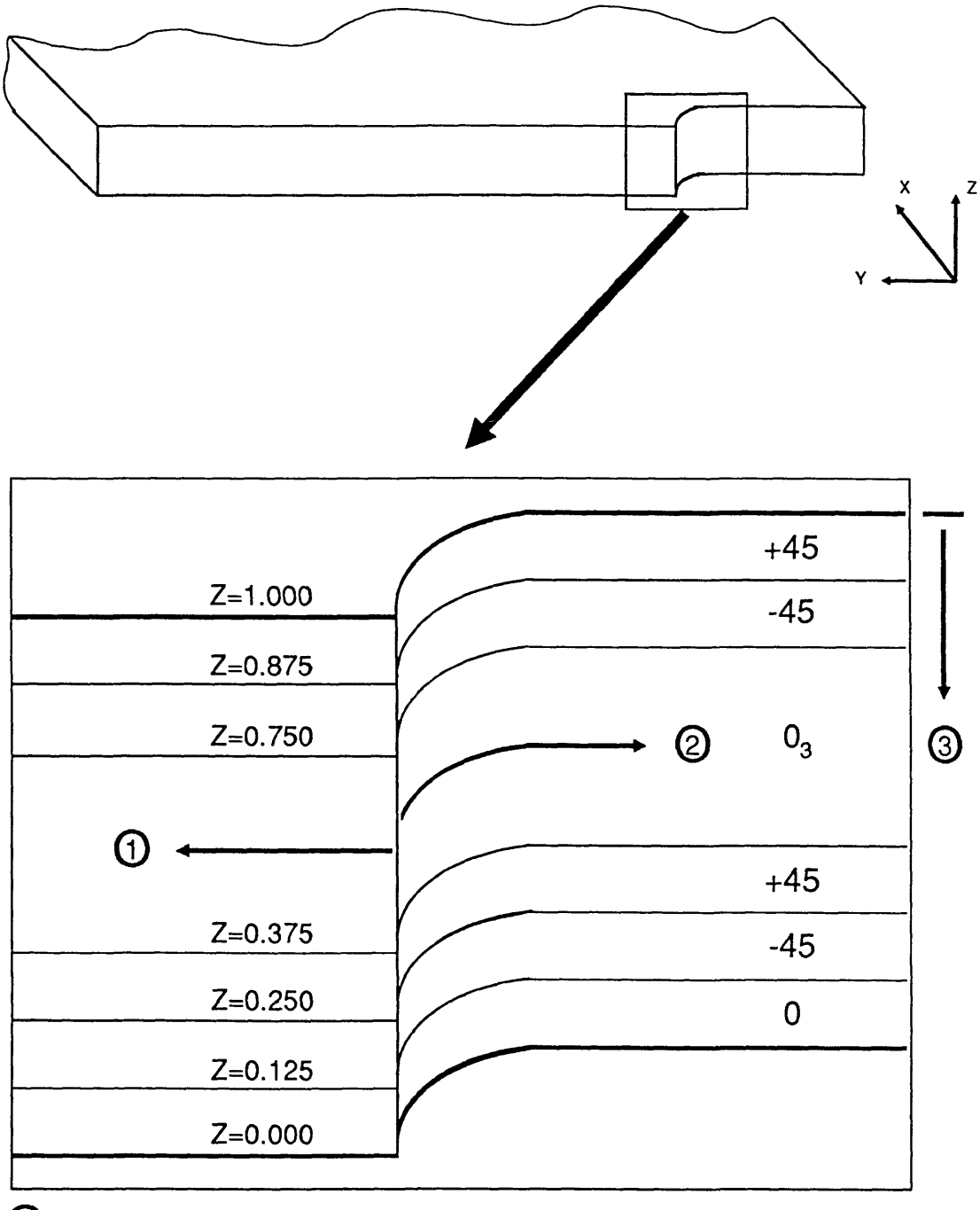


Fig. 4.69: Above, is the deformed shape of the loaded (sharp notched) specimen; the plot scale is X=1, Y=1 and Z=10, where Z is the through-thickness direction; the deformation scale is 10 times. Below, is a close-up view of the notch tip deformation.



① Plot direction (along Y)

② Plot direction (along notch interior)

③ Plot direction (along the thickness)

Fig. 4.70: A schematic representation of the sharp notch tip area of the Finite element model showing the stacking sequence and the through-thickness co-ordinate of each ply interface. The plot directions for the figures to be presented below are also indicated.

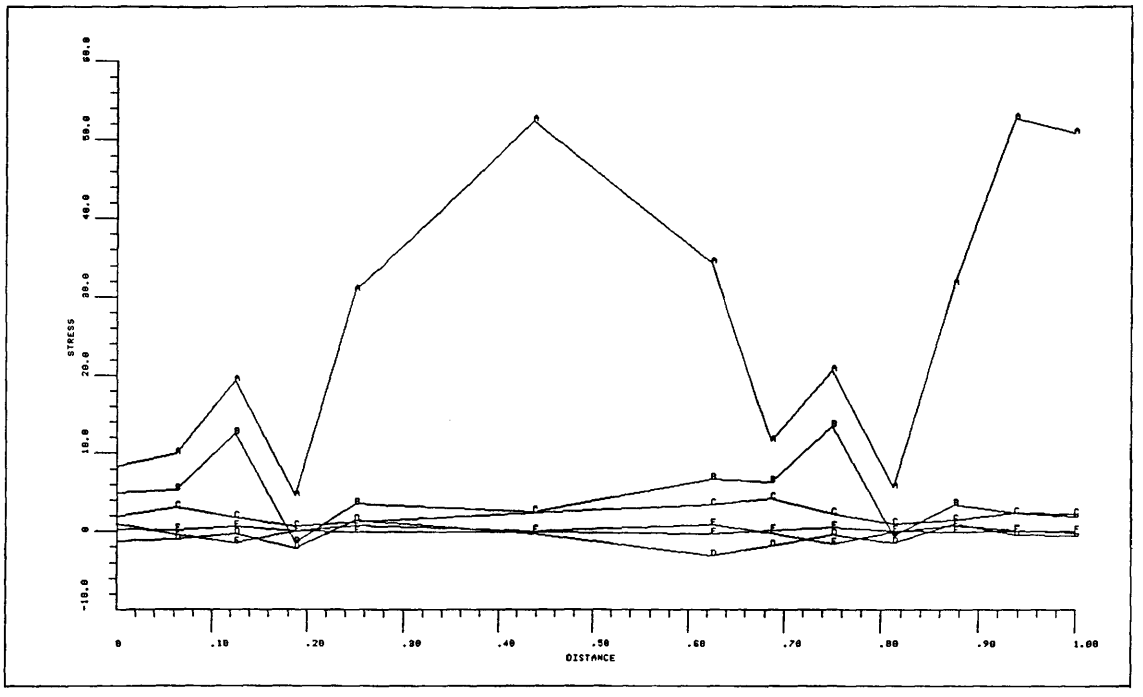


Fig. 4.71: Plots of the through-thickness stress distribution at the tip of the sharp notch (X=0.00, Y=5.00). The direct stresses along the directions X, Y and Z are indicated by the letters A, B and C respectively; the shear stresses in the planes XY, YZ and XZ are indicated by the letters D, E and F respectively.

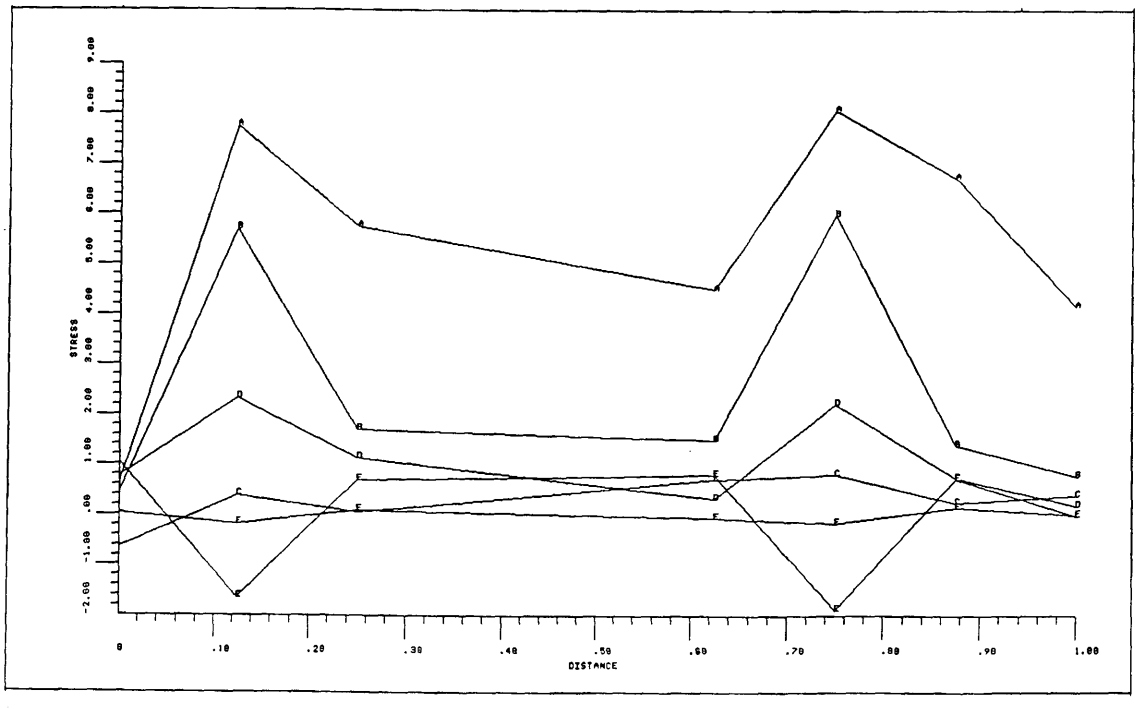


Fig. 4.72: Plots of the through-thickness stress distribution near the tip of the sharp notch at the point X=0.00, Y=5.05. The direct stresses along the directions X, Y and Z are indicated by the letters A, B and C respectively; the shear stresses in the planes XY, YZ and XZ are indicated by the letters D, E and F respectively.

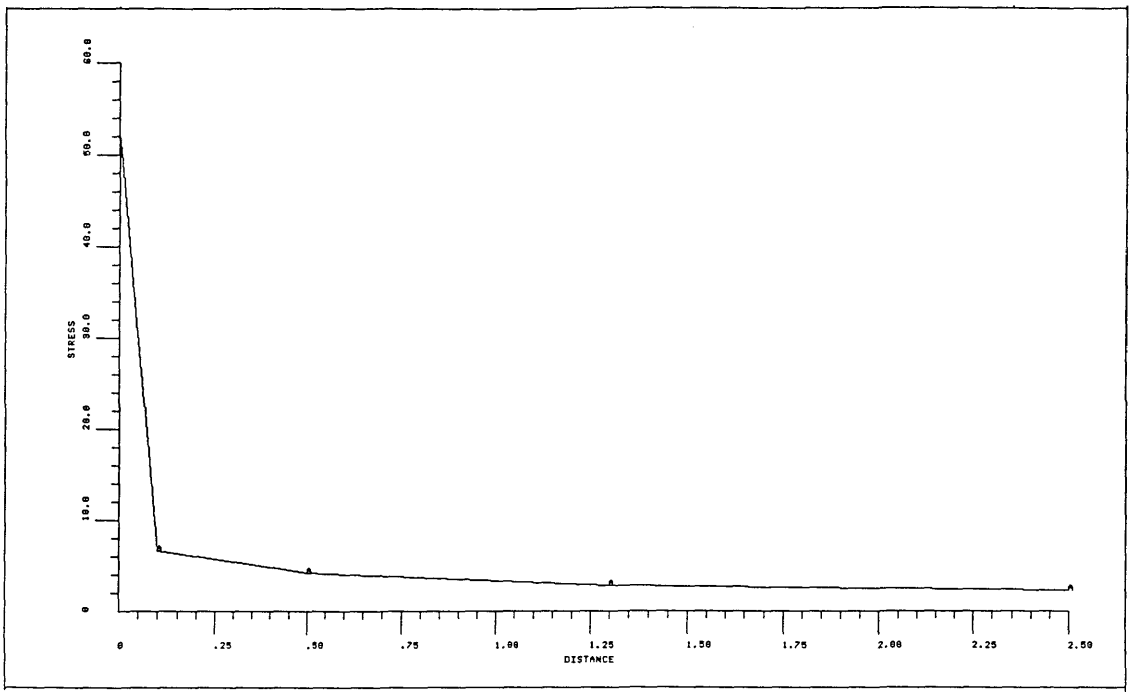


Fig. 4.73: Plot of the direct stress σ_x against the nodal distance (mm) along the Y-direction at Z=0.563 (stack of the three 0° plies), see figure 4.70.

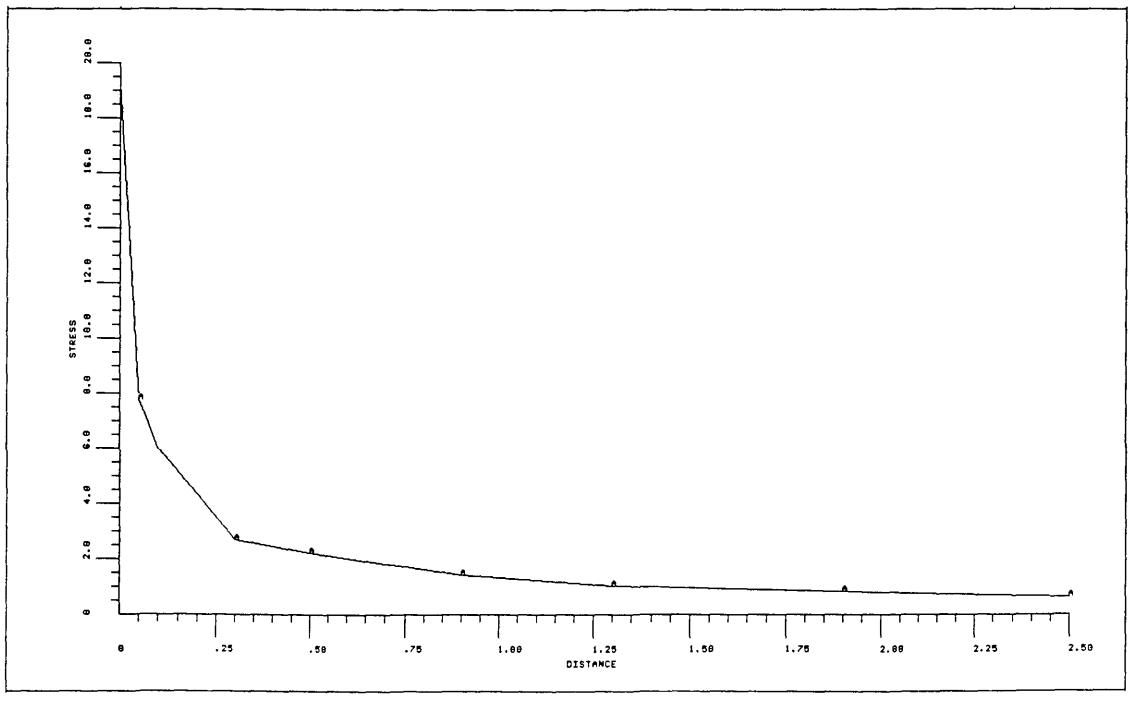


Fig. 4.74: Plot of the direct stress σ_x against the nodal distance (mm) along the Y-direction at Z=0.875 (interface between the surface ±45° plies), see figure 4.70.

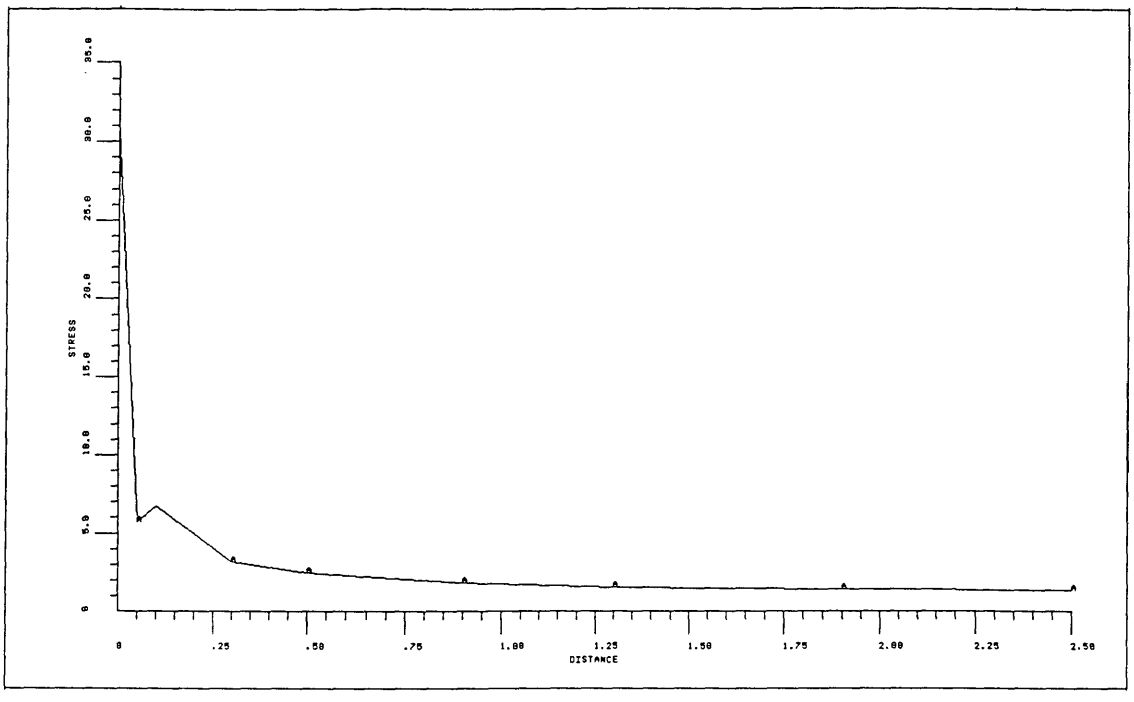


Fig. 4.75: Plot of the direct stress σ_x against the nodal distance (mm) along the Y-direction at Z=0.750 (interface between the outermost ±45° and 0°plies), see figure 4.70.

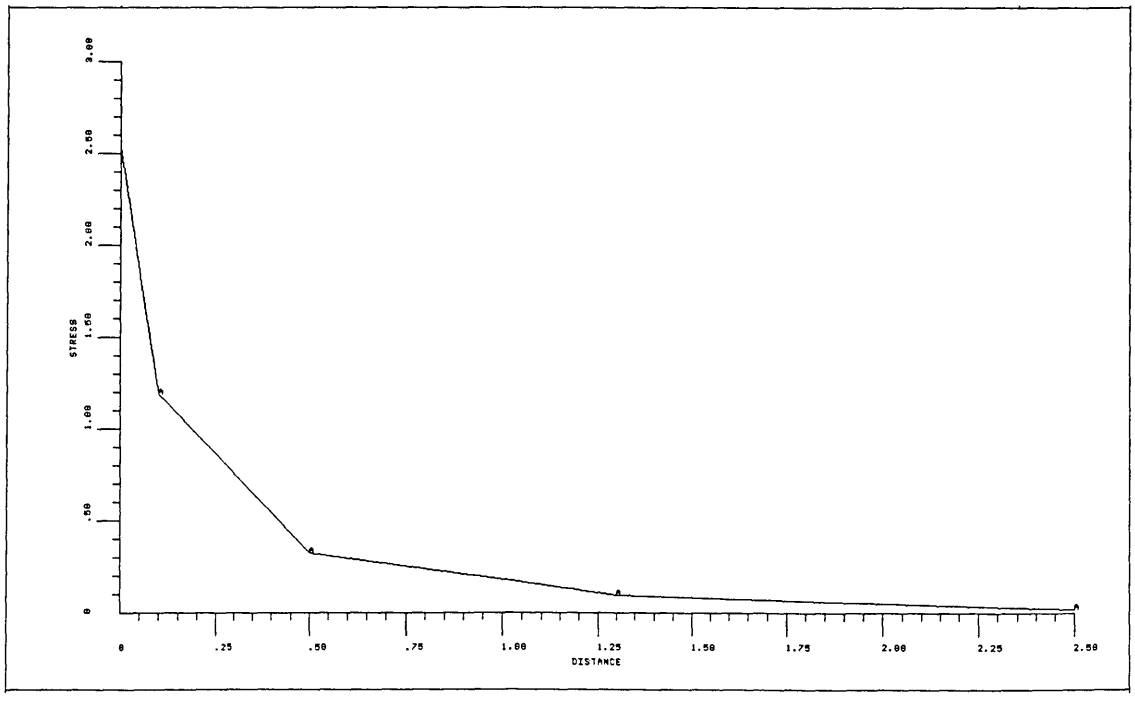


Fig. 4.76: Plot of the direct stress σ_y against the nodal distance (mm) along the Y-direction at Z=0.563 (stack of the three 0° plies), see figure 4.70.

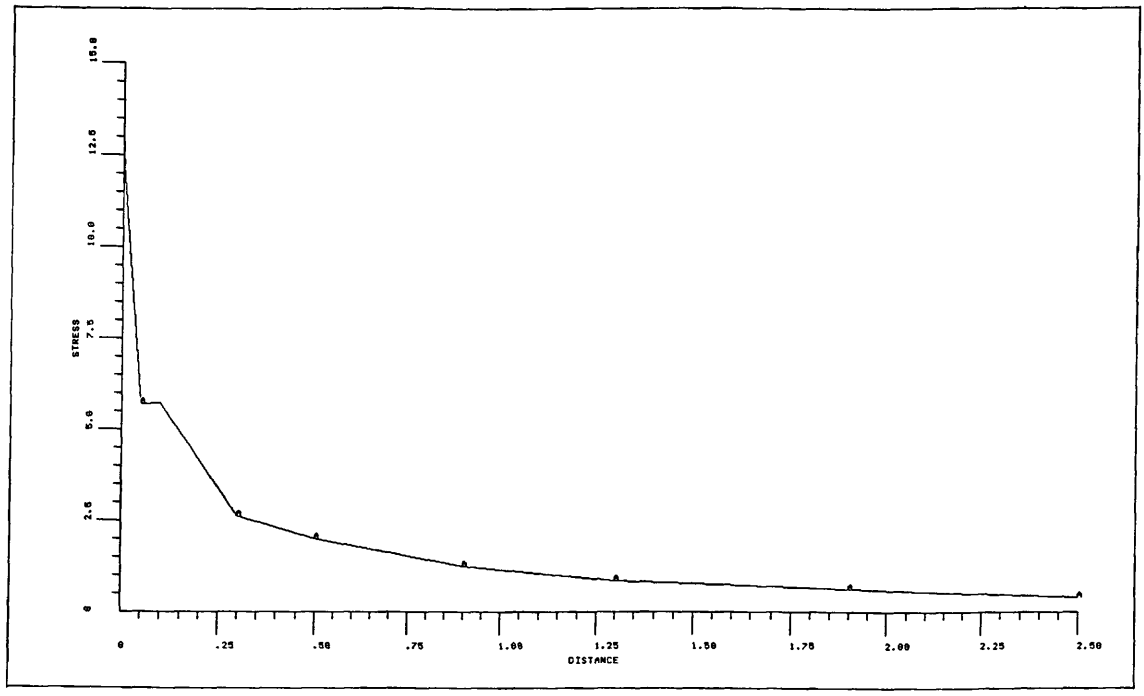


Fig. 4.77: Plot of the direct stress σ_y against the nodal distance (mm) along the Y-direction at Z=0.875 (interface between the surface ±45° plies), see figure 4.70.

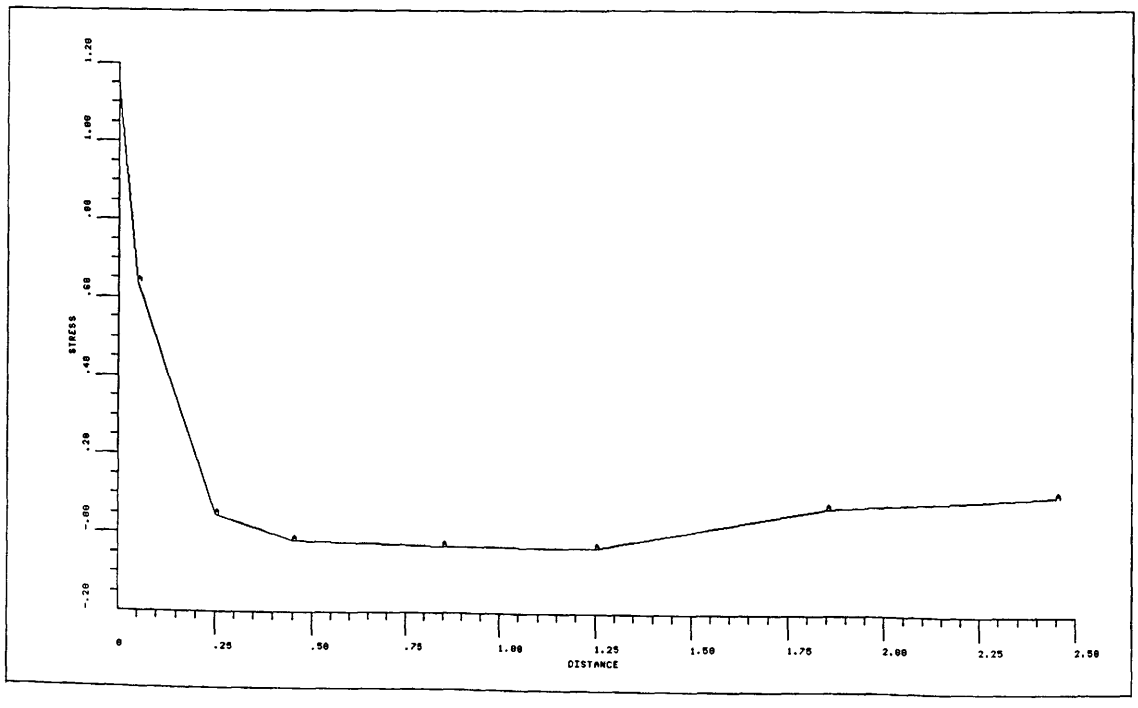


Fig. 4.78: Plot of the shear stress σ_{xy} against the nodal distance (mm) along the Y-direction at Z=0.750 (interface between the outermost ±45° and 0°plies), see figure 4.70.

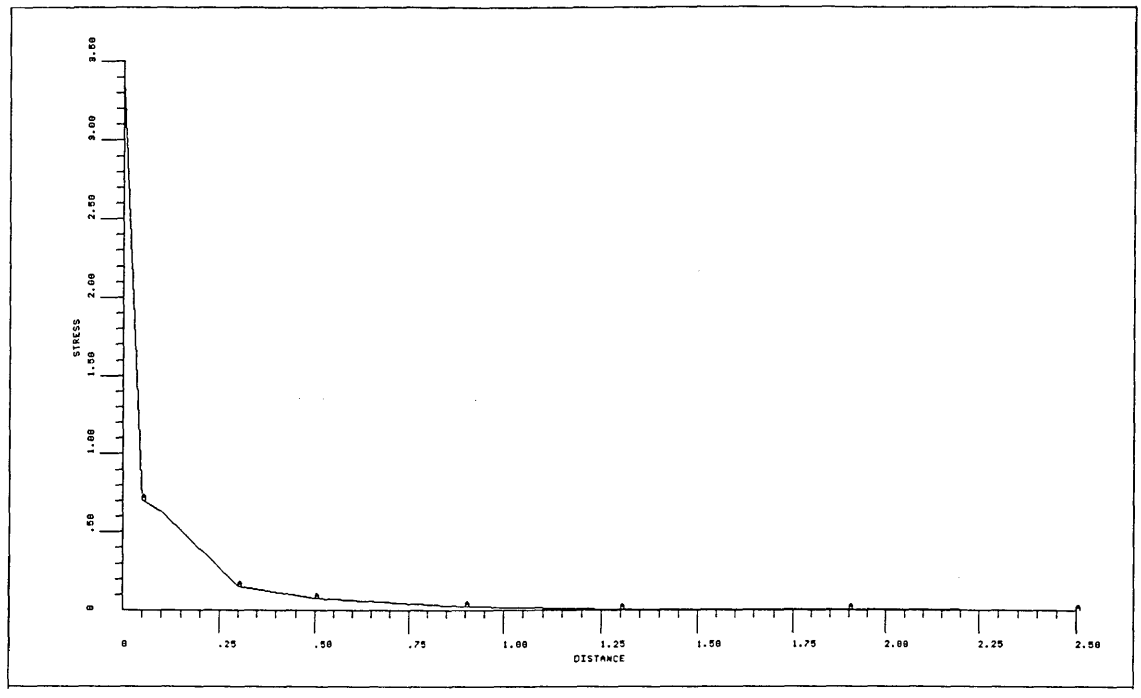


Fig. 4.79: Plot of the direct stress σ_z against the nodal distance (mm) along the Y-direction at Z=0.375 (second interface between the ±45° plies), see figure 4.70.

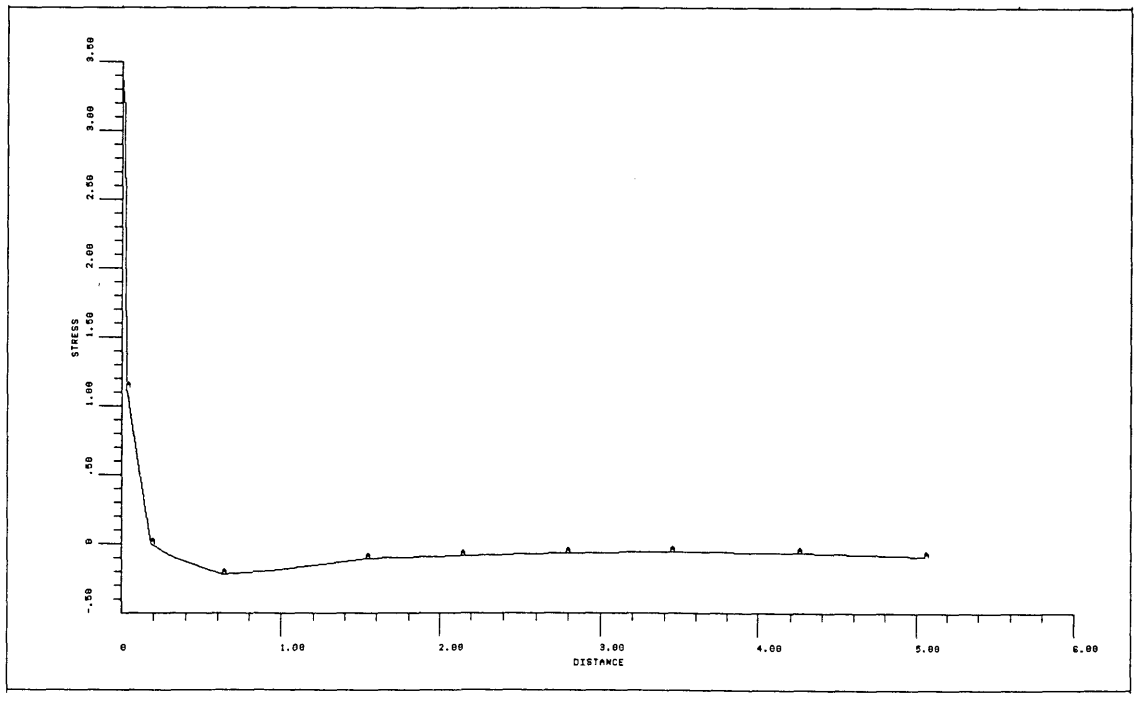
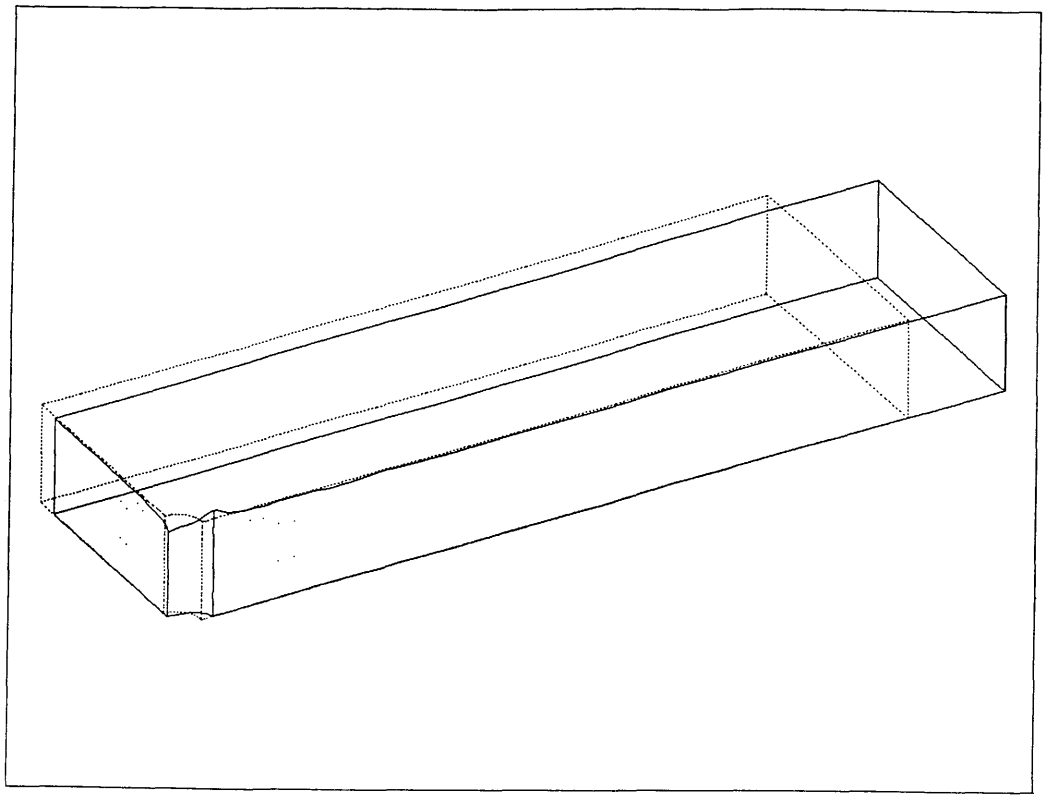


Fig. 4.80: Plot of the direct stress σ_z along the notch interior (plot direction (2)) at Z=0.375 (second interface between the ±45° plies), see figure 4.70.



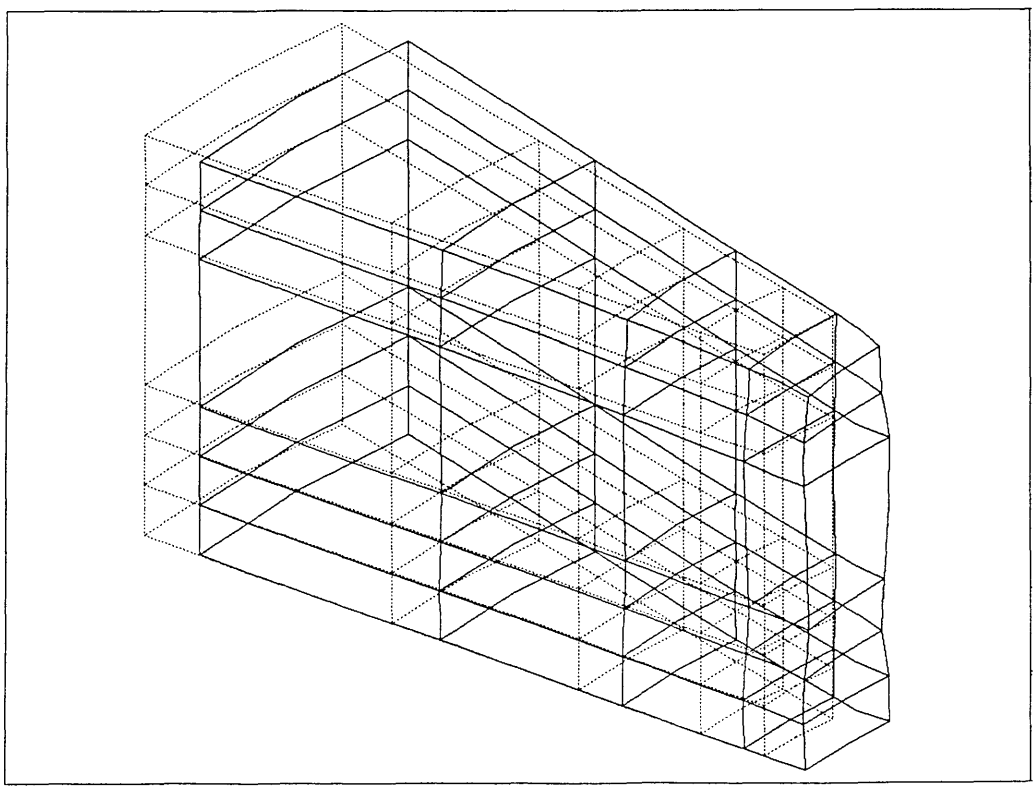


Fig. 4.81: Above, is the deformed shape of the loaded (holed) specimen; the plot scale is X=1, Y=1 and Z=10, where Z is the through-thickness direction; the deformation scale is 10 times. Below, is a close-up view of the "hole tip" deformation.

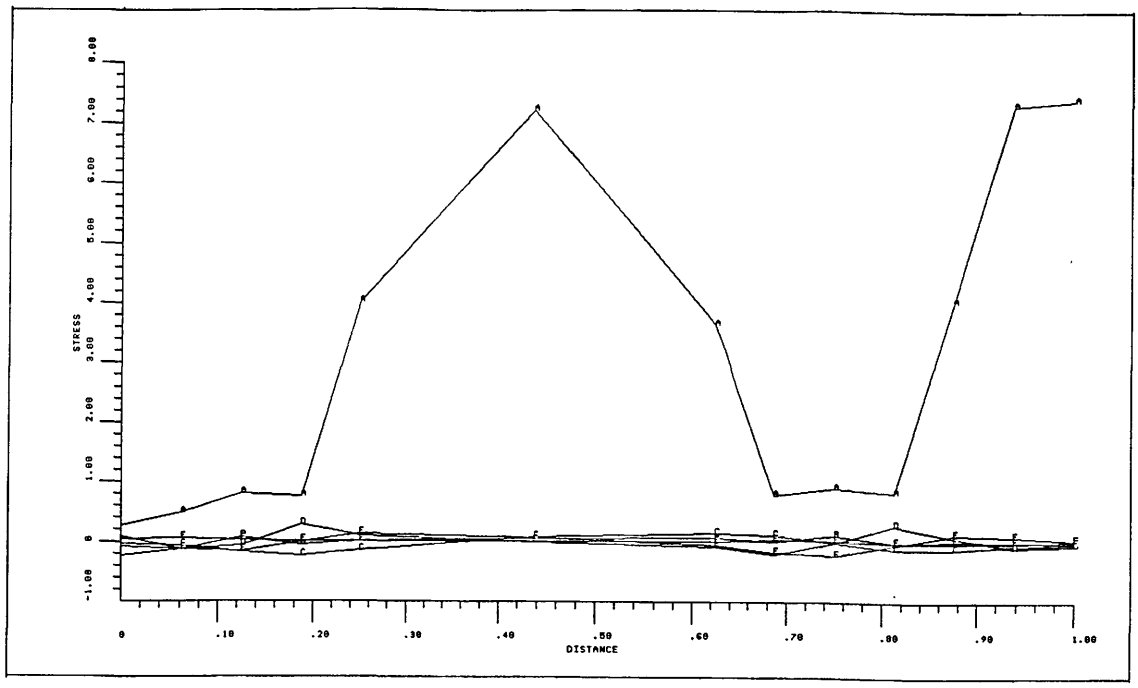


Fig. 4.82: Plots of the through-thickness stress distribution at the "tip" of the circular hole (X=0.00, Y=2.50). The direct stresses along the directions X, Y and Z are indicated by the letters A, B and C respectively; the shear stresses in the planes XY, YZ and XZ are indicated by the letters D, E and F respectively.

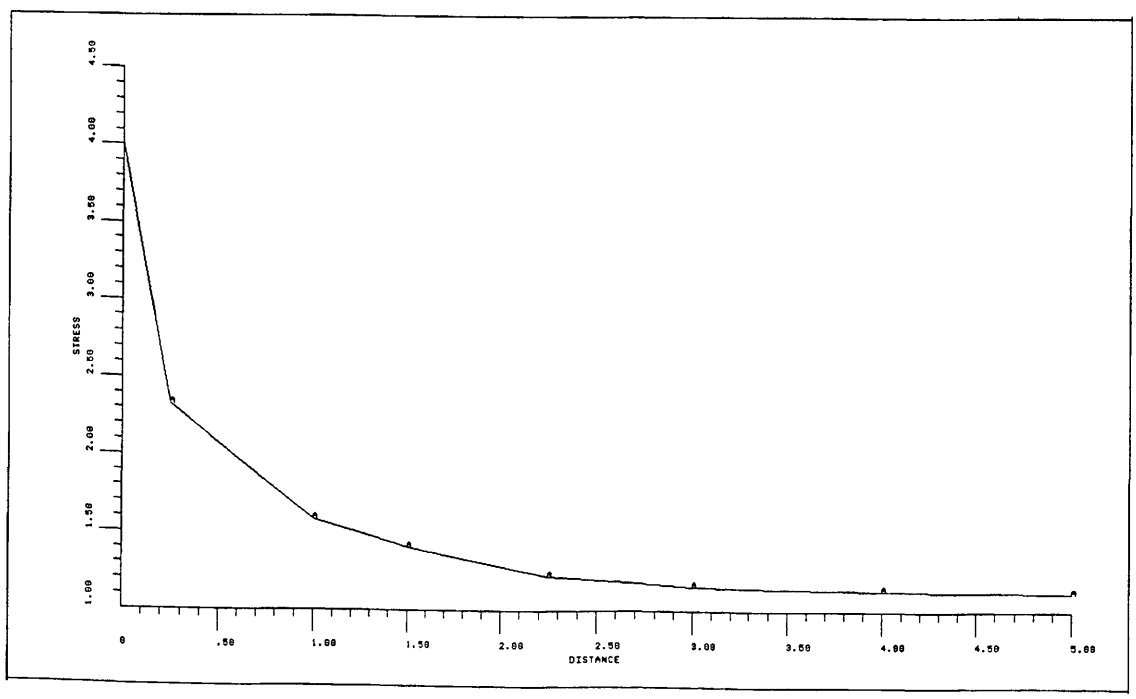


Fig. 4.83: Plot of the direct stress σ_x against the nodal distance (mm) along the Y-direction at Z=0.750 (interface between the outermost ±45° and 0°plies).

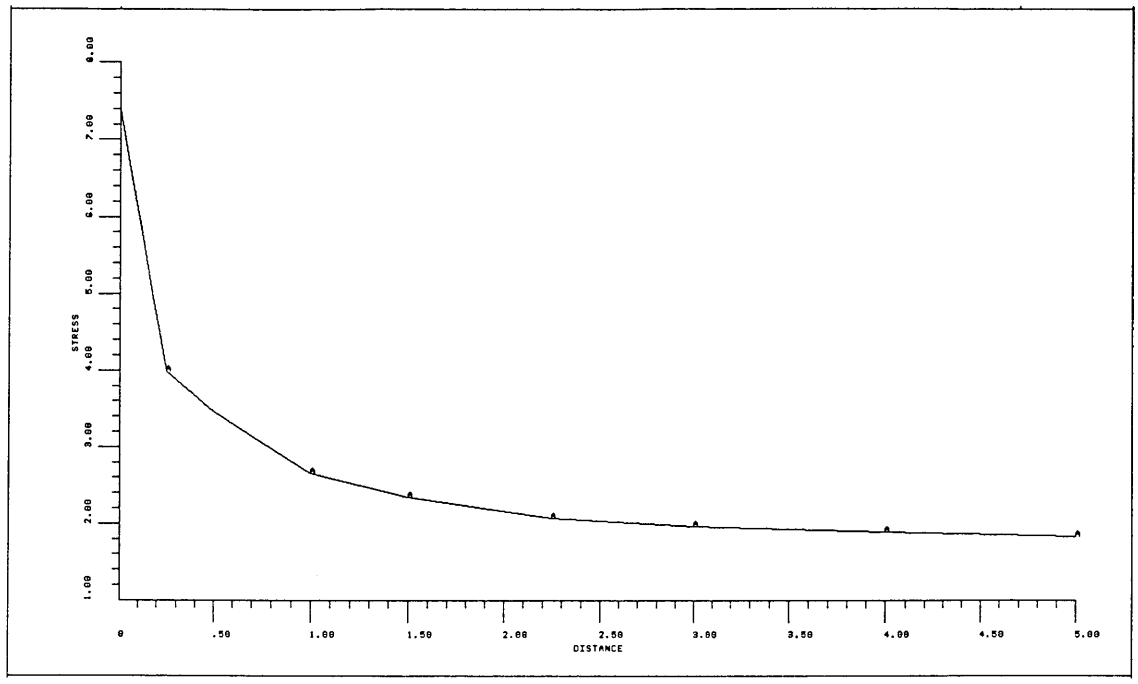


Fig. 4.84: Plot of the direct stress σ_x against the nodal distance (mm) along the Y-direction at Z=0.00 (mid-plane).

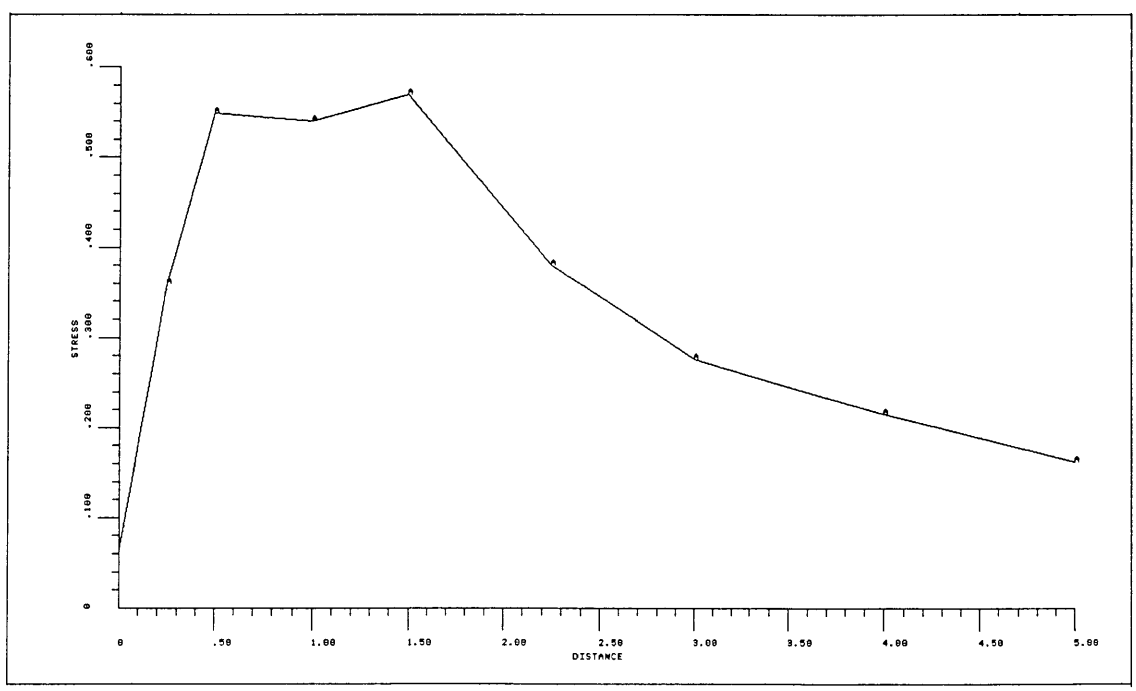


Fig. 4.85: Plot of the direct stress σ_y against the nodal distance (mm) along the Y-direction at Z=0.875 (interface between the surface ±45° plies).

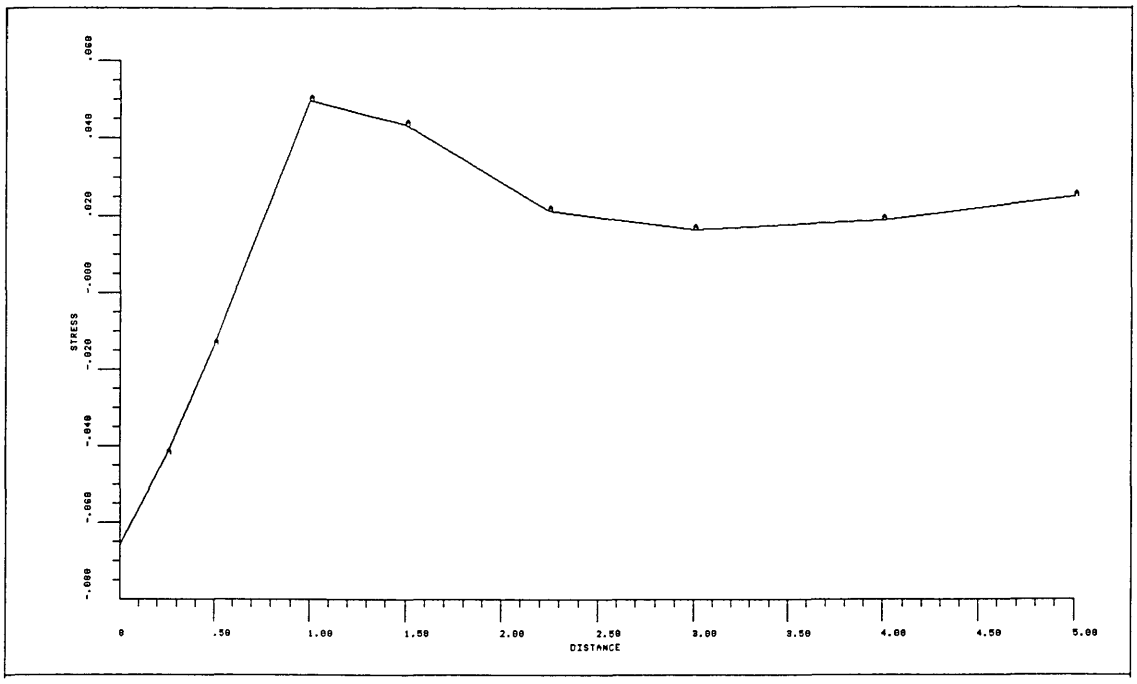


Fig. 4.86: Plot of the shear stress σ_{xy} against the nodal distance (mm) along the Y-direction at Z=0.875 (interface between the surface ±45° plies).

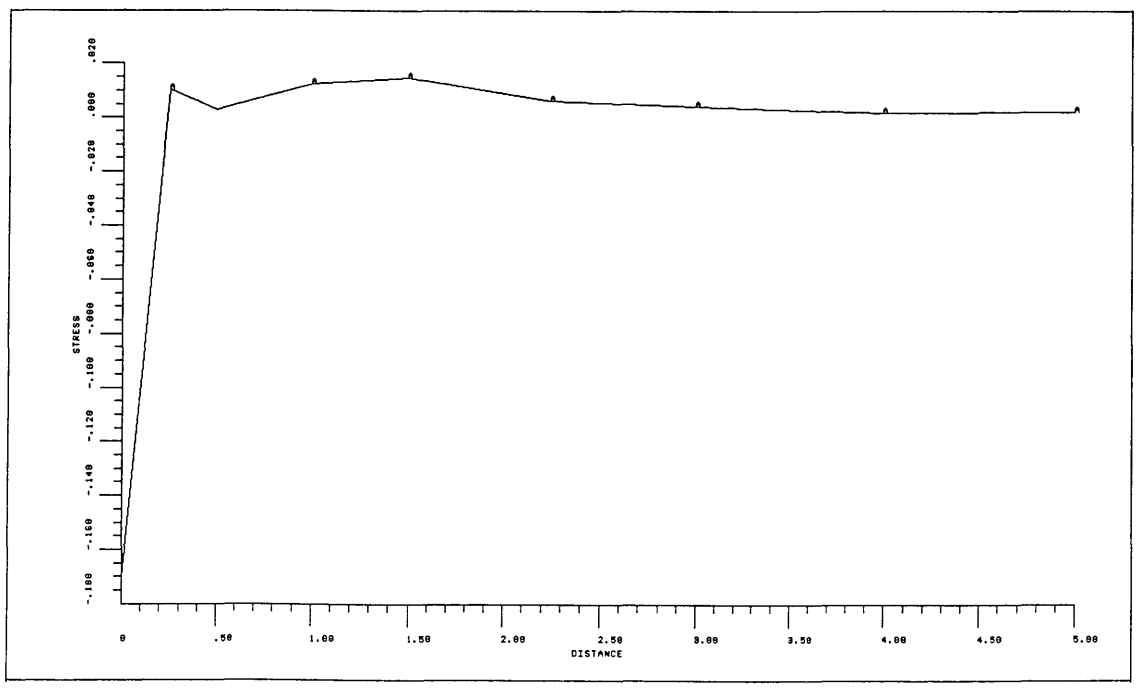


Fig. 4.87: Plot of the direct stress σ_z against the nodal distance (mm) along the Y-direction at Z=0.875 (interface between the surface ±45° plies).

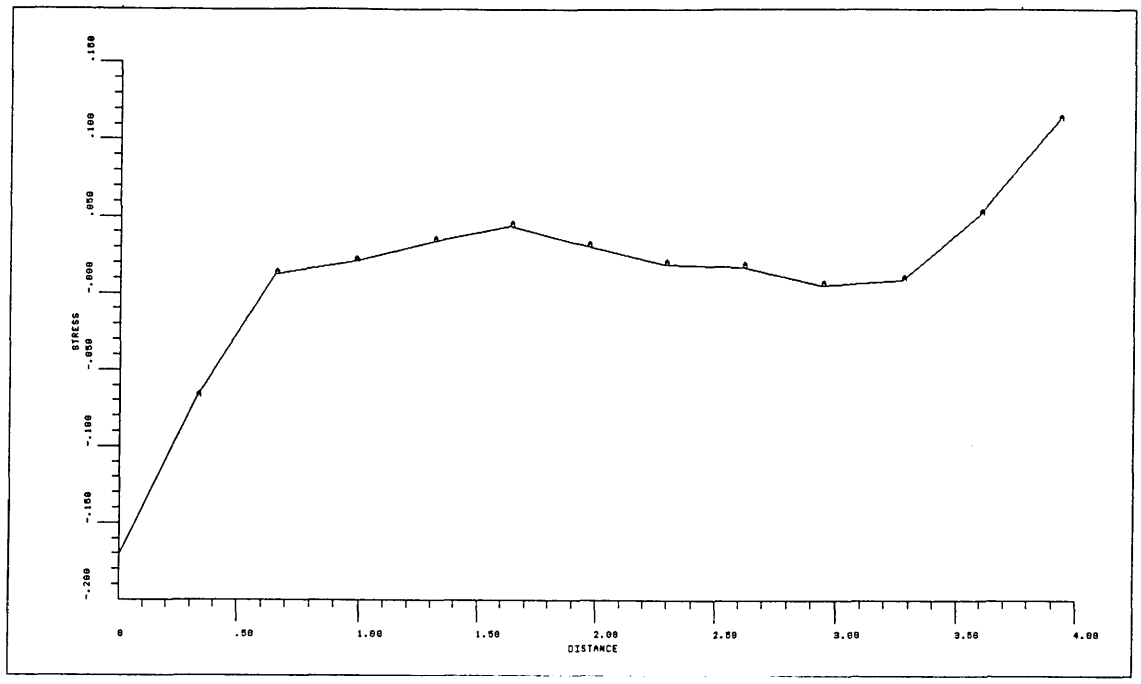


Fig. 4.88: Plot of the direct stress σ_z along the hole's free edge (plot direction (2)) at Z=0.875 (interface between the surface ±45° plies), see figure 4.70 which applies to the circular hole also.

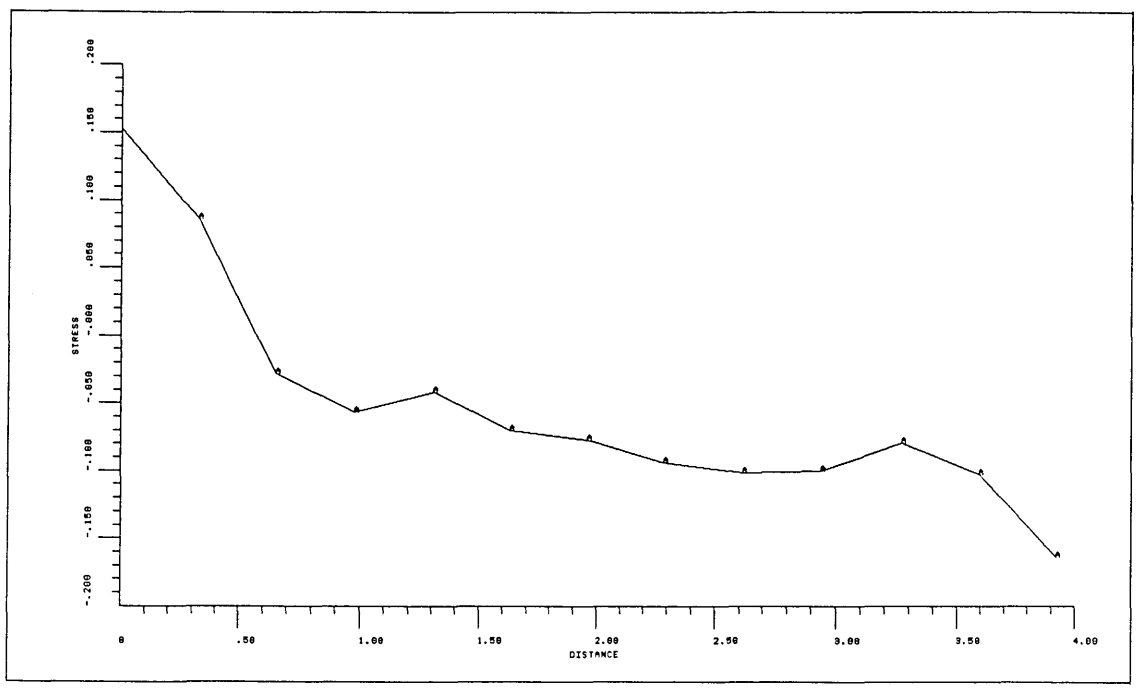


Fig. 4.89: Plot of the direct stress σ_z along the hole's free edge (plot direction (2)) at Z=0.375 (second interface between the ±45° and 0°plies), see figure 4.70 which applies to the circular hole also.

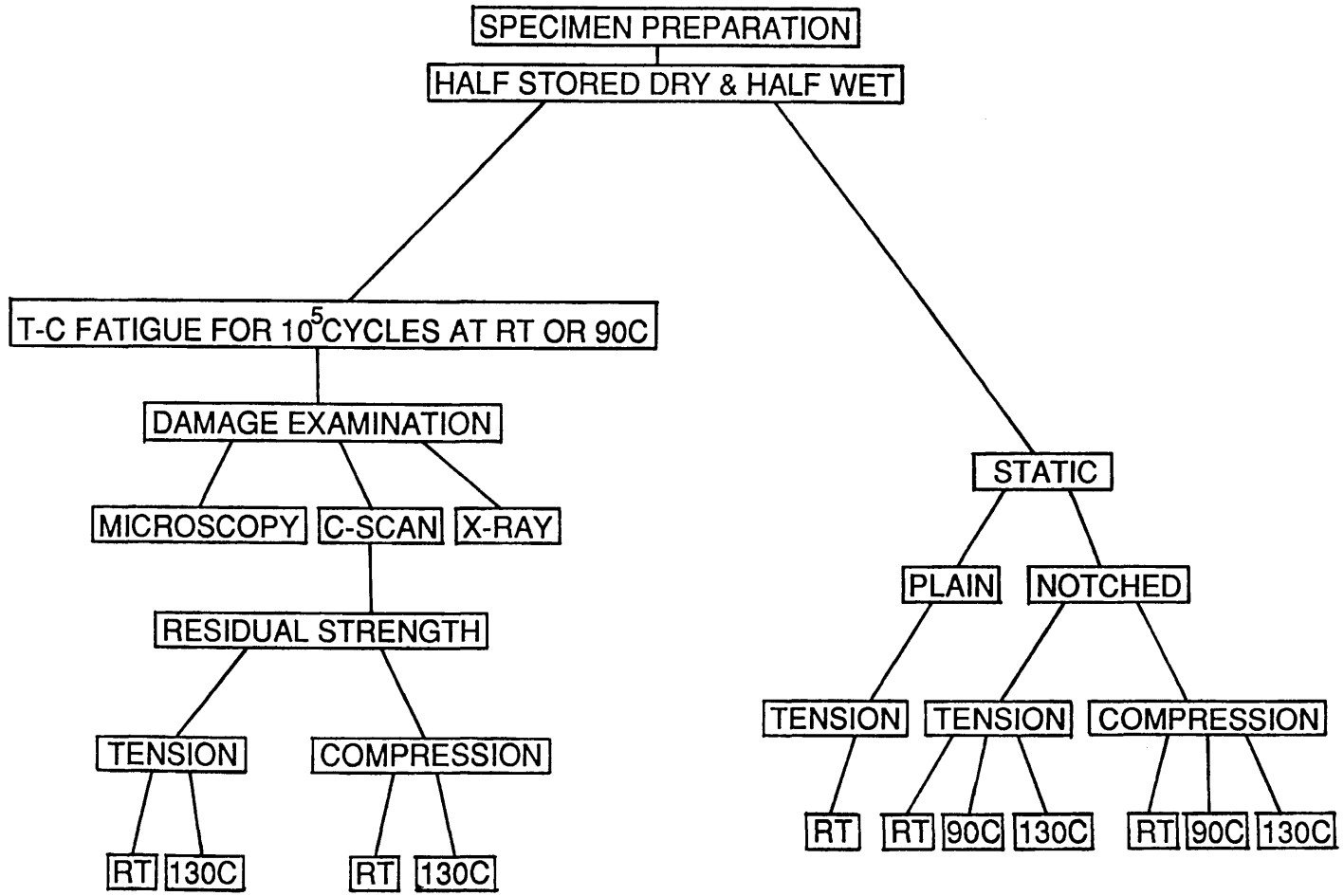


Fig. 5.1: Summary of the experimental programme for **6376C** (stacking sequence A): specimens were notched with sharp notches only.

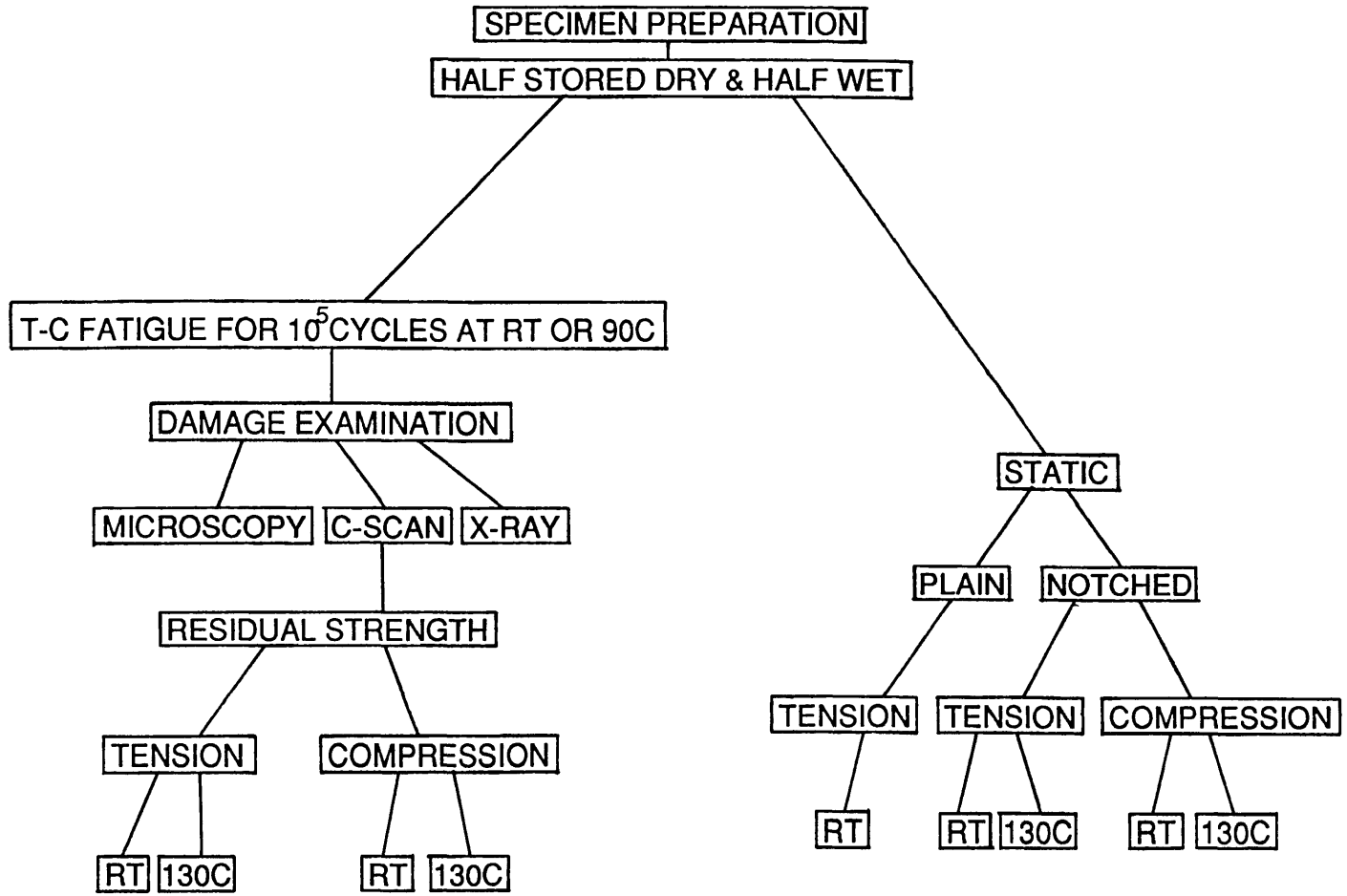


Fig. 5.2: Summary of the experimental programme for **APC-2** (stacking sequence A): specimens were notched with sharp notches only.

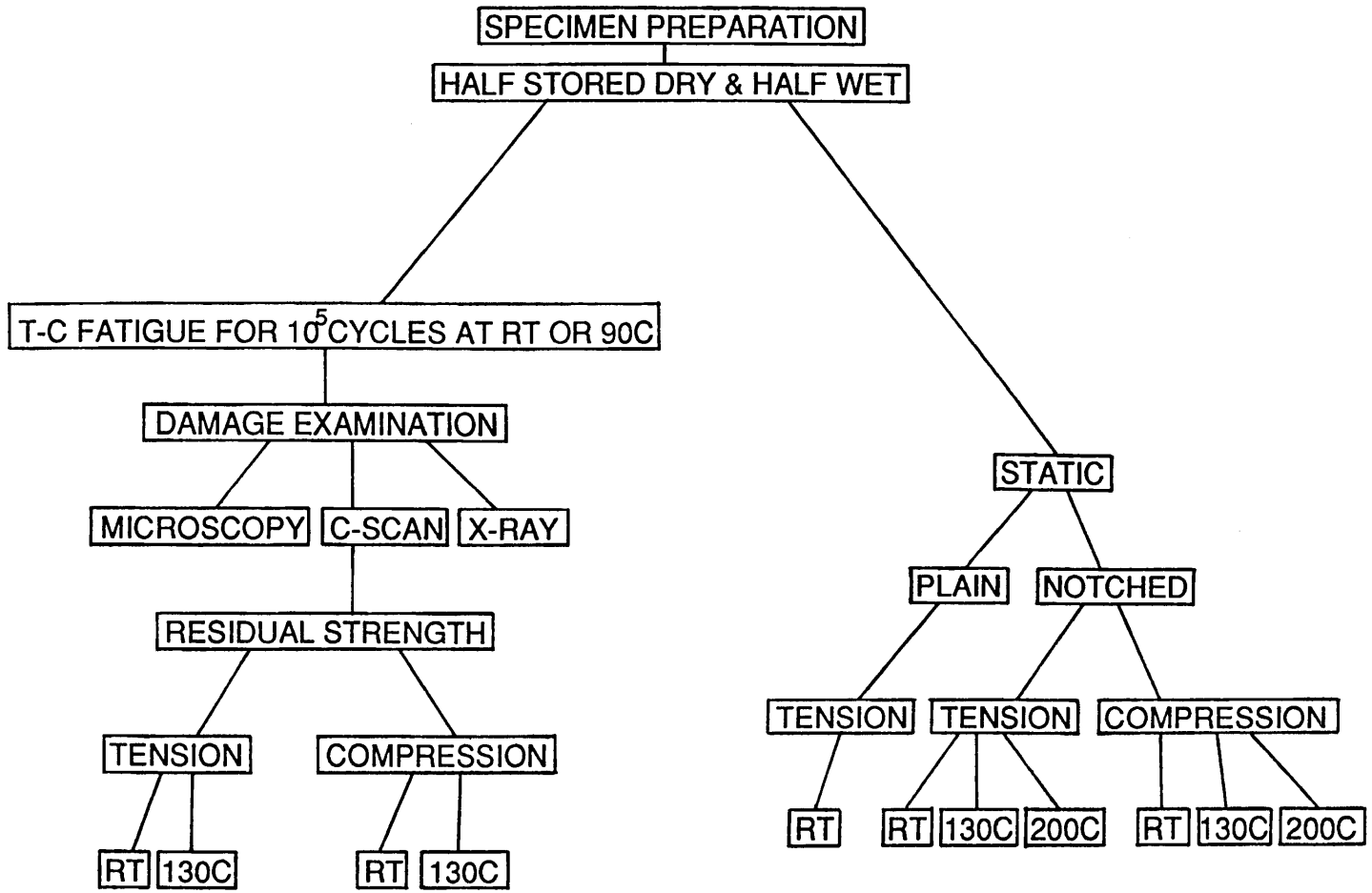


Fig. 5.3: Summary of the experimental programme for **R25** (stacking sequence A): specimens were notched with sharp notches only. Note the additional high temperature (200°C) tests.

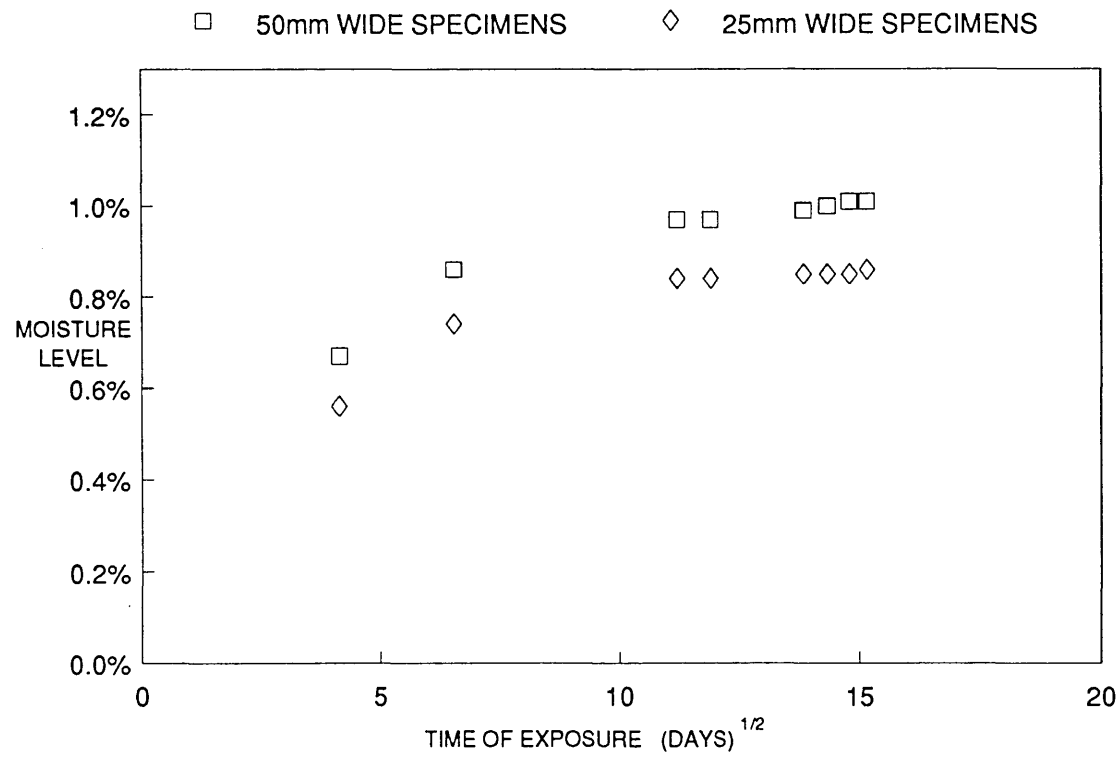


Fig. 5.4: Moisture pickup in **6376C** following environmental exposure at 60°C and 84% RH.

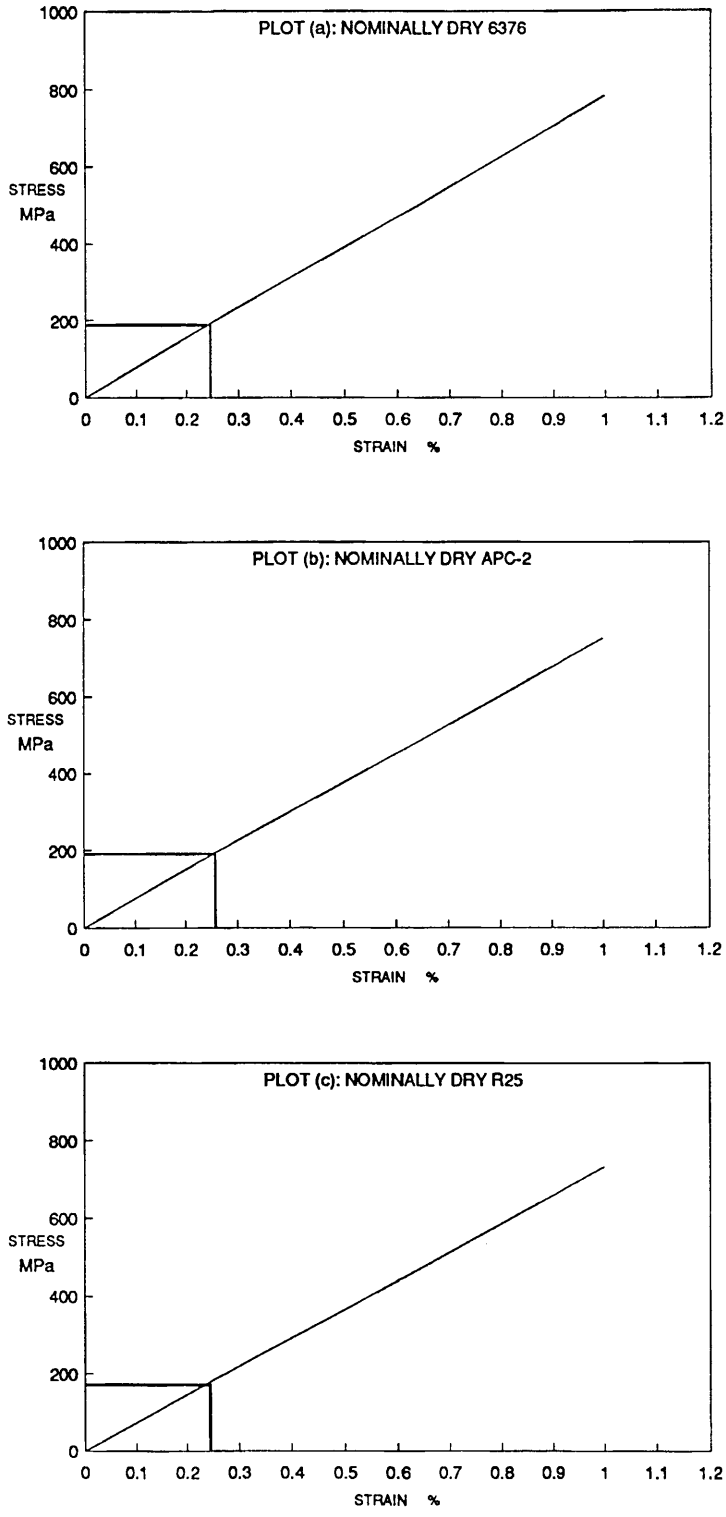


Fig. 5.5: Plots of stress versus strain for 6376C, APC-2 and R25. Note that the fatigue load amplitude of 20 kN does not correspond exactly to 200 MPa; this is a result of the average specimen thickness being different than the nominal thickness of 2mm. The average specimen thickness was 2.14mm, 2.03mm and 2.25mm for 6376C, APC-2 and R25 respectively.

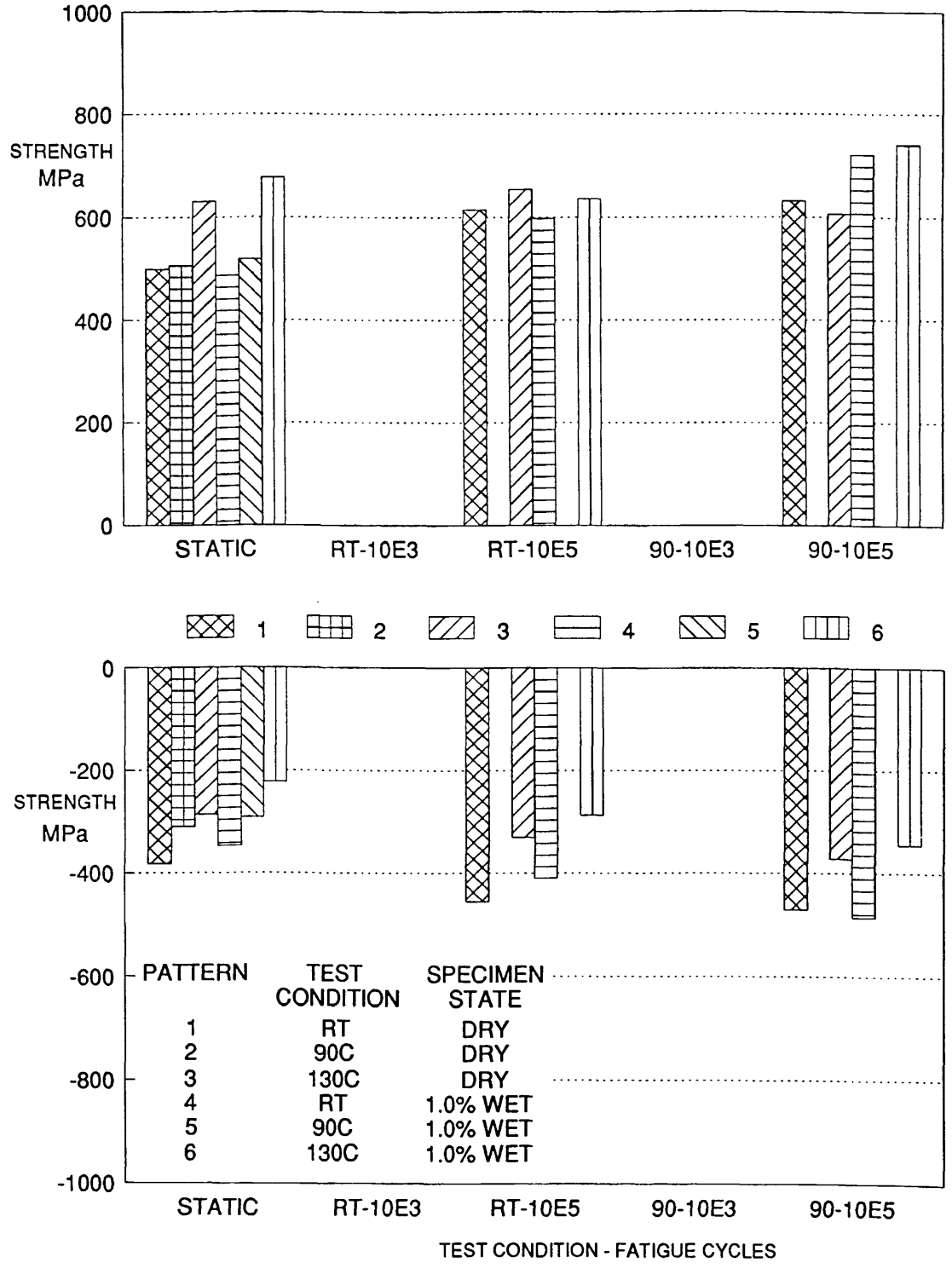


Fig. 5.6: Above, the tensile residual strength results for the dry and wet **6376C** specimens with sharp notches (stacking sequence A): below, the compressive residual strengths. The notched static strength results are also included.

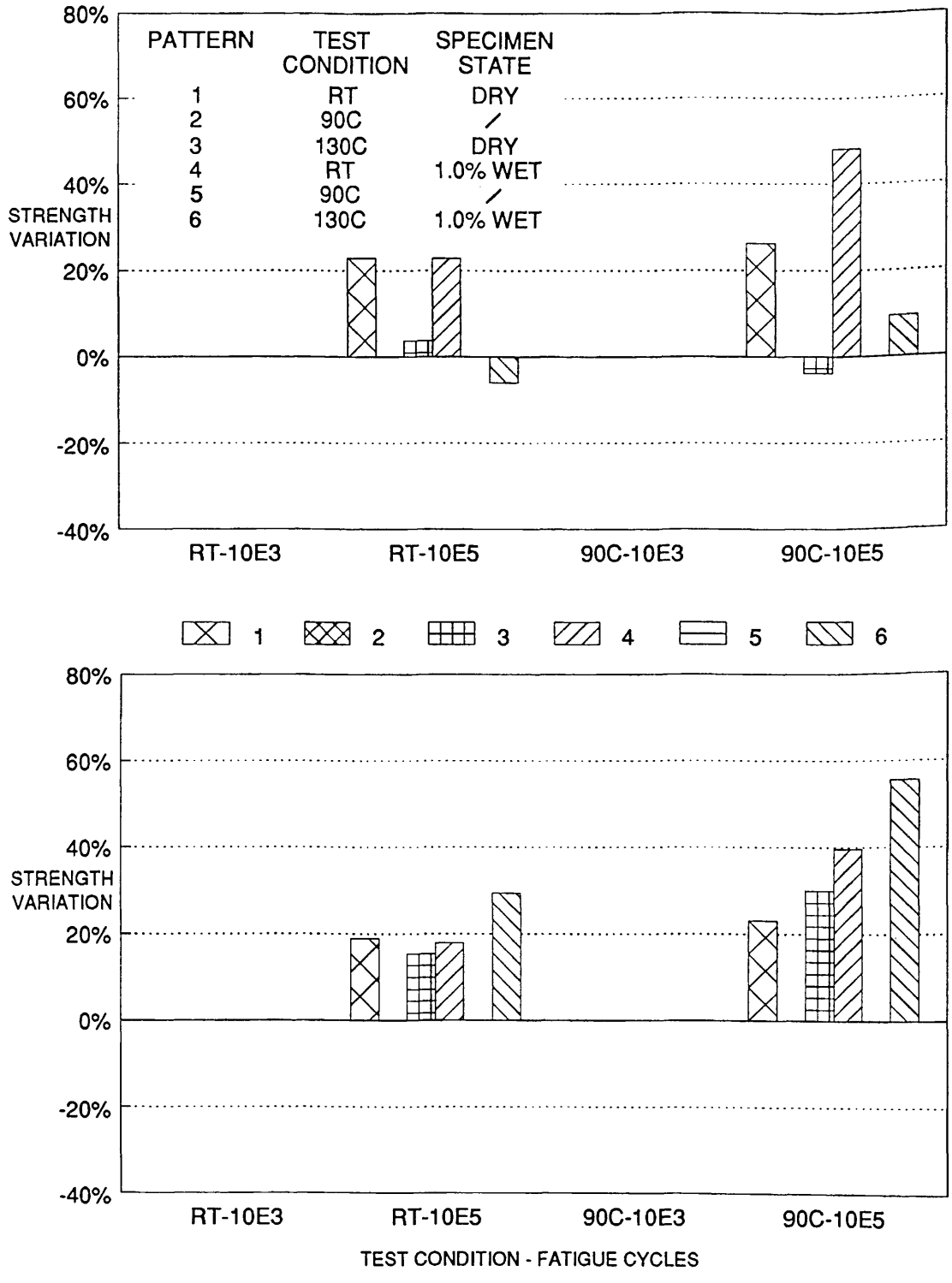


Fig. 5.7: Above, variation of the tensile residual strength with respect to the corresponding static value, for dry and wet **6376C** specimens with sharp notches (stacking sequence A): below, variation of the compressive residual strength.

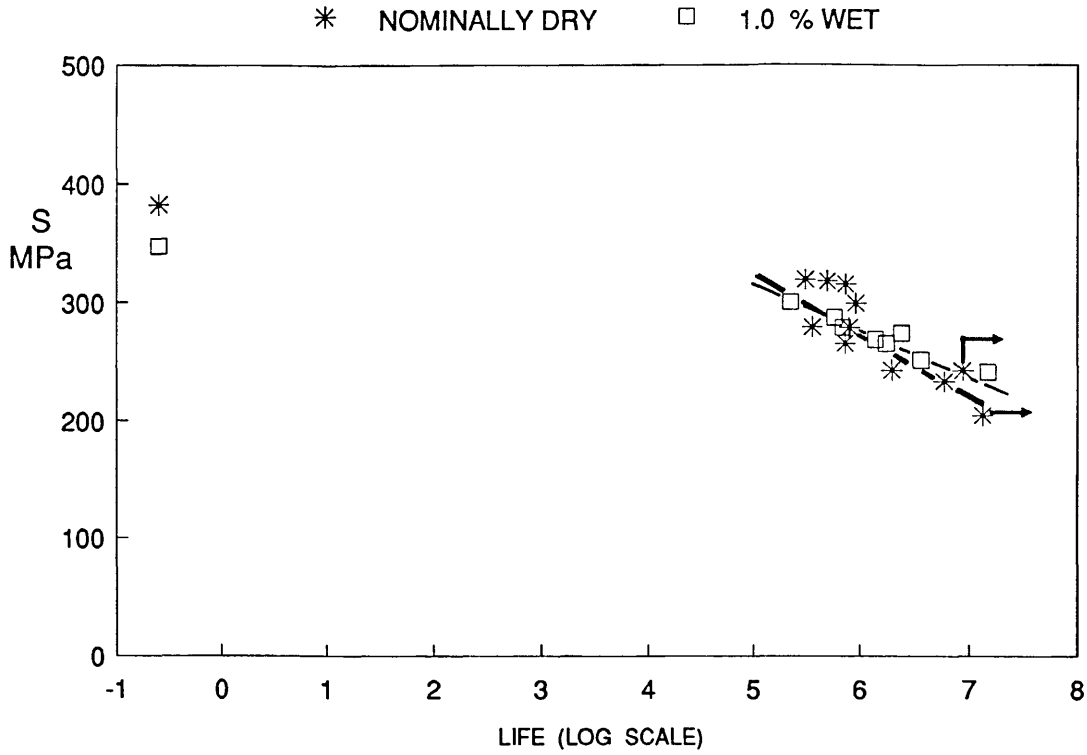


Fig. 5.8: Cyclic stress amplitude versus fatigue life: a comparison between dry and wet **6376C** specimens (stacking sequence A) with sharp notches: all tests were performed in tension-compression at RT. The arrows indicate higher than marked (expected) life.

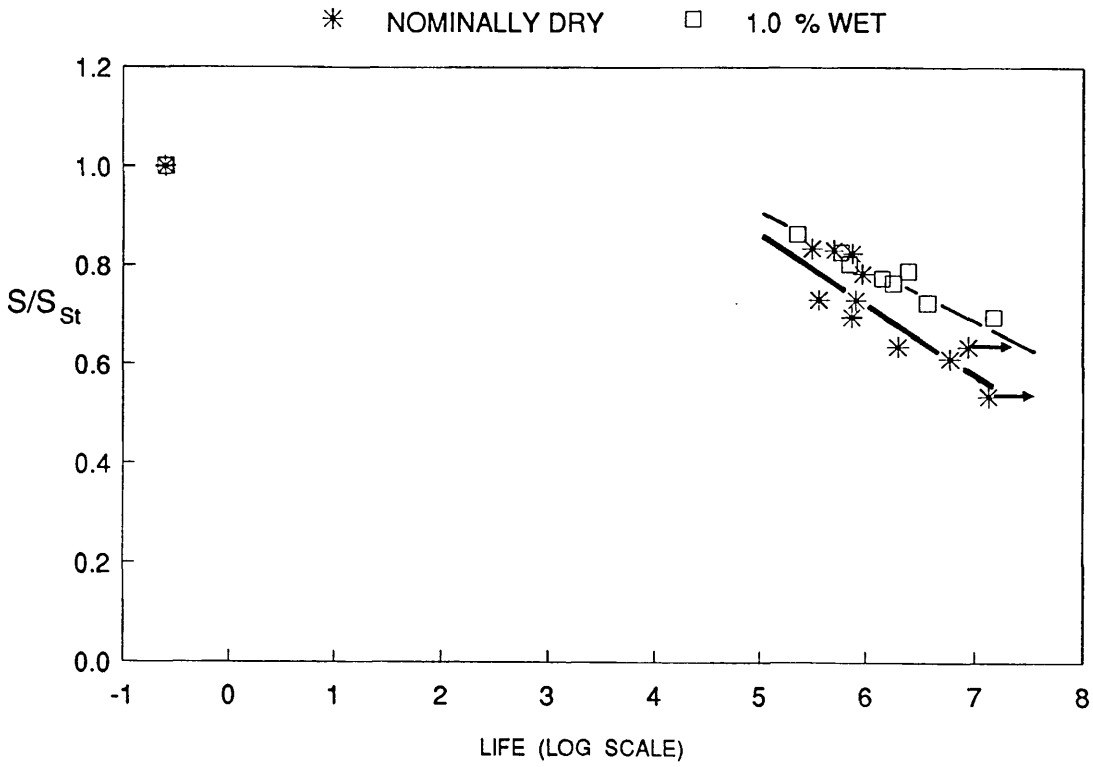
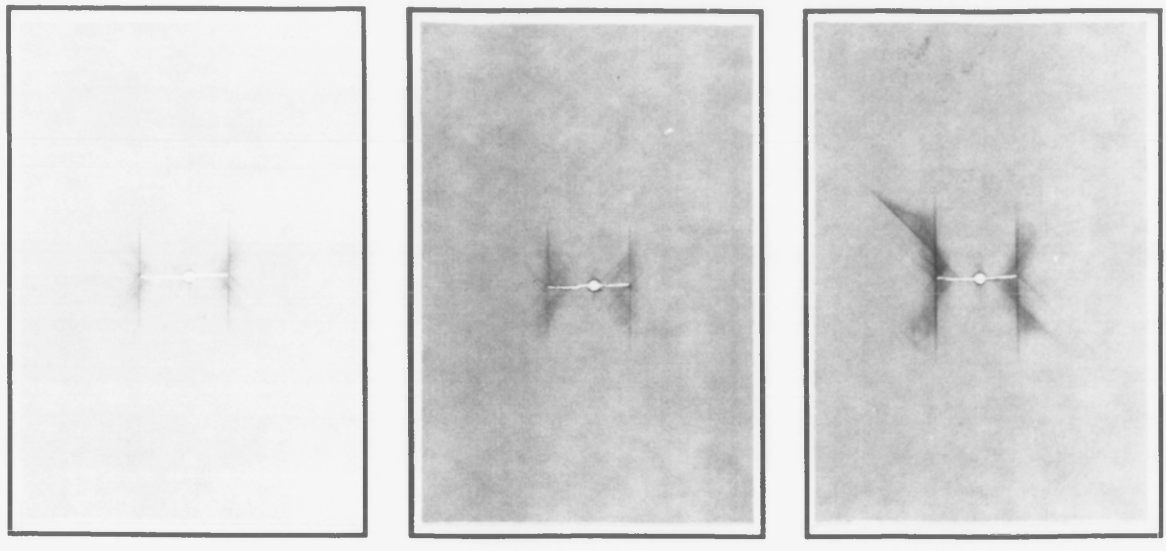


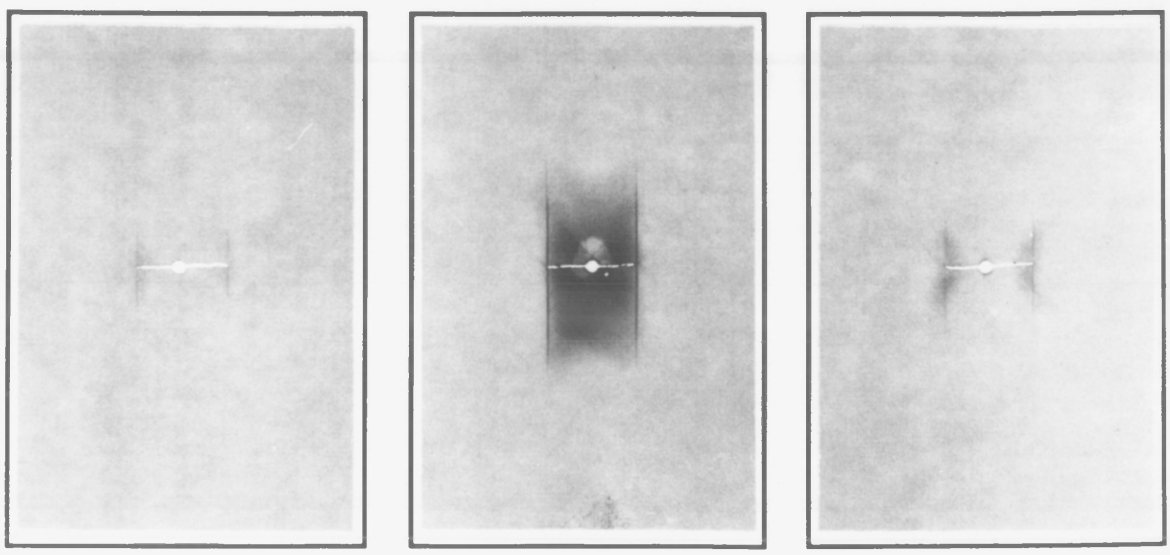
Fig. 5.9: Normalised cyclic stress amplitude versus fatigue life: the cyclic stress has been normalised with respect to the corresponding compressive value: tests include dry and wet **6376C** specimens with sharp notches: all tests were performed in tension-compression at RT. The arrows indicate higher than marked (expected) life.



DRY/RT/10^5 L=20kN

DRY/90C/10^5 L=20kN

DRY/RT/10^6 L=20kN



WET/RT/10^5 L=20kN

WET/90C/10^5 L=20kN

WET/RT/10^6 L=20kN

Fig. 5.10: X-ray radiographs of typical fatigue damage development under various environmental conditions in **6376C** specimens with sharp notches: the load amplitude is denoted L.

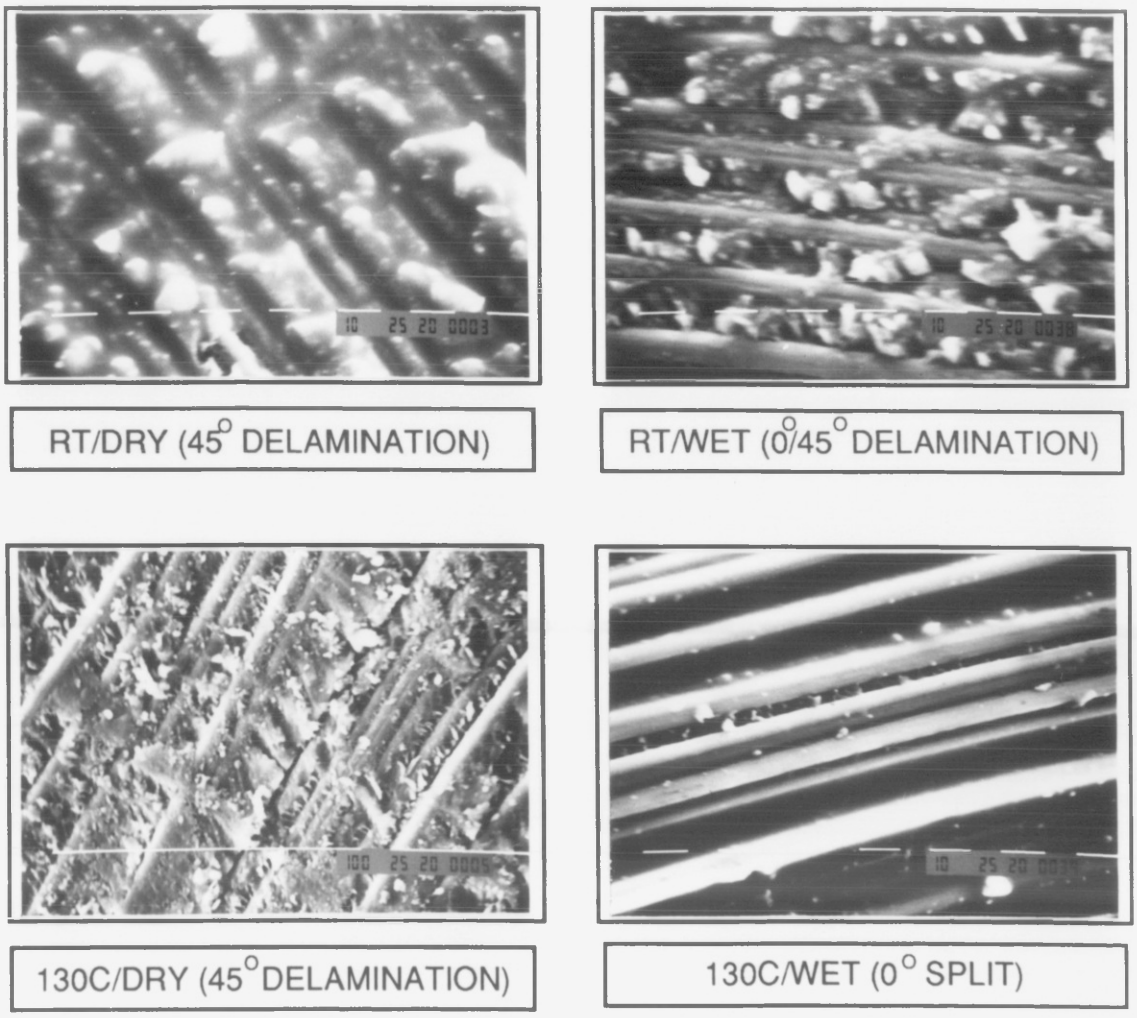


Fig. 5.11: Typical fractographs of delamination or fibre splitting under a range of test temperatures, for both dry and wet **6376C** specimens.

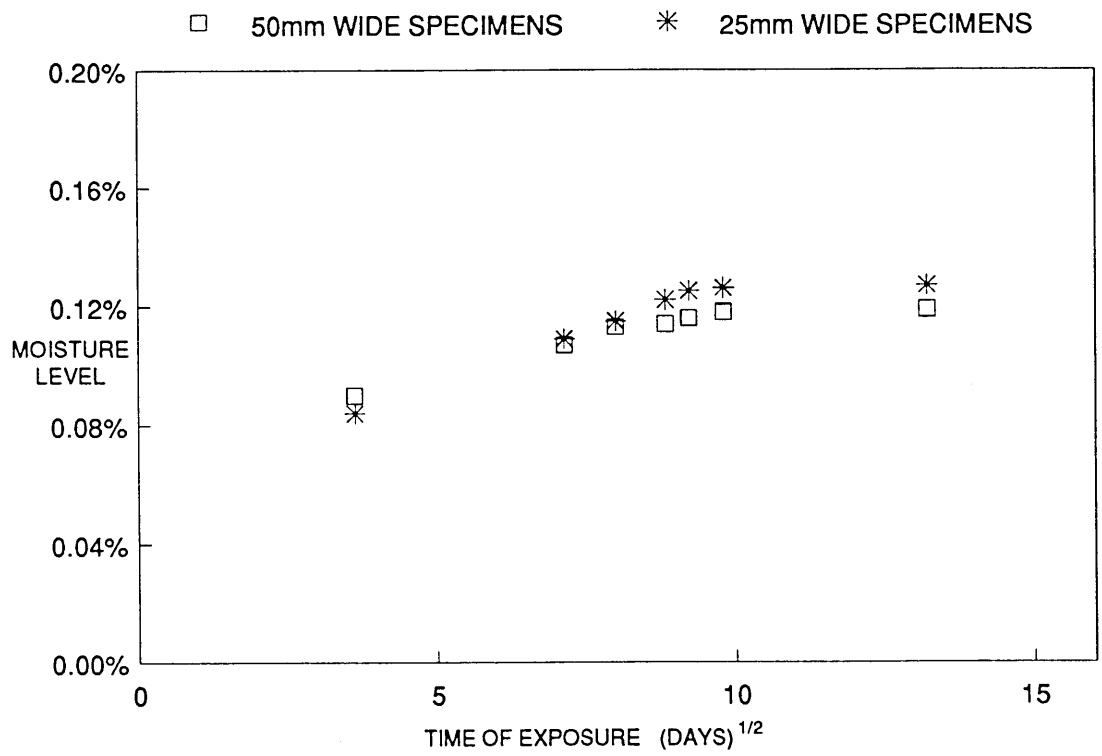


Fig. 5.12: Moisture pickup in **APC-2** following environmental exposure at 60°C and 84% RH.

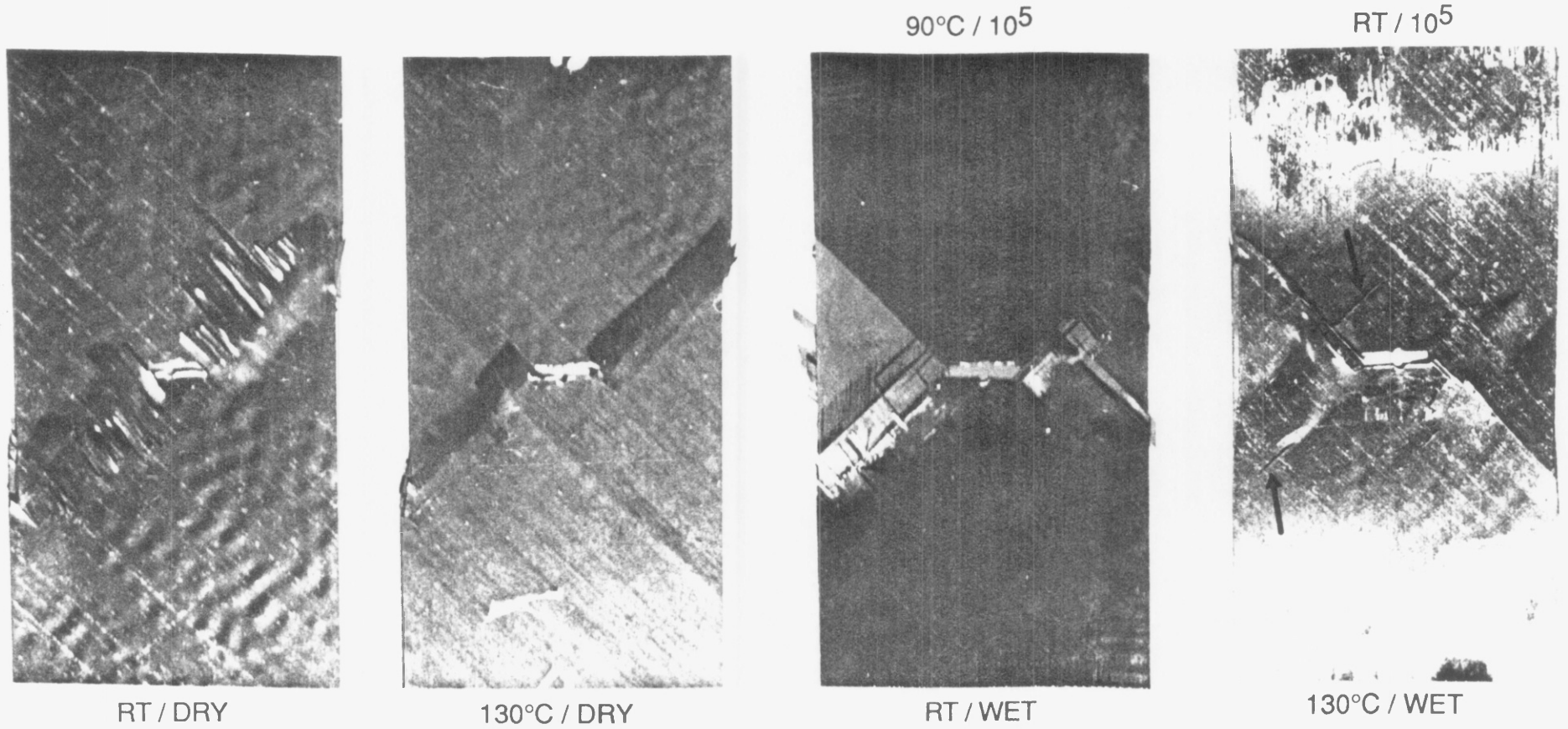


Fig. 5.13: A comparison of tensile failure modes in dry and wet **APC-2** specimens (with sharp notches): the fatigue condition is shown at the top and the static condition at the bottom of each picture.

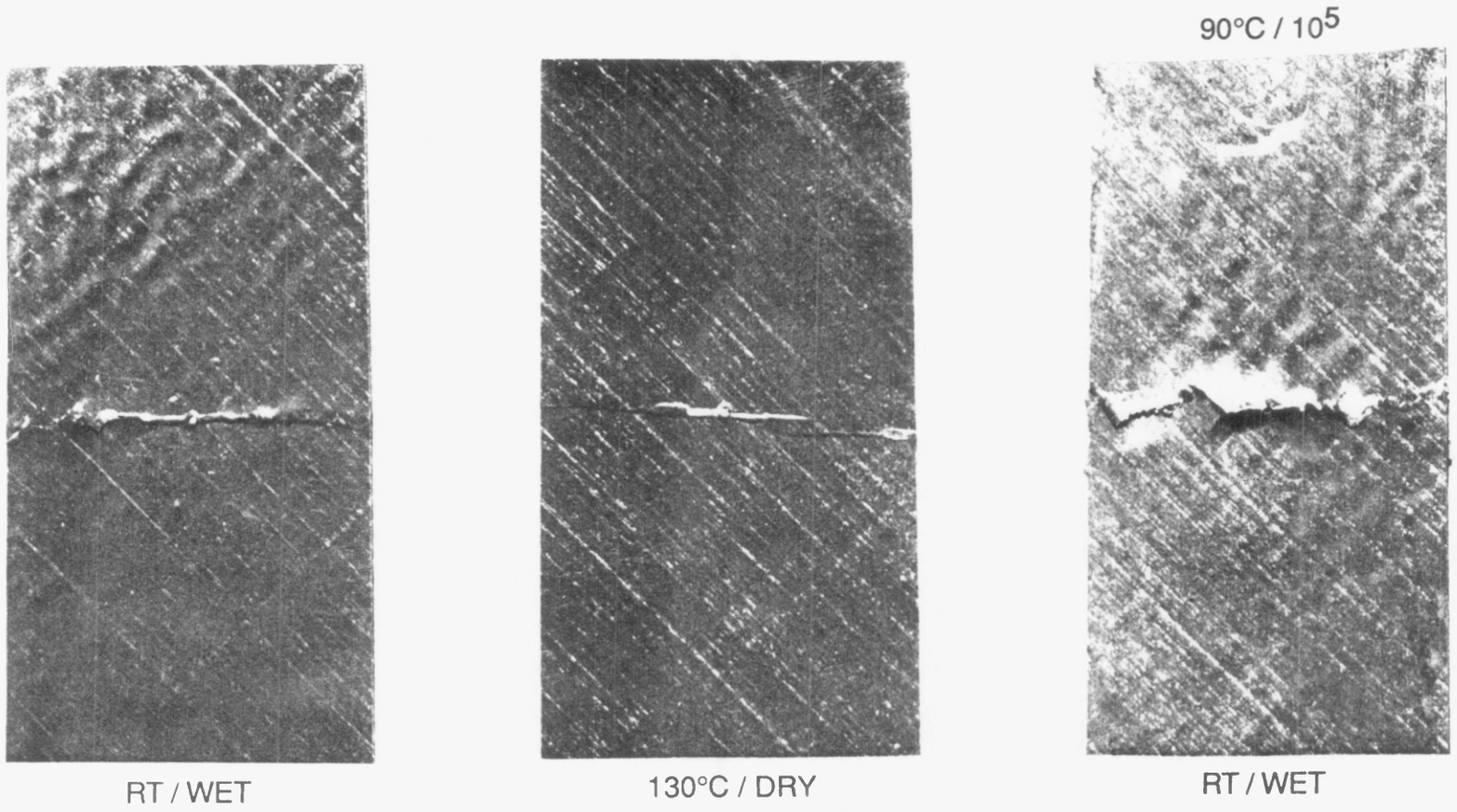


Fig. 5.14: A comparison of compressive failure modes in dry and wet **APC-2** specimens (with sharp notches): the fatigue condition is shown at the top and the static condition at the bottom of each picture.

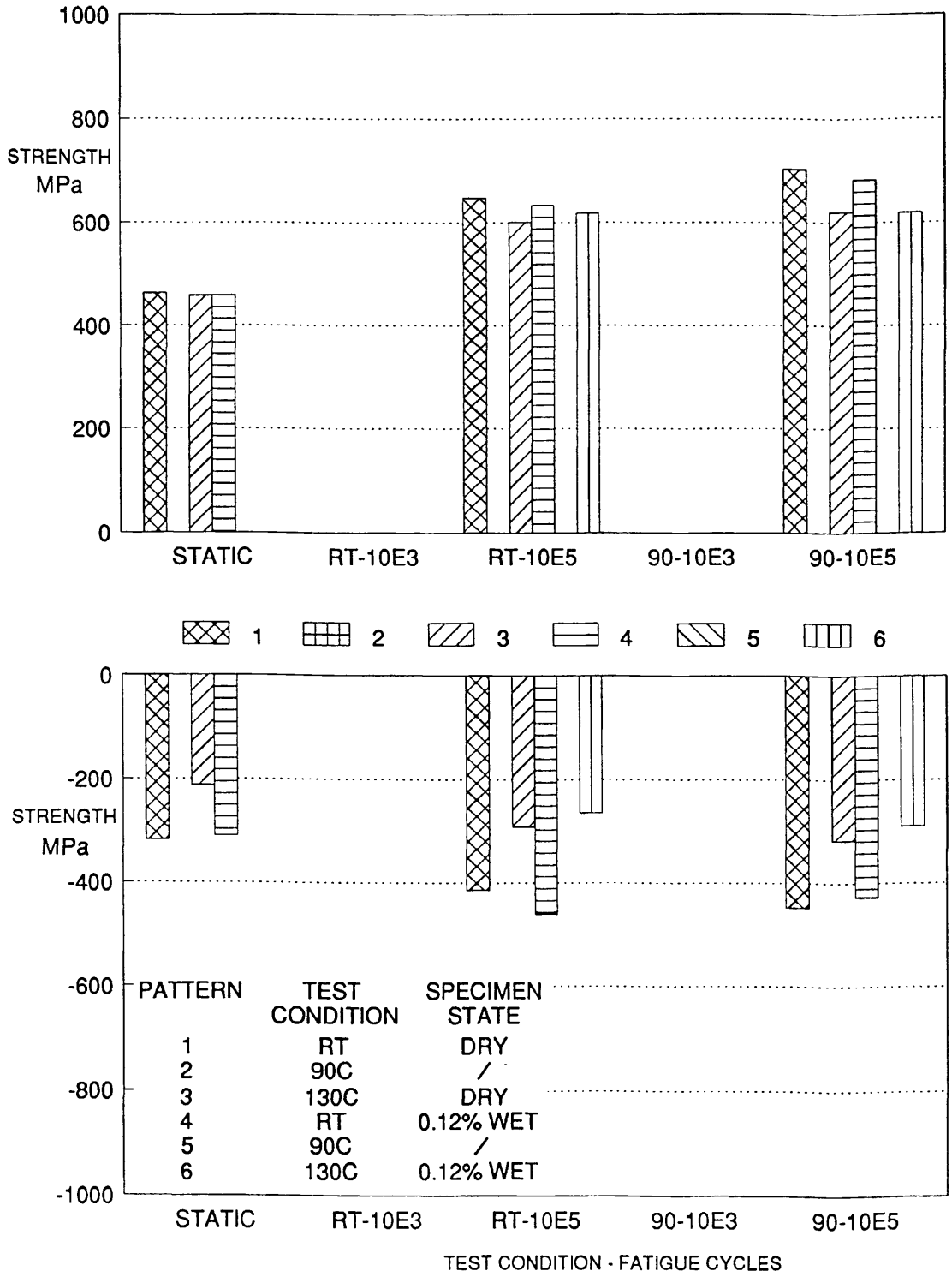


Fig. 5.15: Above, the tensile residual strength results for the dry and wet **APC-2** specimens with sharp notches (stacking sequence A): below, the compressive residual strengths. The notched static strength results are also included.

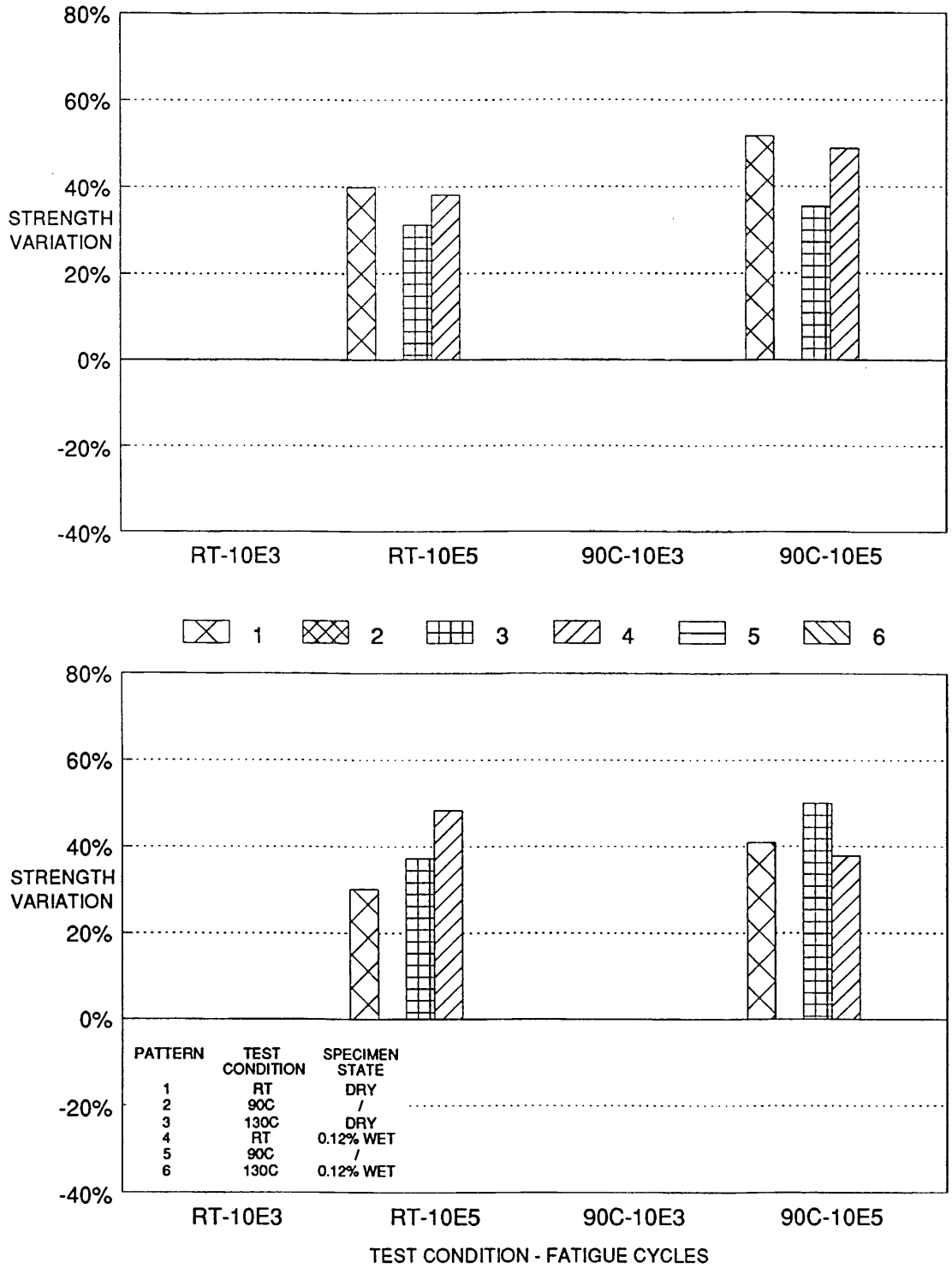


Fig. 5.16: Above, variation of the tensile residual strength with respect to the corresponding static value, for dry and wet **APC-2** specimens with sharp notches (stacking sequence A): below, variation of the compressive residual strength.

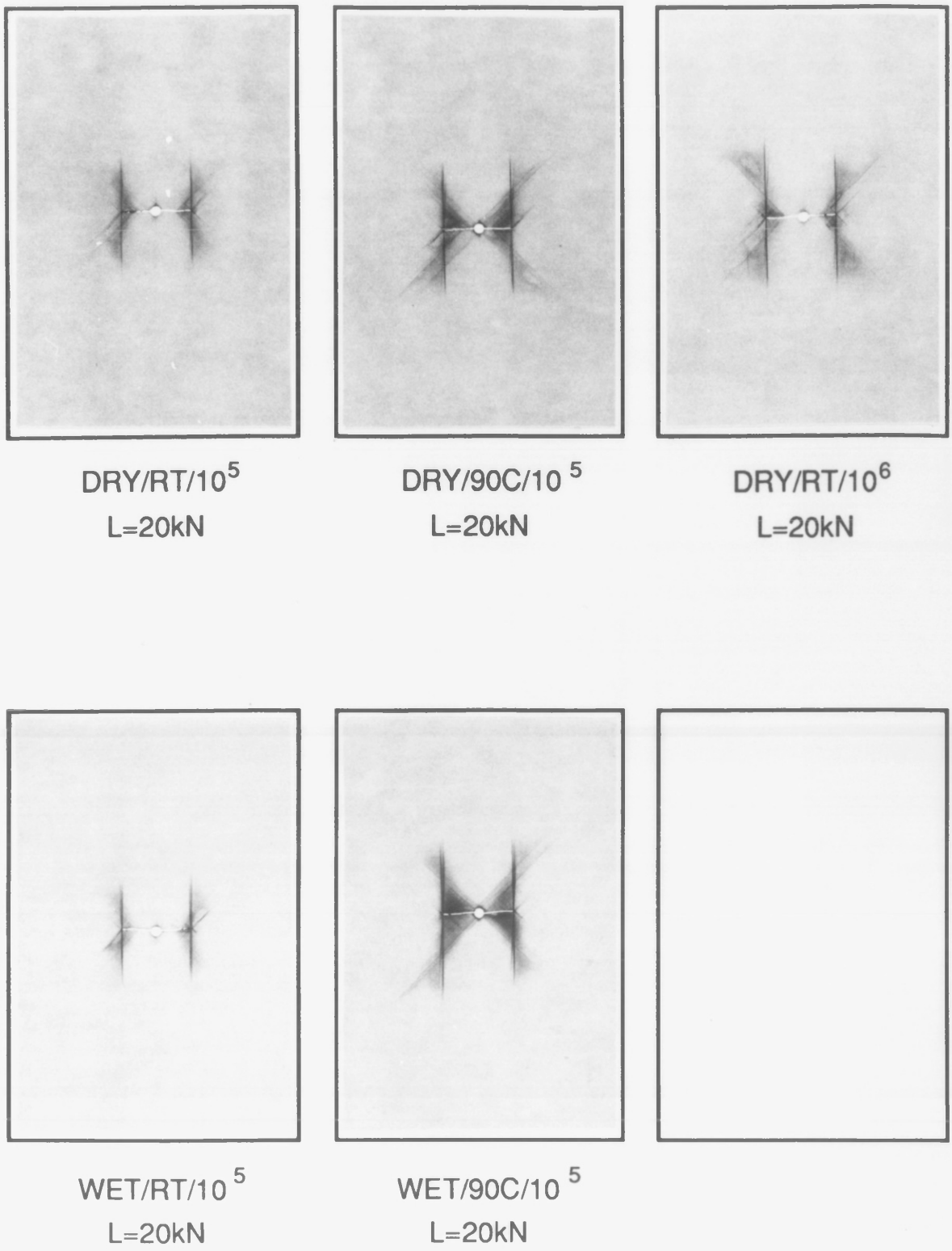


Fig. 5.17: X-ray radiographs of typical fatigue damage development under various environmental conditions in **APC-2** specimens with sharp notches: the load amplitude is denoted L.

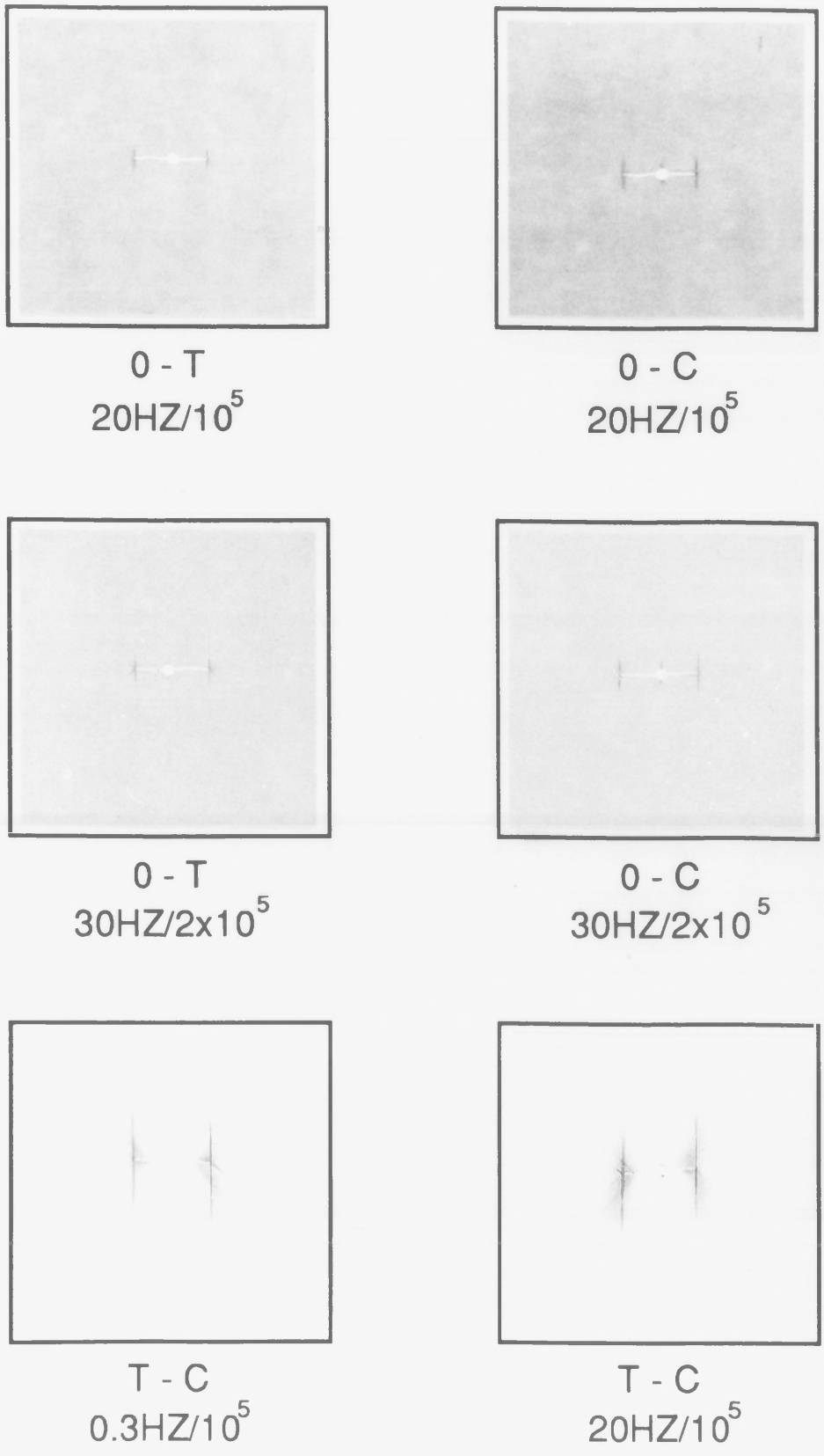


Fig. 5.18: X-ray radiographs of typical fatigue damage development under various fatigue cycles and/or frequency regimes in dry **APC-2** specimens: all tests have been performed at RT at a load amplitude Ln (=20kN).

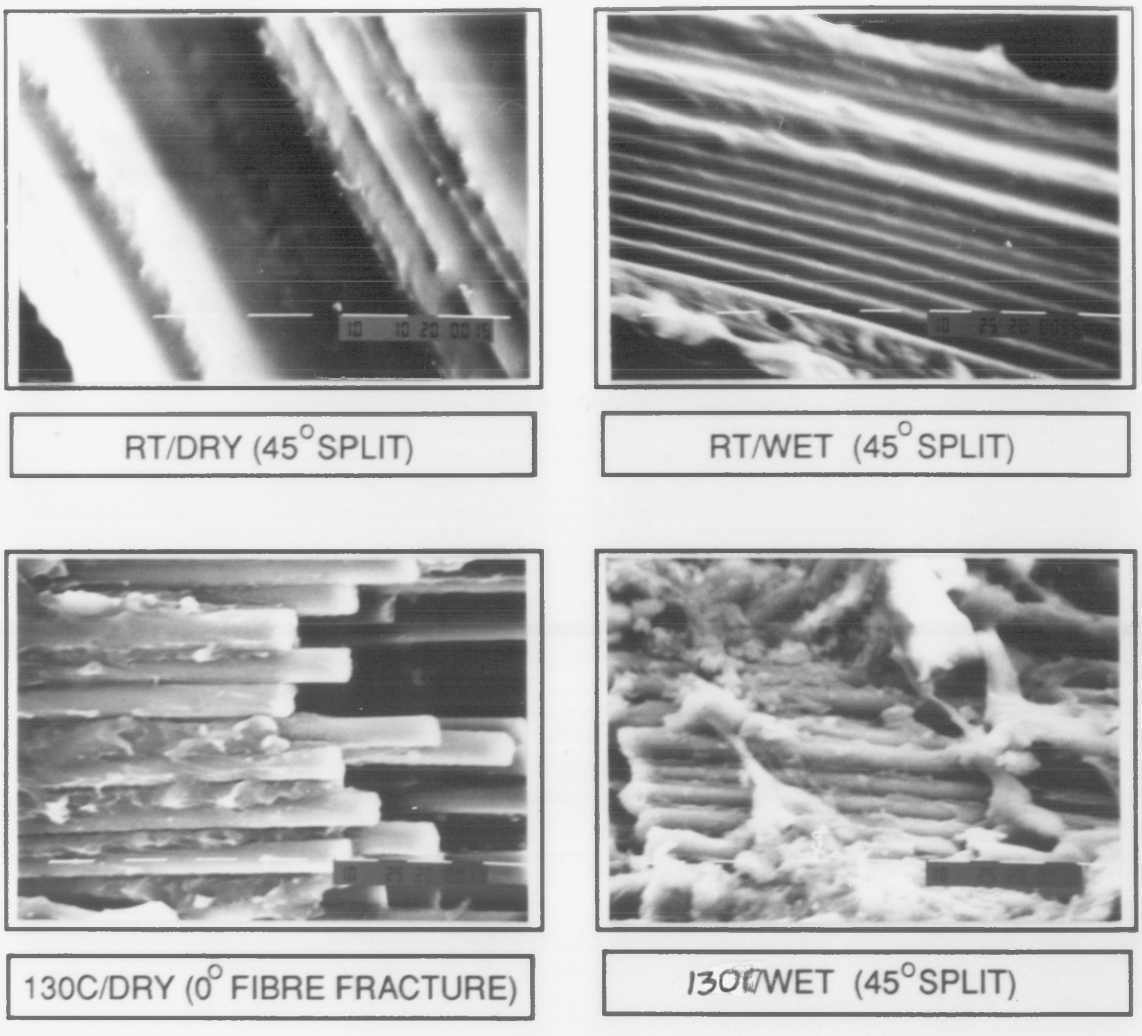


Fig. 5.19: Typical fractographs of delamination or fibre splitting under a range of test temperatures, for both dry and wet **APC-2** specimens.

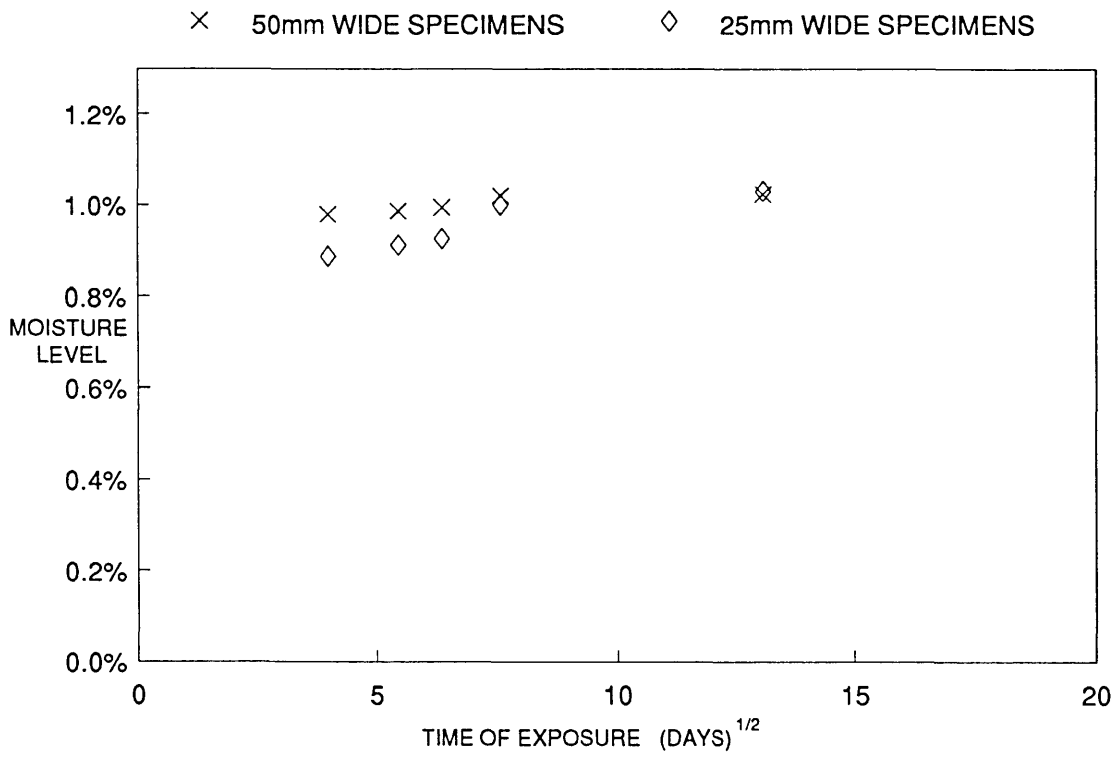


Fig. 5.20: Moisture pickup in **R25** following environmental exposure at 60°C and 84% RH.

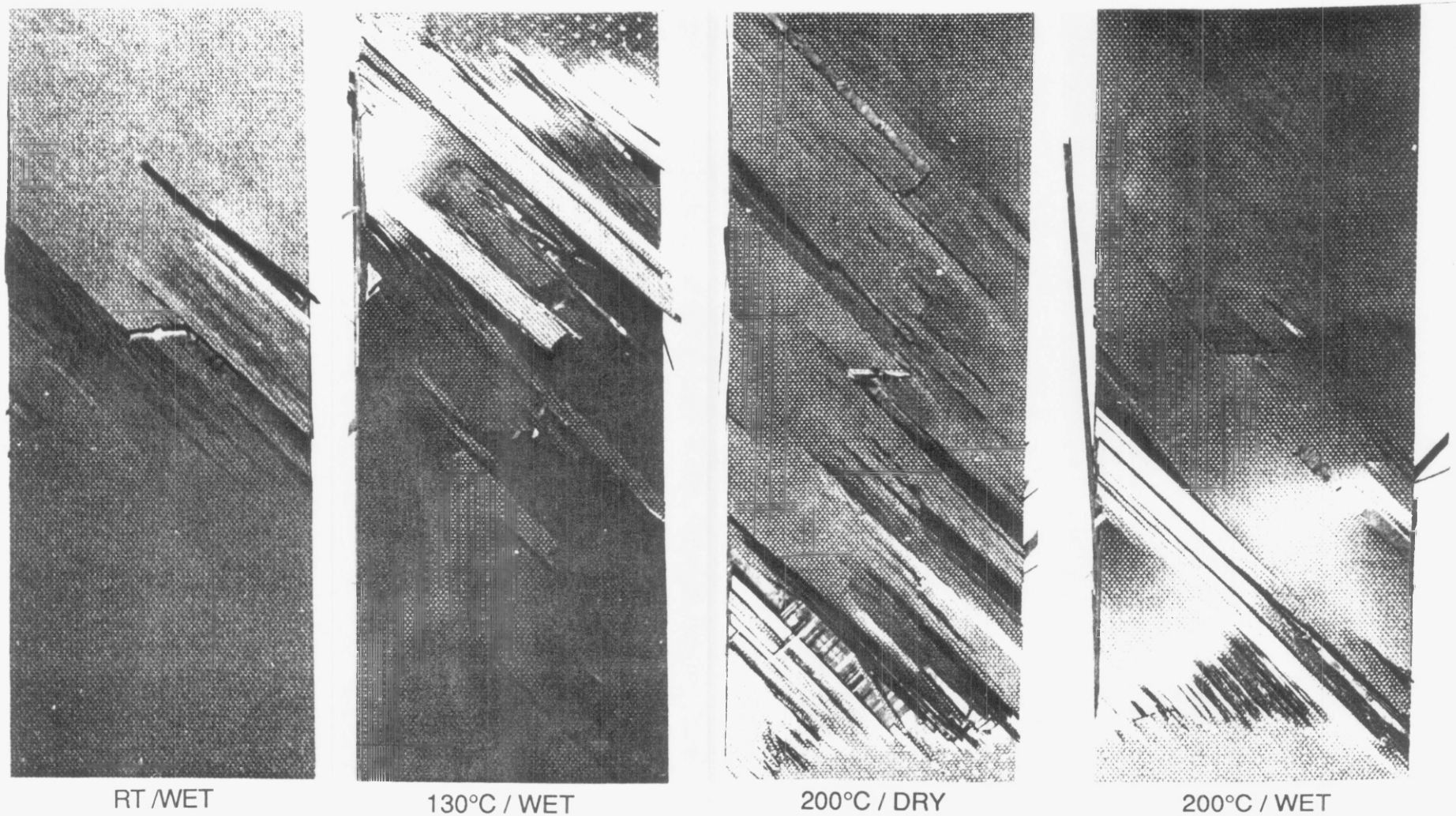


Fig. 5.21: A comparison of static tensile failure modes in dry and wet **R25** specimens (with sharp notches): the test condition is shown at the bottom of each picture.

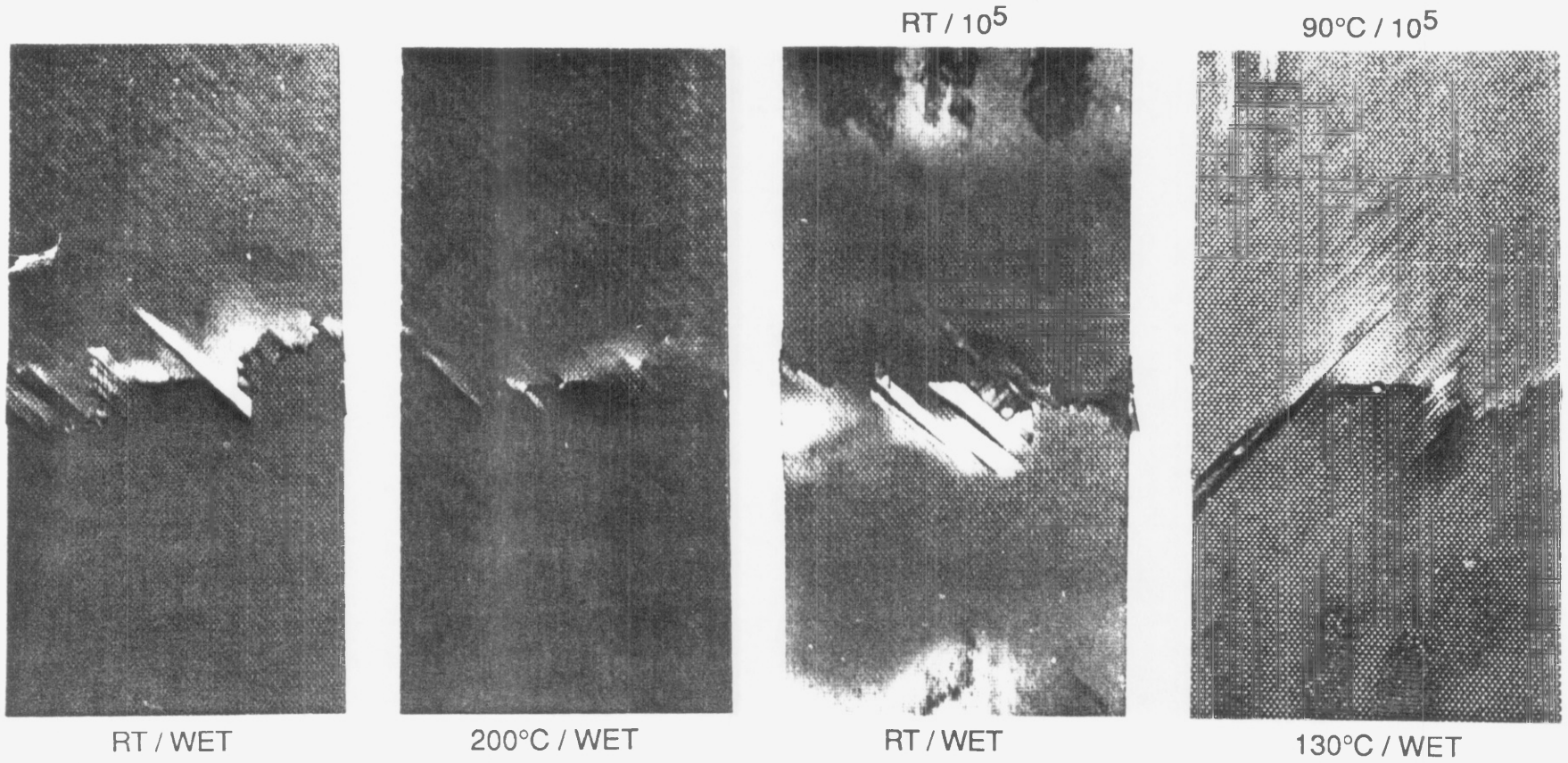


Fig. 5.22: A comparison of compressive failure modes in wet **R25** specimens (with sharp notches): the fatigue condition is shown at the top and the static condition at the bottom of each picture.

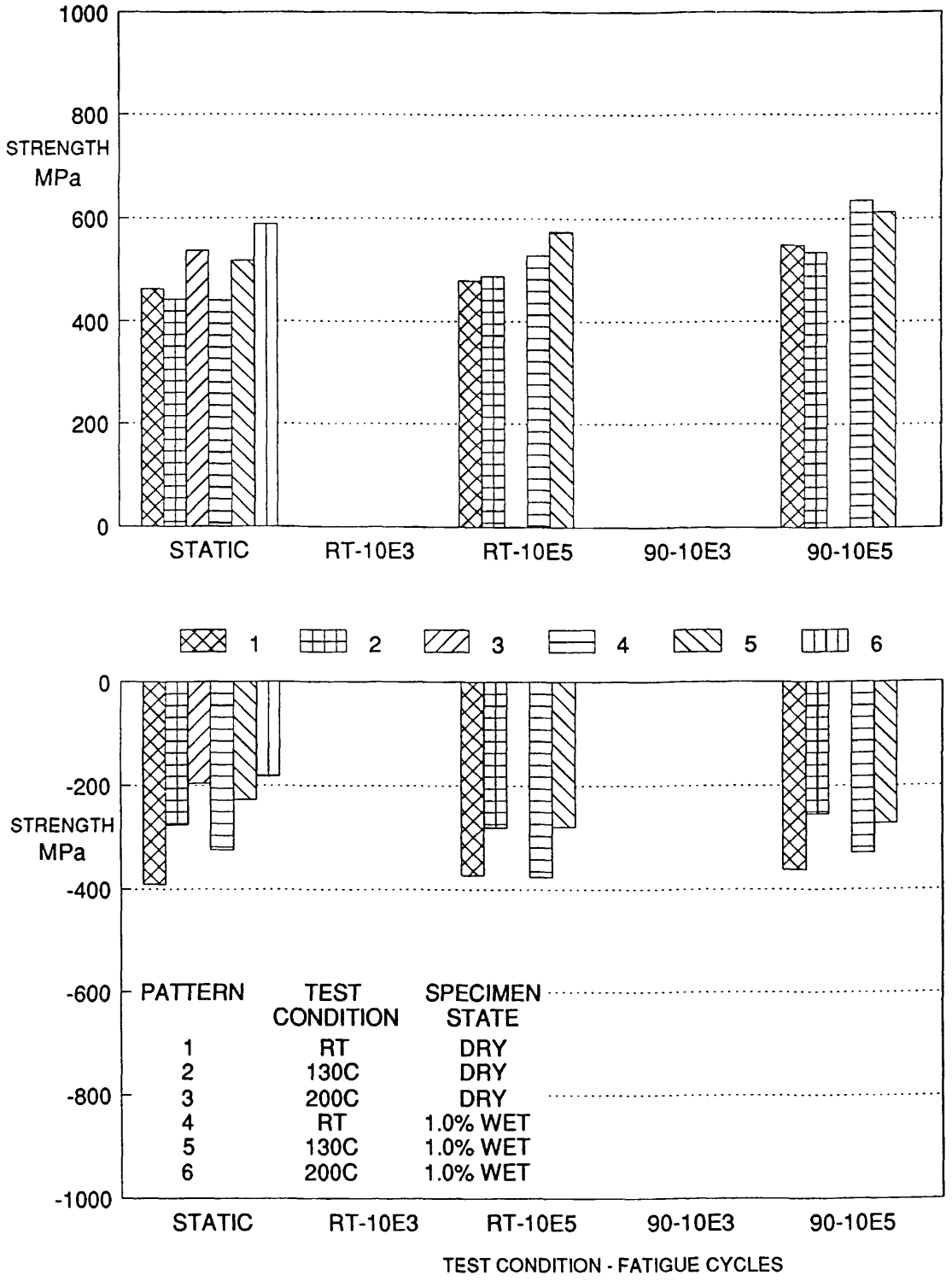


Fig. 5.23: Above, the tensile residual strength results for the dry and wet **R25** specimens with sharp notches (stacking sequence A): below, the compressive residual strengths. The notched static strength results are also included.

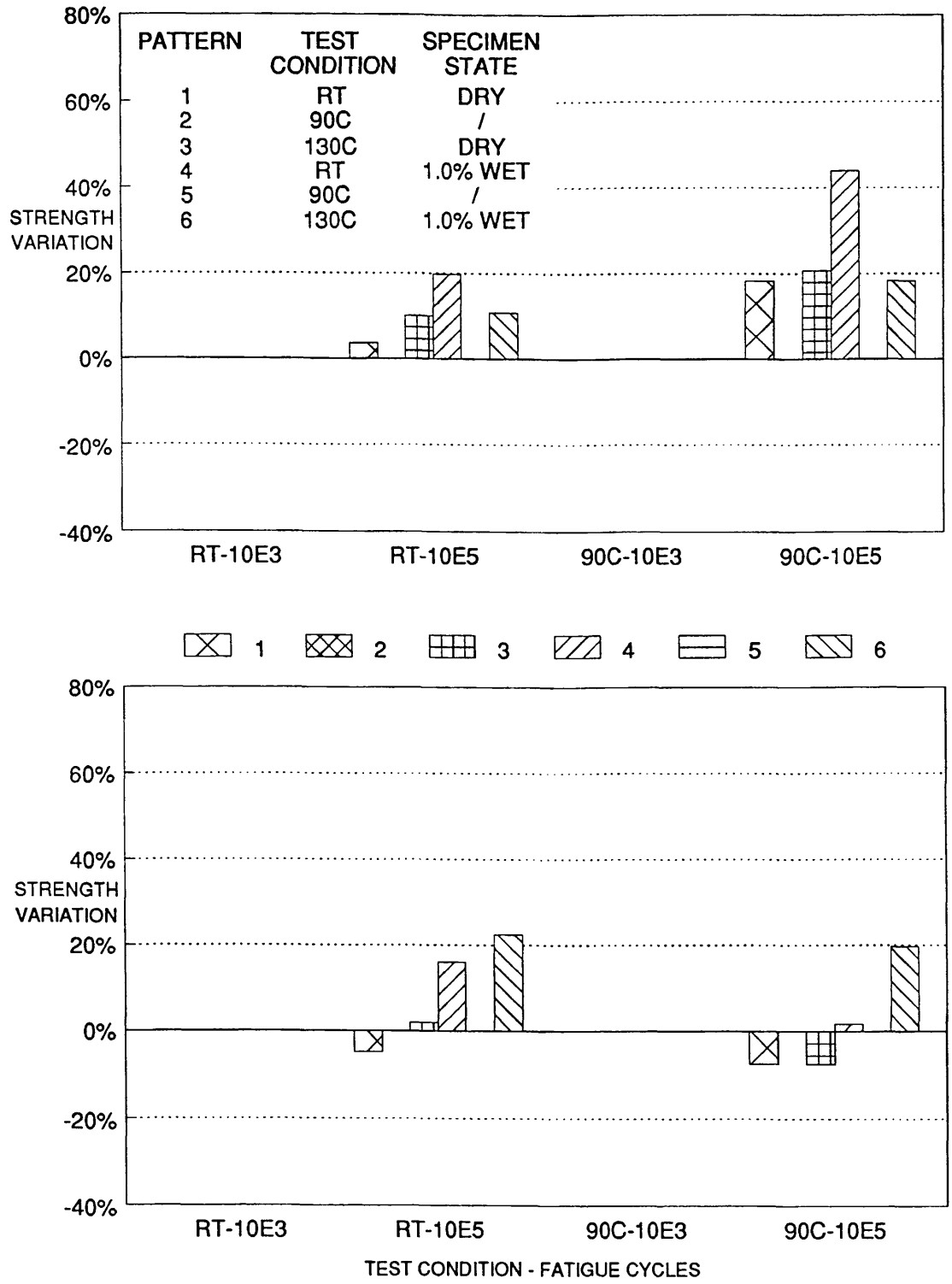
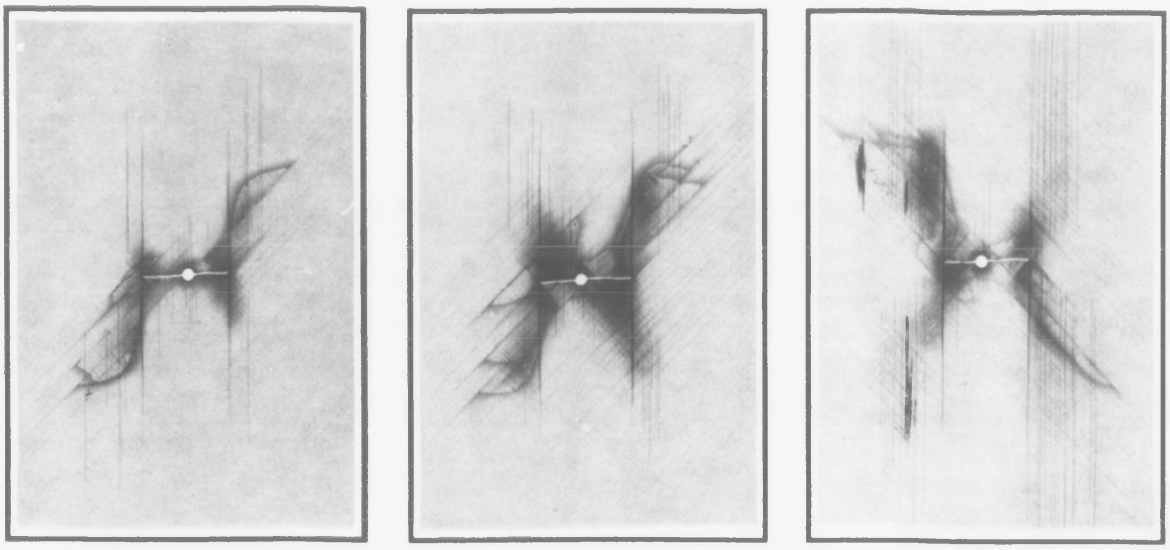


Fig. 5.24: Above, variation of the tensile residual strength with respect to the corresponding static value, for dry and wet **R25** specimens with sharp notches (stacking sequence A): below, variation of the compressive residual strength.



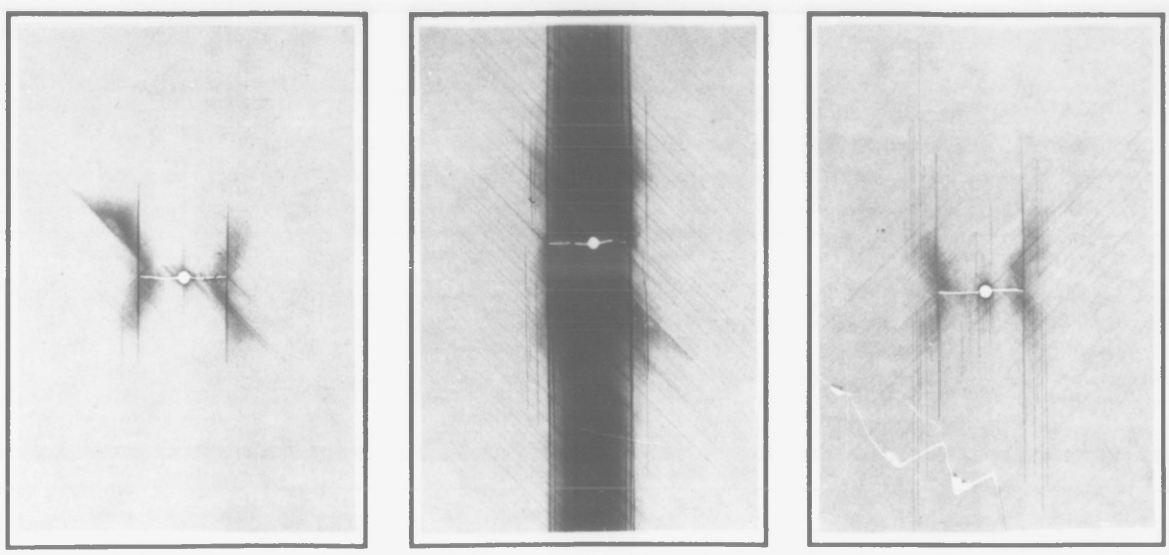
Fig. 5.25: A comparison of tensile failure modes in wet **R25** specimens (with sharp notches): the fatigue condition is shown at the top and the static condition at the bottom of each picture.



DRY/RT/10^5
L=20kN

DRY/90C/10^5
L=20kN

DRY/RT/10^6
L=20kN



WET/RT/10^5
L=20kN

WET/90C/10^5
L=20kN

DRY/RT/4.1×10^6
L=17kN

Fig. 5.26: X-ray radiographs of typical fatigue damage development under various environmental conditions in **R25** specimens with sharp notches: the load amplitude is denoted L.

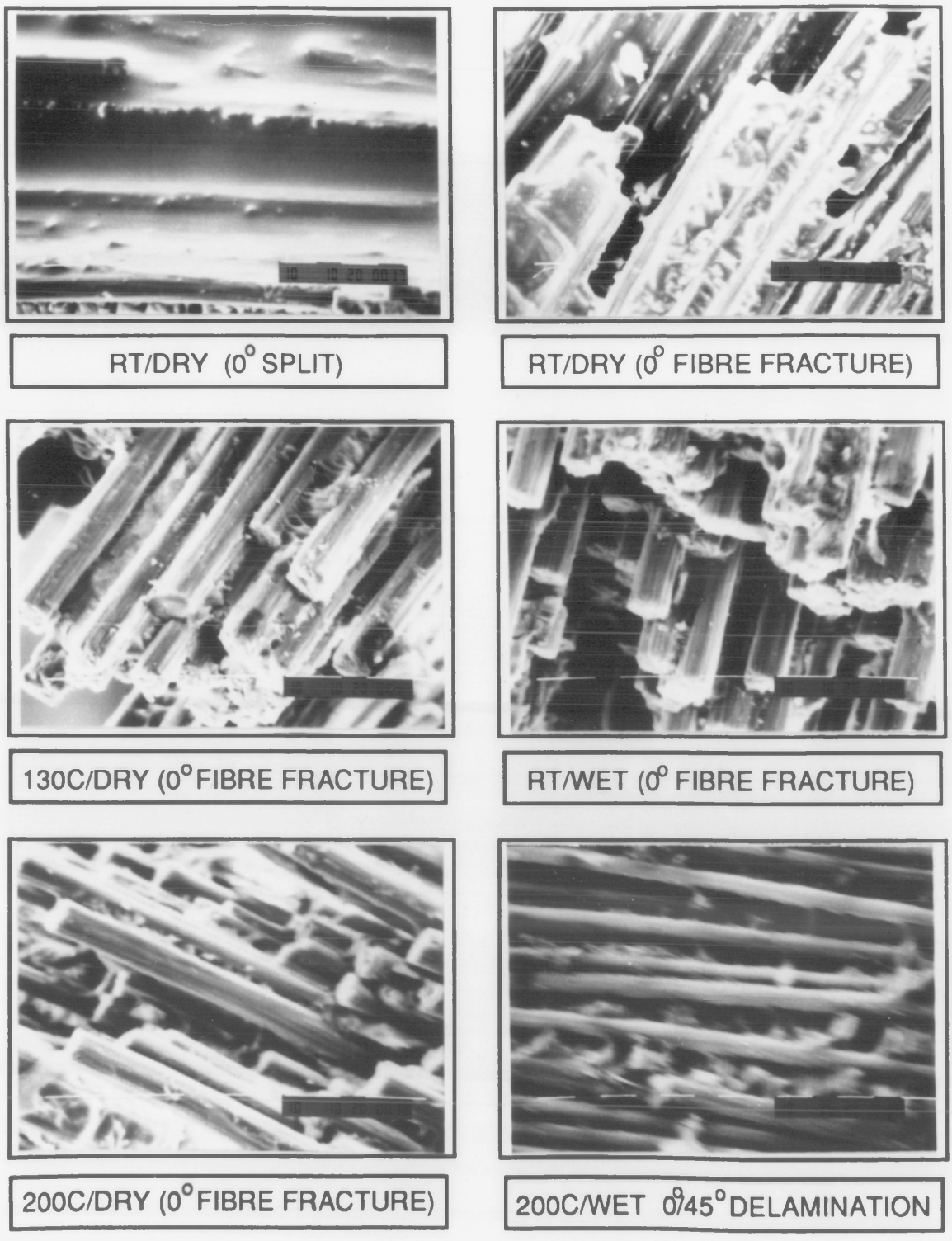
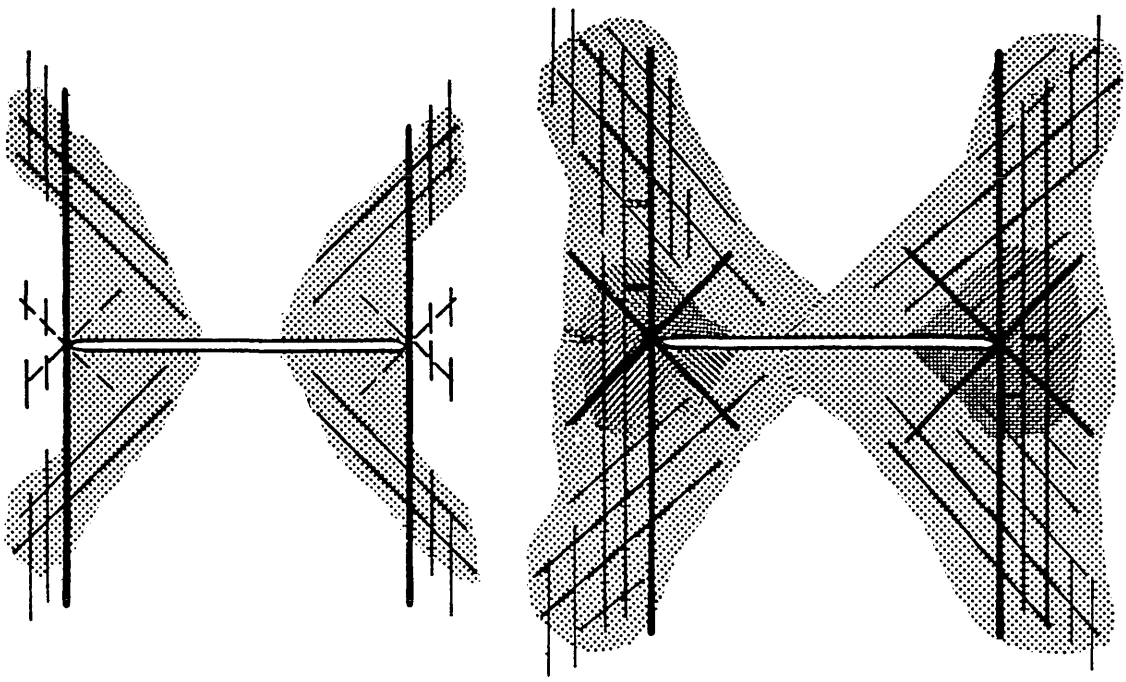
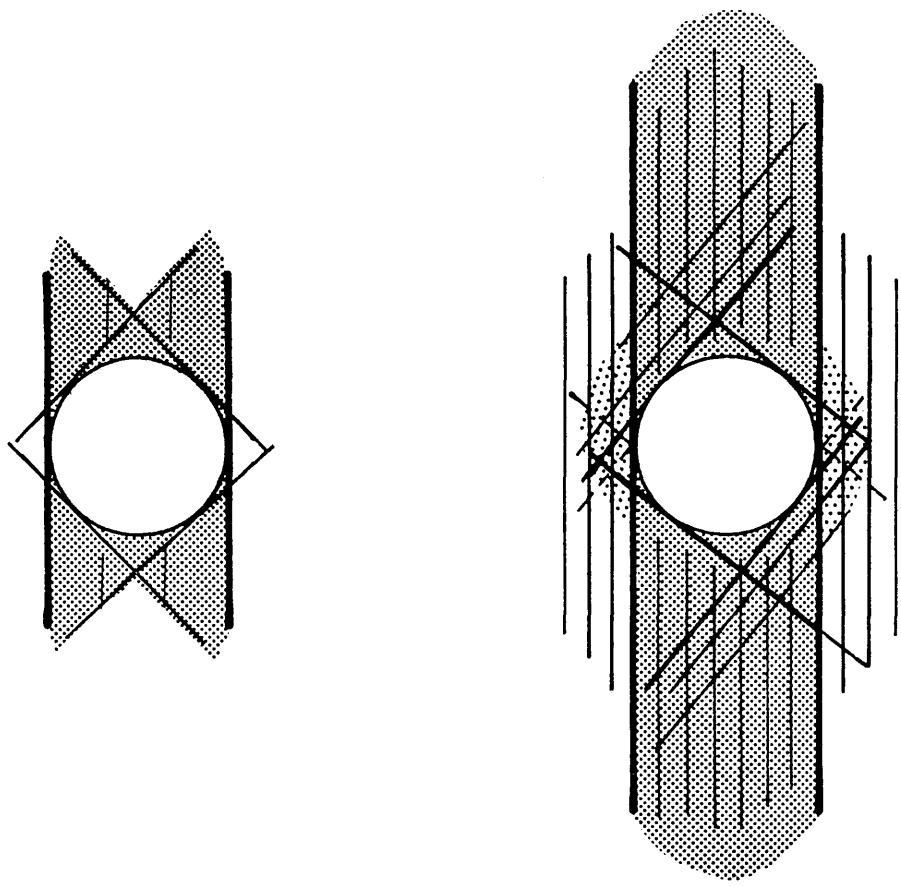


Fig. 5.27: Typical fractographs of delamination or fibre splitting under a range of test temperatures, for both dry and wet **R25** specimens.



(a)



(b)

Fig. 6.1 Schematic representation of the fatigue damage development in notched, 914C specimens.

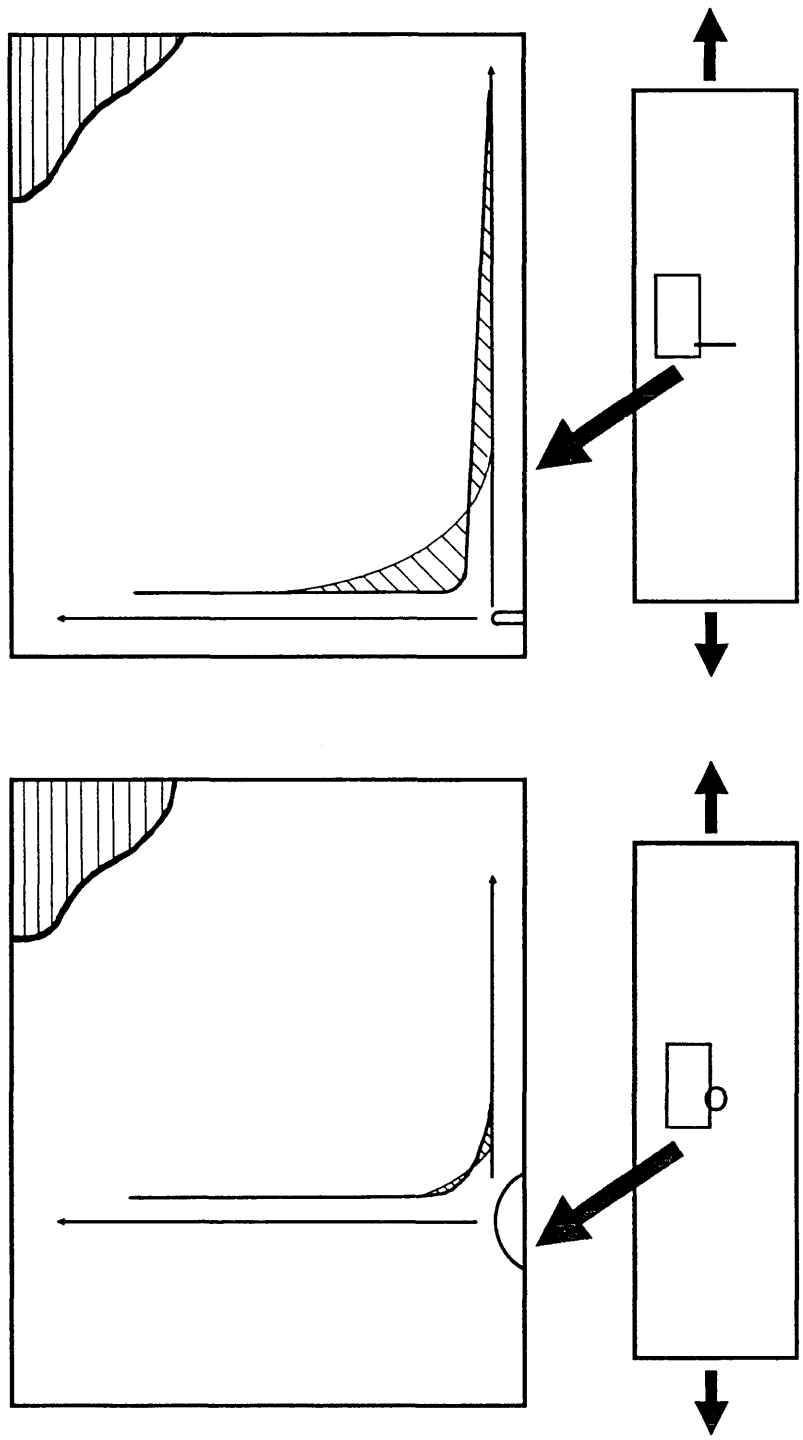


Fig. 6.2 Schematic presentation of the stress concentration, σ_x, near the notch tip area: sharp notch above, and circular hole below. This is a typical variation in stress found in the 0° plies.

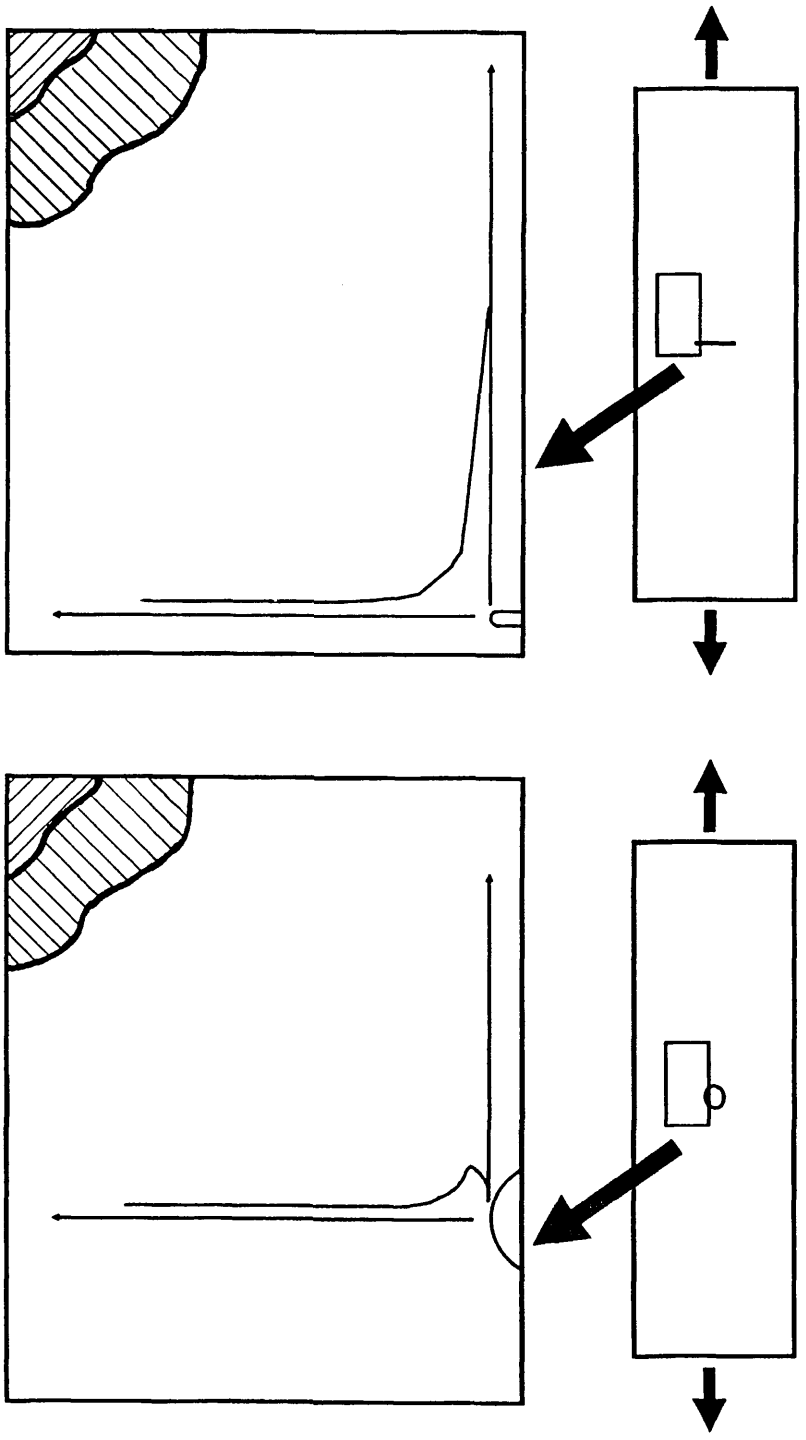


Fig. 6.3 Schematic presentation of the stress concentration, σ_x, near the notch tip area: sharp notch above, and circular hole below. This is a typical variation in stress found in the ±45° plies. NB the stress magnitude, relative to the stress magnitude in figure 6.2, is shown 1.4 times larger.

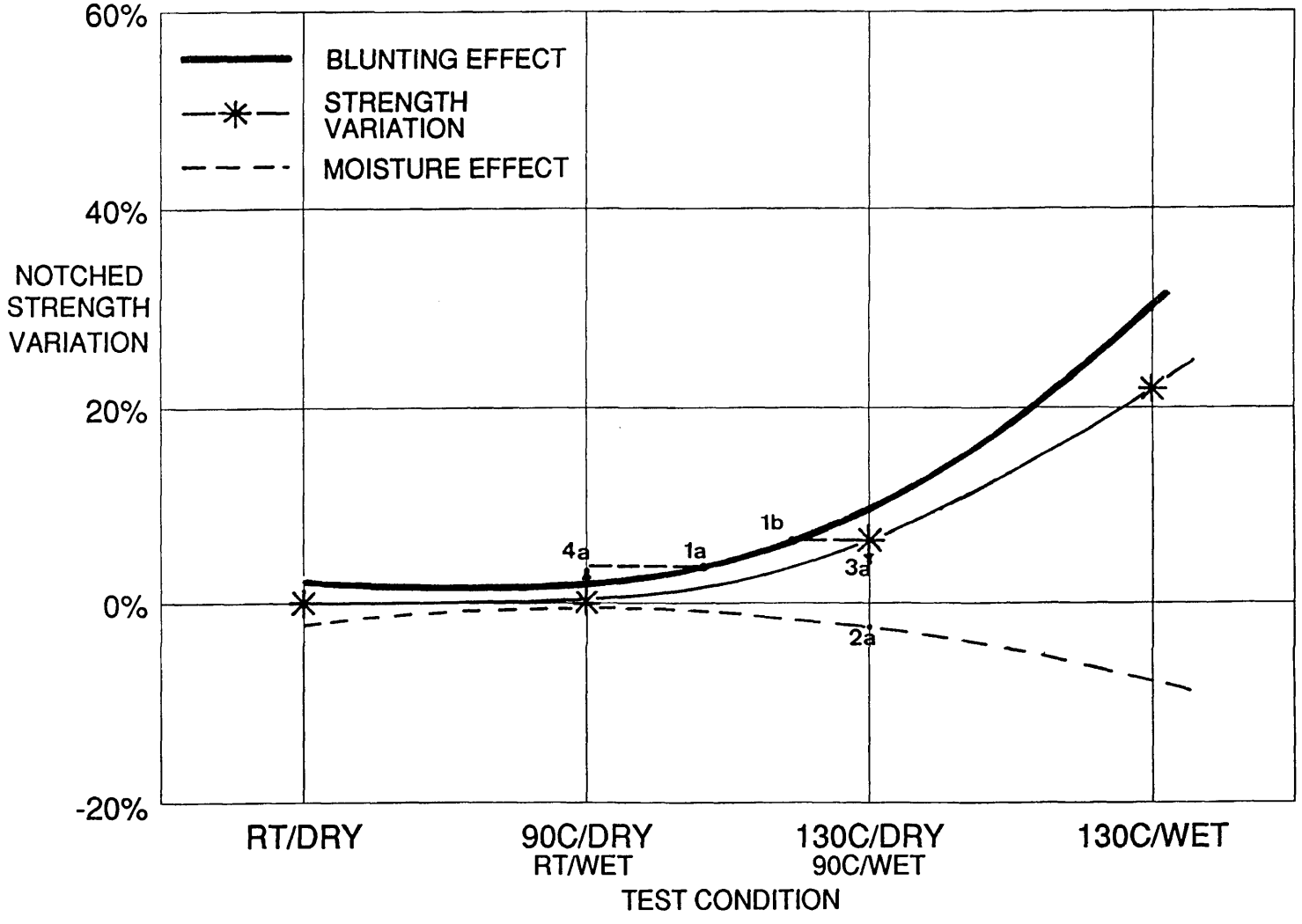


Fig. 6.4 Schematic presentation of the effect of blunting and moisture upon the observed notched static tensile strength increase with increasing temperature and/or moisture content for 914C, stacking sequence **A** specimens containing sharp notches.

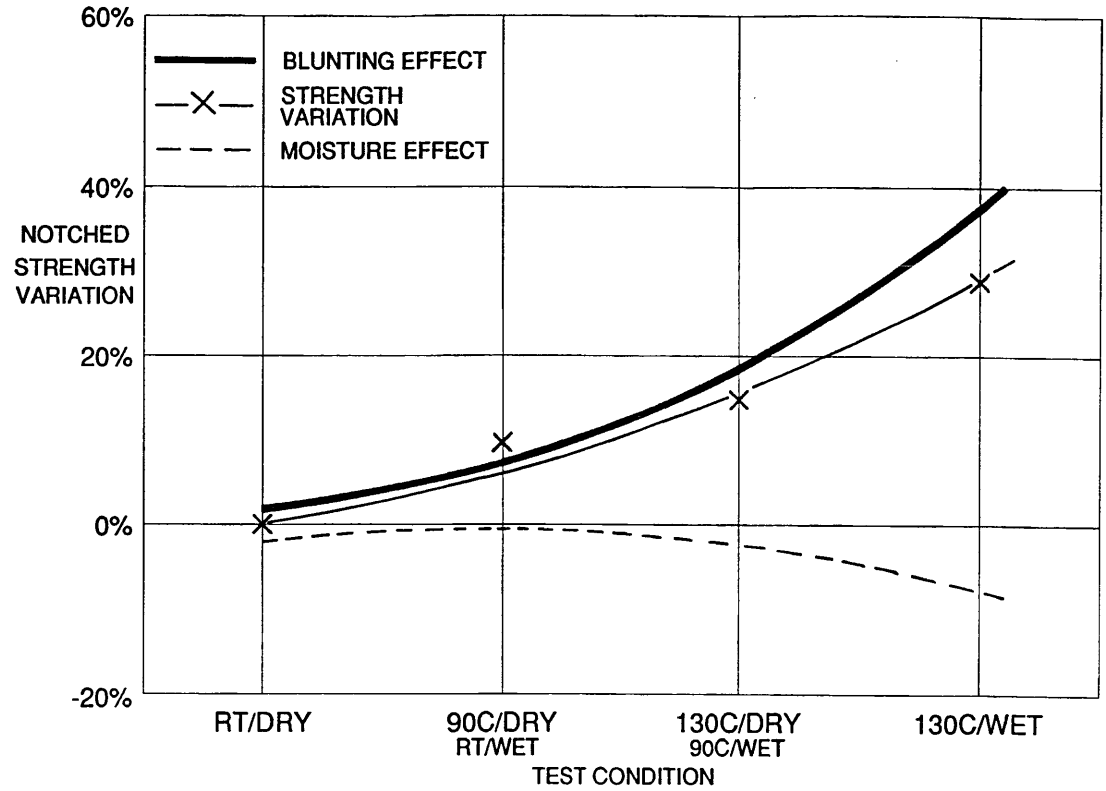


Fig. 6.5 Schematic presentation of the effect of blunting and moisture upon the observed notched static tensile strength increase with increasing temperature and/or moisture content for 914C, stacking sequence **B** specimens containing sharp notches.

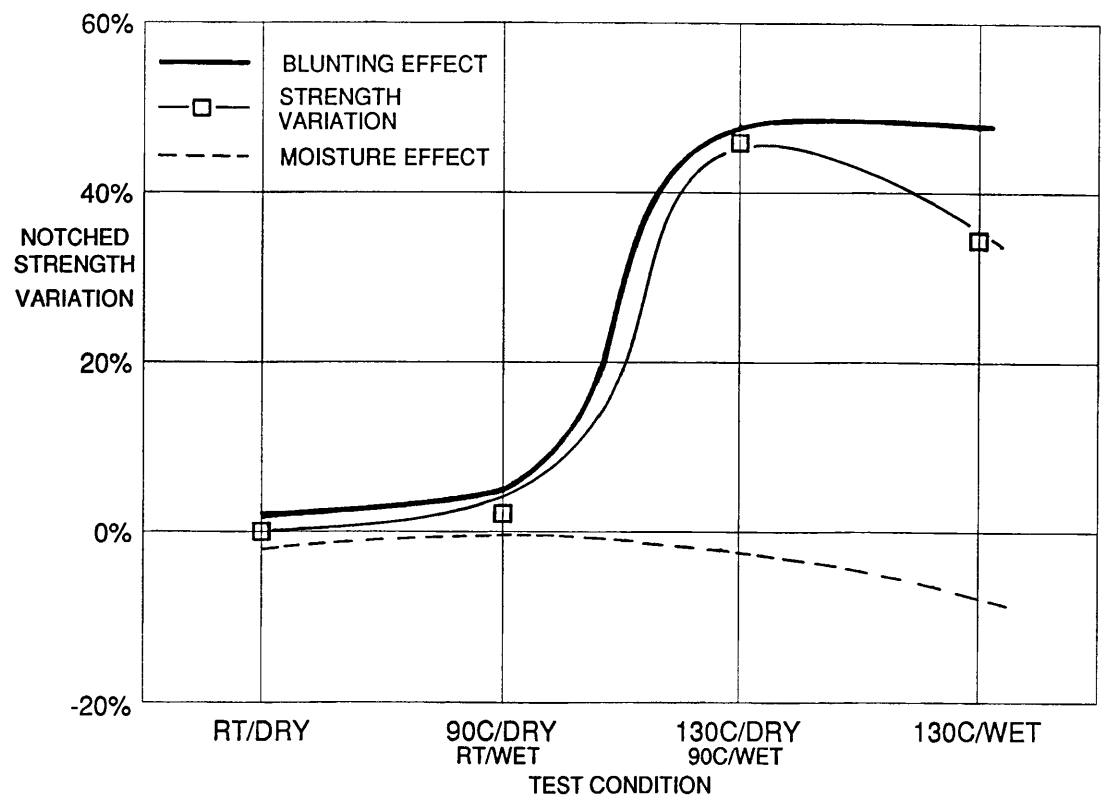


Fig. 6.6 Schematic presentation of the effect of blunting and moisture upon the observed notched static tensile strength increase with increasing temperature and/or moisture content for 914C, stacking sequence **A** specimens containing circular holes.

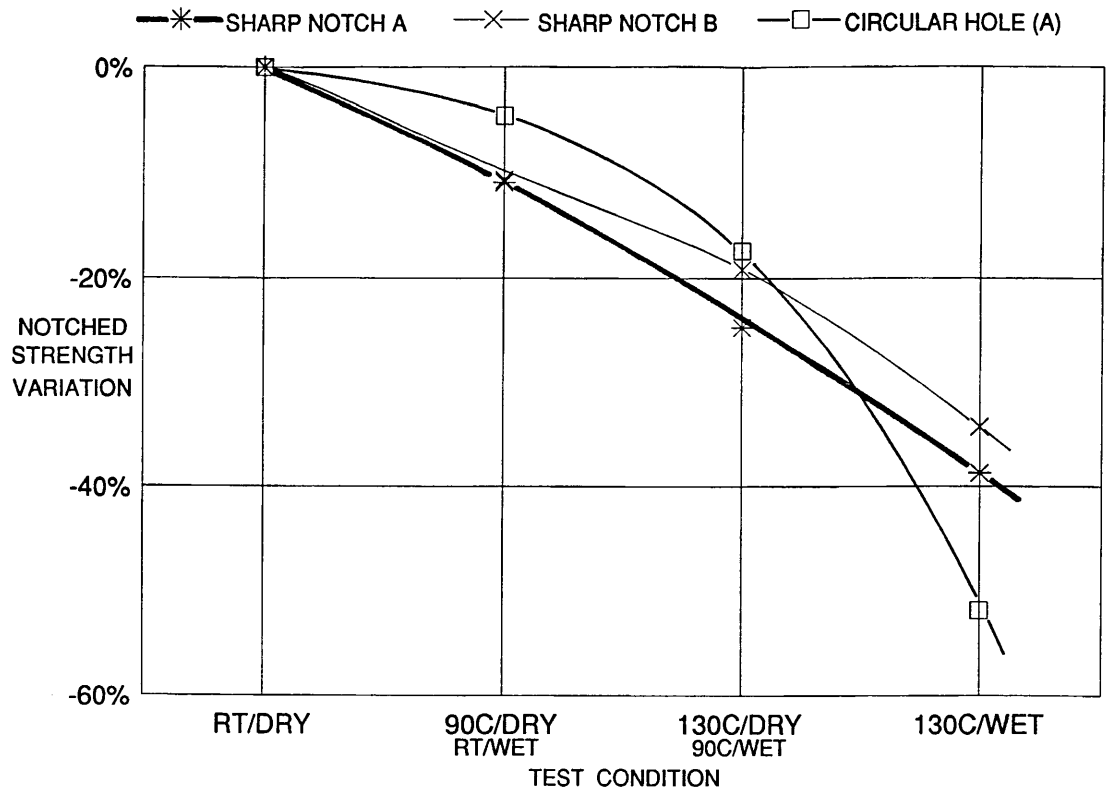


Fig. 6.7 Plot of the notched compressive strength variation with increasing temperature and/or moisture content, in 914C specimens.

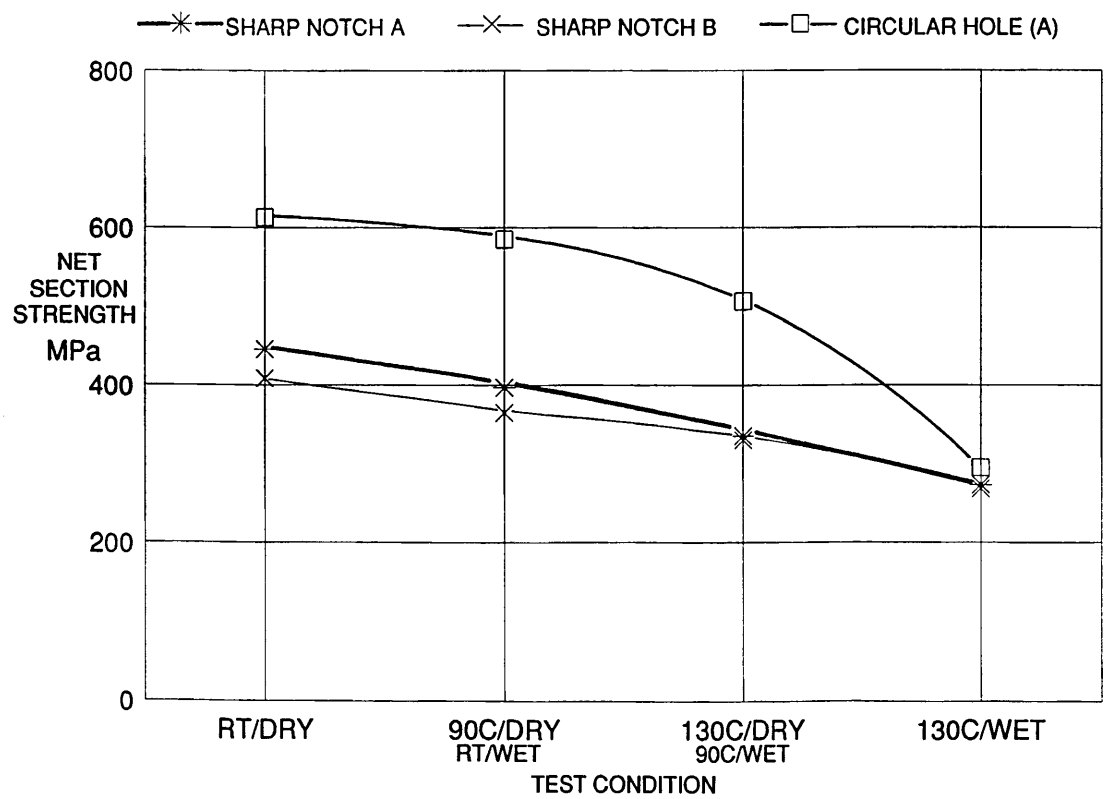


Fig. 6.8 Plot of the compressive net-section strength versus with increasing temperature and/or moisture content, in 914C specimens.

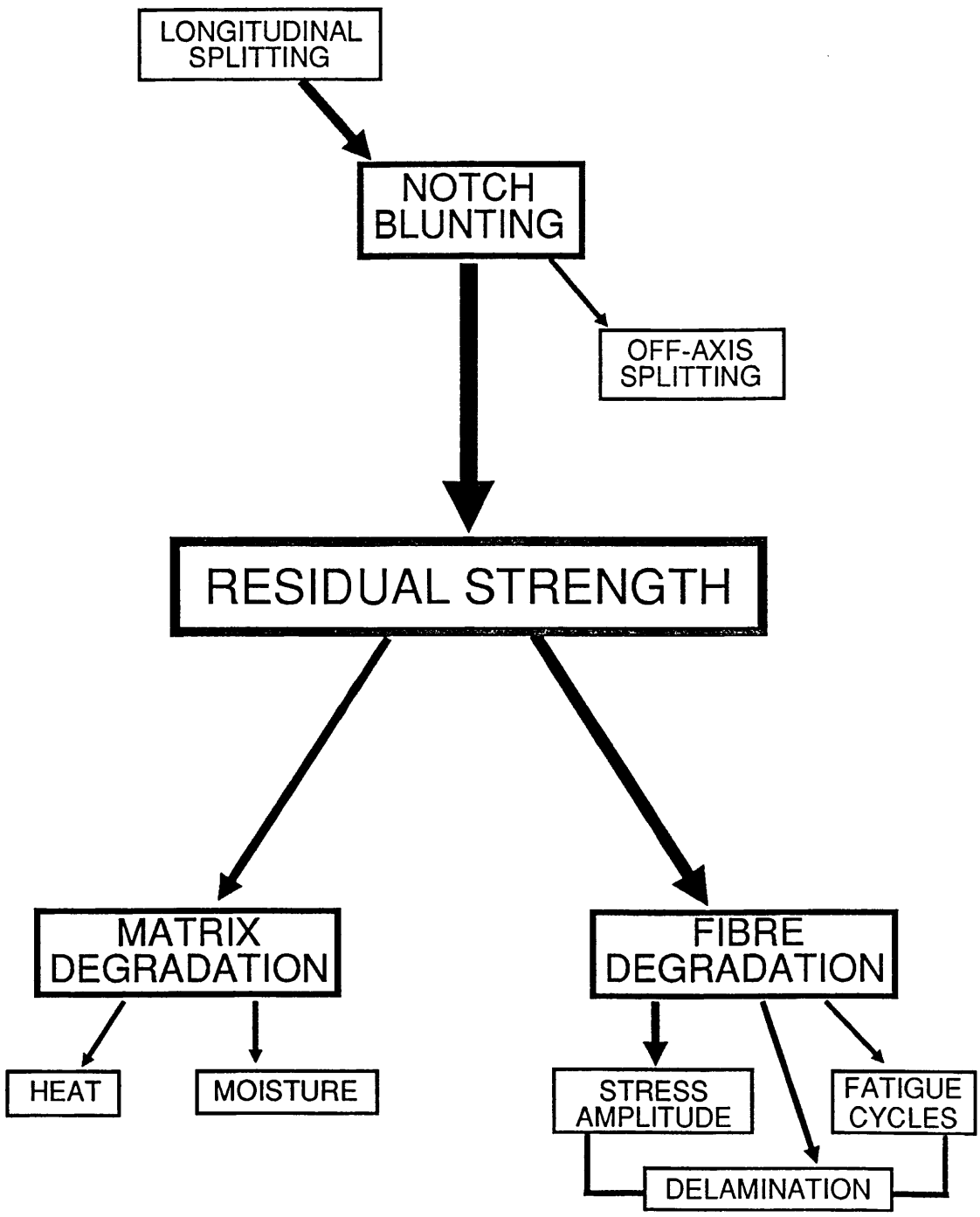


Fig. 6.9 A schematic model, demonstrating the effect of several fatigue damage mechanisms upon residual strength.

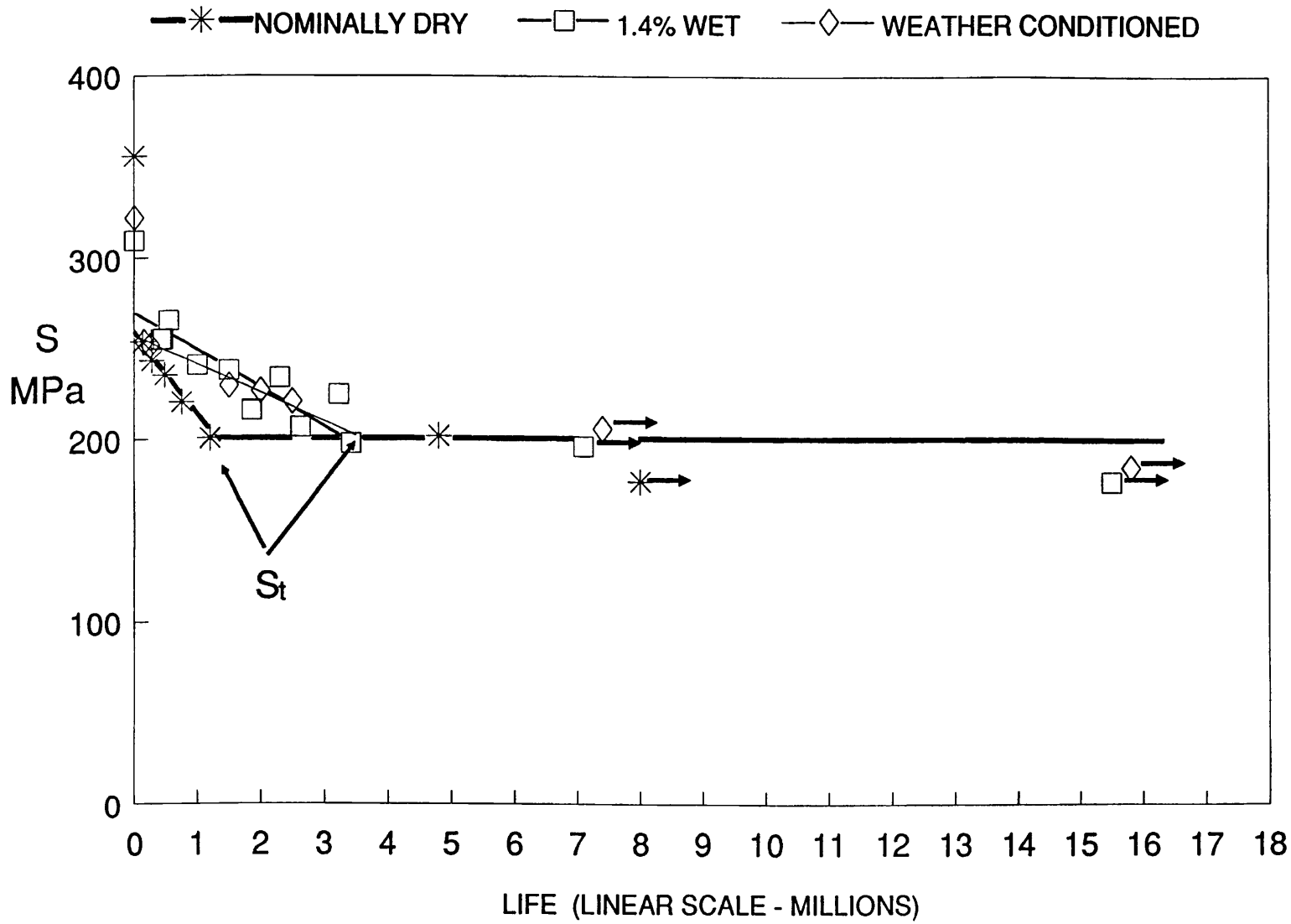


Fig. 6.10 Cyclic stress amplitude versus "linear" fatigue cycles for dry and wet 914C, stacking sequence **A** specimens containing **sharp 10mm notches**, tested at RT. This plot is referred to in the text as a "linear S-N plot".

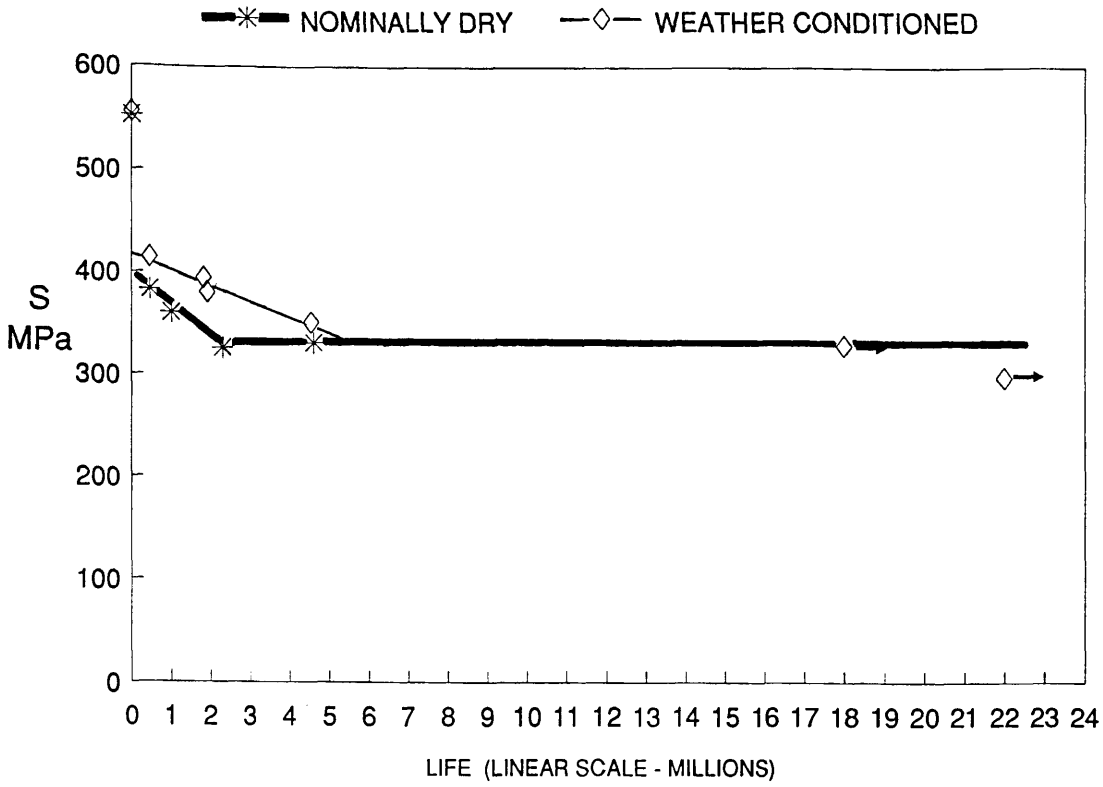


Fig. 6.11 Cyclic stress amplitude versus "linear" fatigue cycles for dry and wet 914C, stacking sequence **A** specimens containing **circular 5mm holes**, tested at RT. This plot is referred to in the text as a "linear S-N plot".

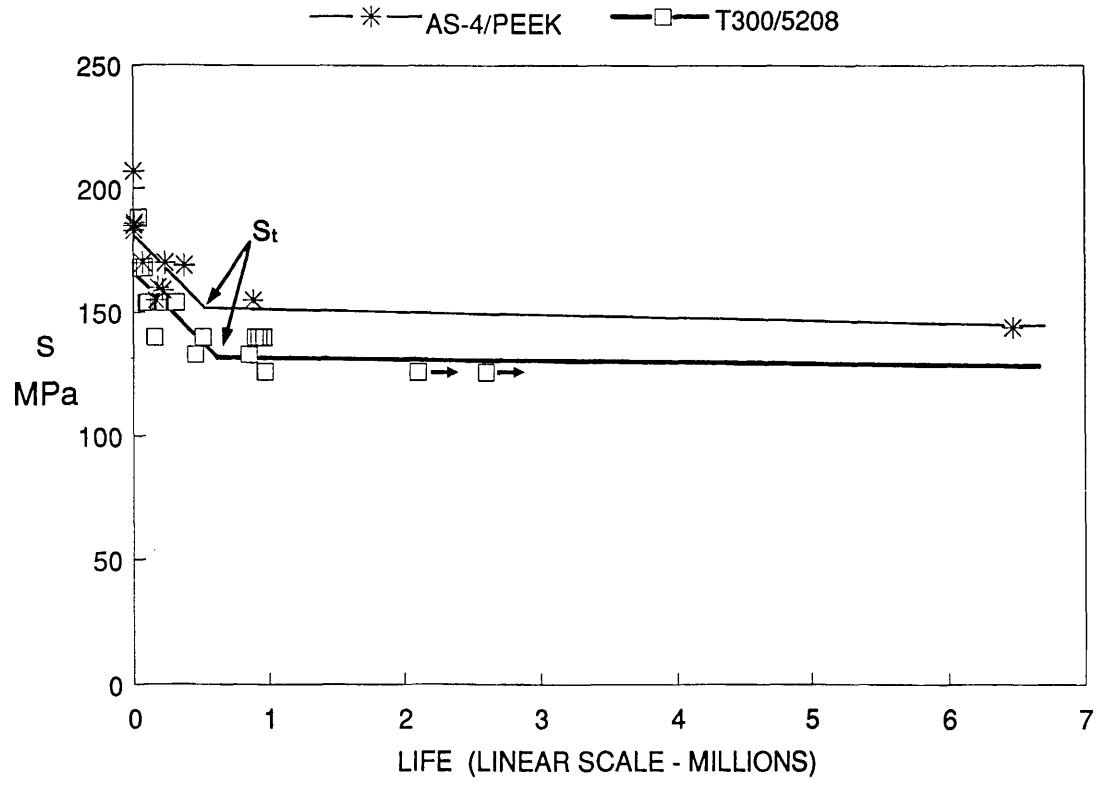


Fig. 6.12 Linear S-N plots for specimens of quas-isotropic lay-up containing a circular hole, tested at RT in tension-compression. The data has been extracted from **reference 101.**

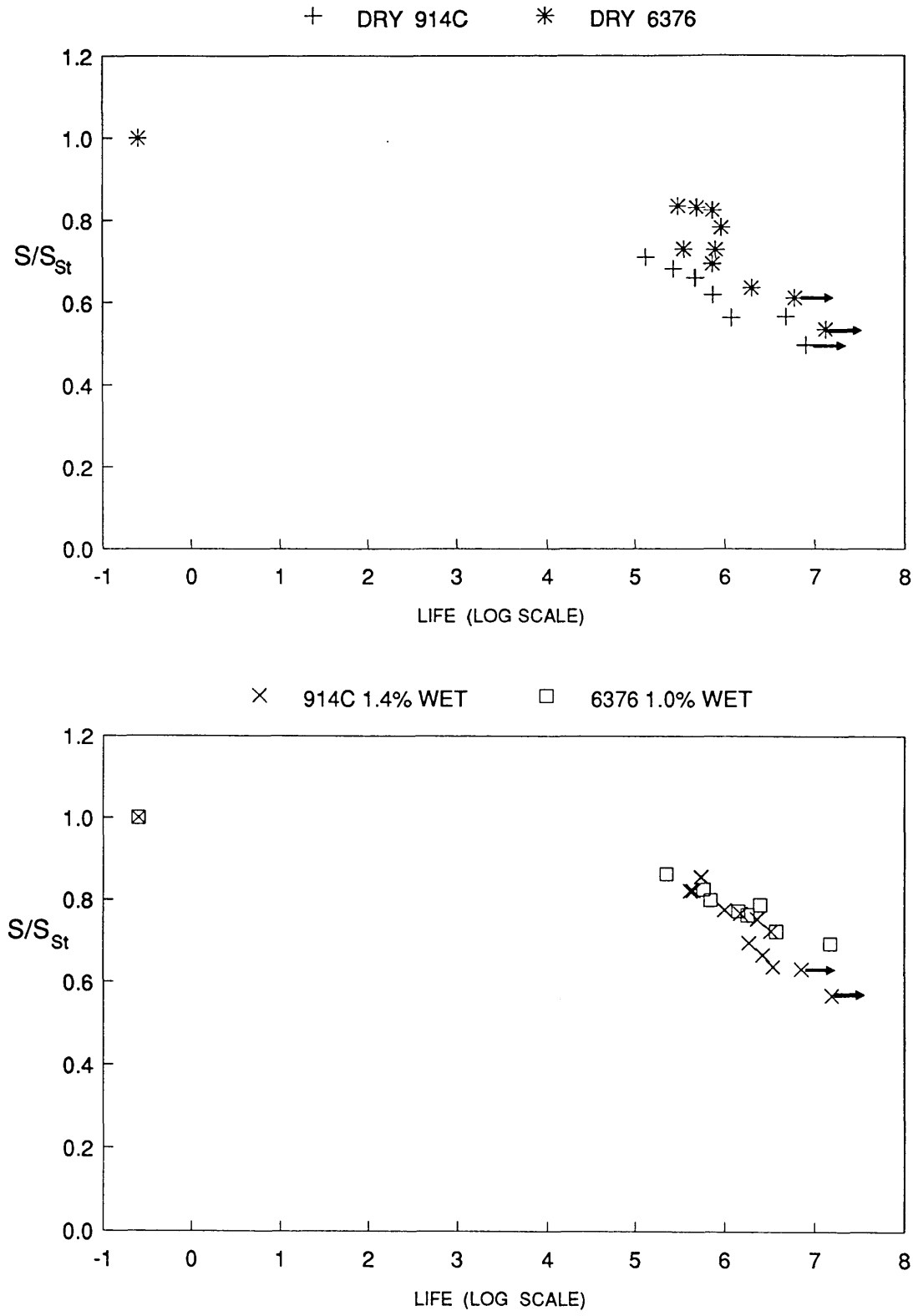


Fig. 6.13 A comparison of S-N plots for **914C** and **6376C.** The cyclic stress amplitude has been normalised with respect to the corresponding RT notched compressive strength.

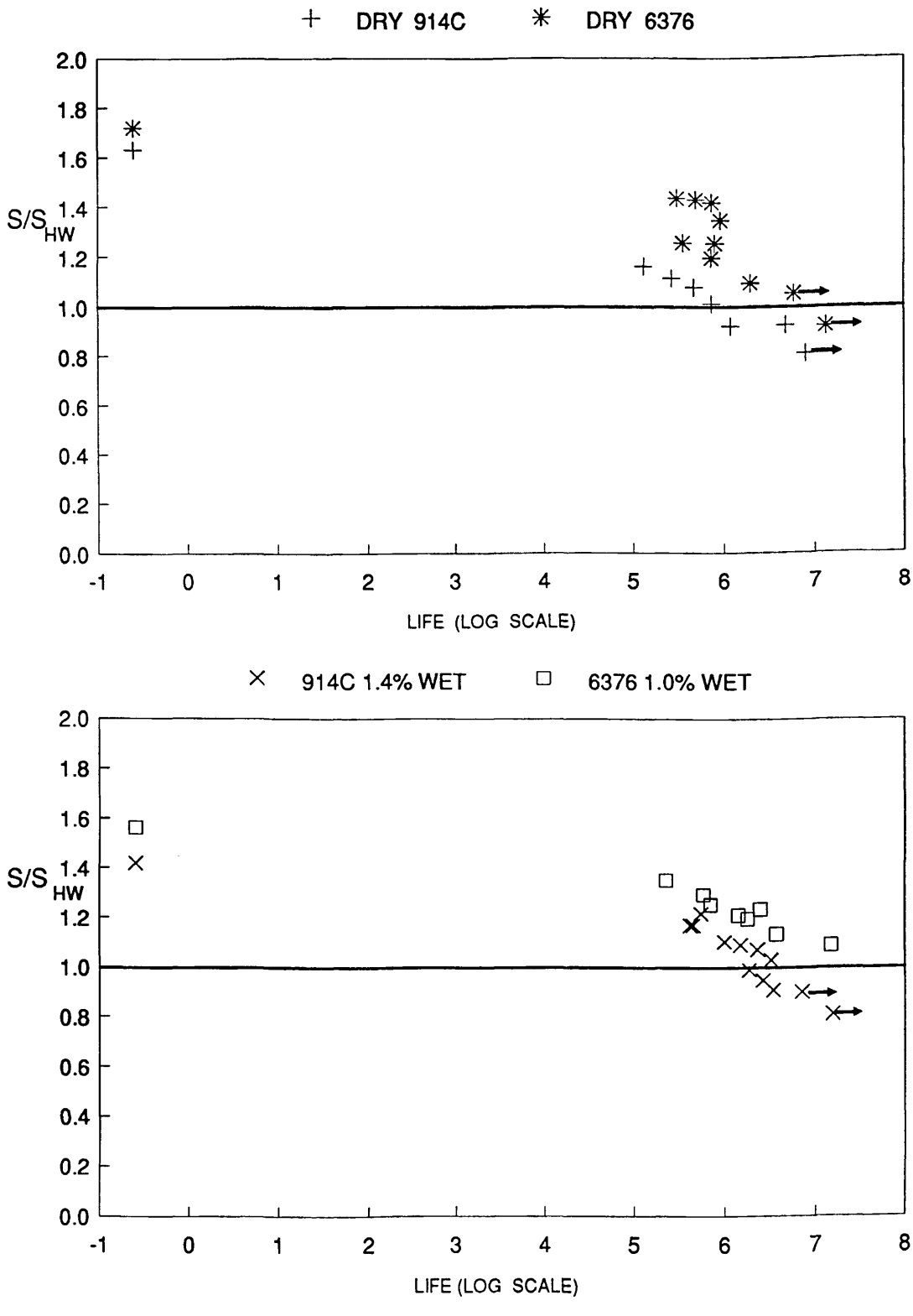


Fig. 6.14 A comparison of S-N plots for **914C** and **6376C.** The cyclic stress amplitude has been normalised with respect to the corresponding hot/wet notched compressive strength.

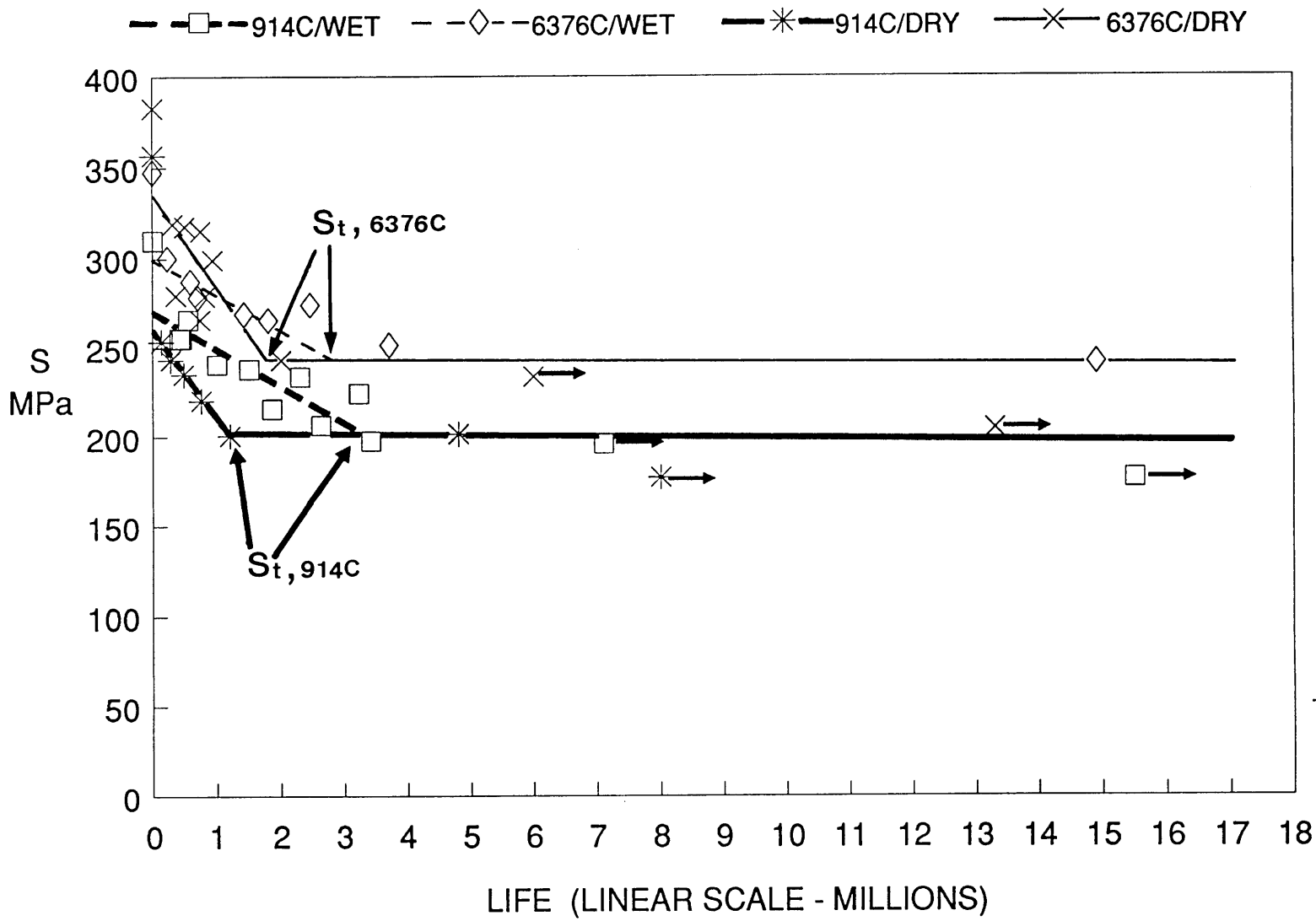


Fig. 6.15 A comparison of linearly plotted S-N data for **914C** and **6376C.**

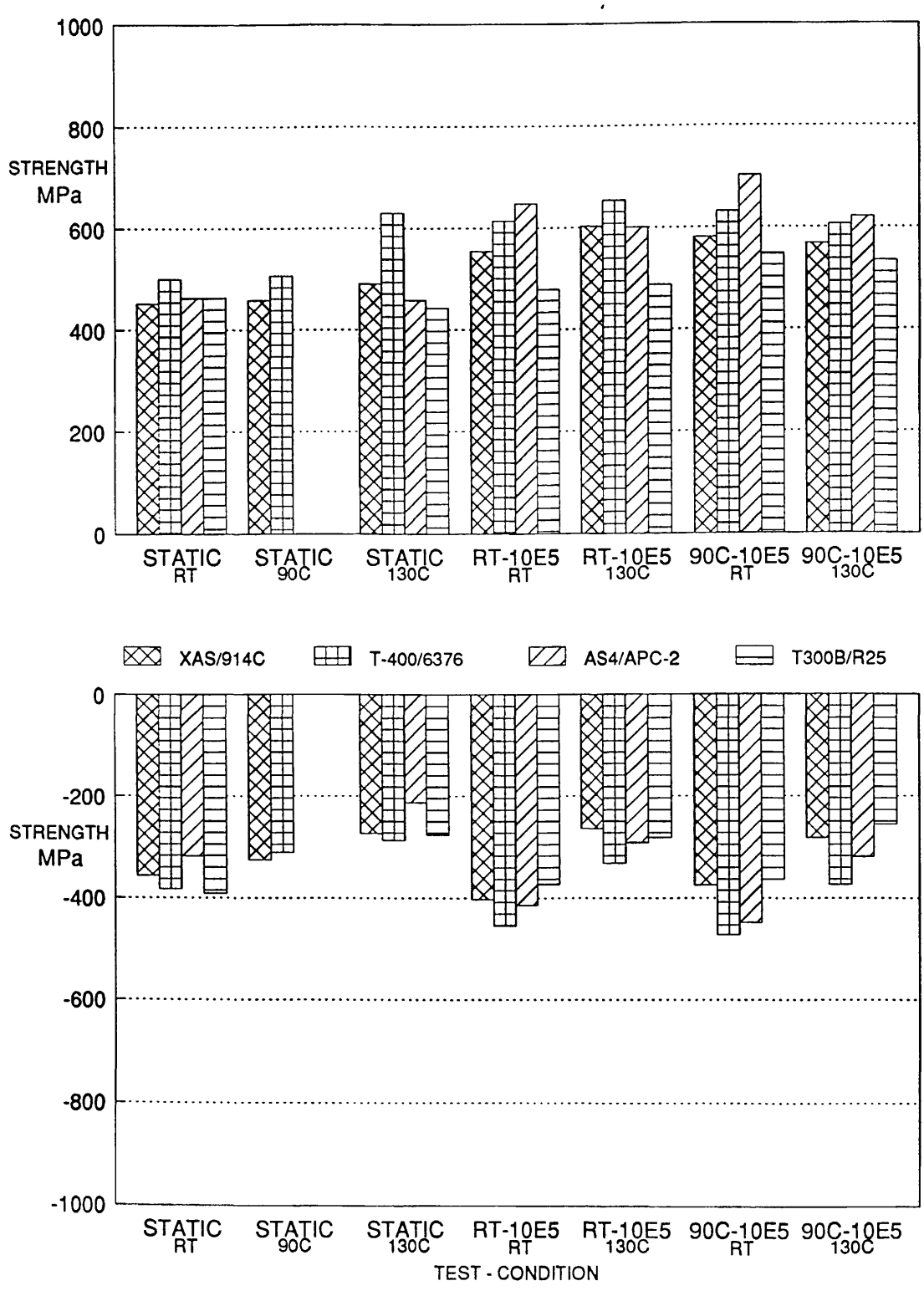


Fig. 6.16 A comparison of the notched static and residual strength results for all material systems examined. All specimens were tested dry.

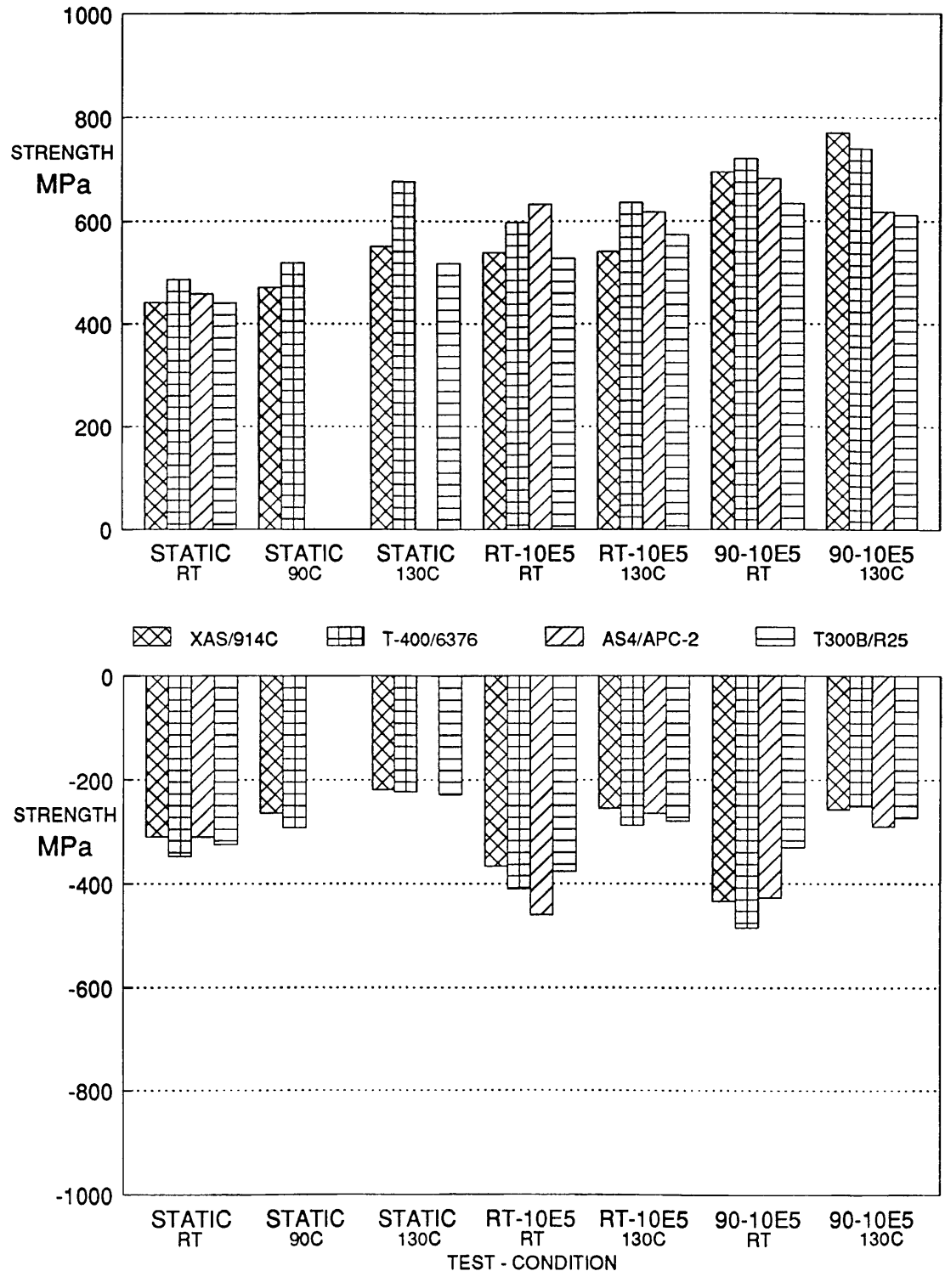


Fig. 6.17 A comparison of the notched static and residual strength results for all material systems examined. All specimens were tested wet.

TABLE 1: PLAIN (UNNOTCHED) TENSILE STRENGTH FOR WET AND DRY 914C, TESTED AT RT

STACKING SEQUENCE	ENVIRONMENTAL EXPOSURE	TIME OF EXPOSURE MONTHS	AVERAGE MOISTURE %	NO. OF VALID TESTS	STRENGTH MPa	STANDARD DEVIATION
A	RT/ 0% RH	17	0.00	9	1132.1	40.7
A	60C/84%RH	17	1.22	13	1189.7	34.1
A	60C/84%RH	29	1.21	9	1209.1	38.9
A	RT/100% RH	16	1.96	5	1091.6	33.0
A	LONDON WEATHER	29	0.53	3	1095.2	64.8
B	RT/ 0% RH	17	0.00	/	/	/
B	60C/84% RH	17	1.24	5	1092.1	30.0

TABLE 2: INTERLAMINAR SHEAR STRENGTH FOR WET AND DRY UNIDIRECTIONAL 914C, AT RT

ENVIRONMENTAL EXPOSURE	TIME OF EXPOSURE MONTHS	AVERAGE MOISTURE %	AVERAGE THICKNESS mm	NO. OF SPECIMENS TESTED	ILSS MPa	STANDARD DEVIATION
RT/ 0% RH	19	0.00	1.98	18	110.3	3.1
RT/ 0% RH	29	0.00	2.00	15	112.7	3.3
60C/84%RH	3	1.29	2.01	17	99.1	2.1
60C/84%RH	13	1.35	1.99	16	103.8	2.6
60C/84%RH	19	1.34	1.97	25	99.2	1.6
60C/84%RH	29	1.37	2.00	20	99.9	2.1

TABLE 3: EXPERIMENTALLY OBTAINED ELASTIC PROPERTIES OF WET AND DRY 914C, RT

ELASTIC PROPERTY	TEST METHOD	SPECIMEN* TYPE	DRY VALUE	WET VALUE
E_{11}	TENSION	②	137.10 GPa	129.40 GPa
E_{22}	TENSION	③	9.86 GPa	9.17 GPa
ν_{12}	TENSION	②	0.32	0.35
ν_{23}	TENSION	③	0.50	0.51
G_{12}	TENSION	④	5.98-2.25 GPa (0%-1% SHEAR STRAIN)	5.98-1.80 GPa
G_{23}	3-P BEND	①	3.89 GPa	3.77 GPa

* See figure 3.12

TABLE 4: NOTCHED STATIC STRENGTH RESULTS
914C, 10mm NOTCH, DRY, STACKING SEQUENCE A

TEST TEMPERATURE	SPECIMEN NUMBER	NOTCH SIZE mm	X-SECTION AREA $(mm)^2$	NORMALISED STRENGTH MPa	AVERAGE STRENGTH MPa
			TENSION		
RT	46	10.06	102.01	444.6	451.8
	77	10.08	102.25	450.2	6.6*
	78	9.93	99.38	460.5	
90C	149	10.05	100.96	457.6	457.8
	160	10.08	100.40	465.5	6.2
	170	9.96	101.97	450.2	
130C	58	9.94	101.59	467.5	490.4
	137	9.94	101.63	504.1	16.3
	140	10.07	100.40	499.7	
			COMPRESSION		
RT	59	9.93	102.85	-368.6	-356.5
	128	10.07	102.95	-364.9	14.5
	167	9.95	102.99	-336.1	
90C	28	9.95	102.12	-312.6	-325.4
	116	9.96	100.46	-327.8	9.6
	119	10.06	101.53	-335.8	
130C	10	10.09	100.48	-263.9	-272.9
	39	10.02	101.56	-281.9	7.3
	166	9.97	98.93	-273.0	

* Standard Deviation

TABLE 5: NOTCHED STATIC STRENGTH RESULTS
914C, 10mm NOTCH, 1.4% WET, STACKING SEQUENCE A

TEST TEMPERATURE	SPECIMEN NUMBER	NOTCH SIZE mm	X-SECTION AREA $(mm)^2$	NORMALISED STRENGTH MPa	AVERAGE STRENGTH MPa
			TENSION		
RT	2	10.02	100.42	459.3	441.5
	33	10.00	103.10	420.8	15.9
	45	9.99	102.83	444.5	
90C	35	9.93	101.50	468.3	470.4
	112	9.99	103.49	463.1	6.9
	123	10.08	102.64	479.7	
130C	102	9.99	102.44	584.4	550.7
	115	10.05	101.91	590.2	51.8
	154	9.98	101.64	477.5	
			COMPRESSION		
RT	72	9.97	101.71	-314.9	-309.9
	84	10.00	101.23	-315.5	7.5
	171	10.04	102.39	-299.3	
90C	25	10.02	102.93	-260.6	-263.6
	31	10.02	99.61	-261.3	3.8
	145	9.98	101.95	-269.0	
130C	73	10.01	102.62	-209.6	-218.5
	164	10.07	102.24	-216.9	8.0
	173	9.93	102.22	-229.1	

TABLE 6: NOTCHED STATIC STRENGTH RESULTS
914C, 10mm NOTCH, STACKING SEQUENCE A
WEATHER CONDITIONED FOR OVER TWO YEARS

TEST TEMPERATURE	SPECIMEN NUMBER	NOTCH SIZE mm	X-SECTION AREA $(mm)^2$	NORMALISED STRENGTH MPa	AVERAGE STRENGTH MPa
			TENSION		
RT	/	/	/	/	/
	/	/	/	/	/
	/	/	/	/	/
90C	/	/	/	/	/
	/	/	/	/	/
	/	/	/	/	/
130C	/	/	/	/	/
	/	/	/	/	/
	/	/	/	/	/
			COMPRESSION		
RT	5	9.57	101.51	-307.4	-322.5
	6	10.13	101.66	-338.6	12.8
	8	10.00	102.62	-321.6	
90C	/	/	/	/	/
	/	/	/	/	/
	/	/	/	/	/
130C	/	/	/	/	/
	/	/	/	/	/
	/	/	/	/	/

TABLE 7: NOTCHED STATIC STRENGTH RESULTS
914C, 10mm NOTCH, DRY, STACKING SEQUENCE B

TEST TEMPERATURE	SPECIMEN NUMBER	NOTCH SIZE mm	X-SECTION AREA $(mm)^2$	NORMALISED STRENGTH MPa	AVERAGE STRENGTH MPa
			TENSION		
RT	6	9.93	101.85	385.9	403.3
	36	10.02	101.24	420.6	17.4
90C	8	9.96	101.40	421.1	431.8
	20	10.02	99.85	442.5	10.7
130C	9	10.14	102.12	460.9	454.1
	28	10.16	99.43	447.2	6.9
			COMPRESSION		
RT	37	9.98	100.40	-315.2	-326.8
	40	10.06	98.99	-338.4	11.6
90C	17	10.10	99.67	-269.2	-281.3
	39	9.90	100.68	-293.4	12.1
130C	16	9.89	100.84	-276.1	-272.5
	48	9.71	101.53	-268.8	3.7

TABLE 8: NOTCHED STATIC STRENGTH RESULTS
914C, 10mm NOTCH, I.4% WET, STACKING SEQUENCE B

TEST TEMPERATURE	SPECIMEN NUMBER	NOTCH SIZE mm	X-SECTION AREA $(mm)^2$	NORMALISED STRENGTH MPa	AVERAGE STRENGTH MPa
			TENSION		
RT	11	9.96	101.98	460.0	452.7
	42	10.05	100.36	445.3	7.4
90C	21	9.93	101.20	470.7	472.3
	31	10.06	98.74	473.9	1.6
130C	3	10.13	101.82	527.2	519.6
	44	9.91	101.10	511.9	7.7
			COMPRESSION		
RT	2	9.97	99.44	-304.7	-302.7
	24	10.00	100.42	-300.7	2.0
90C	33	10.00	99.66	-265.3	-255.6
	45	9.99	99.43	-245.8	9.8
130C	5	9.84	102.22	-211.0	-214.8
	-43	10.17	101.49	-218.6	3.8

TABLE 9: NOTCHED STATIC STRENGTH RESULTS
914C, 5mm HOLE, DRY, STACKING SEQUENCE A

TEST TEMPERATURE	SPECIMEN NUMBER	X-SECTION AREA $(mm)^2$	FAILURE STRESS MPa	AVERAGE STRENGTH MPa
		TENSION		
RT	6	102.28	659.0	645.4
	46	101.66	666.4	24.7
	76	101.43	610.8	
90C	10	100.00	632.0	655.0
	58	101.62	718.4	45.4
	86	101.54	614.5	
130C	30	102.30	924.7	945.0
	37	100.90	916.7	34.5
	66	101.16	993.5	
		COMPRESSION		
RT	8	102.22	-526.8	-551.9
	49	101.60	-601.4	35.0
	77	101.41	-527.6	
90C	18	102.57	-494.8	-527.1
	60	101.52	-531.4	24.8
	90	101.58	-555.2	
130C	28	102.22	-584.0	-502.2
	39	102.49	-448.8	58.8
	67	101.39	-473.9	

TABLE 10: NOTCHED STATIC STRENGTH RESULTS
914C, 5mm HOLE, 1.4% WET, STACKING SEQUENCE A

TEST TEMPERATURE	SPECIMEN NUMBER	X-SECTION AREA $(mm)^2$	FAILURE STRESS MPa	AVERAGE STRENGTH MPa
TENSION				
RT	2	102.02	659.7	663.0
	22	103.74	665.1	2.4
	61	101.62	664.2	
90C	24	101.36	924.9	937.6
	63	101.66	964.5	19.1
	101	100.78	923.3	
130C	4	102.45	872.6	867.4
	44	101.12	860.8	4.9
	115	102.28	868.7	
COMPRESSION				
RT	33	100.32	-454.5	-526.3
	53	100.84	-582.3	53.3
	113	101.28	-542.0	
90C	13	102.99	-491.3	-409.6
	55	99.91	-419.9	71.3
	82	100.91	-317.6	
130C	14	103.07	-247.4	-265.7
	34	101.89	-266.5	14.7
	83	100.79	-283.3	

TABLE 11: NOTCHED STATIC STRENGTH RESULTS
914C, 5mm HOLE, 2.0% WET, STACKING SEQUENCE A

TEST TEMPERATURE	SPECIMEN NUMBER	X-SECTION AREA $(mm)^2$	FAILURE STRESS MPa	AVERAGE STRENGTH MPa
TENSION				
RT	/	/	/	/
	/	/	/	/
90C	/	/	/	/
	/	/	/	/
130C	/	/	/	/
	/	/	/	/
COMPRESSION				
RT	15	100.30	-438.2	-464.7
	16	101.28	-491.2	26.5
90C	17	101.74	-314.5	-317.7
	18	101.30	-320.8	3.2
130C	/	/	/	/
	/	/	/	/

TABLE 12: NOTCHED STATIC STRENGTH RESULTS
914C, 5mm HOLE, STACKING SEQUENCE A
WEATHER CONDITIONED FOR OVER TWO YEARS

TEST TEMPERATURE	SPECIMEN NUMBER	X-SECTION AREA $(mm)^2$	FAILURE STRESS MPa	AVERAGE STRENGTH MPa
		TENSION		
RT	/	/	/	/
	/	/	/	/
	/	/	/	/
90C	/	/	/	/
	/	/	/	/
	/	/	/	/
130C	/	/	/	/
	/	/	/	/
	/	/	/	/
		COMPRESSION		
RT	2	100.84	-511.7	-555.5
	4	99.34	-603.0	37.4
	6	101.30	-551.8	
90C	/	/	/	/
	/	/	/	/
	/	/	/	/
130C	/	/	/	/
	/	/	/	/
	/	/	/	/

TABLE 13; RESIDUAL STRENGTHS AFTER RT/10^3 CYCLES
914C, 10mm NOTCH, DRY, STACKING SEQUENCE A

TEST TEMPERATURE	SPECIMEN NUMBER	NOTCH SIZE mm	X-SECTION AREA $(mm)^2$	NORMALISED STRENGTH MPa	AVERAGE STRENGTH MPa
			TENSION		
RT	26	10.34	99.90	471.7	459.1
	159	10.35	100.46	446.5	12.6
90C	49	10.46	101.05	447.2	463.3
	88	9.67	101.73	479.3	16.1
130C	60	10.39	103.10	485.3	489.6
	129	9.86	101.40	493.9	4.3
			COMPRESSION		
RT	36	10.42	100.67	-392.9	-395.5
	40	9.85	101.23	-398.0	2.6
90C	97	9.96	99.92	-319.6	-325.1
	117	10.27	101.17	-330.5	5.5
130C	79	10.11	102.96	-307.5	-311.8
	106	10.21	100.55	-316.0	4.3

TABLE 14; RESIDUAL STRENGTHS AFTER 90C/10^3 CYCLES
914C, 10mm NOTCH, DRY, STACKING SEQUENCE A

TEST TEMPERATURE	SPECIMEN NUMBER	NOTCH SIZE mm	X-SECTION AREA $(mm)^2$	NORMALISED STRENGTH MPa	AVERAGE STRENGTH MPa
			TENSION		
RT	18	10.77	100.67	456.9	464.8
	37	10.25	100.55	472.6	7.9
90C	69	10.11	101.34	486.2	495.2
	80	10.34	102.59	504.1	9.0
130C	108	9.74	102.37	467.5	480.7
	120	10.13	100.67	493.9	13.2
			COMPRESSION		
RT	47	10.39	101.07	-378.1	-377.9
	67	10.26	99.34	-377.7	0.2
90C	89	10.16	99.42	-329.4	-344.7
	98	9.72	99.97	-360.0	15.3
130C	127	10.48	101.09	-310.9	-312.2
	136	10.18	101.72	-313.4	1.3

TABLE 15; RESIDUAL STRENGTHS AFTER RT/10^5 CYCLES
914C, 10mm NOTCH, DRY, STACKING SEQUENCE A

TEST TEMPERATURE	SPECIMEN NUMBER	NOTCH SIZE mm	X-SECTION AREA $(mm)^2$	NORMALISED STRENGTH MPa	AVERAGE STRENGTH MPa
			TENSION		
RT	30	10.11	101.59	529.7	554.0
	139	10.59	100.17	578.2	24.3
90C	48	10.47	101.76	523.8	562.2
	90	9.82	99.46	600.5	38.4
130C	118	10.67	99.59	615.6	602.4
	130	10.11	100.15	589.2	13.2
			COMPRESSION		
RT	56	10.37	101.85	-404.3	-402.8
	86	9.86	101.94	-401.2	1.6
90C	66	10.17	100.36	-340.0	-341.3
	99	10.15	99.98	-342.5	1.3
130C	107	10.11	102.66	-237.2	-263.4
	110	10.11	98.87	-289.5	26.2

TABLE 16; RESIDUAL STRENGTHS AFTER 90C/10^5CYCLES
914C, 10mm NOTCH, DRY, STACKING SEQUENCE A

TEST TEMPERATURE	SPECIMEN NUMBER	NOTCH SIZE mm	X-SECTION AREA $(mm)^2$	NORMALISED STRENGTH MPa	AVERAGE STRENGTH MPa
			TENSION		
RT	19	10.22	101.82	561.0	580.2
	138	10.47	101.13	599.3	19.2
90C	20	10.43	102.26	574.1	595.3
	126	10.23	101.89	616.4	21.2
130C	70	9.87	100.38	544.8	567.9
	87	10.38	100.84	590.9	23.1
			COMPRESSION		
RT	50	10.16	101.54	-415.0	-374.2
	96	9.62	100.61	-333.4	40.8
90C	100	9.72	100.41	-278.4	-301.5
	146	10.23	100.17	-324.6	23.1
130C	68	9.87	102.37	-274.1	-281.0
	109	9.91	101.63	-287.9	6.9

TABLE 17; RESIDUAL STRENGTHS AFTER RT/10^3CYCLES
914C, 10mm NOTCH, 1.4% WET, STACKING SEQUENCE A

TEST TEMPERATURE	SPECIMEN NUMBER	NOTCH SIZE mm	X-SECTION AREA $(mm)^2$	NORMALISED STRENGTH MPa	AVERAGE STRENGTH MPa
			TENSION		
RT	21	10.26	98.89	485.0	482.0
	65	10.06	102.62	478.9	3.1
90C	14	9.78	100.15	467.1	472.6
	51	9.91	101.51	478.1	5.5
130C	44	10.30	102.64	530.8	550.1
	75	9.79	102.42	569.4	19.3
			COMPRESSION		
RT	55	9.81	101.93	-341.1	-342.3
	85	9.92	101.67	-343.4	1.2
90C	94	9.86	100.94	-309.9	-308.0
	104	10.71	102.62	-306.1	1.9
130C	111	10.23	99.80	-260.9	-266.5
	125	10.50	101.65	-272.1	5.6

TABLE 18; RESIDUAL STRENGTHS AFTER 90C/10^3CYCLES
914C, 10mm NOTCH, 1.4% WET, STACKING SEQUENCE A

TEST TEMPERATURE	SPECIMEN NUMBER	NOTCH SIZE mm	X-SECTION AREA $(mm)^2$	NORMALISED STRENGTH MPa	AVERAGE STRENGTH MPa
			TENSION		
RT	22	10.56	100.38	476.0	482.9
	61	10.42	102.12	489.8	6.9
90C	43	9.90	100.13	472.9	497.5
	91	9.64	101.86	522.0	24.6
130C	52	9.89	102.57	523.4	524.0
	113	10.18	101.75	524.6	0.6
			COMPRESSION		
RT	64	9.60	101.38	-357.5	-371.5
	95	9.84	101.50	-385.5	14.0
90C	81	9.83	101.46	-301.9	-306.4
	133	10.21	102.41	-310.9	4.5
130C	105	9.79	102.69	-237.0	-259.6
	143	10.59	101.74	-282.1	22.6

TABLE 19; RESIDUAL STRENGTHS AFTER RT/10^5CYCLES
914C, 10mm NOTCH, 1.4% WET, STACKING SEQUENCE A

TEST TEMPERATURE	SPECIMEN NUMBER	NOTCH SIZE mm	X-SECTION AREA $(mm)^2$	NORMALISED STRENGTH MPa	AVERAGE STRENGTH MPa
			TENSION		
RT	103	10.36	102.97	496.2	538.5
	114	10.15	100.19	580.7	42.3
90C	62	9.79	100.40	552.9	544.3
	122	10.28	102.39	535.6	8.7
130C	71	10.40	99.96	550.9	540.9
	92	10.08	101.29	530.8	10.1
			COMPRESSION		
RT	42	10.97	101.30	-354.6	-366.3
	82	9.78	102.00	-378.0	11.7
90C	11	10.67	102.83	-315.9	-311.6
	23	10.26	102.68	-307.2	4.4
130C	32	10.26	100.37	-248.3	-254.6
	53	10.96	102.33	-260.8	6.3

TABLE 20; RESIDUAL STRENGTHS AFTER 90C/10^5CYCLES
914C, 10mm NOTCH, 1.4% WET, STACKING SEQUENCE A

TEST TEMPERATURE	SPECIMEN NUMBER	NOTCH SIZE mm	X-SECTION AREA $(mm)^2$	NORMALISED STRENGTH MPa	AVERAGE STRENGTH MPa
			TENSION		
RT	12	10.40	102.35	629.6	695.0
	93	10.14	101.98	760.3	65.4
90C	41	9.88	101.09	628.3	669.1
	101	9.81	101.84	709.0	40.8
130C	74	10.18	102.00	752.1	771.4
	124	10.32	102.83	790.6	19.3
			COMPRESSION		
RT	24	10.29	102.31	-441.2	-433.9
	34	9.65	101.56	-426.6	7.3
90C	54	10.47	100.09	-367.9	-382.1
	63	10.42	101.88	-396.2	14.2
130C	83	10.08	100.82	-242.5	-256.7
	121	10.57	100.59	-270.8	14.2

TABLE 21; RESIDUAL STRENGTHS AFTER RT/10^5CYCLES
914C, 10mm NOTCH, 2.0% WET, STACKING SEQUENCE A

TEST TEMPERATURE	SPECIMEN NUMBER	NOTCH SIZE mm	X-SECTION AREA $(mm)^2$	NORMALISED STRENGTH MPa	AVERAGE STRENGTH MPa
			TENSION		
RT	5	9.86	101.76	548.9	554.9
	6	10.03	100.88	560.9	6.0
90C	1	10.36	100.96	529.3	525.8
	3	9.85	100.71	522.3	3.5
130C	/	/	/	/	/
	/	/	/	/	/
			COMPRESSION		
RT	2	10.31	98.89	-350.1	-360.0
	4	9.83	101.99	-369.9	9.9
90C	7	9.79	101.71	-256.8	-247.1
	8	10.12	98.54	-237.4	9.7
130C	/	/	/	/	/
	/	/	/	/	/

TABLE 22; RESIDUAL STRENGTHS AFTER 90C/10^5CYCLES
914C, 10mm NOTCH, 2.0% WET, STACKING SEQUENCE A

TEST TEMPERATURE	SPECIMEN NUMBER	NOTCH SIZE mm	X-SECTION AREA $(mm)^2$	NORMALISED STRENGTH MPa	AVERAGE STRENGTH MPa
			TENSION		
RT	12	10.41	99.22	848.4	822.2
	17	10.54	101.26	795.9	26.3
90C	15	10.67	101.24	744.8	736.2
	18	10.51	100.76	727.5	8.7
130C	/	/	/	/	/
	/	/	/	/	/
			COMPRESSION		
RT	13	10.17	101.28	-495.4	-465.1
	16	10.75	101.26	-434.7	30.4
90C	10	9.96	101.58	-296.2	-295.4
	14	10.61	100.22	-294.5	0.9
130C	/	/	/	/	/
	/	/	/	/	/

TABLE 23; RESIDUAL STRENGTHS AFTER RT/10^5CYCLES
914C, 10mm NOTCH, DRY, STACKING SEQUENCE B

TEST TEMPERATURE	SPECIMEN NUMBER	NOTCH SIZE mm	X-SECTION AREA $(mm)^2$	NORMALISED STRENGTH MPa	AVERAGE STRENGTH MPa
			TENSION		
RT	26	10.39	100.12	497.8	505.6
	58	10.17	97.25	513.3	7.8
90C	18	10.28	100.40	484.2	511.9
	57	10.50	97.63	539.5	27.7
130C	10	10.35	101.59	527.6	521.4
	56	10.13	93.78	515.2	6.2
			COMPRESSION		
RT	27	10.30	100.99	-336.1	-338.1
	30	10.22	99.72	-340.1	2.0
90C	29	10.44	100.53	-303.3	-317.1
	38	10.18	100.28	-330.9	13.8
130C	47	9.60	101.30	-302.7	-299.0
	49	10.18	101.85	-295.2	3.8

TABLE 24; RESIDUAL STRENGTHS AFTER RT/10^5CYCLES
914C, 10mm NOTCH, 1.4% WET, STACKING SEQUENCE B

TEST TEMPERATURE	SPECIMEN NUMBER	NOTCH SIZE mm	X-SECTION AREA $(mm)^2$	NORMALISED STRENGTH MPa	AVERAGE STRENGTH MPa
			TENSION		
RT	/ /	/ /	/ /	/ /	/ /
90C	1	10.39	101.46	526.8	513.5
	14	9.76	98.87	500.1	13.4
130C	4	9.83	100.82	506.8	488.2
	32	9.75	100.10	469.5	18.7
			COMPRESSION		
RT	/ /	/ /	/ /	/ /	/ /
90C	15	9.60	101.42	-287.4	-285.9
	34	9.92	100.20	-284.3	1.6
130C	22	9.86	100.22	-225.9	-225.1
	41	10.38	98.60	-224.2	0.9

TABLE 25; RESIDUAL STRENGTHS AFTER RT/10^3CYCLES
914C, 5mm HOLE, DRY, STACKING SEQUENCE A

TEST TEMPERATURE	SPECIMEN NUMBER	X-SECTION AREA $(mm)^2$	FAILURE STRESS MPa	AVERAGE STRENGTH MPa
		TENSION		
RT	19	103.30	667.5	682.1
	47	99.75	696.7	14.6
90C	87	102.41	652.3	651.5
	97	95.29	650.6	0.9
130C	100	97.73	1035.5	998.2
	147	97.42	960.8	37.4
		COMPRESSION		
RT	50	100.29	-548.4	-534.7
	69	101.66	-520.9	13.8
90C	107	96.62	-522.7	-504.3
	157	98.90	-485.8	18.5
130C	136	96.86	-331.9	-386.2
	150	94.35	-440.4	54.3

TABLE 26; RESIDUAL STRENGTHS AFTER 90C/10^3 CYCLES
914C, 5mm HOLE, DRY, STACKING SEQUENCE A

TEST TEMPERATURE	SPECIMEN NUMBER	X-SECTION AREA $(mm)^2$	FAILURE STRESS MPa	AVERAGE STRENGTH MPa
		TENSION		
RT	29	101.97	691.4	716.9
	48	101.85	742.3	25.5
90C	89	102.14	629.0	679.1
	96	99.36	729.2	50.1
130C	118	98.37	1047.1	1003.7
	129	97.38	960.2	43.5
		COMPRESSION		
RT	68	102.85	-559.1	-549.6
	70	100.00	-540.0	9.6
90C	106	96.85	-570.0	-555.6
	110	98.85	-541.2	14.4
130C	138	96.38	-473.1	-458.0
	146	96.88	-442.8	15.2

TABLE 27; RESIDUAL STRENGTHS AFTER RT/10^5 CYCLES
914C, 5mm HOLE, DRY, STACKING SEQUENCE A

TEST TEMPERATURE	SPECIMEN NUMBER	X-SECTION AREA $(mm)^2$	FAILURE STRESS MPa	AVERAGE STRENGTH MPa
		TENSION		
RT	78	101.64	934.2	994.5
	117	95.38	1054.7	60.3
90C	56	99.87	945.7	941.1
	159	97.23	936.4	4.7
130C	36	101.99	911.9	927.0
	126	94.85	942.0	15.1
		COMPRESSION		
RT	99	96.33	-738.6	-723.5+
	130	95.92	-708.4+	/
90C	108	96.25	-626.0	-610.5
	148	97.90	-595.0	15.5
130C	16	100.69	-587.0	-611.5
	140	93.39	-636.0	24.5

TABLE 28; RESIDUAL STRENGTHS AFTER 90C/10^5CYCLES
914C, 5mm HOLE, DRY, STACKING SEQUENCE A

TEST TEMPERATURE	SPECIMEN NUMBER	X-SECTION AREA $(mm)^2$	FAILURE STRESS MPa	AVERAGE STRENGTH MPa
		TENSION		
RT	57	101.18	993.3	990.9
	156	97.73	988.4	2.5
90C	80	99.85	881.3	935.7
	137	98.22	990.1	54.4
130C	79	102.14	993.7	1030.9
	119	98.31	1068.1	37.2
		COMPRESSION		
RT	120	95.32	-737.0+	-648.1+
	49	98.38	-559.1+	/
90C	40	101.95	-662.1	-637.0+
	109	95.79	-611.8+	/
130C	98	97.81	-599.1	-602.1
	127	97.50	-605.1	3.0

TABLE 29; RESIDUAL STRENGTHS AFTER RT/10^3CYCLES
914C, 5mm HOLE, 1.4% WET, STACKING SEQUENCE A

TEST TEMPERATURE	SPECIMEN NUMBER	X-SECTION AREA $(mm)^2$	FAILURE STRESS MPa	AVERAGE STRENGTH MPa
		TENSION		
RT	92	102.33	680.2	668.9
	121	98.86	657.5	11.4
90C	74	101.14	894.8+	884.2+
	131	101.32	873.5	/
130C	65	101.06	876.2+	885.0+
	133	100.80	893.8	/
		COMPRESSION		
RT	32	101.44	-546.1	-528.5
	144	99.84	-510.8	17.7
90C	11	102.30	-469.7	-465.6
	85	98.62	-461.4	4.2
130C	45	101.39	-396.0	-388.8
	153	98.30	-381.5	7.3

TABLE 30; RESIDUAL STRENGTHS AFTER 90C/10^3 CYCLES
914C, 5mm HOLE, 1.4% WET, STACKING SEQUENCE A

TEST TEMPERATURE	SPECIMEN NUMBER	X-SECTION AREA $(mm)^2$	FAILURE STRESS MPa	AVERAGE STRENGTH MPa
		TENSION		
RT	31	100.85	761.0	849.8
	93	102.28	938.6	88.8
90C	15	100.08	843.3+	890.4+
	71	101.87	937.5	/
130C	43	100.58	837.6	855.2
	145	100.84	872.7	17.6
		COMPRESSION		
RT	75	99.35	-624.1	-638.5+
	91	101.26	-652.8+	/
90C	122	101.28	-573.7	-510.1
	154	100.80	-446.4	63.7
130C	125	100.86	-381.7	-382.8
	132	100.32	-383.8	1.1

TABLE 31; RESIDUAL STRENGTHS AFTER RT/10^5 CYCLES
914C, 5mm HOLE, 1.4% WET, STACKING SEQUENCE A

TEST TEMPERATURE	SPECIMEN NUMBER	X-SECTION AREA $(mm)^2$	FAILURE STRESS MPa	AVERAGE STRENGTH MPa
		TENSION		
RT	41	101.62	973.2	980.4
	123	99.28	987.6	7.2
90C	95	101.28	914.3	893.6
	112	101.34	872.8	20.8
130C	1	102.32	895.2	867.8
	62	100.62	840.3	27.5
		COMPRESSION		
RT	23	103.03	-626.5+	-631.6+
	152	101.32	-636.6+	/
90C	72	100.64	-571.3	-525.3
	84	99.31	-479.3	46.0
130C	134	101.15	-476.0	-429.5
	142	100.64	-383.0	46.5

TABLE 32; RESIDUAL STRENGTHS AFTER 90C/10^5CYCLES
914C, 5mm HOLE, 1.4% WET, STACKING SEQUENCE A

TEST TEMPERATURE	SPECIMEN NUMBER	X-SECTION AREA $(mm)^2$	FAILURE STRESS MPa	AVERAGE STRENGTH MPa
		TENSION		
RT	94	101.26	1013.2	1015.1
	5	102.07	1016.9	1.9
90C	25	101.95	1005.4	968.5
	151	100.80	931.5	37.0
130C	21	101.04	914.5	923.4
	42	101.37	932.2	8.9
		COMPRESSION		
RT	12	102.03	-651.8+	-663.7+
	155	100.82	-675.5	/
90C	114	99.80	-631.3	-612.2
	124	100.34	-593.0	19.2
130C	64	99.60	-465.9	-453.0
	81	101.14	-440.0	13.0

TABLE 33; RESIDUAL STRENGTHS AFTER RT/10^5CYCLES
914C, 5mm HOLE, 2.0% STACKING SEQUENCE A

TEST TEMPERATURE	SPECIMEN NUMBER	X-SECTION AREA $(mm)^2$	FAILURE STRESS MPa	AVERAGE STRENGTH MPa
		TENSION		
RT	3	101.26	982.6	979.0
	4	102.26	975.4	3.6
90C	5	101.26	879.9	897.8
	8	101.30	915.6	17.9
130C	/	/	/	/
	/	/	/	/
		COMPRESSION		
RT	6	101.24	-626.7	-638.8
	7	101.80	-650.8	12.1
90C	1	98.84	-581.2	-557.8
	2	100.76	-534.4	23.4
130C	/	/	/	/
	/	/	/	/

TABLE 34: FATIGUE RESULTS FOR 10mm NOTCHED 914C SPECIMENS TESTED DRY AT RT

FATIGUE LIFE	S MPa	$\frac{S}{S_{St}}$	$\frac{S}{S_{HW}}$
0.25	356.5	1.00	1.63
$1.33X10^5$	253.3	0.71	1.16
$2.73X10^5$	243.1	0.68	1.11
$4.80X10^5$	235.1	0.66	1.08
$7.50X10^5$	220.4	0.62	1.01
$1.20X10^6$	200.7	0.56	0.92
$4.81X10^6$	201.7	0.57	0.92
$8.00X10^6 \rightarrow^*$	177.0	0.50	0.81

* Arrow indicates higher expected life

TABLE 35: FATIGUE RESULTS FOR 10mm NOTCHED 914C SPECIMENS TESTED WET AT RT

FATIGUE LIFE	S MPa	$\frac{S}{S_{St}}$	$\frac{S}{S_{HW}}$
	1.4% WET		
0.25	309.9	1.00	1.42
$4.20X10^5$	254.9	0.82	1.17
$4.50X10^5$	255.0	0.82	1.17
$5.50X10^5$	265.5	0.86	1.22
$1.00X10^6$	240.6	0.78	1.10
$1.50X10^6$	237.8	0.77	1.09
$1.86X10^6$	215.7	0.70	0.99
$2.30X10^6$	233.6	0.75	1.07
$2.63X10^6$	206.6	0.67	0.95
$3.23X10^6$	224.4	0.72	1.03
$3.42X10^6$	197.8	0.64	0.91
$7.10X10^6 \rightarrow$	196.1	0.63	0.90
$15.50X10^6 \rightarrow$	176.5	0.57	0.81
	WEATHER CONDITIONED		
0.25	322.5	1.00	1.48
$1.56X10^5$	253.5	0.79	1.16
$2.50X10^5$	251.5	0.78	1.15
$1.50X10^6$	229.3	0.71	1.05
$2.00X10^6$	226.4	0.70	1.04
$2.50X10^6$	220.6	0.68	1.01
$7.40X10^6 \rightarrow$	205.6	0.64	0.94
$15.81X10^6 \rightarrow$	184.4	0.57	0.84

TABLE 36: FATIGUE RESULTS FOR 5mm HOLED 914C SPECIMENS TESTED DRY AT RT

FATIGUE LIFE	S MPa	$\frac{S}{S_{St}}$	$\frac{S}{S_{HW}}$
0.25	551.9	1.00	2.08
$4.62X10^5$	382.9	0.69	1.44
$9.98X10^5$	360.3	0.65	1.36
$2.30X10^6$	326.2	0.59	1.23
$4.60X10^6$	331.0	0.60	1.25

TABLE 37: FATIGUE RESULTS FOR 5mm HOLED 914C SPECIMENS TESTED WET (WEATHER CONDITIONED) AT RT

FATIGUE LIFE	S MPa	$\frac{S}{S_{St}}$	$\frac{S}{S_{HW}}$
0.25	555.5	1.00	2.09
$4.53X10^5$	414.4	0.75	1.56
$1.82X10^6$	394.7	0.71	1.49
$1.91X10^6$	380.6	0.69	1.43
$4.53X10^6$	351.0	0.63	1.32
$18.00X10^6 \rightarrow$	328.9	0.59	1.24
$22.00X10^6 \rightarrow$	297.5	0.54	1.12

TABLE 38: PLAIN (UNNOTCHED) TENSILE STRENGTH FOR "NEW" MATERIAL SYSTEMS TESTED WET AND DRY AT RT

MATERIAL SYSTEM	ENVIRONMENTAL EXPOSURE	TIME OF EXPOSURE MONTHS	AVERAGE MOISTURE %	NO. OF VALID TESTS	STRENGTH MPa	STANDARD DEVIATION
6376	RT/ 0% RH	12	0.00	8	1334.9	57.3
6376	60C/84%RH	12	0.94	6	1383.6	35.3
APC-2	RT/ 0% RH	8	0.00	5	1160.2	38.4
APC-2	60C/84% RH	8	0.13	5	1174.0	35.4
R25	RT/ 0% RH	6	0.00	6	753.2	38.2
R25	60C/84%RH	6	1.01	5	769.8	71.4

TABLE 39; NOTCHED STATIC STRENGTH RESULTS
6376, 10mm NOTCH, DRY, STACKING SEQUENCE A

TEST TEMPERATURE	SPECIMEN NUMBER	NOTCH SIZE mm	X-SECTION AREA $(mm)^2$	NORMALISED STRENGTH MPa	AVERAGE STRENGTH MPa
		TENSION			
RT	9	9.95	105.48	477.6	499.8
	69	10.05	106.04	521.9	22.2
90C	27	9.96	106.48	487.4	506.3
	53	10.04	107.06	525.1	18.9
130C	65	10.04	100.92	641.4	630.0
	95	9.98	101.10	618.6	11.4
		COMPRESSION			
RT	11	9.98	106.02	-381.6	-382.5
	13	10.02	106.00	-383.4	0.9
90C	49	10.07	107.00	-300.1	-310.2
	71	9.94	106.46	-320.3	10.1
130C	85	10.00	101.00	-294.1	-286.8
	105	10.02	100.99	-279.5	7.3

TABLE 40; NOTCHED STATIC STRENGTH RESULTS
6376, 10mm NOTCH, 1.0% WET, STACKING SEQUENCE A

TEST TEMPERATURE	SPECIMEN NUMBER	NOTCH SIZE mm	X-SECTION AREA $(mm)^2$	NORMALISED STRENGTH MPa	AVERAGE STRENGTH MPa
		TENSION			
RT	20	9.93	99.50	500.8	486.4
	42	9.96	103.58	472.1	14.3
90C	48	10.02	106.50	498.2	518.7
	84	9.98	104.50	539.2	20.5
130C	92	10.00	105.13	651.6	676.4
	96	9.97	103.08	701.3	24.9
		COMPRESSION			
RT	68	9.99	104.04	-345.9	-347.5
	102	10.01	104.00	-349.2	1.7
90C	32	10.15	105.58	-290.1	-291.5
	104	9.90	103.96	-292.9	1.4
130C	24	10.03	105.71	-208.8	-222.4
	44	9.93	105.58	-236.0	13.6

TABLE 41; RESIDUAL STRENGTHS AFTER RT/10^5CYCLES
6376, 10mm NOTCH, DRY, STACKING SEQUENCE A

TEST TEMPERATURE	SPECIMEN NUMBER	NOTCH SIZE mm	X-SECTION AREA $(mm)^2$	NORMALISED STRENGTH MPa	AVERAGE STRENGTH MPa
			TENSION		
RT	1	10.03	104.50	608.6	614.3
	15	10.16	101.60	620.0	5.7
90C	/	/	/	/	/
	/	/	/	/	/
130C	3	9.84	105.00	656.6	653.4
	17	9.57	104.44	650.1	3.3
			COMPRESSION		
RT	21	9.88	104.35	-427.7	-455.0
	31	10.50	105.37	-482.3	27.3
90C	/	/	/	/	/
	/	/	/	/	/
130C	23	10.43	106.54	-328.8	-331.0
	45	9.74	101.02	-333.1	2.2

TABLE 42; RESIDUAL STRENGTHS AFTER 90C/10^5CYCLES
6376, 10mm NOTCH, DRY, STACKING SEQUENCE A

TEST TEMPERATURE	SPECIMEN NUMBER	NOTCH SIZE mm	X-SECTION AREA $(mm)^2$	NORMALISED STRENGTH MPa	AVERAGE STRENGTH MPa
			TENSION		
RT	25	9.41	101.90	644.5	631.1
	33	9.81	106.00	617.6	13.5
90C	/	/	/	/	/
	/	/	/	/	/
130C	37	10.35	106.50	634.3	605.7
	47	10.27	108.02	577.0	28.7
			COMPRESSION		
RT	29	10.88	106.02	-437.8	-471.3
	57	10.18	106.96	-504.7	33.5
90C	/	/	/	/	/
	/	/	/	/	/
130C	41	10.45	104.98	-377.8	-372.9
	51	10.35	105.92	-367.9	5.0

TABLE 43; RESIDUAL STRENGTHS AFTER RT/10^5CYCLES
6376, 10mm NOTCH, 1.0% WET, STACKING SEQUENCE A

TEST TEMPERATURE	SPECIMEN NUMBER	NOTCH SIZE mm	X-SECTION AREA $(mm)^2$	NORMALISED STRENGTH MPa	AVERAGE STRENGTH MPa
			TENSION		
RT	16	10.18	103.92	597.1	597.3
	62	10.55	104.00	597.5	0.2
90C	/	/	/	/	/
	/	/	/	/	/
130C	22	10.71	105.50	637.6	635.6
	34	10.27	106.54	633.5	2.1
			COMPRESSION		
RT	12	10.70	104.00	-422.7	-409.7
	52	10.35	105.13	-396.8	13.0
90C	/	/	/	/	/
	/	/	/	/	/
130C	38	10.45	105.13	-285.9	-287.8
	56	10.56	106.08	-289.7	1.9

TABLE 44; RESIDUAL STRENGTHS AFTER 90C/10^5CYCLES
6376, 10mm NOTCH, 1.0% WET, STACKING SEQUENCE A

TEST TEMPERATURE	SPECIMEN NUMBER	NOTCH SIZE mm	X-SECTION AREA $(mm)^2$	NORMALISED STRENGTH MPa	AVERAGE STRENGTH MPa
			TENSION		
RT	14	10.53	103.46	725.0	720.7
	30	10.59	101.00	716.3	4.4
90C	/	/	/	/	/
	/	/	/	/	/
130C	26	10.28	104.83	707.5	740.4
	36	10.50	103.50	773.2	32.9
			COMPRESSION		
RT	18	10.32	105.04	-488.4	-485.5
	50	10.73	101.97	-482.5	2.9
90C	/	/	/	/	/
	/	/	/	/	/
130C	90	10.20	98.54	-366.9	-346.0
	98	9.83	105.08	-325.1	20.9

TABLE 45: FATIGUE RESULTS FOR 10mm NOTCHED 6376 SPECIMENS TESTED DRY AT RT

FATIGUE LIFE	S MPa	$\frac{S}{S_{St}}$	$\frac{S}{S_{HW}}$
0.25	382.5	1.00	1.72
3.10×10^5	319.1	0.83	1.43
3.60×10^5	279.1	0.73	1.25
5.00×10^5	317.8	0.83	1.43
7.40×10^5	265.5	0.69	1.19
7.46×10^5	315.2	0.82	1.42
8.10×10^5	278.6	0.73	1.25
9.32×10^5	299.1	0.78	1.34
2.00×10^6	242.9	0.64	1.09
6.00×10^6	233.6	0.61	1.05
8.80×10^6 →	242.8	0.63	1.09
13.30×10^6 →	204.6	0.53	0.92

TABLE 46: FATIGUE RESULTS FOR 10mm NOTCHED 6376 SPECIMENS TESTED WET AT RT

FATIGUE LIFE	S MPa	$\frac{S}{S_{St}}$	$\frac{S}{S_{HW}}$
0.25	347.5	1.00	1.56
2.25×10^5	300.1	0.86	1.35
5.85×10^5	287.1	0.83	1.29
7.00×10^5	278.7	0.80	1.25
1.42×10^6	268.7	0.77	1.21
1.80×10^6	265.3	0.76	1.19
2.46×10^6	273.9	0.79	1.23
3.71×10^6	251.4	0.72	1.13
14.90×10^6	241.4	0.69	1.09

TABLE 47: NOTCHED STATIC STRENGTH RESULTS
APC-2, 10mm NOTCH, DRY, STACKING SEQUENCE A

TEST TEMPERATURE	SPECIMEN NUMBER	NOTCH SIZE mm	X-SECTION AREA $(mm)^2$	NORMALISED STRENGTH MPa	AVERAGE STRENGTH MPa
		TENSION			
RT	21	10.07	103.66	473.9	462.9
	71	9.92	103.62	451.8	11.1
90C	/	/	/	/	/
	/	/	/	/	/
130C	54	9.97	103.07	465.0	457.8
	81	9.95	105.17	450.5	7.3
		COMPRESSION			
RT	22	10.11	101.65	-302.7	-317.8
	74	9.88	101.65	-317.8	7.6
90C	/	/	/	/	/
	/	/	/	/	/
130C	51	9.98	99.51	-209.8	-212.2
	63	9.91	103.96	-214.5	2.4

TABLE 48: NOTCHED STATIC STRENGTH RESULTS
APC-2, 10mm NOTCH, 0.12% WET, STACKING SEQUENCE A

TEST TEMPERATURE	SPECIMEN NUMBER	NOTCH SIZE mm	X-SECTION AREA $(mm)^2$	NORMALISED STRENGTH MPa	AVERAGE STRENGTH MPa
		TENSION			
RT	16	9.97	101.69	455.6	458.3
	67	10.02	100.56	460.9	2.7
90C	/	/	/	/	/
	/	/	/	/	/
130C	/	/	/	/	/
	/	/	/	/	/
		COMPRESSION			
RT	66	10.09	99.59	-316.2	-309.9
	75	9.92	99.09	-303.6	6.3
90C	/	/	/	/	/
	/	/	/	/	/
130C	/	/	/	/	/
	/	/	/	/	/

TABLE 49: RESIDUAL STRENGTHS AFTER RT/10^5CYCLES
APC-2, 10mm NOTCH, DRY, STACKING SEQUENCE A

TEST TEMPERATURE	SPECIMEN NUMBER	NOTCH SIZE mm	X-SECTION AREA $(mm)^2$	NORMALISED STRENGTH MPa	AVERAGE STRENGTH MPa
			TENSION		
RT	11	10.76	100.52	658.9	647.5
	23	10.29	101.28	636.0	11.5
90C	/	/	/	/	/
	/	/	/	/	/
130C	41	9.84	102.15	602.1	600.6
	42	9.81	100.20	599.0	1.6
			COMPRESSION		
RT	13	9.59	102.19	-421.7	-413.8
	61	10.26	107.30	-405.9	7.9
90C	/	/	/	/	/
	/	/	/	/	/
130C	32	10.41	101.61	-295.7	-291.2
	73	9.72	103.20	-286.6	4.6

TABLE 50: RESIDUAL STRENGTHS AFTER 90C/10^5CYCLES
APC-2, 10mm NOTCH, DRY, STACKING SEQUENCE A

TEST TEMPERATURE	SPECIMEN NUMBER	NOTCH SIZE mm	X-SECTION AREA $(mm)^2$	NORMALISED STRENGTH MPa	AVERAGE STRENGTH MPa
			TENSION		
RT	12	10.58	100.10	668.9	702.4
	31	9.70	102.53	735.8	33.5
90C	/	/	/	/	/
	/	/	/	/	/
130C	34	10.20	98.05	621.1	620.0
	43	9.82	102.15	618.9	1.1
			COMPRESSION		
RT	14	9.56	100.64	-445.9	-447.8
	83	10.30	99.63	-449.7	1.9
90C	/	/	/	/	/
	/	/	/	/	/
130C	52	9.58	101.02	-285.3	-318.3
	72	10.22	103.16	-351.3	33.0

TABLE 51: RESIDUAL STRENGTHS AFTER RT/10^5CYCLES
APC-2, 10mm NOTCH, 0.12% WET, STACKING SEQUENCE A

TEST TEMPERATURE	SPECIMEN NUMBER	NOTCH SIZE mm	X-SECTION AREA $(mm)^2$	NORMALISED STRENGTH MPa	AVERAGE STRENGTH MPa
			TENSION		
RT	44	10.98	101.69	628.6	633.2
	65	9.83	99.51	637.7	4.6
90C	/	/	/	/	/
	/	/	/	/	/
130C	27	10.75	102.19	603.7	617.6
	46	10.26	97.85	631.5	13.9
			COMPRESSION		
RT	15	10.49	100.60	-473.4	-460.0
	36	10.11	95.48	-446.5	13.5
90C	/	/	/	/	/
	/	/	/	/	/
130C	25	10.35	100.60	-281.6	-264.6
	57	10.24	107.14	-247.5	17.1

TABLE 52: RESIDUAL STRENGTHS AFTER 90C/10^5CYCLES
APC-2, 10mm NOTCH, 0.12% WET, STACKING SEQUENCE A

TEST TEMPERATURE	SPECIMEN NUMBER	NOTCH SIZE mm	X-SECTION AREA $(mm)^2$	NORMALISED STRENGTH MPa	AVERAGE STRENGTH MPa
			TENSION		
RT	37	10.24	108.65	665.0	682.4
	64	10.96	101.36	699.8	17.4
90C	/	/	/	/	/
	/	/	/	/	/
130C	17	10.24	103.54	625.5	618.6
	26	10.67	100.14	611.7	6.9
			COMPRESSION		
RT	47	10.50	101.61	-413.5	-427.2
	56	10.54	103.41	-440.8	13.7
90C	/	/	/	/	/
	/	/	/	/	/
130C	24	9.80	103.12	-307.2	-289.5
	45	10.99	98.59	-271.7	17.8

TABLE 53: NOTCHED STATIC STRENGTH RESULTS
R25, 10mm NOTCH, DRY, STACKING SEQUENCE A

TEST TEMPERATURE	SPECIMEN NUMBER	NOTCH SIZE mm	X-SECTION AREA $(mm)^2$	NORMALISED STRENGTH MPa	AVERAGE STRENGTH MPa
			TENSION		
RT	2	10.10	105.19	525.5	462.9
	36	9.94	107.72	400.3	62.6
130C	15	10.03	107.13	437.5	442.8
	23	9.98	102.56	448.1	5.3
200C	19	10.12	106.17	522.6	536.7
	33	9.90	97.19	550.8	14.1
			COMPRESSION		
RT	4	10.03	108.17	-386.5	-391.2
	25	9.97	107.98	-395.8	4.7
130C	16	9.99	106.04	-278.1	-275.5
	17	10.03	105.73	-272.8	2.7
200C	26	10.08	109.13	-196.0	-195.9
	34	9.92	109.34	-195.8	0.1

TABLE 54: NOTCHED STATIC STRENGTH RESULTS
R25, 10mm NOTCH, 1.0% WET, STACKING SEQUENCE A

TEST TEMPERATURE	SPECIMEN NUMBER	NOTCH SIZE mm	X-SECTION AREA $(mm)^2$	NORMALISED STRENGTH MPa	AVERAGE STRENGTH MPa
			TENSION		
RT	2	9.92	101.34	452.1	440.3
	35	10.09	105.25	428.5	11.8
130C	6	9.94	97.64	516.7	517.7
	22	10.05	99.56	518.6	1.0
200C	26	9.96	92.93	627.2	588.0
	38	10.03	103.12	548.7	39.3
			COMPRESSION		
RT	3	9.94	106.08	-319.5	-324.3
	5	10.06	106.67	-329.1	4.8
130C	8	9.89	106.63	-211.7	-227.8
	21	10.13	93.04	-243.9	16.1
200C	10	9.96	103.21	-188.1	-181.6
	42	10.04	100.16	-175.1	6.5

TABLE 55: RESIDUAL STRENGTHS AFTER RT/10^5CYCLES
R25, 10mm NOTCH, DRY, STACKING SEQUENCE A

TEST TEMPERATURE	SPECIMEN NUMBER	NOTCH SIZE mm	X-SECTION AREA $(mm)^2$	NORMALISED STRENGTH MPa	AVERAGE STRENGTH MPa
			TENSION		
RT	9	10.13	93.65	515.9	479.6
	18	9.80	107.63	443.3	36.3
90C	/	/	/	/	/
	/	/	/	/	/
130C	3	10.18	108.22	476.4	487.6
	7	10.48	102.62	498.8	11.2
			COMPRESSION		
RT	22	10.44	104.67	-443.7	-372.6
	24	10.19	97.14	-301.4	71.2
90C	/	/	/	/	/
	/	/	/	/	/
130C	12	10.66	105.50	-294.6	-280.8
	28	10.50	106.71	-267.0	13.8

TABLE 56: RESIDUAL STRENGTHS AFTER 90C/10^5CYCLES
R25, 10mm NOTCH, DRY, STACKING SEQUENCE A

TEST TEMPERATURE	SPECIMEN NUMBER	NOTCH SIZE mm	X-SECTION AREA $(mm)^2$	NORMALISED STRENGTH MPa	AVERAGE STRENGTH MPa
			TENSION		
RT	13	10.46	107.15	554.6	547.6
	20	10.36	99.70	540.6	7.0
90C	/	/	/	/	/
	/	/	/	/	/
130C	10	10.22	102.71	566.0	534.5
	39	10.22	105.13	502.9	31.6
			COMPRESSION		
RT	8	10.20	105.21	-359.0	-362.5
	27	10.22	107.72	-366.0	3.5
90C	/	/	/	/	/
	/	/	/	/	/
130C	31	9.75	104.67	-250.9	-255.0
	37	9.94	109.68	-259.1	4.1

TABLE 57: RESIDUAL STRENGTHS AFTER RT/10^5CYCLES
R25, 10mm NOTCH, 1.0% WET, STACKING SEQUENCE A

TEST TEMPERATURE	SPECIMEN NUMBER	NOTCH SIZE mm	X-SECTION AREA $(mm)^2$	NORMALISED STRENGTH MPa	AVERAGE STRENGTH MPa
			TENSION		
RT	14	9.84	93.35	520.7	527.7
	28	10.99	104.92	534.6	7.0
90C	/	/	/	/	/
	/	/	/	/	/
130C	9	9.59	97.04	630.7	573.7
	20	10.66	104.92	516.6	57.1
			COMPRESSION		
RT	4	9.83	105.63	-394.2	-376.3
	16	10.35	105.92	-358.3	18.0
90C	/	/	/	/	/
	/	/	/	/	/
130C	24	10.59	105.50	-296.6	-279.0
	30	10.44	105.69	-265.4	13.6

TABLE 58: RESIDUAL STRENGTHS AFTER 90C/10^5CYCLES
R25, 10mm NOTCH, 1.0% WET, STACKING SEQUENCE A

TEST TEMPERATURE	SPECIMEN NUMBER	NOTCH SIZE mm	X-SECTION AREA $(mm)^2$	NORMALISED STRENGTH MPa	AVERAGE STRENGTH MPa
			TENSION		
RT	32	10.83	106.71	619.3	633.9
	43	10.67	107.54	648.4	14.6
90C	/	/	/	/	/
	/	/	/	/	/
130C	15	10.19	101.66	645.4	612.3
	19	10.52	104.04	579.2	33.1
			COMPRESSION		
RT	17	9.66	105.20	-344.7	-330.0
	25	10.62	106.24	-315.3	14.7
90C	/	/	/	/	/
	/	/	/	/	/
130C	11	10.39	107.17	-271.1	-272.6
	33	10.33	106.08	-274.0	1.5